Synthesis, characterisation and optimisation of novel adsorbents for CO_2 capture

Esegboria Obhielo

A thesis submitted in partial Fulfilment of the Requirements for the Degree of

Doctor of Philosophy

University of Strathclyde

Department of Chemical and Process Engineering

Glasgow, UK

April, 2015

Copyright declaration

This thesis is the result of the author's original research. It has been composed by the author and has not been previously submitted for examination which has led to the award of a degree.'

Signed: Date:

Acknowledgments

This thesis would not have been completed without the support and cooperation of many people; firstly, I would like to extend the deepest sense of gratitude to my supervisor, Dr. Ashleigh Fletcher, for her help, guidance, patient, encouragement and excellent advice throughout my PhD programme. I have been very fortunate to work with someone of such a high level of professionalism and the willingness and availability to help when needed, I will be forever grateful to her for the success and completion of my PhD.

I would also like to extend my appreciation to colleagues and staff within the chemical engineering department, for the help and support received through my programme, with a special mention of Dr. Thomas Yip for his help during the initial period of my research, a big thank you and also to Dr. Stewart Taylor, for his assistance with coming to grips with gel making, another big thank you.

I would like to thank, my lovely wife, Karly, for her patience, understanding and sacrifice over the last 36 months, and to my lovely children, Ayesha, Noah and Evie, for their love, support and constant reminder of how proud you were of me.

Finally, I want to use this medium to acknowledge my parents Chief and Mrs E.A. Obhielo for their support all through the years, and if not for them, I would not have been here today, I want to say thank you MUM, thank you DAD, and last and by no mean the least, to all my friends and research colleagues, thank you.

Obhielo Esegboria

Abstract

In this study, a suite of novel CO_2 capture sorbents were prepared employing three facile synthetic routes: amine assimilation (co-synthesis), wet impregnation and in situ-impregnation synthesis, to develop a range of materials capable of efficiently adsorbing CO_2 while demonstrating their applicability as alternative materials for CO_2 capture from coal and gas fired power plants via post-combustion carbon capture. Prepared sorbents were characterised for individual physical and chemical properties, using, scanning electron microscopy, infrared spectroscopy, thermogravimetric analysis, elemental analyses and N_2 sorption at 77 K. CO_2 capture capacities were determined using gravimetric analysis under a range of analysis conditions (different temperature and pressure), with the corresponding effects of materials characteristics on CO_2 capacities investigated. The effect of amine incorporation was explored in detail, with findings first bench-marked against the corresponding amine free counterparts, and, then, the effect of increasing amine content analysed. So far, within the context of this study, results suggest that materials prepared via the synthetic routes adopted, exhibit high degrees of synthetic control; in addition, CO_2 capture capacities were determined to be dependent upon both textural properties but, more importantly, the basic nitrogen functionalities contained within these materials. This observation was prominent with amine in-situ impregnated silica and melamine resorcinol formaldehyde samples, but not wholly for bio-inspired amine silica samples, as the degree of amine functionalisation could not be controlled by the synthetic route chosen. Irrespective, all materials have shown enhanced adsorption performance as a result of the incorporation of basic nitrogen functionalities into the sorbent structures. Furthermore, prepared materials exhibited easy regeneration and maintained stable sorption capacities $\leq$ 99.9% over the cycles analysed, with results obtained suggesting new strategies for carbon capture materials development for efficient CO_2 capture from power plant flue gas and other relevant applications.

Dedication

This work is dedicated to my wife Karly N. Obhielo, and my children; Ayesha, Noah and Evie Obhielo.

TABLE OF CONTENT

Table of Figures

Table of Tables

Nomenclature

AIIS	Amine In-Situ Impregnated Silica
AOAC	Association of Official Analytical Chemists
ASAP	Accelerated Surface Area and Porosimetry
B13P	Bis 3-Aminopropyl-1-3 Propanediamine
B3A	Bis 3-Aminopropyl amine
BDDT	Brunauer, Deming, Deming And Teller
BET	Brunauer, Emmett And Teller
BIAS	Bio-Inspired Amine Silica
BJH	Barrett-Joyner-Halenda
BPEI	Branched-Polyethyleneimine
CCS	Carbon Capture and Storage
CHN/O	Carbon, Hydrogen, Nitrogen and Oxygen
CO_2	Carbon dioxide
CRT	Cathode Ray Tube
CSA	Concentration Swing Adsorption
C_t	Catalyst
DA	Dubinin-Astakhov
DCM	Dichloromethane
DEA	Diethanolamine
DETA	Diethylenetriamine
DR	Dubinin-Radushkevich
DSC	Differential Scanning Calorimetry
DTA	Differential Thermal Analysis
F	Formaldehyde
FTIR	Fourier Transform Infrared Spectroscopy
GHG	Greenhouse Gases
HPLC	High Performance Liquid Chromatography
ICDD	International Centre for Diffraction Data
IGA	Intelligent Gravimetric Analyser
IGCC	Integrated Gasification Combined Cycle

IIAC	Ionic Liquid Impregnated Activated Carbon
ILs	Ionic Liquids
IPCC	Intergovernmental Panel on Climate Change
IR	Infra-Red
IUPAC	International Union of Pure and Applied Chemistry
M	Melamine
MEA	Monoethanolamine
MOF	Metal Organic Framework
MRF	Melamine Resorcinol Formaldehyde
MSD	Micropore Size Distribution
NGCC	Natural Gas Combined Cycle
NRDC	National Research Development Council
PAH	Poly-Allylamine Hydrochloride
PC	Pulverised Coal
PCCC	Post Combustion Carbon Capture
PDADMAC	Polydiallyl dimethyl ammonium chloride
PEHA	Pentaethylenehexamine
PEI	Polyethylemimine
PMMA	Poly(methyl methacrylate)
ppm	parts per million
PSA	Pressure Swing Adsorption
PSD	Pore Size Distribution
PXRD	Powder X-Ray Diffraction
R	Resorcinol
R/C_t	Resorcinol to Catalyst ratio
R/F	Resorcinol to Formaldehyde ratio
rpm	revolutions per minute
SEM	Scanning Electron Microscopy
TEA	Triethanolamine
TEPA	Tetraethylenepentamine
TETA	Triethylenetetramine
TGA	Thermo-Gravimetric Analysis

TSA	Temperature Swing Adsorption
UNFCCC	United Nations Framework Convention on Climate Change
VSA	Vacuum Swing Adsorption
W_d	Deionized water
wt%	Weight percent

CHAPTER 1

INTRODUCTION, AIMS AND OBJECTIVES

1 INTRODUCTION

Carbon dioxide (CO_2) is an odourless, colourless, slightly acidic and non-flammable gas composed of a single carbon atom covalently bonded by two oxygen atoms forming a linear molecule. In its ground state, CO_2 has no permanent dipole moment, however, it interacts with passing (electromagnetic) radiation by vibrating (symmetric stretch, asymmetric stretch, and a doubly degenerate bending mode), which causes absorption and emission of infra-red (IR) radiation [1]. Although, some IR radiation is emitted, there is a continuous absorption, emission and re-adsorption cycle that stores radiant IR, which when re-emitted back to the Earth, causes the Earth to warm up, this term is known as global warming and the overall process is called the greenhouse effect.

The concentration of CO_2 in the atmosphere has reached roughly 400 ppm [2], a record high for the last 800,000 years, and is predicted to exceed 600 ppm, by the end of the century, if emissions continue at current rates. Intergovernmental Panel on Climate Change (IPCC) report, amongst others, suggest that, unless measures are taken to reverse this trend, likely and already existing scenarios that could result from global warming include:

- Melting of the polar ice caps that would ultimately lead to a rise in sea levels.
- Reports from IPCC, suggest that human induced global warming has been linked to increased intensity of rain events over the last 50 years [2-4]. Hence, warmer temperatures could lead to increased precipitation, as a result of increased energy within the climate system, which can, potentially, result in widespread flooding in some areas.
- Increased intensity of hurricanes and storms, in the last 35 years, the number of category 4 and 5 storms has increased according to the Natural Resources Defence Council (NRDC) [5].

Although the list of plausible effects of global warming is numerous, those outlined above are some of the impacts that could result from taking no action to curb human influence on global climate.

The increase in CO_2 emissions into the atmosphere resulting from increased utilisation of fossil fuels is believed to be a major cause of global warming, and can

be traced back to the 1800s when the concentration of CO_2 was approximately 280 parts per million (ppm) and, compared to the 1999 figure of 367 ppm, the difference can be attributed to increased utilisation of fossil fuels [6]. Svante Arrhenius postulated in 1896, that CO_2 emissions could someday bring about global warming [7], however, his concepts were not generally accepted until mid-1900s, when scientists discovered that the possibility of global warming was a reality. In the late 1950s to early 1960s, scientists confirmed that the level of CO_2 in the atmosphere was not only increasing, but rising quickly [8-10]. Berger *et al.* [11] estimated that in the last 150 years, the average surface temperature of the Earth has risen by approximately 1 ^{o}C and could potentially increase by 5.8 ^{o}C by the year 2100 [11-13].

Currently, it is proposed that as much as 87% of all anthropogenic emissions result from burning fossil fuels like coal, crude oil and natural gas; resulting in 39%, of total emissions released, from electricity generation [14], 23% from transport, 22% from industry [15, 16], ~4% from commercial process, like cement production, and the balance from other sources e.g. deforestation [17]. Prior to the industrial revolution, the concentration of atmospheric CO_2 was relatively constant suggesting an equilibrium between the amounts generated and the amounts absorbed naturally, however, Morrissey *et al.* [17] stated that there was evidence suggesting that anthropogenic emissions, since that time, have created an imbalance with only half of the total CO_2 emitted absorbed by natural processes [18]. As stated above, a significant amount of emissions result from supplying the World's energy demand via fossil fuels, e.g. electricity production from coal-fired power plants [19]; as fossil fuels are both a primary energy source and a driving force for sustainable global economic growth, it is likely that human dependence on such energy sources will continue for the remainder of this century. Future transitions to alternative energy sources, such as renewables and fuel cells are required to reduce the accumulation of greenhouse gases (GHGs). Currently, such energy alternatives are not main stream; hence, fossil fuels will continue to play an important role in the energy industry, consequently, continued CO_2 emissions are expected.

In response to calls for concerted efforts to tackle climate change, the United Nations Framework Convention on Climate Change (UNFCCC) [20, 21] and the Kyoto protocol [4] were adopted to provide global strategies to combat the climatic changes

evidenced and confirmed by the IPCC [3, 22], attributed as the result of human activities. Both UNFCCC and the Kyoto protocol set out targets to be met by industrialised countries to reduce their CO_2 emissions, sometimes allowing interim increased emissions as determined on a country by country basis. On average, a target reduction of 5.2% was proposed, relative to 1990 levels. The United Kingdom (UK) was given a target to cut its net CO_2 emissions by 12.5% relative to the 1990 baseline (approximately 778 million tonnes of CO_2). In 2008, The Climate Change Act (CCA) was passed to established a framework to develop an economically credible emissions reduction path, and also strengthen the UK's leadership internationally by highlighting the role it would take in contributing to urgent collective action to tackle climate change under the Kyoto Protocol [23]. The CCA outlined new targets for the UK with reductions of 20% by 2020 and 80% by 2050 expected. To meet these targets, concerted efforts are required to mitigate against increasing CO_2 emissions, notwithstanding technological advances in more efficient utilisation of energy or increased energy input from the renewable sector, more still needs to be done. Despite these regulatory demands, in 2012, final figures for the UK greenhouse gas emissions [24] showed a net CO_2 emission increase of 4.4%, compared to the previous year, while globally, in 2010, CO_2 emissions increased by ~5.9% [24, 25]. This further highlights the need for greater efforts to tackle CO_2 emissions.

In order to combat this rising trend, urgent technological solutions need to be applied to control CO_2 emissions such as potential Carbon (CO_2) Capture and Storage (CCS) technologies. The capture of CO_2 followed by its storage in geological formations is viewed as an important strategy in achieving substantial reduction in emissions levels, but firstly, the main emission sources need to be assessed in order to design proposed technologies capable of mitigating against increasing CO_2 emissions [3, 6, 26], by considering CO_2 emission sources, proximity to CCS technology and applicable CCS methods [3].

1.1 CO_2 Emission sources (commercial and industrial)

The two main sources of CO_2 emissions into the atmosphere, are human (anthropogenic), and natural. Natural sources include respiration, decomposition and ocean releases; while anthropogenic sources vary depending on the emission source,

e.g. combustion of fossil fuels, industrial processes like cement production, electricity generation from coal and gas fired power plants, land use changes etc. Natural sources are not discussed further in this section as such emissions are much lower in concentration and often mobile (e.g. respiration), making capture restrictive [16].

1.1.1 Land use changes

Land use changes come about when the natural environment is converted for alternative use e.g. for agriculture, settlement and recreational activities etc. The main type of land use change responsible for reducing CO_2 emissions removal is known as deforestation. As trees act as a carbon sink (CO_2 removal via photosynthesis), their removal impacts GHG emissions when these forests are either burnt or allowed to rot, hence, adding to the overall CO_2 in the atmosphere. It is estimated that between the year 1850 and 2000, 28 – 40% (396 - 690 billion tonnes) of the total anthropogenic CO_2 emissions were related to land use changes, and more recently it has been shown that as much as 9% of the total emissions in 2011 were land use related, contributing ~3.3 billion tonnes of CO_2 [16].

1.1.2 Commercial/industrial processes

Different industrial processes produce differing amounts of CO_2; some produce CO_2 directly, i.e. during the combustion of fossil fuels (e.g. electricity generation), while others produce CO_2 as by-product during manufacturing processes (e.g. steel production). In 2013, Le Quéré *et al*. [16], reported that industrial processes accounted for up to 4% of anthropogenic CO_2 emissions, contributing ~1.7 billion tonnes of CO_2 [17].

1.1.3 Fossil fuel emissions

Fossil fuels account for the largest contribution to human sources of CO_2 emissions, accounting for ~87% of the total anthropogenic emissions, and result predominately from burning fossil fuels for electricity, transportation, heat generation etc. Le Quéré *et al*. [16] reported that in 2011, ~33.2 billion tonnes of CO_2 were emitted from the combustion of fossil fuels worldwide (Figure 1-1).

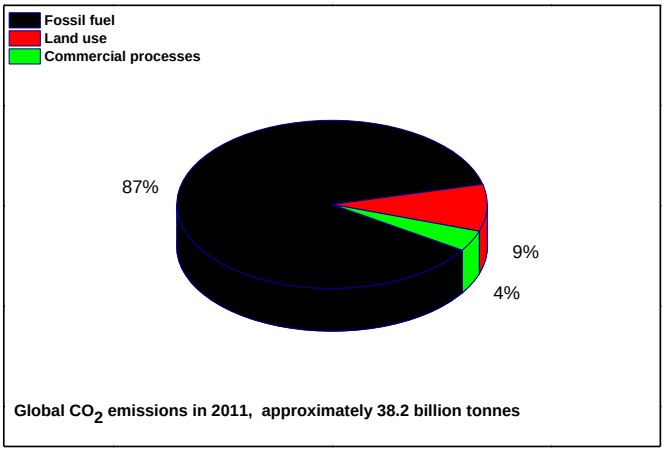

Figure 1-1: Anthropogenic CO_2 percentage emissions (source Le Quéré, C. *et al.* [16]. The global carbon budget (1959-2011)

More recently, environmental concerns, resulting from climate change, have motivated research towards stabilising the imbalance of CO_2 concentration in the atmosphere [26]. At present, point sources, such as coal-fired power stations are receiving the most attention as they contribute significantly to this excess [27] (Figure 1-2).

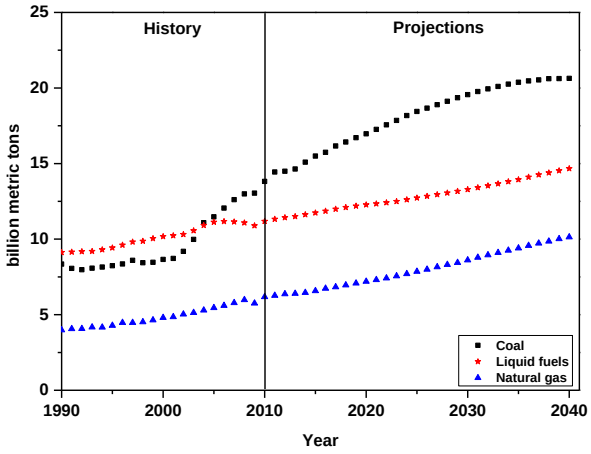

Figure 1-2: World energy related CO_2 emissions by fuel type. 1990 – 2040 [28].

The implication of this increase is that commercial-scale CCS technologies are required [29] and, over the last fifteen years, various CCS mitigation technologies have emerged.

If the UK intends to remain a major player in CCS technology development now, and in the future, and to also meet with the European Commission's 2020 and 2050 CO_2

reduction targets, there is need for the deployment of such commercial-scale CCS technologies. However, as coal is the major source of CO_2 emissions, emphasis is being placed on developing CCS technology specifically for coal fired plants. Using the cost of CO_2 capture as a defining benchmark; of all of the different technologies available for CO_2 capture from flue gas streams in coal based power plants, adsorption on porous solid media is an emerging alternative that addresses the often prohibitive cost issues of competitor processes (reduced energy requirements for sorbent regeneration compared to aqueous solvent) [3, 30].

In this work, we have developed range a of novel CO_2 capture sorbents with special emphasis on sorbent efficiency, practicability and ease of synthesis, making practical use of these sorbents as alternative materials for CO_2 capture by post-combustion carbon capture technology from coal/gas fired power plants. The materials synthesised have been subsequently characterised and screened for CCS potential.

1.2 Aims and objectives

The aim of the research work was to develop a range of novel CO_2 capture sorbents capable of efficiently adsorbing CO_2 while demonstrating their applicability as alternative materials for CO_2 capture from coal and gas fired power plants via post-combustion carbon capture.

1.3 Objective

The objectives set to achieve the overall aims were:

- Synthesis of a range of novel materials using simplistic preparation methods;
    - Bio-inspired amine silicas and nitrogen enriched resorcinol formaldehyde xerogels preparation; termed amine assimilated syntheses.
    - Ionic liquids impregnation on activated carbon; termed wet impregnation synthesis.
    - Amine in-situ impregnated silica prepared using a combination of the amine assimilated and wet impregnated synthesis methods; referred to as in situ-impregnated synthesis.

- Determination of chemical and physical properties of materials synthesised using a range of characterisation techniques.
- Evaluate the effect of nitrogen content on the CO_2 capture capacities of synthesised materials using a range of working conditions (temperatures and pressures).
- Investigation of optimum regeneration methods and effect of cycling on sorbent CO_2 capture capacities.
- Optimisation of synthesis method to reduce synthesis time and associated costs.

CHAPTER 2

INTRODUCTION TO CARBON CAPTURE

2 CO_2 CAPTURE TECHNIQUES AND ASSOCIATED CAPTURE COSTS

Presently, CO_2 can be recovered from flue gases emitted by power plants (Integrated Gasification Combined Cycle (IGCC)), steel mills, and cement factories etc. by using any of the following proposed CO_2 capture technologies, which are categorised into three main strategies (Figure 2-1):

- Pre-combustion carbon capture
- Oxy-fuel combustion carbon capture
- Post-combustion carbon capture

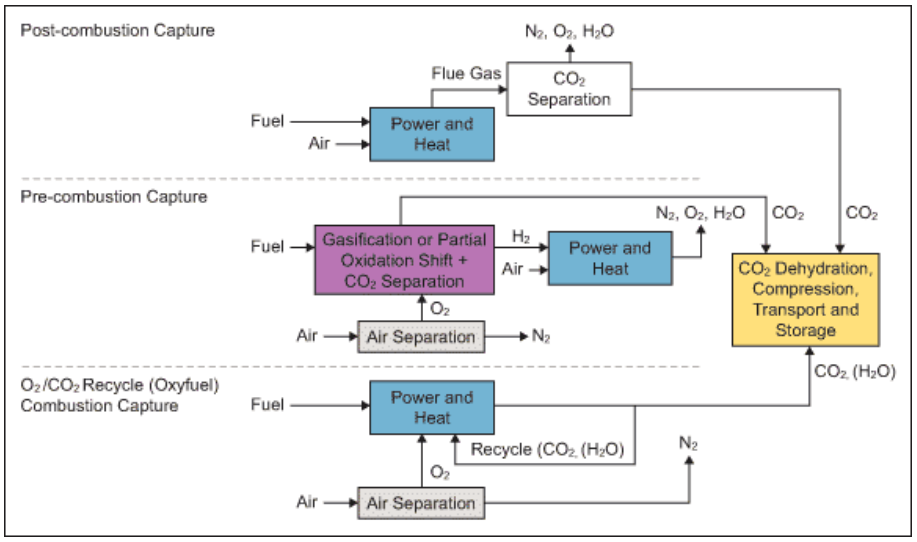

Figure 2-1: Schematic diagram of different CO_2 capture routes [31].

Each technological approach has associated pros and cons; some already proven in chemical industries involved in CCS, while others are currently only viable on a laboratory scale but which indicate potential future application.

2.1 Pre-Combustion Carbon Capture

This category of technologies involves the removal of CO_2 before combustion in an IGCC plant; firstly, the fossil fuel is converted to synthetic gas, composed primarily of CO and H_2, either by coal gasification or natural gas reforming with oxygen. The CO formed is converted to CO_2, generating H_2 by the water-gas-shift reaction, and is separated from the flue gases using an absorbent, leaving a H_2 rich gas supply. As H_2 produces no CO_2 on combustion, it is a clean source of fuel, being burned in a gas

turbine or used for other purposes e.g. the operation of fuel cells or in transportation methods [32, 33].

2.1.1 Advantages of pre-combustion capture

- It is a scalable process, with existing applications in the oil and gas industries.
- The CO_2 separation step consumes less energy than in other processes (post and oxy-combustion carbon capture), involving smaller reaction volumes, lower volumetric flow rates, elevated pressures, and higher component concentrations. The higher concentration reduces energy intensity and energy generation penalties are typically 10-16%, i.e. roughly half those of post-combustion carbon capture methods [34]. It is an efficient technology, which allows the use of simple inexpensive techniques, usually by either physical or chemical absorption process e.g. physical solvents (Selexol and Rectisol), membranes, pre-combustion sorbents (lithium silicate-based (Li_4SiO_4) etc., to separate the highly concentrated CO_2 from syngas resulting in a hydrogen-rich fuel which can be used in many applications, such as boilers, furnaces, gas turbines, engines and fuel cells; efficiencies up to 95% CO_2 capture have been achieved.

- It is applicable to both natural gas and coal fired IGCC power plants.
- The hydrogen by-product provides a good source of energy for different industrial processes [32, 35].

2.1.2 Disadvantages of pre-combustion capture

- The new structures that have to be retrofitted to older IGCC plants make pre-combustion capture expensive and limited only to newer plants.
- Process equipment like gas turbines, boilers and heaters must be modified for hydrogen firing, and the feed fuel must first be converted to syngas before CO_2 removal [36].

2.2 Oxy-Combustion Carbon Capture (OCCC)

Oxy-combustion carbon capture is another form of CO_2 capture, which involves the modification of the combustion process so that the post combustion flue gas has a high concentration of CO_2. Here, fossil fuels are burnt in high purity oxygen ($\geq$ 95%), rather than air, resulting in an exhaust stream of highly concentrated CO_2

(~90%) and water vapour [34], with nitrogen eliminated completely from the combustion process.

2.2.1 Advantages of oxy-combustion capture

- It offers the option of retrofitting, and is a more promising process than post-combustion capture for new plants, because the need for a CO_2 separation unit is eliminated from the process.
- High CO_2 concentration of the flue gas (~90%), which can be purified using inexpensive methods (i.e. flue gas is dried to remove H_2O, removal of O_2 to prevent corrosion in transport pipelines, and possibly removal of other contaminants and diluents, such as Ar, N_2, SO_2, and NOx by oxidation).
- Due to the higher boiler efficiencies offered by this method and the elimination of N_2 from the combustion process, lower NO_x formation is achieved, hence, eliminates the need for NO_x control equipment.
- H_2O is the only by product; it is non-toxic and easily separated by condensation.

2.2.2 Disadvantages of oxy-combustion capture

- Decreased process efficiencies due to cost and environmental concerns of using high purity oxygen (recently Praxair Incorporated started a project to investigate alternative approaches to oxy-combustion, proposing the use of an oxygen transport membrane as an alternative to the popular cryogenic method of producing oxygen, this was done to overcome the large energy requirements of conventional cryogenic air separators vital for O_2 production, which make the process cost intensive [35].
- There are concerns with higher CO emissions, which are also environmentally unfriendly because of reaction with hydroxyl radicals to produce CO_2, as well as associated health issues [32].

2.3 Post Combustion Carbon Capture (PCCC)

As the name implies, PCCC involves the removal of CO_2 from flue gas streams, produced from the combustion of fossil fuels or carbonaceous materials, by the addition of a separate CO_2 capture system. It is also beneficial, before CO_2 separation commences, to separate other combustion constituents like N_2, H_2O, O_2, NO_x, SO_x,

and a host of heavy metals, using existing technologies like selective catalytic reduction (reduces NO_x emissions), electrostatic precipitation (reduces ash), flue gas desulphurisation (reduces sulphur i.e. SO_x). PCCC is an end of pipeline treatment for flue gas, and is plagued by low economic efficiencies because of the requirement for large, expensive equipment needed to treat high volumes of flue gas and significant associated efficiency penalties of 25 – 35%. PCCC can be retrofitted to the majority of existing coal fired power plants, as it does not affect the upstream part of the plant during retrofitting, causing no disturbance to production, and has cost savings, as no new plant is built [26, 34]; such methods have shown promise in reducing GHG emissions as a direct result of retrofitting [37, 38].

2.3.1 Types of PCCC methods

Different PCCC systems have been developed over time (Figure 2-2), including:

- Absorption capture (Figure 2-2a)
- Adsorption capture (Figure 2-2a)
- Membrane capture (Figure 2-2b)
- Cryogenic separation(Figure 2-2c)

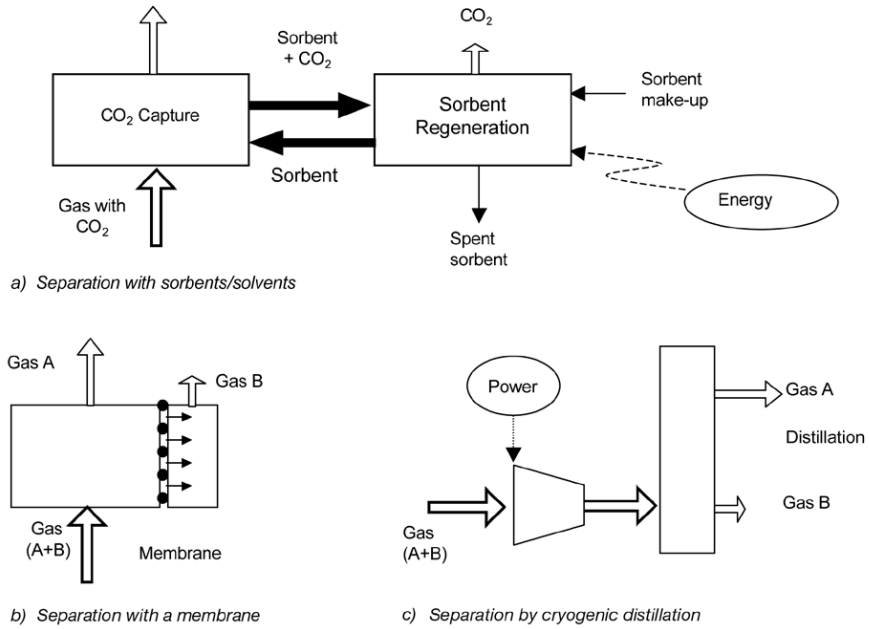

Figure 2-2: General schematics of the main separation processes relevant for PCCC [39].

2.3.1.1 Absorption capture systems

Capturing CO_2 from a gas stream using either physical or chemical absorption is a mature technology and has been applied, at industrial scale, for a few decades, although not for CO_2 capture from power plants; such systems are applicable to gas streams with the following key characteristics: high CO_2 partial pressure and high acidic content of the flue gas. Based on the information obtained from the application of absorption capture systems to high pressure feeds, CO_2 recovery methods for lower partial pressure systems, and even directly from air, have been developed. CO_2 capture, based on absorption methods, can be sub-divided into two main categories: **physical absorption,** when absorption occurs without involving a chemical reaction, and **chemical absorption,** which occurs when a solvent reacts chemically with an adsorbate to form a new chemical compound from which CO_2 can be recovered by heating, at elevated temperatures [40]. Different systems exist by which CO_2 is captured chemically; the next section provides a brief overview of some of the major absorption systems currently available.

2.3.1.1.1 Amine-based systems

Typically, chemical absorption processes require an absorber and a stripper, by which the absorbent is thermally regenerated. Here, a flue gas stream is exposed to an aqueous amine solution and the CO_2 present reacts reversibly with the amines to form stable carbamates salts from which CO_2 is released by heating the solution in the stripper (37); the degree of hydrolysis of these carbamates to form bicarbonate depends on the chemical stability of the carbamate, which is influenced by the temperature and solvent molecular structure. Alkanolamines are generally used as absorbents for chemical CO_2 absorption and consist of an ammonia group with one or more hydrogen atoms replaced by an alkyl or aryl group.

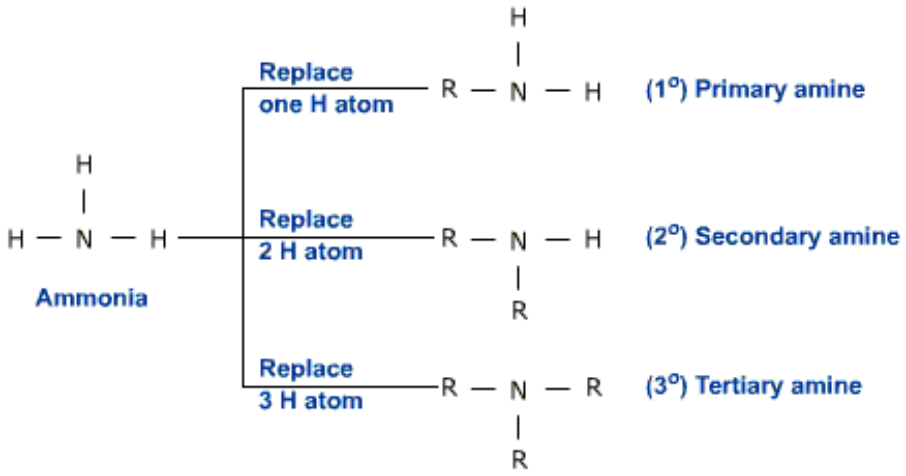

Figure 2-3: Different types of amines.

Depending on the groups replacing the hydrogen, alkanolamines exist in one of three structural forms; primary, secondary, and tertiary, each containing at least one OH and one amine group e.g. monoethanolamine (MEA), diethanolamine (DEA) and triethanolamine (TEA).

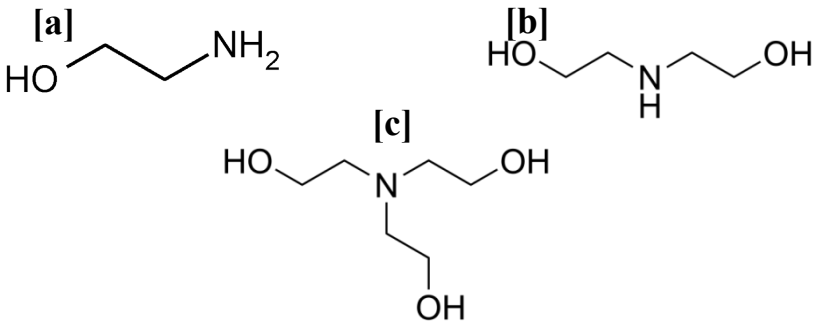

Figure 2-4: Groups of amine, (a) monoethanolamine (primary amine), (b) diethanolamine (secondary amine) and (c) triethanolamine (tertiary amine).

The reactivity of these amines, increases in the order of primary < secondary < tertiary, hence, their CO_2 loading capacities reduce in the same order, with tertiary amines showing the highest CO_2 loading capacities. Capacities of 1.0 mol of CO_2 per mol of amine have been recorded for tertiary amines while, both primary and secondary amines have shown loading capacities of between 0.5 and 1.0 mol of CO_2 per mol of amine. Equation 1 shows how amines (primary and secondary) react with CO_2 to form a carbamate, this is known as the zwitterion mechanism (originally proposed in 1968 by Caplow [41] and reintroduced in 1979 by Danckwerts [39]). The mechanism by which tertiary amines react with CO_2 (Equation 3) was proposed by Donaldson and Nguyen [40]. The reaction mechanism is essentially the base

catalysed hydration of CO_2, as CO_2 reacts directly with tertiary amines by physical absorption [42, 43]. Tertiary amines catalyse the formation of bicarbonates by homogeneous hydrolysis, in which H_2O reacts with the zwitterion type complex to form a bicarbonate (Equation 4) [44, 45].

Zwitterion mechanism:

$$RR'NH + CO_2 \longleftrightarrow RR'NH^+COO^-$$

Equation 1

$$RR'NH^+COO^- + RR'NH \longleftrightarrow RR'NCOO^- \left(Carbamate\right) + RR'NH_2^+$$

Equation 2

The zwitterion mechanism comprises two steps, the first is the formation of a CO_2– amine zwitterion (Equation 1) and the second, is the based catalysed deprotonation of the zwitterion (Equation 2)

Comparatively, the overall reaction with tertiary amines is:

$$2RR'NH + CO_2 \longleftrightarrow RR'NCOO^- + RR'NH_2^+$$

Equation 3

$$RR'NCOO^- + H_2O \longleftrightarrow RR'NH + HCO_3^- \left(bicarbonate\right)$$

Equation 4

Amine regeneration (alkanolamine) is a major issue affecting chemical absorption processes because of associated economic, environmental and operational problems. According to Arnold *et al.* [46], degradation losses of ~2.2 kg of MEA occur when capturing 1 t of CO_2, which leads to increased operational costs, while Rochelle *et al.* [44] reported that amine absorption/stripping increases the overall CO_2 capture cost by \$52 – 77/t and regeneration costs up to 4.2 GJ/t CO_2 for conventional coal fired plants [47].

2.3.1.1.2 Carbonate based systems

These systems are based on the ability of a soluble carbonate to react with CO_2 to form bicarbonate that, when heated, releases CO_2 and reverts back to the carbonate, which can be recycled for further CO_2 capture cycles. The overall reaction occurring

when CO_2 is absorbed in a solution of an alkali metal carbonate (e.g. potassium carbonate) is as follows:

$$CO_2 + K_2CO_3 + H_2O \leftrightarrow 2KHCO_3$$

Equation 5

As potassium carbonate and bicarbonate are both strong electrolytes, their metals remain only in the ionic form; hence, Equation 5 is rewritten as:

$$CO_2 + CO_3^{2-} + H_2O \leftrightarrow 2HCO_3^-$$

Equation 6

A major advantage of this system, compared with amine-based systems, is that significantly lower energy is required for regeneration [48]. Hanna *et al.* [49], from their work on the feasibility of CO_2 capture using sodium carbonate slurry, concluded that, compared to MEA-based capture systems, the energy requirement was lower by 3.2 MJ/kg CO_2 captured [49].

2.3.1.1.3 Ammonia based systems

The use of ammonia as a solvent for CO_2 capture has generated increased interest over the last decade, and is a method similar to amine based systems; here ammonia and its derivatives react with CO_2 via a range of reaction mechanisms. One mode of interaction is the aqua-ammonia process, where aqueous ammonia is used to capture CO_2 at room temperature, and Bai *et al.* [47] have reported CO_2 removal efficiencies from flue gas > 95% , while absorption capacities of ~0.9 kg CO_2 per kg NH_3 have also been reported [50]. Another reaction mechanism, is the chilled ammonia process, patented in 2006 by Eli Gal [51], CO_2 capture is performed under refrigeration conditions (temperatures of 273–283 K). The reaction mechanisms for ammonia based CO_2 capture follow the format presented below, as proposed by Brooks and Audrieth, [52], Hatch and Pigford, [46, 50] and Koutinas *et al.* [51]:

$$CO_2(g) + 2NH_3(g) \leftrightarrow NH_2COONH_4(s)$$

Equation 7

$$NH_2COONH_4(s) + H_2O(g) \leftrightarrow (NH_4)_2CO_3(s)$$

Equation 8

$$CO_2(g) + 2NH_3(g) \leftrightarrow CO(NH_2)_2(s) + H_2O(g)$$

Equation 9

$$CO_2(g) + 2NH_3(aq) \leftrightarrow NH_4^+(aq) + NH_2COO^-(aq)$$

Equation 10

$$NH_3(g) + CO_2(g) + H_2O(g) \leftrightarrow NH_4HCO_3(s)$$

Equation 11

$$2NH_3(l) + CO_2(g) + H_2O(l) \leftrightarrow (NH_4)_2CO_3(s)$$

Equation 12

$$NH_3(l) + CO_2(g) + H_2O(l) \leftrightarrow NH_4HCO_3(s)$$

Equation 13

The above reactions proceed at different temperatures and under various operating conditions, for example, the formation of ammonium carbamate (NH_2COONH_4) results from a reaction between ammonia and CO_2 under ambient conditions (room temperature and pressure). A major advantage of this system is that, the energy requirement for regeneration is significantly reduced because of the lower heat of reaction, also there is no degradation of the reactants during adsorption/desorption regeneration cycles. Ammonia based systems are also tolerant to flue gases containing oxygen, and reacts with flue gas impurities (NO_x and SO_x) to form useful and economic by products (fertilizers), although one disadvantage is the requirement for lower operating temperatures, as ammonia is highly volatile, and extensive losses can occur during regeneration at elevated temperatures [53, 54].

2.3.1.1.4 Sodium hydroxide based absorption

CO_2 absorption using sodium hydroxide first forms carbonic acid, from the dissolution of CO_2 in water, which eventually reacts with sodium hydroxide to form sodium carbonate, hence the proposed reaction mechanism:

$$2NaOH(aq) + CO_2(g) \rightarrow Na_2CO_3(aq) + H_2O(l)$$

Equation 14

The Na_2CO_3 produced exists only as dissociated Na^+ and CO_3^{2-}; as more CO_2 is absorbed, the reaction proceeds to the next phase:

$$Na_2CO_3(aq) + CO_2(g) + H_2O(l) \rightarrow 2NaHCO_3(aq)$$

Equation 15

Regeneration is achieved by the addition of lime ($Ca(OH)_2$) to the carbonation products to regenerate sodium hydroxide and produce calcium carbonate (Equation 16), which is heat treated to release pure CO_2 (Equation 17), for either capture or hydrolysis to lime mud (Equation 18):

$$Na_2CO_3 + Ca(OH)_2 \leftrightarrow 2NaOH + CaCO_3$$

Equation 16

$$CaCO_3 \leftrightarrow CaO + CO_2 \quad \text{(Heat treated at ~1173 K)}$$

Equation 17

$$CaCO_3 + H_2O \leftrightarrow Ca(OH)_2 \quad \text{(Regeneration of lime mud)}$$

Equation 18

The main advantage of this system is that the chemicals used are inexpensive and readily available, but the drawback is the high energy requirement for CO_2 recovery [55]. Ranjani *et al.* [53] reported that regeneration temperatures of 973 K were required, compared to 423 K for MEA systems [56], while Bacicchi *et al.* [54] reported, for their work on process design and energy requirements for CO_2 capture using NaOH, regeneration temperatures of 1173 K and energy requirements of 179 kJ/mol CO_2 [57]. Maryam *et al.* [58] reported similar energy requirements to those of the MEA system reported by Roa *et al.* [46], (~130 KJ/mol CO_2) although the heat required for regeneration of CaO was supplied at 1073 K. These demands further highlight the drawbacks associated with the use of hydroxides as CO_2 capture solvents.

2.3.1.2 Cryogenic separation

The process of cryogenic separation involves the separation of a gas mixture by fractional condensation, and distillation at low temperature. It involves cooling the gas mixture (< 200 K) to induce the phase changes needed for effective separation. Separation is based on the different boiling points and volatilities of the components present in the cooled gas mixture. In a typical cryogenic separation process for CO_2 capture, the gas mixture containing CO_2 is initially compressed and preheated to

remove any water present, then cooled, before being cryogenically distilled where after the liquefied CO_2 is separated and collected for storage [59].

2.3.1.3 Membranes

A relatively new technique using selective membranes to separate certain components from a gas stream based on the different gas permeabilities; here, membranes act as semi-permeable barriers that preferentially allow certain gases to pass through them by various mechanisms (solution-diffusion, adsorption-diffusion, molecular sieve and ionic transport). Membranes come in different forms: organic (e.g. polymeric) and inorganic (e.g. carbon, zeolites), and can be porous or non-porous. Polymeric membranes are generally used for gas transport, adopting separation mechanisms like solution-diffusion, Knudsen diffusion and molecular sieve etc., while inorganic membranes are generally used in highly selective separations e.g. H_2 (non-porous inorganic membrane), or CO_2 , large pore zeolites such as those used by Falconer *et al.* [60] (SAPO-34 membrane separated CO_2 from CH_4 with a selectivity of 67 at 297 K). The use of membranes in conjunction with chemical absorption has been suggested for CO_2 capture; it involves passing flue gas through a bundle of membranes composed of polymer i.e. hollow fibres arranged in a tube and shell configuration, with amine solution flowing through the shell side. CO_2 preferentially filters through the membrane and is absorbed into the amine leaving behind the flue gas contaminants. Once the process is complete the amine is regenerated and the concentrated CO_2 captured [61, 62]. Although membranes have several advantages over absorption and adsorption processes (no regeneration energy required, simple modular systems, no waste streams), membranes cannot always achieve high degrees of separation, which makes multiple stages or recycling necessary. Another disadvantage of membranes is the insensitivity to sulphur compounds and other trace elements [59, 63].

2.3.1.4 Adsorption capture systems

In adsorption capture systems, the adsorbate remains on the surface of the adsorbent either by formation of a chemical bond (chemical adsorption) or by weak physical attractive forces of the van der Waals type (pole-ion and pole-pole interactions between the quadrupole of CO_2 and the ionic and polar sites of the adsorbent surface [64], known as physical adsorption). Adsorption capture systems have several advantages including, no liquid waste, any solid waste is usually environmentally

friendly, and sorbents can operate at a variety of temperatures making their applicability widespread.

A wide variety of physisorbent materials exist with more being developed, a few examples are; porous carbonaceous materials (activated carbon based adsorbents), zeolites, alumina, silica gels, ionic liquids (physical solvents) and metal organic frameworks (MOFs). The three systems used in this work are discussed further.

2.3.1.4.1 Adsorption by activated carbon

Activated Carbons (AC), including charcoal, have well developed micro/mesoporosities, which are applicable to a wide range of industrial and technological processes. ACs are versatile adsorbents used extensively for the removal of colour, odour, taste, organic and inorganic impurities both industrially and domestically, they have applications in solvent recovery and air purification, amongst a host of others, the Egyptians used charcoal as an adsorbent for medical purposes in 1500 BC; ancient Hindus in India purified drinking water by filtering through charcoal etc. The surface chemistry of AC is governed by the presence of heteroatoms, such as oxygen, nitrogen, sulphur and hydrogen derived from the starting material or incorporated during activation or other preparatory methods. ACs are generally prepared by the pyrolysis of carbonaceous materials at elevated temperatures (< 1273 K), via two main process steps; the first involves carbonising the carbonaceous materials at temperatures up to 1073 K, while the second involves activating the carbonised materials at elevated temperatures (up to 1273 K). Carbonisation removes most of the non-carbon components as volatile gaseous products leaving behind bare elemental carbon, comprised of stacks of irregularly arranged aromatic sheets with free interstices between the sheets. The interstices make carbons excellent adsorbents, as they give rise to porous structure, which can be further enhanced upon activation [65].

Activated carbons on their own, sometimes do not have the desired chemical nature or suitable porous structure for a given application, hence, chemical modification, to develop the internal porous structure is required. Carbon modification has been reported to improve the surface chemistry (acidic) and enhance the adsorptive properties; the formation of a range of surface groups can be achieved, for example carbon-oxygen surface groups, formed by oxidation of the carbon surface with oxidising gases or solutions, carbon-hydrogen groups obtained by treatment with

hydrogen gas at elevated temperatures, carbon-nitrogen surface groups obtained by treatment with ammonia or amines, carbon-sulphur surface groups obtained by treatment with elementary sulphur, CS_2, H_2S or SO_2, and carbon-halogen surface groups formed by treatment with halogens in gaseous or solution phase. Chemical modification of carbons with regards CO_2 capture has been extensively studied by a host of authors using a variety of modification techniques. All report that surface modification with basic groups increases the overall sorbent adsorption capacity, although a compromise with porosity is often involved depending on the modification route [25, 66-70]

2.3.1.4.2 Adsorption by silica

Silica gel is a partially dehydrated form of colloidal silicic acid; its chemical formula is $SiO_2.nH_2O$, where the water of crystallisation is as chemically bonded hydroxyl groups called silanol. The bulk structure of SiO_2 consists mainly of silanol (Si-OH) and siloxane (-O-Si-O-) bridges with oxygen atoms, the silanol groups are formed from incomplete condensation-polymerisation reaction of $Si(OH)_4$ or by the rehydroxylation of dehydroxylated silica when it is treated with water or aqueous solutions (Figure 2-5).

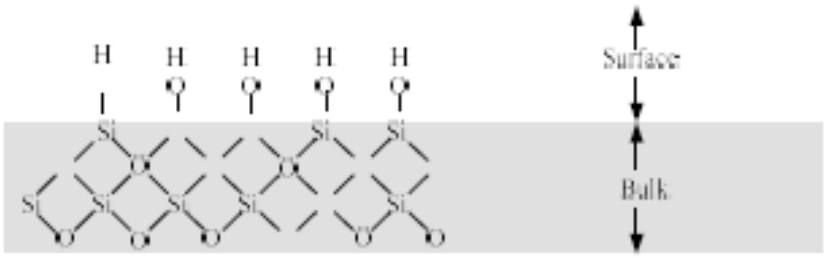

Figure 2-5: Structure of SiO_2 showing siloxane bridges and surface silanol groups

The hydroxyl groups on the silica surface act as centres for molecular adsorption during their interaction with adsorbates capable of forming hydrogen bonds with surface hydroxyl groups, i.e. donor-acceptor interactions. The surface hydroxyl groups can either react or be replaced with different chemicals (e.g. alcohols, phenols, and amines) allowing desired surface properties to be tailored. For CO_2 capture, the surface chemistry can be modified with amines, to increase a sorbents CO_2 adsorption capacity; generally there are two main methods of modification:

Post synthetic grafting technique

Silica surfaces are well adapted to grafting with organosilanes, functionalisation is achieved by grafting the desired functionality onto the silica surface or pore walls

(Figure 2-6). Llewellyn *et al*. [71] grafted MCM-41 with chloromethyl octyl silane groups and, with respect to CO_2 capture, different authors have grafted amine containing ligands onto the surface of mesoporous silica [71-74]. Depending on the amine type, the resulting extent of basicity on the silica surface, affects the CO_2 adsorption behaviour. Zelenak *et al.* [74] functionalised SBA-12 using different amines with varying base strength, and their results showed that the higher basicity of amino ligands increased the CO_2 adsorption capacity of the sorbents [75].

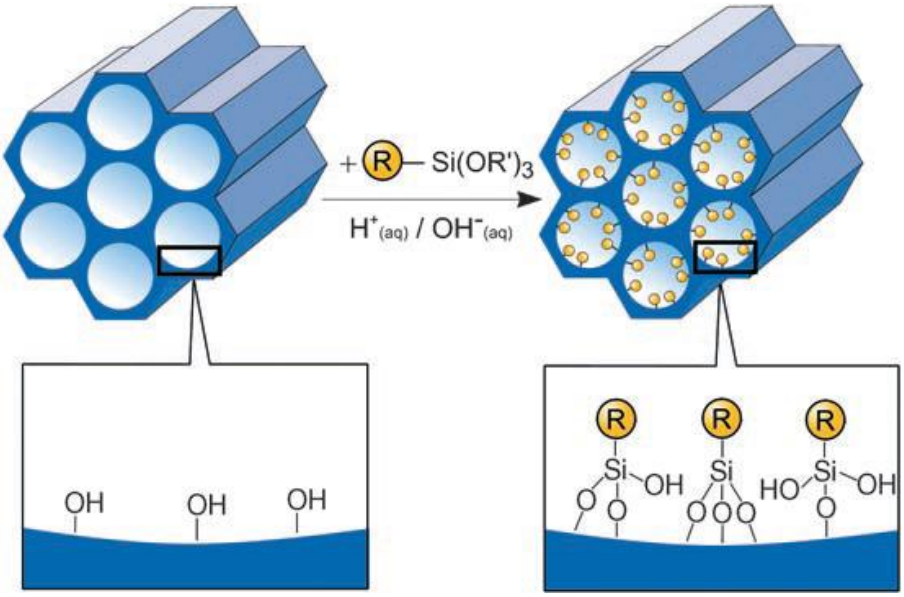

Figure 2-6: Modification (post-synthetic functionalisation) by grafting organic moieties (organosilanes) onto mesoporous silica [75].

Co-condensation (one-pot synthesis) functionalisation technique

An alternative method to synthesise organically functionalised mesoporous silica, uses silane $(R'O)_4$ Si (TEOS and TMOS) and organosilane $(R'O)_3$ Si-R (where R′ is ethanol or methanol and R is non-hydrolysable ligand) precursors, which co-assemble in the presence of amphiphilic surfactants (Figure 2-7). Organically functionalised silica is prepared in such a way that the organic groups are within the pores (i.e. organic functionalities are direct components of the silica matrix), hence, the problem of pore blocking is overcome and, also worth mentioning, the organic groups are well distributed within the silica matrix (homogenous), while a range of organic functional groups can be readily introduced into the mesoporous silica allowing anchorage of organic functional ligands to the mesopore walls in a single step, and enabling a higher and more homogenous surface coverage of organosilane functionalities. One main disadvantage of this technique, however, is that there is a

limit to the amount of organic functionalities that can be incorporated, exceeding 40 mol% [76]. has proven to lead to disordering of the pore network; another issue is that of predicting the quantity of organic functionality within the pore walls, as it is not possible to determine this in advance as the proportion of terminal organic groups incorporated into the pore-wall network is generally lower when compared to the starting concentration in the reaction mixture [76].

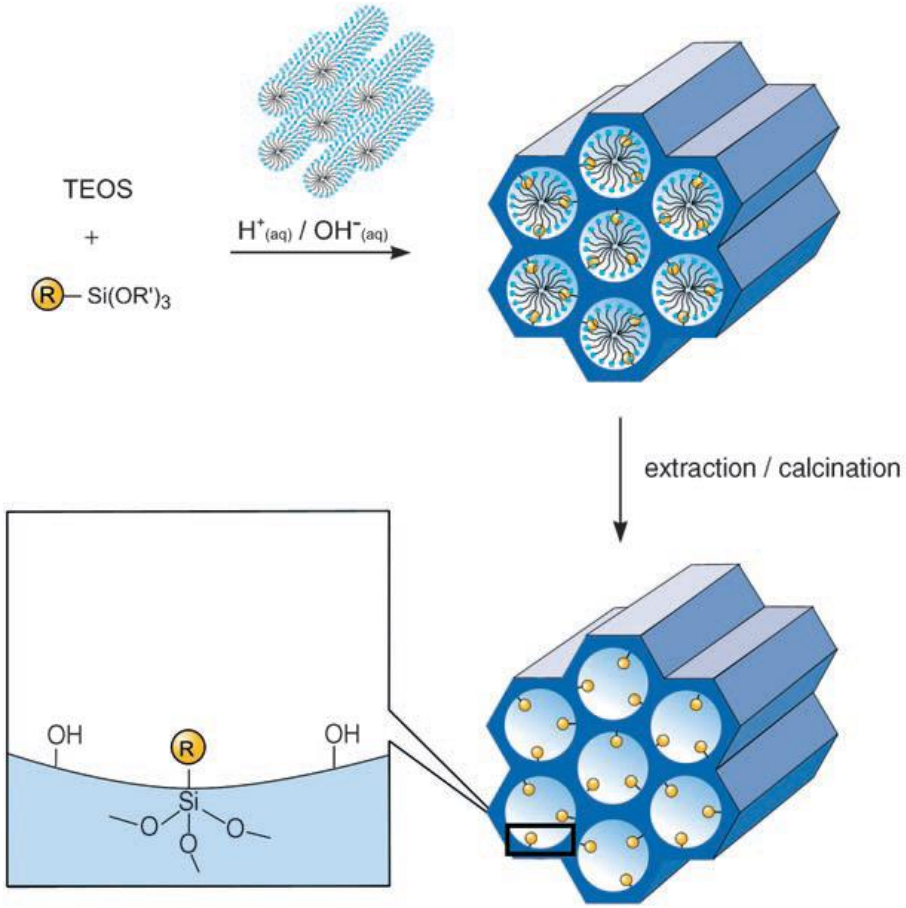

Figure 2-7: Co-condensation method (direct synthesis) for the organic modification of mesoporous silica [75].

2.3.1.4.3 Adsorption by ionic liquids

Ionic liquids (ILs) are a diverse group of salts, which are liquid at room temperature [77, 78], and consist solely of ions (cations and anions) [79] as opposed to an ionic solution. Generally, ILs are composed in the main of large asymmetric cations, where the cationic centre most often involves a positively charged nitrogen and, on the basis of the cations present, ionic liquids can be divided into five groups:

- Five-membered heterocyclic
- Six-membered and benzo-fused heterocyclic
- Ammonium, phosphonium and sulphonium based

- Functionalised imidazolium
- Chiral

Recent attention has focused on the use of ILs as CO_2 capture sorbents because of their virtually unlimited chemical tunability; these chemical properties, amongst a host of other unique properties, such as low/non volatility, non-flammability and high thermal stability, makes ILs a promising alternative to conventional sorbents. Their unique non-volatile nature makes them excellent candidates for gas separation, as the issue of contaminating the gas stream is avoided making them a superior option over conventional solvents like MEA. The solubility of CO_2 in ILs is, therefore, of significance and has been investigated; Anthony *et al.* [79] investigated the solubility of different gases in conventional ILs using gravimetric methods and their results showed CO_2 to have the highest solubility, possessing the strongest interaction with the ILs used, as a result of the large quadrupole moment of CO_2. Blanchard *et al.* [78] studied the solubility of CO_2 in a series of imidazolium-type ILs, and showed that ILs with $[PF_6]^-$ anions had the highest solubilities [80]; Anthony *et al*. [79] also investigated a series of ILs with the same cation but different anions, showing CO_2 solubility to be significantly dependent on the anion choice, and that CO_2 solubility decreased with increasing temperature but increased with pressure [81].

In the last two decades, research has been geared towards the covalent immobilisation of ILs on porous solid materials (silica) as this is regarded as a promising strategy to synthesise advanced sorbents for CO_2 capture. Wang *et al*. [80] immobilised amino acid-functionalised [EMIM]-type ILs into nanoporous polymethylmethacrylate (PMMA) microspheres to produce new sorbents for post-combustion CO_2 removal [26], with the aim of enhancing CO_2 capacity.

Due to the complex nature of individual adsorption capture materials, different mechanisms for CO_2 capture exist, for example, adsorption of CO_2 by zeolites and activated carbon can be most easily represented as;

$$CO_2 + \text{surface} \longleftrightarrow (CO_2)^*(\text{surface})$$

One major disadvantage of physisorbents as CO_2 capture materials is that conventional sorbents, like activated carbon, zeolites or carbon nanotubes, all suffer from low CO_2 capture capacities at low CO_2 partial pressures, and low selectivity,

over competing species in a flue gas stream; thus enhancing the surface chemistry of these physisorbents, by incorporating basic functional groups (e.g. -NH_2) into the porous structure that are capable and available to interact with acidic CO_2, should, in theory increase their CO_2 capture capacities and selectivities. Alkaline carbonates and amines are common sources of basic functional groups used to modify physisorbents to form chemisorbents, and examples include alkali-metal carbonate based sorbents and amine functionalised solid sorbents (amine functionalised carbonaceous materials, functionalised zeolite based sorbents, functionalised polymer based sorbents, functionalised silica supported materials and impregnated alumina supported sorbents). Song and co-workers [81] reported the effects of polyethylenimine (PEI) impregnation on CO_2 capture performance of mesoporous silicas (MCM-41 and SBA-15), with capacities as high as 178 mg CO_2/g adsorbent reported for 50 wt% PEI impregnated MCM-41 (99% CO_2, 348 K) compared to 89.2 mg CO_2/g adsorbent for pristine MCM-41. Similar results were reported for SBA 15 impregnated with PEI of similar loading (50 wt% PEI on SBA 15, 240 mg CO_2/g adsorbent) and pristine SBA 15 (140 mg CO_2/g adsorbent). Despite both materials having the same PEI loading, they exhibit different CO_2 capture performances and capacities [81], hence, it is essential that suitable support materials and/or adsorbents are chosen.

2.4 Comparison of carbon capture technologies

Different studies have compared all three established technologies in terms of efficiency, increased capture cost and cost of electricity generated (Figure 2-8), Kanniche *et al.* [32] concluded that, from an energetics perspective (within economic consideration), PCCC showed the highest efficiency for Natural Gas Combined Cycle (NGCC) systems, pre-combustion carbon capture favoured IGCC, while oxy-combustion carbon capture favoured Pulverised Coal (PC); nevertheless, PCCC application to PC plants seems inevitable even though it has shown lower efficiencies when compared to Oxy-Combustion Carbon Capture (OCCC), because it can be retrofitted to coal-fired power stations that will be built between now and 2020 and retrofittable OCCC technology is currently unavailable. These reasons, some listed below, amongst others have made PCCC the main focus of this study;

- Can be retrofitted to existing plants allowing the continued operation of valuable resources.
- In either new build or retrofit application, PCCC enables the continued deployment of the well-established PC technology familiar to power industries worldwide.
- Extensive research and development into improved sorbents and capture equipment should reduce the energy penalty of PCC capture systems.

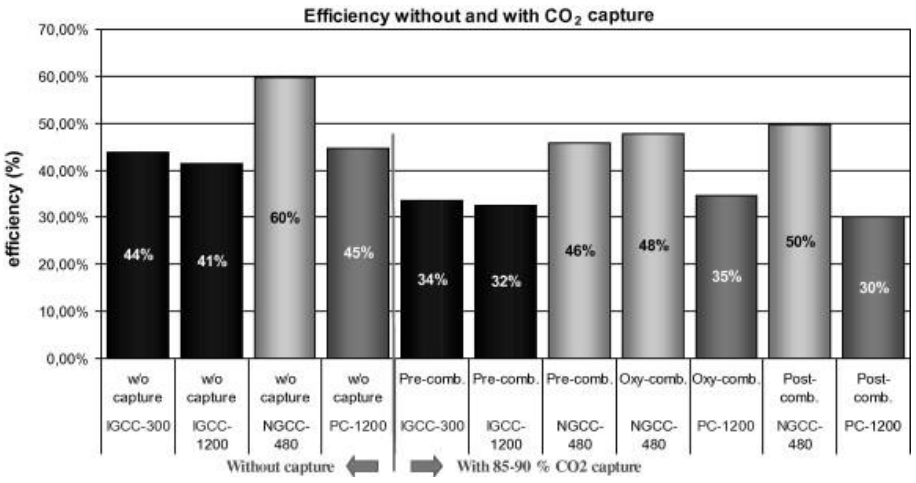

Figure 2-8: Efficiencies of different systems with and without CO_2 capture [41].

As is also the case for pre- and oxy-combustion methods, development of PCCC is required before practical deployment to coal-based power plants for several reasons [82]:

- No large-scale process has been demonstrated to date to show that there is a sustainable route to CO_2 capture, although, the Saskpower boundary dam (Canada) and Mississippi's Power Kemper IGCC are expected to come online sometime in 2014; if these go ahead, useful data could be collected, over time, to show whether CO_2 capture is sustainable on a large scale.
- The required parasitic loads (loses attributed to capture and compression of CO_2) to supply both power and steam to the CO_2 capture plant would reduce the overall power generation capacity of the plant by approximately one-third [26, 38].
- Assuming scale-up is possible; at present it is still not cost-effective [32].

The next section presents important criteria to be considered when selecting suitable support materials.

2.4.1 Criteria for selection of CO_2 adsorbent material

Adsorbent selection is an important aspect of CO_2 capture and it is essential that the selection process is both economical and operational; a summary of the important characteristics is presented to serve as a guide to sorbent selection:

2.4.1.1 Adsorption capacity

The equilibrium adsorption capacity of any sorbent is of major importance as it affects the amount of sorbent required, hence, the vessel size, thus, sorbents with high CO_2 capacities would reduce both quantity or sorbent required and equipment sizes. In a commercial sense, the instantaneous capacity (total adsorption capacity over a specified time interval; for example, adsorption capacity after 30 min) is the preferred measure rather than a sorbents equilibrium capacity, because of the variation in sorption kinetics between sorbents [26]; for a given instantaneous capacity, slow sorption kinetics would lead to reduced capacity while fast sorption kinetics would lead to higher sorption capacity.

2.4.1.2 CO_2 Selectivity

Selectivity is defined as the ratio of CO_2 capacity to that of another component present in a flue gas stream. A typical example is that of a flue gas stream from fossil-fuel fired power plants containing mainly air. A good sorbent material should exhibit high CO_2 selectivities over the N_2 and O_2 present in the flue gas stream, while also exhibiting a high affinity for CO_2 in a flue gas stream containing significant amounts of water vapour [26].

2.4.1.3 Adsorption - desorption kinetics

As previously mentioned, it is essential that selected sorbents show fast sorption kinetics under set conditions. Sorption kinetics control the time taken for one cycle of a fixed-bed adsorption system. For functionalised sorbents, the overall kinetics of CO_2 sorption are influenced by the interaction between CO_2 and the functional groups present, coupled with mass transfer or CO_2 diffusion resistance through the porous structure of the sorbent. Adsorbents can be designed to limit this CO_2 diffusivity resistance, hence, promoting faster kinetics [26].

2.4.1.4 Mechanical strength of sorbent particles

An essential requirement for solid sorbents is that they show micro-structural and morphological stability while maintaining stable CO_2 capacities during repeated

cycles (regeneration). Operating conditions, such as high volumetric flue gas flow rates, high temperatures, grinding, and vibration should not appreciably degrade the sorbent structurally after repeated use. Thus, to keep the process cost effective, sorbents with adequate mechanical strength are essential [26].

2.4.1.5 Chemical stability and/or tolerance to impurities

It is important that sorbents are stable in oxidising environments and resistant to flue gas contaminants, e.g. SO_x and NO_x, to prevent degradation and/or reduced selectivity for CO_2 in a competing environment.

2.4.1.6 Adsorbent regeneration

Although, sorbents can be recyclable, it is important to consider the energy requirements for regeneration, to do this the heat of adsorption is determined. This value should be relatively low, for physisorption processes, the heat of adsorption is typically 5 – 45 $kJmol^{-1}$, while heats of 80 – 400 $kJmol^{-1}$ are expected for chemisorption processes. It is, therefore, essential that cycling of the sorbent should be suited for the choice of regeneration process, bearing in mind the CO_2 adsorption efficiency and the cost implication involved. There are three main routes used for sorbent regeneration:

- **Temperature Swing Adsorption (TSA) –** here sorbent regeneration is achieved by the application of increased temperature at a constant concentration and pressure, provided the sorbent is not degraded in the process. Commercially, increased temperatures are not sufficient for complete regeneration, so a hot purge stream is used to sweep out the desorbed CO_2 [83]. This makes the desorption process energy intensive (vapour cost in heating the column) and mainly suitable for chemisorbents.
- **Pressure Swing Adsorption (PSA) –** this concept was developed by the Esso research and engineering company and published in a 1960 patent [84]. The concept of PSA for gas separation is relatively simple because, after selective adsorption of certain components of a gas mixture onto the sorbents porous structure, performed by contacting the gas stream with sorbents in a packed column at relatively high pressures to produce a rich gas stream of components with lower affinity for the sorbent; desorption is achieved by reducing the partial pressure of the incumbent gas phase to enhance recovery of the desorbed species, for complete regeneration, a purge gas is passed at

the lowest pressure used. Since no heating is involved, PSA is a cheaper and less energy intensive method, making it a preferred industrial option [85].

- **Vacuum Swing Adsorption (VSA) –** this is a modification of the PSA outlined above; VSA was developed to improve regeneration efficiencies and to lower energy consumption [26]. The main difference between VSA and PSA is the use of a partial vacuum in the desorption step, although complete regeneration is dependent on the interactions between the adsorbate and the adsorbent.

2.4.1.7 Adsorbent costs

According to the sensitivity analysis conducted by Tarka *et al.* [86], the cost of an adsorbent should be ~ $10/kg for the process to be economical. The study also suggested that a cost of $5/kg adsorbent is a very good scenario (economically viable), while a cost in excess of $15/kg sorbent is prohibitive [29].

Although the aforementioned characteristics are all desirable for an ideal sorbent, rarely would a single sorbent possess the full range of attributes hence, it is essential that new sorbents be tailored as closely as possible to these needs ensuring efficient and economical capture of CO_2 from flue gas streams [87].

CHAPTER 3

THEORY OF CHARACTERISATION TECHNIQUES

This chapter provides an insight into the background of the experimental techniques used to characterise materials synthesised in this work. Details of the relevant adsorption theories utilised for data analysis are also given. The characterisation techniques serve first as a method of selection, and then as a comparison tool; for example, gravimetric adsorption methods were used to determine the potential of sorbents as CO_2 capture materials, and also to compare adsorption capacities of a range of sorbents.

In order to validate selection of the theoretical techniques used to analyse the data obtained, the techniques are discussed in detail, with equations, models, assumptions and limitations presented and critically appraised. To complement the information presented here, Chapter 4 will discuss the operational methodology of the experimental techniques used. Listed below are details of the range of experimental techniques used for each material type.

Bio-inspired amine silica

- N_2 adsorption (volumetric)
- CO_2 adsorption (gravimetric)
- Fourier transform infrared spectrometry
- Elemental analysis
- Powder X-ray diffraction
- Scanning electron microscopy
- Thermo-gravimetric analysis

Silica in-situ impregnated silica

- N_2 adsorption (volumetric)
- CO_2 adsorption (gravimetric)
- Fourier transform infrared spectrometry
- Elemental analysis
- Scanning electron microscopy
- Thermo-gravimetric analysis

Nitrogen doped RF organic and carbon xerogels

- N_2 adsorption (volumetric)
- CO_2 adsorption (gravimetric including Dubinin-Astakhov analysis)

- Fourier Transform Infrared Spectrometry
- Elemental analysis
- Scanning electron microscopy
- Thermo-gravimetric analysis

Ionic liquid impregnated onto activated carbon

- N_2 adsorption (volumetric)
- CO_2 adsorption (gravimetric)
- Scanning electron microscopy

3 ADSORPTION (SOLID – GAS INTERFACE)

Adsorption is a surface phenomenon that occurs whenever a substance accumulates at an interface or in an interfacial region. It can be simply defined as the enrichment of a material at an interfacial layer and happens within a system containing both an adsorbent (often a solid) and an adsorptive (usually a gas or liquid) [64, 88-90] by van der Waals intermolecular attraction, forming a molecular or atomic film (the adsorbate). There are a few general terminologies associated with adsorption, defined below:

- Adsorbate – a substance in the adsorbed state.
- Adsorptive – a substance that is capable of being adsorbed.
- Adsorbent – a surface (material) on which adsorption occurs.

As stated above, adsorption is, by nature, a surface phenomenon, and is governed by the unique property of discontinuity that occurs at the surface of a bulk material due to bonding deficiencies. The adsorbate molecules within close proximity to the surface try to satisfy this bonding deficiency and are, consequently, attracted to these surface sites, hence, a continuous surface attraction over the interfacial layer causes a monolayer, i.e. a single thickness layer of adsorbate, to form (Figure 3-1) [62, 89-91].

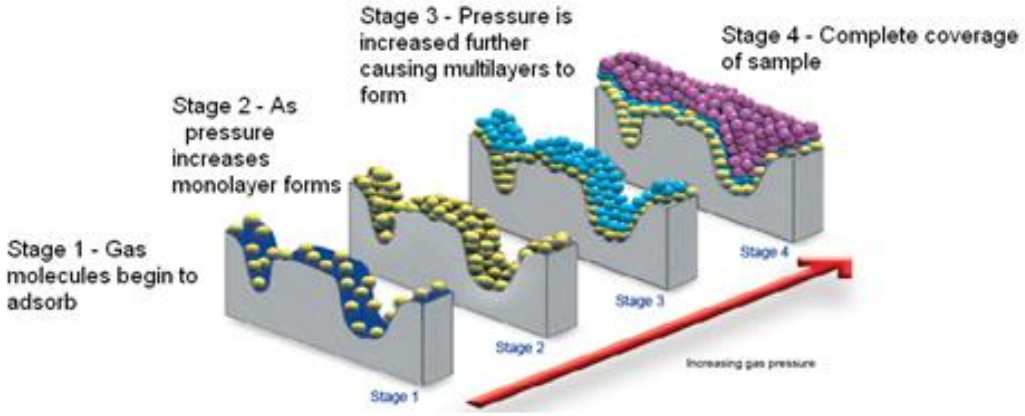

Figure 3-1: Monolayer and multilayer formation during gas adsorption on a solid surface [91].

3.1 Types of adsorption

Adsorption can be split into two broad categories, depending on the interactions involved:

- Chemisorption
- Physisorption

3.1.1 Chemisorption

This involves interactions between the adsorbent and the adsorbate that results in the formation of new chemical bonds. In such processes, the adsorbate is usually adsorbed at specific sites, although this is sometimes not the case when there is surface diffusion [92]. Generally, the heat of adsorption for chemisorption is larger than that for physisorption; typically within the range of 80 – 400 kJ mol^{-1}.

3.1.2 Physisorption

Physisorption is intrinsically weak and is characterised by relatively small heat of adsorption, usually close to the iquefaction of the adsorptive and typically in the range of 5 – 45 kJ mol^{-1}. During physisorption the adsorbate adheres to the solid surface via weak intermolecular forces (e.g. van der Waals interactions) similar to those responsible for the imperfection of real gases and condensation of vapours, which do not result in significant changes to the electronic structures of the species involved [86]. This phenomenon is witnessed at low temperatures due to the weakness of the forces involved. At low pressures, the gas molecules begin to adsorb onto the surface of the adsorbent and, as pressure rises, a monolayer will be formed,

if pressure is increased further it can lead to the formation of a multilayer, which is not in direct contact with the sorbent. Continually increasing pressure causes more multilayers to form [93, 94].

3.1.3 Adsorption isotherms

An adsorption isotherm (Figure 3-2) can be mathematically represented as the amount of condensed material, in this case gas adsorbed on a solid surface, which is dependent on absolute temperature (T), pressure (P) and the interaction potential *E* between the adsorbate and the adsorbent.

When the system achieves equilibrium, at a given temperature and pressure, the weight of gas adsorbed in a unit weight of adsorbent (W) is a function of these variables, defined as:

$$W = f(T, P, E)$$

Equation 19

At constant temperature, this relationship reduces to:

$$W = f(P, E)_T$$

Equation 20

Plotting W against P, at constant T, is referred to as an adsorption isotherm, which can vary in shape depending on the gas used for analysis, the structure of the porous solid and the type of interactions that occur within the system [94].

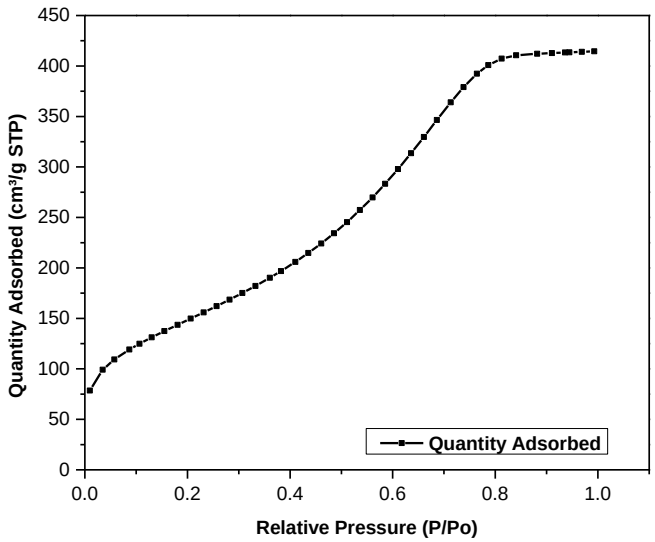

Figure 3-2: An example of an adsorption isotherm.

Adsorption isotherms have long been used to determine the textural properties of sorbents, with the first attempt to interpret adsorption isotherms on gas–solid interfaces reported by Brunauer, Deming, Deming and Teller (BDDT) in 1940 [93]. The resulting BDDT classification formed the basis of the International Union of Pure and Applied Chemistry (IUPAC) classification of adsorption isotherms, which categorised adsorption isotherms into six types, the first five of which (Type I-V) are attributable to BDDT [93] sometimes being referred to simply as the Brunauer classification of 1945, and in 1985 IUPAC proposed the sixth isotherm type [95]; all isotherm shapes are represented below in Figure 3-3.

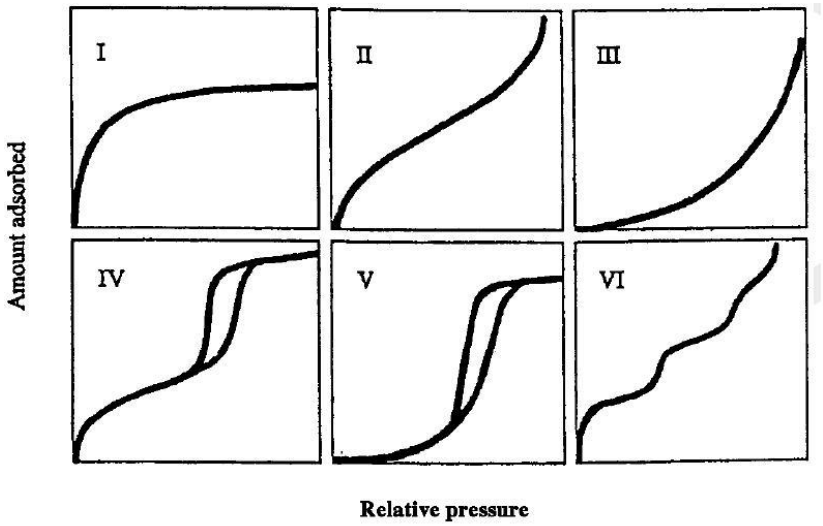

Figure 3-3: The six isotherm Types for gas physisorption, according to the IUPAC classification [95].

Type I isotherm – Typical of adsorbents with predominantly microporous structures, the majority of micropore filling occurs at relative pressures (P/P^o) below 0.1, and the adsorption process is usually complete at a partial pressure of ~0.5. An example of a material that exhibits a Type I isotherm is nitrogen adsorption on microporous carbon at 77 K [89].

Type II isotherm – This isotherm type has a unique shape; it is initially concave to the pressure axis, then almost linear, before finally becoming convex to the pressure axis. Predominantly observed for physical adsorption of gases on non–porous solids; monolayer coverage is followed by multi-layering at higher relative pressures (P/P^o). The adsorbed layer becomes the bulk liquid or solid when the equilibrium pressure

equals the saturated pressure. Examples of materials exhibiting Type II adsorption isotherms include adsorption of nitrogen at 77 K on iron or on silica gel [89].

Type III isotherm – This isotherm type is obtained when the amount of gas initially adsorbed is low but increases without a limit as the relative pressure approaches unity. It is characteristic of weak adsorbate-adsorbent interactions and is usually associated with non-porous and microporous adsorbents. The shape is convex to the P/P^o axis over the complete range of relative pressures. Although, Type III isotherms are uncommon, adsorption of bromine on silica gel, at 352 K, demonstrates a Type III isotherm [89, 96].

Type IV isotherm – A variation of the Type II isotherm, but with limited multi-layer formation corresponding to complete filling of the capillaries, the process ends as the relative pressure tends to unity. It also includes a hysteresis loop, which is often related to the presence of mesoporosity [89, 97].

Type V isotherm – This isotherm is convex to the pressure axis for the entirety of the range, and is usually characteristic of weak adsorbate-adsorbent interactions, in the same way that the Type III isotherm is formed. Type V isotherms are suggestive of microporous or mesoporous solids [89].

Type VI isotherm – Initially introduced as a hypothetical isotherm, Type VI isotherms are relatively rare and associated with layer by layer adsorption on highly homogeneous, non-porous surfaces [89].

3.2 Hysteresis loops

The phenomenon of hysteresis occurs in the multilayer range (usually at $P/P^o > 0.42$) of physisorption isotherms, and is generally associated with capillary condensation. The presence of capillary condensation and the resulting hysteresis loop can make analysing a material's pore size distribution rather complicated but, on the other hand, correct interpretation, can provide significant information on the textural (pore structure and network) properties of the material. De Boer *et al.* [97, 98] reported that most mesoporous adsorbents give unique hysteresis loops [99],and an empirical classification was given by IUPAC [95] for the main loops, as presented in Figure 3-4.

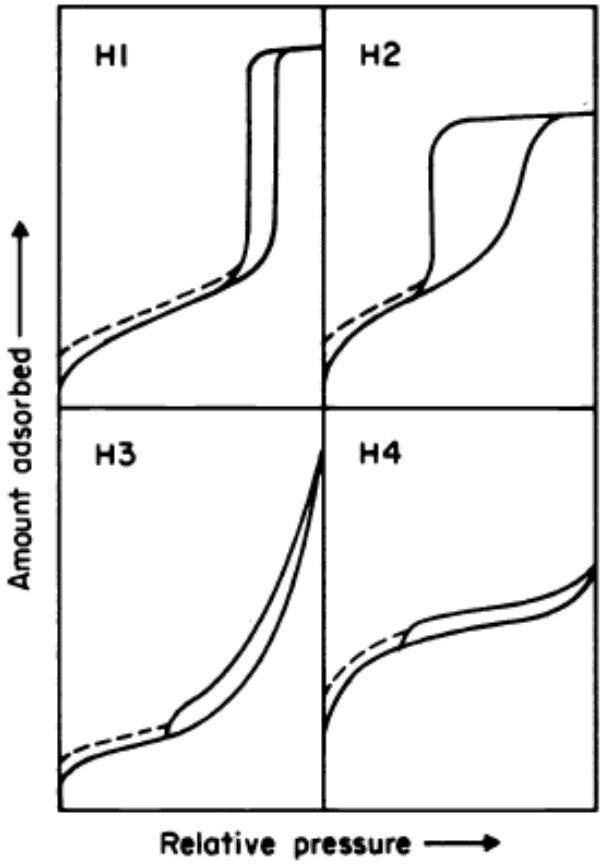

Figure 3-4: The IUPAC classification system for hysteresis loops [95].

Types H1, H2 and H3 were those originally included in the classification proposed by De Boer *et al*. [97], while H4 was included in the 1985 IUPAC classification developed by Sing *et al*. [95]. H1 is a fairly narrow loop with very steep, nearly parallel, adsorption and desorption branches. In contrast, H2 loops are broad, with long, almost flat, plateaus and steep desorption branches. H3 and H4, at high partial pressures, do not terminate at the plateau, causing difficulty in establishing the limiting desorption boundary curve [100-103].

Certain hysteresis loops are associated with well-defined pore structures, for example H1 loops are ascribed to adsorbents with a narrow distribution of uniform pores, and an example is SBA-15, which consists of open ended tubular pores. H2 loops are associated with complex pore structures that tend to be made up of interconnected pores of varying sizes and shapes; an example is inorganic oxides gels. H3 loops are normally observed for aggregates of plate-like particles, while Type H4 loops are associated with activated carbons and other adsorbents that have slit pores within the microporous range [103, 104].

3.3 Porosity of solid adsorbents

The porosity of a solid can be defined as the total volume of pores in 1 g of adsorbent, it can also be represented in terms of percentage pore volume in the total volume of 1 g of adsorbent, as shown in Equation 24 [89]:

$$Porosity = \frac{V\ pores}{V\ adsorbents}$$

Equation 21

3.3.1 Qualitative description of a porous solid

Solid materials that contain cavities, channels, or interstices can be regarded as being porous, although it is important to choose the exact terminology in order to prevent ambiguity, hence, the classification of porous materials is made with respect to the types of pores within the material as well as the materials form. Pores can be classified into four categories as follows [92]:

Closed pores – pores that are totally secluded from their neighbouring pores; they usually affect the macroscopic properties of the sorbent such as thermal conductivity and bulk density.

Open pores – connected to the external surface of the material, there are two sub-categories of open pore, through (or transport) pore and blind pores.

Through open pores: - open at both ends, they begin at one location on the materials surface, extending into the particle and re-emerging on the surface, usually at a different location.

Blind open pores: - open only at one end, they are also called dead-end or saccate pores.

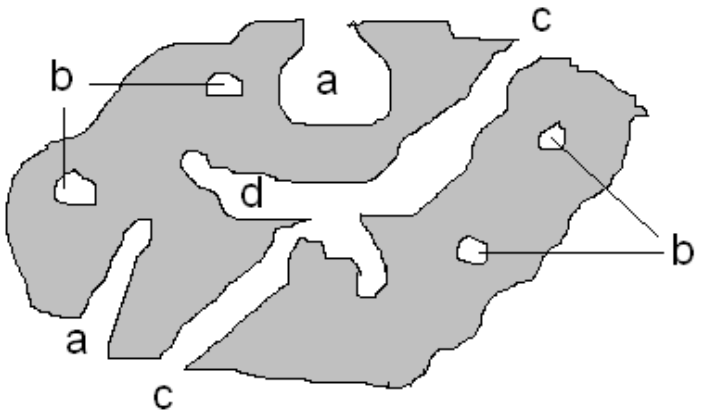

Figure 3-5: Schematic cross-section of a porous solid material: (a) open pores (ink-bottle) (b) closed pores, (c) transport pores (cylindrical) and (a, d) blind pores [92].

Pores can also be classified according to their topology; common pore shapes include cylindrical, ink-bottle, funnel and slit [89, 103, 105].

3.4 Adsorption theory

To determine the pore size, and specific surface area, by gas adsorption, the Langmuir or Brunauer, Emmett and Teller (BET) methods can be used. It is essential that the pores must be accessible to the adsorptive molecules used for analysis, generally N_2; thus it is important to classify these pores by size. According to the IUPAC classification of pore sizing [88]:

- Micropores have pore widths less than 2 nm.
    - Ultramicropores below 0.7 nm
    - Supermicropores 0.7 – 2 nm
- Mesopores have pore widths between 2 and 50 nm.
- Macropores have pore widths larger than 50 nm.

3.5 Langmuir adsorption isotherm model

The Langmuir equation evaluates the relationship between the pressure of a gas, in equilibrium with a flat surface, and the volume of gas adsorbed on that surface. It was first reported for surface area determination based on the following assumptions:

- The surface of a solid consists of a collection of adsorption sites and the ability of a molecule to adsorb at a given site is independent of neighbouring sites.
- All sites on the surface are equivalent and each adsorption site can adsorb only one molecule.
- Adsorption cannot proceed beyond monolayer coverage, i.e. there are no adsorbate–adsorbate interactions.

From this approach, Langmuir equated the number of gas molecules evaporating from the surface as equal to the number of molecules condensing on the surface, hence, the following adsorption equation was derived [88, 89, 104-106]:

$$P = V\left(\frac{1}{V_m K} + \frac{P}{V_m}\right)$$

Equation 22

Where P = partial pressure (mmHg)

K = equilibrium constant of adsorption (L mg^{-1})

V = volume of adsorbed gas at pressure P (mol)

V_m = amount of gas adsorbed on material that forms the monolayer (mol)

The Langmuir equation can be used to calculate the surface area of microporous solids, which exhibit Type I isotherms, using the equation as derived below.

$$\theta = \frac{V}{V_m}$$

Equation 23

Where all terms are defined as above and θ is the fraction of sites covered with adsorbed particles.

If V_m is the amount of gas adsorbed by the material forming the monolayer (i.e. θ = 1) then the fraction of sites covered at equilibrium, θ is equal to V/V_m, as V = volume of adsorbate adsorbed at equilibrium. Thus, Equation 23 can be expressed linearly, by first substituting the value of θ into the Langmuir equation:

$$\theta = \frac{KP}{1 + KP} = \frac{V}{V_m}$$

Equation 24

$$V_m KP = V + VKP$$

Equation 25

Equation 25 is rearranged to a linear form and presented in terms of pressure:

$$P = \frac{VKP}{KV_m} + \frac{V}{KV_m}$$

Equation 26

which can be rewritten as:

$$P = V\left(\frac{1}{V_m K} + \frac{P}{V_m}\right)$$

Equation 27

or

$$\frac{P}{V} = \frac{1}{KV_m} + \frac{P}{V_m}$$

Equation 28

A plot of $\frac{P}{V}$ against P will have a gradient of $\frac{1}{V_m}$ and the specific surface area can be calculated as:

$$S = \frac{V_m A_m L}{m}$$

Equation 29

Where S = specific surface area ($m^2 g^{-1}$)

A_m = average area occupied by one molecule during monolayer coverage (m^2 $molecule^{-1}$)

L = Avogadro's constant (6.023×10^{23} molecules mol^{-1})

m = mass (g)

3.5.1 Limitations of Langmuir adsorption theory

- Langmuir proposed that the adsorbate behaves ideally in the vapour phase; this condition can only be satisfied at low pressures, hence, limiting its application.
- It is also assumed that adsorption is complete at the monolayer; although, monolayer formation is possible under low pressure conditions, at higher pressures the assumption breaks down as adsorbed molecules attract more adsorptive molecules towards themselves. The BET theory proposed by Brunauer, Emmett and Teller [94] becomes valid under these conditions, as it provides a more realistic model for multilayer adsorption processes (see section 3.6).
- The surface of the solid adsorbent is also assumed to be homogeneous, with all sites on the solid surface equal in size and shape, with equal affinity for adsorbate molecules, this has been debunked as it is widely acknowledged that solid surfaces are, in general, heterogeneous [94].
- Lastly, the Langmuir equation assumes that molecules do not interact with each other. This is again invalid as weak forces of attraction exist even between molecules of the same species (e.g. London dispersion forces) [98].

3.6 Brunauer-Emmett-Teller (BET) adsorption isotherm model

The specific surface area of porous materials can be determined using the theory proposed, in 1938, by Brunauer, Emmett and Teller (BET) [94], before which, the Langmuir theory was used, as previously described. In the theory proposed, the authors tried to generalise the concept of localised monolayer formation to include multilayer adsorption using the basis that the assumptions developed in the Langmuir adsorption model could be applied to each separate adsorption layer. This allowed the following additional assumptions to be made:

- Each monolayer formed acts as a series of base sites for the adsorption of molecules for a subsequent second layer, which, in turn, acts as a base for a third layer and so on; hence multilayer formation is limitless and the Langmuir theory can be applied to each layer (Figure 3-1).

- The forces of attraction between adsorbed neighbouring molecules are not taken into consideration.

Based on these assumptions, the BET equation was derived as:

$$\frac{P}{V\left(P^o - P\right)} = \frac{1}{V_m C} + \frac{\left(C-1\right)P}{P^o V_m C}$$

Equation 30

Where P = equilibrium pressure (mmHg)

V = amount adsorbed at P (mol)

V_m = amount of adsorbate at monolayer formation (mol)

C = BET Constant (dimensionless quantity)

P^o = saturation vapour pressure (mmHg)

P/P^o = relative pressure

Equation 30 above can be linearized and a plot of $\frac{1}{V\left(\left(\frac{P^o}{P}\right)-1\right)}$ against $\frac{P}{P^o}$ gives a linear isotherm with slope (Sl) and intercept (i),

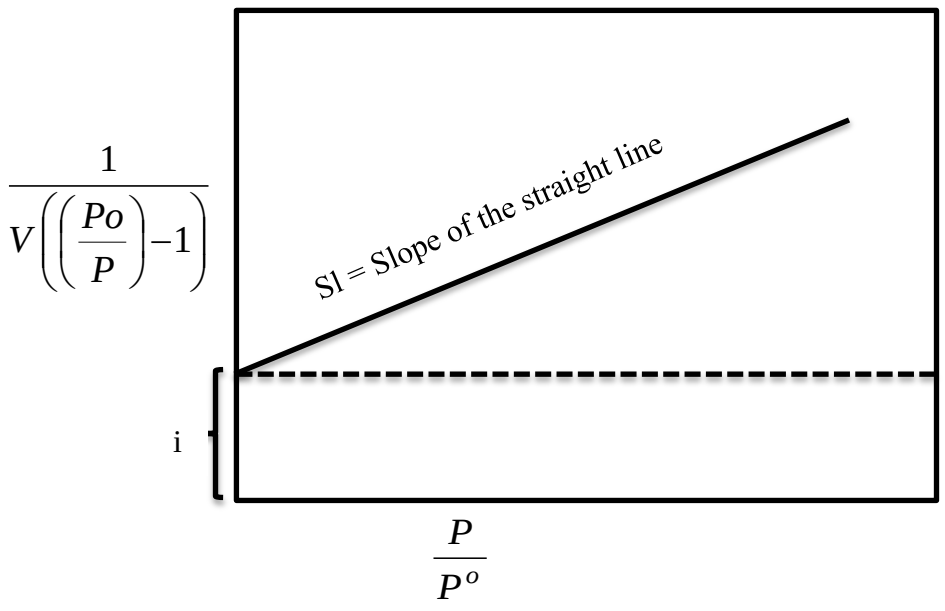

Figure 3-6: BET linearisation of isotherm data for the determination of surface area.

The slope can be represented by:

$$Sl = \frac{(C-1)}{V_m C}$$

Equation 31

and the intercept as:

$$i = \frac{1}{V_m C}$$

Equation 32

From Equation 31and Equation 32, the amount of adsorbate condensed at monolayer formation can be determined as:

$$V_m = \frac{1}{S+i}$$

Equation 33

The surface area is subsequently determined as presented in Equation 29.

3.6.1 Limitations of BET adsorption theory

Although BET theory has extensive uses, it suffers from the following limitations:

- It assumes, as the Langmuir model does, that all adsorption sites are energetically identical but, in reality, the surfaces of real solids are generally heterogeneous [107, 108].
- In deriving the BET equation, Brunauer, Emmett and Teller [94] postulated that the number of adsorbed molecular layers become infinite as the saturated vapour pressure is approached when, in fact, there have been cases were the molecular layers adsorbed are finite even at the saturated vapour pressure.
- BET theory assumes that there are vertical forces between the adsorbent and the adsorbate molecules but does not acknowledge the horizontal interactions between adsorbed molecules [88, 89].

BET analysis represents a standard technique used to evaluate the specific surface area of adsorbents, its results characterise the porous structure of adsorbents into two

main categories, microporous and/or mesoporous structures. Alternative methods can be used to evaluate the microporous and/or mesoporous structures of porous adsorbents, as discussed below.

3.7 Analysis of microporous character of materials

3.7.1 t-plot method

This method, proposed by Lippins and De Boer [106], is used to compare a microporous adsorbent with a standard Type II isotherm, the observed differences allowing information about the porous structure to be elucidated. Multi-layer formation is modelled mathematically to calculate a layer thickness, t, as a function of increasing relative pressure (P/P^o). The resulting t-curve is compared with the experimental isotherm in the form of a t-plot, allowing the micropore volume, surface area and, in principle, the average pore size to be determined. The model is valid only in a narrow relative pressure range, for adsorption after monolayer formation, typically pressures are taken between $P/P^o = 0.2$ to 0.5 or layer thicknesses between 0.35 to 0.5 nm. As this relative pressure range lies between the monolayer and capillary condensation, the t-plot method is not suitable for highly microporous materials, hence, micropores are not included as they are filled during monolayer formation at lower relative pressures outside the range indicated above. Under favourable conditions, a t-plot can provide a means of assessing the micropore volume and the external area.

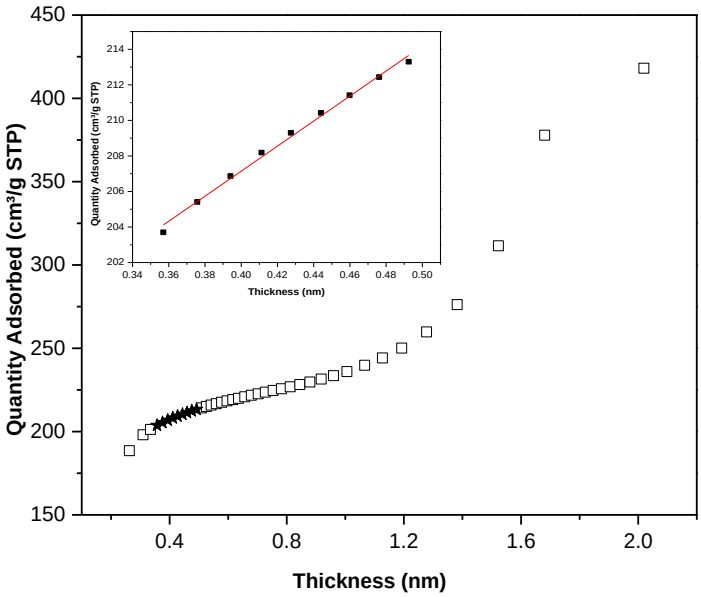

Figure 3-7: Example of a t- plot.

The relative pressure range used for analysis is adjusted, for each data set modelled by this theory, until the best linear plot is obtained. The slope of the t-plot gives the external surface area. If the intercept goes through the origin, the total surface area can be determined as follows:

Let V be the monolayer volume, the number (n) of layers is given as Va/V and n is also equal to t/ρ, where t is the statistical film thickness of a flat surface corresponding to the amount of adsorbate adsorbed (V_a), and ρ is the thickness of one layer (ρ = 0.35 nm). Hence:

$$V = \rho\left(\frac{V_a}{t}\right)$$

Equation 34

The slope, Va/t, as earlier stated, coupled with knowledge of the monolayer coverage, allows the surface area to be calculated:

$$S_{Total} = V \times A_m \times L$$

Equation 35

With L = Avogadro's number ($6.02214129 \times 10^{23}$ mol^{-1})

A_m = adsorbate cross sectional area (16.2 $Å^2$ for N_2)

V = monolayer capacity

using $S_{ext} = 1.5468 \times \frac{V_a}{t}$, gives the external surface area, where Va/*t* is the slope of the linear range taken between relative pressures P/P^o, of ~0.35 to 0.5.

3.7.2 Dubinin-Astakhov (DA) analysis

In 1947, Dubinin proposed a modification to Polanyi's potential theory of 1932 [108-110] for the analysis of adsorption data to characterise microporous materials. Dubinin showed that the micropore volume of a material plays a more significant role than its surface area in microporosity characterisation. A major problem Dubinin faced was evaluation of the parameters that characterise the microporous structure. Dubinin and Radushkevich (DR) [111] proposed an equation to describe the physical adsorption of gases on microporous solids, which had some success in describing the pore size distribution of carbonaceous solids with a low degree of burn-off during activation, although it had limited use for materials with a relatively high burn off, which results in materials with more heterogeneous pore size distributions. Based on this limitation Dubinin and Astakhov modified the DR equation proposing a form that allows for surface heterogeneity to be considered [109, 111, 112]:

$$W = W_o \exp\left[-\left(\frac{A}{\beta E_o}\right)^n\right]$$

Equation 36

Where

n – describes the surface heterogeneity

A – is the adsorption potential and ΔG is the change in Gibbs free energy given by Equation 37below

W – is the amount adsorbed in the micropores when the adsorption potential is A

W_o – is the limiting volume of adsorption or the maximum micropore adsorption capacity, usually when A = 0

β – is the similarity coefficient of the characteristic curve

E_o – is the characteristic energy of adsorption of a reference vapour, usually benzene

The adsorption potential is given as,

$$A = -\Delta G = RT \ln\left(\frac{P^o}{P}\right)$$

Equation 37

At n = 2, the DA equation reduces to the DR equation, hence, rewriting the DA equation in terms of the vapour characteristic energy, E_o:

Substituting Equation 37 into Equation 36, gives;

$$W = W_o \exp\left[-\left(\frac{RT \ln\left(\frac{P^o}{P}\right)}{\beta E_o}\right)^n\right]$$

Equation 38

The heterogeneity parameter (n) can be used as a macroscopic measurement for the sharpness of the Micropore Size Distribution (MSD), for solids with a narrow MSD, n = 3 effectively describes the MSD data. For n < 3, the DA equation describes such systems as having a broad MSD. To determine the microporous parameters of a porous solid, Equation 38 is linearized as:

$$\ln W = \ln W_o - \left(\frac{RT}{\beta E_o}\right)^n \left(\ln\left[\frac{P^o}{P}\right]\right)^n$$

Equation 39

Plotting $\left(\ln\left[\frac{P^o}{P}\right]\right)^n$ vs. $\ln W$ gives a straight line with the intercept representing the limiting micropore capacity, W_o. If the density (ρ) of the adsorbed phase is known, the micropore volume can be calculated as:

$$\text{Intercept} = \left[Log_{10} Wo\right]$$

Equation 40

Once W_o has been determined, the limiting micropore volume (V_{micro}) can be estimated:

$V_{micro} = W_o \times$ *density correction factor*

Equation 41

The density correction factor for CO_2 at 273 K is 1.5876×10^{-3} [113].The characteristic energy of adsorption, E_o can be determined from $\left(\frac{RT}{\beta E_o}\right)^n$ using the following expression;

$$E_o = RT\left(\frac{2.303^{n-1}}{D}\right)^{\frac{1}{n}}$$

Equation 42

This is done by selecting the value of n that is in best accordance of the equation with the experimental adsorption data. Analysis of mesoporous character of materials

3.7.3 Barrett-Joyner-Halenda (BJH) theory

The Barrett-Joyner-Halenda (BJH) [114] theory is a common method used to analyse the Pore Size Distribution (PSD) and total pore volume of mesoporous materials that exhibit capillary condensation. It is based on a modified Kelvin equation, which predicts the pressure at which capillary condensation occurs, and applies to only the mesopores and small macropore ranges. It assumes a hemispherical liquid-vapour meniscus and a well-defined surface tension:

$$\ln\frac{P}{P_0} = \frac{-2\lambda V_L}{rRT}\cos\theta$$

Equation 43

Where

γ = surface tension of the adsorbate (assumed to be that of the bulk material (dyne cm^{-1})

V_L = molar volume of adsorbate ($m^3\ mol^{-1}$)

r = pore radius (nm) of the largest cylindrical capillary filled with condensate (if cylindrical pores are assumed)

R = universal gas constant (8.314 $J\ K^{-1}\ mol^{-1}$)

T = temperature (K)

θ = contact angle (assumed to be = 0) (degrees)

P/P^o = the relative pressure is the ratio of the actual pressure P to the vapour pressure of the bulk adsorbate P^o

The negative sign indicates that P is less than P^o when the contact angle is smaller than 90^o. To quantitatively use the Kelvin equation, it is assumed that is applicable over the complete mesopore range, the meniscus curvature is controlled by the pore size and shape, and the contact angle. At θ = 0, the pores are rigid and of well-defined shape, the distribution is confined to the mesopore range; filling (or emptying) of each pore does not depend on its location within the pore network and adsorption on the pore walls proceeds in exactly the same way as on the corresponding open surface.

With the contact angle, θ = 0. Equation 43 then simplifies to:

$$In\frac{P}{P_0}=\frac{-2\lambda V_L}{rRT}$$

Equation 44

If the total pore volume is assumed to be the volume of gas adsorbed at saturation, two assumptions can be made:

- Pores should be open ended and cylindrical
- A porous network should be absent

From Equation 44, r, for a hemispherical meniscus, will be equal to r_k , the Kelvin radius [115]:

$$r_k(A) = \frac{4.15}{\log(P/P_o)}$$

Equation 45

The pore size of a material can then be determined using:

$$r_p = r_k + t$$

Equation 46

Where r_p = actual radius of pore (nm)

r_k = Kelvin radius of pore (nm)

t = thickness of the physically adsorbed layer at the corresponding value of P/P^o [114, 116]

Hence, r_k indicates the radius into which condensation occurs at the corresponding relative pressure. The Kelvin radius is not the actual pore radius, adsorption commences on the pore walls prior to condensation, thus the adsorbed film remains on the pore walls during desorption of the fluid from the central core. Equation 46 represents this fact; here the thickness of the adsorbed film when condensation or evaporation occurs is given as r_p.

The total pore volume is the volume at a specific relative pressure after the condensation step, usually at $P/P^o = 0.95$. The amount of adsorbed gas reflects the adsorption capacity and the total specific pore volume can be calculated by converting the amount adsorbed into a liquid volume, assuming that the density of the adsorbate is equal to the bulk liquid density at saturation. Then the pore volume, V (cm^3) is given by:

$$V = \frac{M_a}{\rho}$$

Equation 47

Where M_a = adsorbed amount (g)

ρ = liquid density at saturation (g cm^{-3})

Assuming that no alternative surface exists, other than the inner walls of the pores and that the pores are cylindrical, the total pore volume can be calculated from the expression used to determine the average pore radius (r_{ap}):

$$V_p = \frac{S_{BET} r_{ap}}{2}$$

Equation 48

Where;

Vp = Total pore volume ($cm^3\ g^{-1}$)

S_{BET} = BET specific surface area ($m^2\ g^{-1}$)

r_{ap} = average pore radius (nm)

3.8 Characterisation of material porous structure

3.8.1 Gravimetric method

The solubility of gases on either solids or liquids can be determined by measuring the change in mass upon adsorption of the adsorbate on the adsorbent. Gravimetric methods are better suited to measuring adsorption of gases on solids than absorption involving liquids, although there are a few exceptions of liquids with which this technique can be utilised; primarily, the limitation is losses due to evaporation in liquids, which cannot be accurately accounted for during absorption measurements. One such exception is ionic liquids, where absorption is achievable because they are non-volatile so mass changes are attributed to those of the dissolved gases.

To precisely measure the magnitude and dynamics of gas and vapour adsorption on the materials studied in this work, a Hiden Isochema Ltd. Intelligent Gravimetric Analyser (IGA) was used; it utilises gravimetric techniques to accurately measure adsorption parameters. The IGA design integrates precise computer-control and measurement of weight change, pressure, temperature, gas flow and composition [113]. The incorporated computerised system can automatically and reproducibly measure adsorption/desorption isotherms as well as investigate thermal desorption in diverse operating conditions. The unique IGA method exploits the relaxation behaviour of the interaction process after pressure/gas composition/temperature changes to simultaneously evaluate kinetic parameters and the asymptotic uptake [117].

The operational procedure of the IGA system starts with an accurate microbalance system, which has a sample container hung against a counterbalance to monitor the sample weight change veries time at specific temperatures and pressures. The weight change is measured as a function of time and when the approach to equilibrium is established at the set pressure point, the pressure is increased to the next set pressure value and the subsequent uptake is measured until equilibrium is again established. It is important to note that in gravimetric sorption, the size of the sample determines the accuracy of the capacity measurement. In some cases accuracy can be improved by increasing the sample size. The IGA instrument used in this work has a microbalance calibrated for maximum capacity of 200 mg, with a resolution of around ± 0.1 μg, sufficient to perform accurate measurements on porous samples studied. However, if necessary the IGA microbalance can be easily set to run larger samples, by changing the counterweight configuration.

3.8.2 Fourier Transform Infrared Spectroscopy (FTIR)

FTIR is a useful technique for the determination of different organic or inorganic functional groups within a material [115, 118]. The majority of organic samples absorb IR radiation in the mid infrared region, which falls between 4000 and 400 cm^{-1}; for reference the IR region consists of wavelengths between 14000 and 20 cm^{-1}. Molecules absorb radiation when a bond in the molecule vibrates at the same frequency as the incident radiation energy. Once absorbed, the excess energy causes vibrations at higher amplitudes. The frequency absorbed depends on the mass of the atoms in the bond, the geometry of the molecule, as well as bond strength, in addition to other factors, such as the fact that a change in dipole moment during vibration must occur before a molecule can absorb IR radiation [118-120].

There are some common bond vibrations sensitive to IR radiation, including stretching and bending vibrations. Stretching involves a change in the bond length resulting in a change in the interatomic distance, while bending involves a change in the bond angle. Bending vibrations can also result from a change in the position of the atoms with respect to the rest of the molecule. For example, a group of three or more atoms, of which at least two are the same, have two stretching modes which are, symmetric and asymmetric stretching vibrations. For the bending modes, different types of bending vibration exist, such as, scissoring/rocking in-plane vibrations, and wagging/twisting out of plane vibrations. These different vibrations

give a good indication of the chemical structure of the molecule and form the basis for the qualitative structural identification of materials by IR spectroscopy. Unknown materials can also be identified using this technique; in this work the recorded spectra of the unknown materials are compared with absorption frequencies of known functional groups [113, 120, 121].

The absorbance spectrum of a sample can be calculated using the following equation:

$$A = \log\left(\frac{Io}{I}\right)$$

Equation 49

Where A is the Absorbance

I_o is the intensity of the background spectrum

I is the intensity of the sample spectrum

Absorbance, A is related to the concentration of molecules in a material using Beer's Law equation presented in Equation 50:

$$A = \varepsilon Ic$$

Equation 50

Where, $\mathcal{E}$ = absorptivity

I = Path-length

c = Concentration.

The area or height of an absorption peak is proportional to the concentration; instead of absorbance, percentage transmittance (%T) can be used to determine the IR spectrum of a given material.

$$\%T = 100\left(\frac{Io}{I}\right)$$

Equation 51

Where, $\%T$ = Percentage transmittance

I_o = Intensity of the background spectrum

I = Intensity of the sample spectrum

A major advantage of this technique is that it can be used for a wide variety of materials, making it an important tool for materials characterisation [119, 122].

3.8.3 Elemental Analysis (CHN/O)

All organic materials contain carbon (C) and hydrogen (H) and according to the Association of Official Analytical Chemists (AOAC) methods of analysis report published in 1990 [120], the Pregl gravimetric method was the standard

recommended for the determination of carbon and hydrogen contents in materials. Although the Pregl apparatus is no longer manufactured, its method is still used in a few laboratories, while the majority have been replaced by the CHNS/O analyser, the modern equipment designed for the determination of elemental constituents [113, 120]. Elemental analysis is the qualitative detection and quantitative determination of chemical elements present in a material. Elements present are usually in the form of atoms/ions with the most common species being carbon, nitrogen, and hydrogen. It is a fast and essential technique used to prove the elemental composition of an organic material in the form of weight percentage (wt%) composition.

Elemental analysis works on the principle that all atoms prefer to be in their oxidative state, thus, combusting these materials at elevated temperature in an oxidising atmosphere (1273 K) encourages this to happen. During this process, the carbon present is converted into CO_2, the nitrogen into nitrogen oxides and the hydrogen to water. Any subsequent elements present would be converted to their respective combustion products:

$$Sample \xrightarrow{O_2\ 1273K} CO_2 + NO_x + H_2O$$

Equation 52

After combustion, the oxidised products are carried, via an inert gas stream (helium), into the combustion chamber. Nitrogen oxides formed are reduced to elemental nitrogen (N_2) in the presence of elemental copper (Cu) (~873 K), residual oxygen is also removed at this stage.

$$NO_x \xrightarrow{Cu\,(873K)} N_2$$

Equation 53

A Perkin-Elmer elemental analyser model 2400 was used to carry out the CHNS/O analysis and the gases from the combustion chamber (CO_2, H_2O and N_2) were separated via a high sensitivity chromatographic technique measured in a thermal conductivity cell. The corresponding wt% values were calculated with reference to the original sample weight [113].

3.8.4 Powder X-Ray Diffraction (PXRD)

X-Ray Diffraction (XRD) involves monitoring the diffraction of X-rays upon interaction with a solid medium (material being analysed). XRD is a non-destructive

[113] crystallographic technique used to identify the exact crystal structure of a pure single crystal material and quantifying (whether crystalline, amorphous or semi-crystalline) the phases present in solids and powders. When X-rays are beamed onto a regular crystalline material, the portion of the diffracted rays form a pattern, which can be used to determine the crystal phases present, this is done by comparing the pattern to those of internationally recognized standards managed by the International Centre for Diffraction Data (ICDD) [119, 121].

XRD is a common technique used in the characterisation of organic and inorganic materials. It works on the principle that the materials to be characterised have a space lattice with ordered three dimensional distribution of atoms forming a series of parallel planes, separated by a distance, *d*, which varies with material. This crystal lattice spacing, can be determined using Bragg's law [120, 122], presented in Equation 54;

$$n\lambda = 2d\sin\theta$$

Equation 54

The X-ray beam, of wavelength λ, is irradiated onto a crystalline material of spacing *d*, at an angle θ; diffraction only occurs when the distance travelled by the reflected rays differ by an integer *n*. By varying the incidence angle θ, only the X-rays at particular wavelengths would be diffracted by the crystal and, on plotting the angular position against the intensities, a diffraction pattern is produced, which is particular to the individual material.

The X-ray instrumentation consists of three basic elements, the X-ray tube, the sample holder and the X-ray detector. X-rays are generated when the target material is bombarded with electrons, this process is usually accelerated by applying a voltage and, when the energy of the electrons is sufficient enough to dislodge the inner electrons from the materials, an X-ray spectrum is produced. The detector records the X-ray signal and coverts it into a count rate that can be interpreted by the detector. A typical XRD pattern is produced by plotting the diffracted intensity against 2θ (typically from 5 to 90^{o}) and the resulting peaks are assigned labels to indicate the crystal plane spacing [120, 122, 123].

3.8.5 Scanning Electron Microscopy (SEM)

Scanning Electron Microscopy (SEM) is designed to provide high-resolution, high-magnification images of a sample. SEM is a commonly used technique for characterising organic or inorganic nano-materials to obtain an electron image with nano-scale resolution allowing the morphological and topographical characteristics of a material to be analysed. SEM resolution can be a few nanometres and its magnification can be adjusted from 10 to about 300,000 times [113].

SEM analysis is carried out by scanning an electron probe (primary electron) over the surface of a material while monitoring the secondary electrons that are being emitted (when the primary electron hits a material, it shares a fraction of its energy with the materials electrons and this results in the emission of secondary electrons). These emitted electrons are collected by a detector (Everhart-Thornley detector), then converted to a voltage, which is amplified to form images that are displayed on a Cathode Ray Tube (CRT) screen. By synchronising the CRT scan to that of the primary electron scan, the CRT display represents the morphology of the materials scanned surface. The CRT image magnification is the ratio of the image display size to the sample scanned by the primary electron beam. It is important that materials to be analysed must be either conductive or covered with a thin coating of metal (gold) to avoid electric charging [113, 119, 120].

3.8.6 Thermo-Gravimetric Analysis (TGA or TG)

TGA is one of the most widely used methods for thermal analysis of materials. It measures changes in the mass of a material as a function of temperature, or time at a controlled temperature and environment. This mass change occurs as a result of evaporation of the physisorbed (surface water) or chemically bound water (molecular water), pyrolysis of the organic contents and the decomposition of the material at elevated temperatures. TG measurements can be carried out using either air or in an inert atmosphere, often argon or nitrogen, depending on how the material decomposes in a specific atmosphere; an example is that mass loss increases more in oxidative environments owing to the oxidation of metals to oxides and the carbonation of oxides. Hence, for thermal analysis to be investigated, an inert environment is recommended. There are two broad generalisations of TG instruments used for analysis; they include the vertical and horizontal balance type

TG analysers. The presence or absence of a reference pan is used to differentiate between both TG types. The vertical analyser type lacks this feature and is not reliable for the determination of Differential Scanning Calorimetry (DSC) or Differential Thermal Analysis (DTA) measurements while the horizontal balance type can accurately carry out DSC or DTA analyses.

For DTA measurements, the temperature change is measured between the material and the reference pan, and for DSC; this involves the heat flow into the material when compared with the reference pan. DSC monitors the energy changes, either absorbed or released during reactions (chemical) that occur when a sample is heated, cooled or held isothermally. These energy changes allow the identification and quantification of transitions (chemical changes) that occur in the material as well as the temperatures at which these changes occur. This information is especially useful for characterising the melting process, glass transition temperatures and other characteristics of the materials [124, 125].

CHAPTER 4

EXPERIMENTAL METHODS

4 METHODOLOGY

This chapter is divided into two sections: the first describes the methodologies used for sample preparation, including synthetic protocols, and the second outlines the experimental techniques used for the subsequent characterisation of these materials. All experimental methods are discussed in generalised terms to accommodate the complexity of the materials investigated.

Materials prepared in this study include:

- Bio-Inspired Amine Silicas (BIAS)
- Amine In-situ Impregnated Silicas (AIIS)
- Nitrogen enriched Resorcinol Formaldehyde (RF) organic and carbon xerogels
- Ionic-liquid Impregnated Activated Carbons (IIAC)

All chemicals used in this study were of analytical grade and used as received, unless otherwise stated. Where solutions have been prepared or dilutions performed, deionised water was used as the diluent, unless otherwise stated.

Chemicals used in the synthesis of both BIAS and AIIS:

- Sodium metasilicate pentahydrate ($SiO_3Na_2 \cdot 5H_2O$), general purpose grade
- 1M HCl
- Methanol
- Small molecular amines:
    - Diethylenetriamine (DETA)
    - Triethylenetetramine (TETA)
    - Tetraethylenepentamine (TEPA)
    - Pentaethylenehexamine (PEHA)
    - Bis 3-aminopropyl amine (B3A)
    - Bis 3-aminopropyl-1-3 propanediamine (B13P)
- Polymeric amines:
    - Poly-allylamine hydrochloride (PAH)
    - Branched polyethyleneimine (BPEI)
    - Polydiallyl dimethyl ammonium chloride (PDADMAC)

Chemicals used for the synthesis of nitrogen enriched RF organic xerogels:

- Resorcinol (99%)
- Formaldehyde (10 – 15% methanol, 37% in H_2O)
- Catalyst (Na_2CO_3, Li_2CO_3, K_2CO_3, Cs_2CO_3)
- Melamine (99%)
- Acetone (> 99.5%)

Chemicals used for the synthesis of IIAC:

- Activated carbon – Pellets
- Activated carbon – Powder
- Activated carbon – Grains
- Dichloromethane (> 99.8%, HPLC grade)
- Ionic liquids:
    - (Emim-OAc (1-ethyl-3-methylimidazolium acetate)
    - Bmpy-NTF_2 (1-buty-3-methypridinium bis(trifluormethylsulfonyl) imide)
    - Bmim-NTf_2 (1-buty-3- methylimidazolium bis(trifluoromethylsulfonyl) imide)
    - Bmim-OTf (1-buty-3- methylimidazolium trifluoromethanesulfonate)

4.1 Equipment used for materials characterisation.

Equipment used to characterise the as-synthesised materials prepared includes:

- An Intelligent Gravimetric Analyser (IGA), supplied by Hiden Isochema, was used for gas sorption experiments, cyclic measurements, regeneration and micropore analysis on selected samples.
- An ABB MB3000 laboratory Fourier Transform Infrared Spectrometer (FTIR) was used to obtain FTIR spectra of synthesised materials.
- A Perkin-Elmer Series II CHNS/O 2400 analyser was used to determine the elemental composition of the materials produced.
- Textural properties of synthesised materials were determined using a Micrometrics Accelerated Surface Area and Porosimetry Analyser (ASAP) 2420.

- A Hitachi Co. SU6600 Field Emission-Scanning Electron Microscope (FE-SEM) was employed to examine the surface morphology of selected materials.
- The thermal stabilities, dehydration characteristics and proximate analyses, of prepared materials, were investigated using a Netzsch STA 449 F1 Jupiter combined Thermo-Gravimetric Analyser and Differential Scanning Calorimeter (TGA-DSC).
- Powder X-ray diffraction patterns were obtained using a PANalytical X'Pert Powder X-ray Diffractometer (PXRD).

4.2 Synthetic overview for Bio-Inspired Amine Silicas (BIAS)

A commercially viable, bio-inspired synthetic approach, for the preparation of carbon capture sorbents, was adapted in this study. The one-pot synthesis occurs in deionised water (W_d), at room temperature (~298 K), under near neutral pH (7.00 ± 0.05), which serves to maximise the solubility and dissolution rates of silica. The initial synthesis process is complete within a matter of minutes (~5 min) and the process uses readily available chemicals, such as sodium meta-silicate and synthetic amines [126].

The synthesis of BIAS assumed an initial baseline ratio for silica to nitrogen of 1:1, based on the stoichiometric ratio of one molecule of silica (Si) reacting with one molecule of nitrogen (N) to give an optimised product; however, it should be noted that this ratio was subsequently used as a variable within the synthetic procedure. The initial calculated mass of silica precursor (sodium metasilicate pentahydrate ($SiO_3Na_2{\cdot}5H_2O$)) was 0.3182 g, while the mass of amine varied, dependent on two key factors, the molecular weight of the amine and the percentage of nitrogen within its structure. When polymeric amines were used, the reactant mass required was calculated as: one milligram of polymeric amine for every millilitre of total reaction volume, i.e. 1 mg/ml, due to the fact that polymeric amines have large molecular weights, which vary within the sample as a result of the specific polymerisation structure of their repeating monomer units.

4.2.1 Determination of reactant mass for BIAS synthesis

Determination of the reactant mass required to synthesise BIAS is as shown below; note that the same steps were used for other materials synthesised using amines; hence, diethylenetriamine (DETA) has been selected as an illustrative amine source.

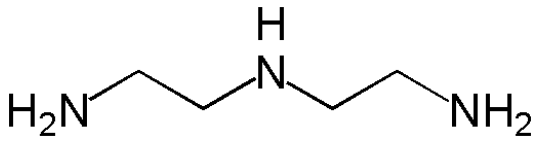

Figure 4-1: Chemical structure of diethylenetriamine (DETA).

The reactant mass calculation was based on the following assumptions:

- Solution concentration of 30 mmol
- Total reaction volume of 50 ml
- Starting Si:N ratio of 1:1

Calculation method:

Molecular weight of $Na_2SiO_3.5H_2O$ = 212.2g

Molecular weight of DETA = 103.1g

The number of moles of solute (silica precursor) can be determined as:

$$Mols\ of\ solute = \frac{reactingmass}{molecularweight}$$

Equation 55

So, for $Na_2SiO_3 \cdot 5H_2O$:

$$Moles\ of\ solute = \frac{x\ g}{212.139 g\ mol^{-1}} = 4.714 \times 10^{-3}\ xmol$$

Equation 56

Using the assumed total reaction volume (50 ml), the number of moles of silica precursor, determined above, and the volume of the silica solution in

Equation 57, gives the mass of $Na_2SiO_3.5H_2O$ required as:

$$Molarity(M) = \frac{mol\ of\ solute}{volume\ of\ solution}$$

Equation 57

$$30 \times 10^{-3}\, mol\, l^{-1} \;=\; \frac{4.714 \;\times\; 10^{-3} x\; mol}{0.05\, l}$$

Equation 58

Hence, x = 0.318 g.

The mass of DETA, calculated using a similar approach as above, must be divided by the number of nitrogen atoms present in the structural formula (i.e. 3, (Figure 4-1)), in order to preserve the initial assumed basis of a 1:1 Si:N ratio:

$$Moles\ of\ \ solute = \frac{x\, g}{103.1\, g\ mol^{-1}} = 9.7 \times 10^{-3} x\, mol$$

Equation 59

Substitute Equation 59 into Equation 57, hence, x = 0.15646 g, adjusting for the proportion of nitrogen in the formula, gives a required mass of 0.0516 g of amine. This process was repeated to determine the reagent mass for all amine types used, refer to Table 4-1 for a summary of all required masses calculated.

Table 4-1: Reagent masses for small and polymeric amines used for BIAS synthesis with associated percentage errors ($Na_2SiO_3 5H_2O$ = 0.318 g).

Sample code	MW of amine/polymer (g/mol)	Amine ID	Amine mass (g)	Vol. of HCl used (ml)	Yield (g)	Yield (%)
DETA_1-1	103.2	C2N3	0.05	3.79	0.033	22.9
TETA_1-1	146.2	C2N4	0.055	3.52	0.057	39.2
TEPA_1-1	189.3	C2N5	0.057	3.54	0.067	45.3
PEHA_1-1	232.4	C2N6	0.058	3.43	0.072	48.8
B13P_1-1	188.3	C3N4	0.071	4.17	0.076	46.8
B3A_1-1	131.2	C3N3	0.066	4.22	0.041	26.1
BPEI_1-1	10000.0	0	0.050	2.88	0.082	72.3
PAH_1-1	15000.0	0	0.050	2.46	0.103	85.3
PDADMAC_1-1	150000.0	0	0.048	2.65	0.035	35.3

4.2.2 Step by step DETA_1-1 synthesis

To eliminate synthetic error and to demonstrate repeatability, five replicates were performed for all small molecular amines analysed, as illustrated in Table 4-2 through to Table 4-5. Using the example BIAS synthesis discussed above, with DETA as the representative amine, synthesis started with 0.052 g of DETA and 0.318 g of silica precursor ($Na_2SiO_3.5H_2O$) being placed into two separate plastic

vials, with 25 ml of deionised water (W_d) added to the silica precursor and the resulting mixture stirred until complete dissolution of the $Na_2SiO_3.5H_2O$ was achieved. 20 ml of W_d was added to the DETA solution, and the mixture lightly shaken to prevent aggregation of the long chains, which could ultimately affect the morphology of the final product formed (when polymeric amines were used, mixing was more vigorous, as such amines are usually solid at room temperature). The prepared solutions were subsequently mixed together, before ~3.79 ml 1M HCl was added to the DETA-silica solution, and the total volume was made up to the required 50 ml by adding W_d, as required.

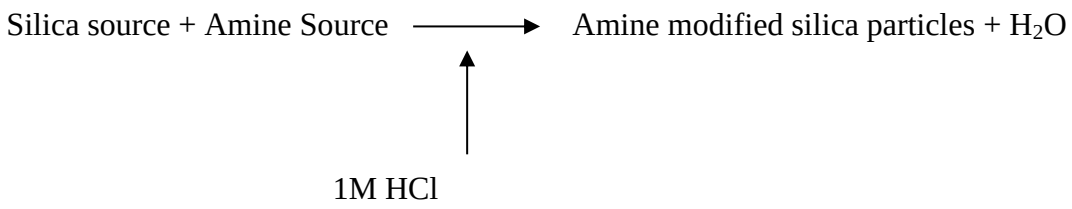

Figure 4-2: Schematic of experimental procedure for BIAS.

The added acid acts to neutralise the alkaline solution while also speeding up the aggregation of silica from solution. After 5 min, the reaction was terminated by decanting into a centrifuge vial to begin the washing/centrifugation process. Note that pH was monitored throughout the synthesis process, with a successful synthetic procedure resulting in a final pH of 7.00 +/- 0.05. A pH of 7.00 +/- 0.05 was chosen to mimic the ability of diatoms to grow beautiful and complicated silica structures adopting conditions similar to those stated in Chapter 5, section 5; hence, following a chemical approach to achieve similar results and ultimately keeping the process green (Figure 4-3).

Table 4-2: Neutralising acid volumes and yields obtained for DETA repeats (silica precursor = 0.318 g).

Sample code	Vol. of HCl used (ml)	Yield (g)	Amine-silica yield (%)
DETA_1-1A	3.76	0.042	29.4
DETA_1-1B	3.80	0.029	20.7
DETA_1-1C	3.79	0.029	20.7
DETA_1-1D	3.78	0.021	14.8
DETA_1-1E	3.79	0.041	28.9
Average	3.78	0.033	22.9
Standard dev	0.01	0.008	5.6
Relative sdev	0.00	0.242	0.2

Table 4-3: Neutralising acid volumes and yields obtained for TETA repeats (silica precursor = 0.318 g).

Sample code	Vol. of HCl used (ml)	Yield (g)	Amine-silica yield (%)
TETA_1-1A	3.56	0.049	33.5
TETA_1-1B	3.52	0.057	39.1
TETA_1-1C	3.53	0.059	40.7
TETA_1-1D	3.50	0.063	43.2
TETA_1-1E	3.50	0.057	39.5
Average	3.52	0.057	39.2
Standard dev	0.02	0.005	3.2
Relative sdev	0.01	0.081	0.1

Table 4-4: Neutralising acid volumes and yields obtained for TEPA repeats (silica precursor = 0.318 g).

Sample code	Vol. of HCl used (ml)	Yield (g)	Amine-silica Yield (%)
TEPA_1-1A	3.48	0.057	39.1
TEPA_1-1B	3.55	0.071	48.1
TEPA_1-1C	3.57	0.065	44.1
TEPA_1-1D	3.55	0.069	47.1
TEPA_1-1E	3.56	0.070	47.8
Average	3.54	0.067	45.2
Standard dev	0.03	0.005	3.4
Relative sdev	0.01	0.075	0.1

Table 4-5: Neutralising acid volumes and yields obtained for PEHA repeats (silica precursor = 0.318 g).

Sample code	Vol. of HCl used (ml)	Yield (g)	Amine-silica Yield (%)
PEHA_1-1A	3.42	0.073	49.0
PEHA_1-1B	3.45	0.071	48.1
PEHA_1-1C	3.43	0.076	51.4
PEHA_1-1D	3.42	0.071	48.2
PEHA_1-1E	3.45	0.070	47.3
Average	3.43	0.072	48.8
Standard dev	0.01	0.002	1.4
Relative sdev	0.00	0.029	0.0

4.2.4 Washing procedure for BIAS samples

Post reaction, the solution was poured into vials and centrifuged using a universal laboratory centrifuge (SIGMA 2-16) for 15 min at 8000 rpm. Solid BIAS particles collected at the base of the tube and, upon completion of centrifugation, the excess solution was decanted and fresh W_d added (~50 ml). The vials were shaken vigorously to thoroughly mix and dislodge as much of the chloride ion (Cl^-) impurity formed during synthesis; the process was repeated twice to maximise Cl^- removal.

4.2.5 Drying procedure for BIAS samples

Upon completion of the final centrifugation step, the excess solution was decanted, and the wet solid BIAS collected and placed in a ceramic crucible before transference to a Memmert universal oven, set to 358 K, wherein the BIAS particles were allowed to dry for 3-4 h. Once dried, the samples were collected, weighed and stored in small storage bottles awaiting further analysis.

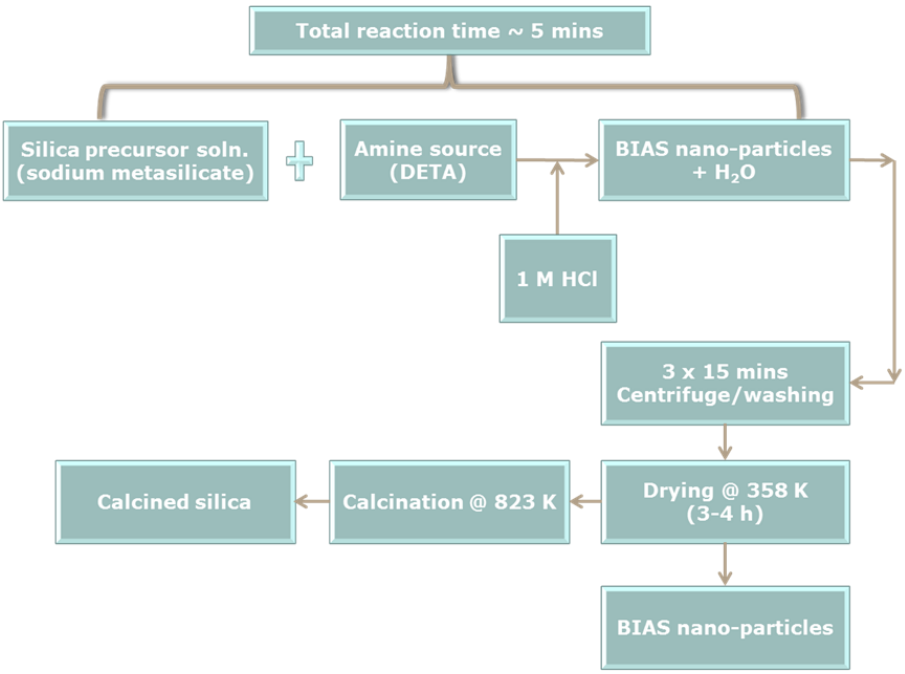

Figure 4-3: Synthesis flow diagram for BIAS nanoparticles prepared in this study.

4.2.6 Preparation of calcined BIAS

The influence of amines on both physical and chemical properties of BIAS was investigated by calcining selected samples to remove the amines incorporated during synthesis, producing amine free silicas, which served as comparators. ~100 mg of a selected BIAS was weighed into a ceramic boat and placed in a horizontal tube

furnace (Carbolite), before heating under flowing air (200 cm^3 min^{-1}) to 823 K, using the heating regime outlined below (Figure 4-4), and held for 2 h (Figure 4-4):

- Ramp at 1 K min^{-1} from room temperature to 393 K, hold for 30 min.
- Ramp at 5 K min^{-1} from 393 to 823 K, hold for 2 h.
- Cool to room temperature (~298 K at 5 K min^{-1}) under flowing air (200 cm^3 min^{-1})

Post calcination samples were designated as amine type_S-N_{cal} e.g. DETA_1-1_{cal}

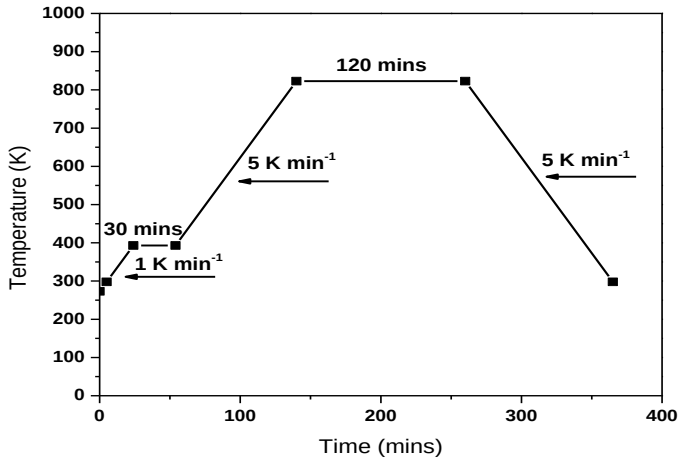

Figure 4-4: The calcination temperature - time profile applied for bio-inspired amine silica.

4.2.7 Preparation of BIAS with varied reactant concentration

The effects of varying reagent concentrations (molar, amine and silica concentration ratios, respectively) were investigated by varying the assumed initial concentration of 30 mmol, depending on the reactant investigated, while all other assumed variables remained constant, e.g. total reaction volume 50 ml. Samples synthesised as such were labelled amine type_X(Si)-Y(N) i.e. X and Y are integer values dependent upon the reactant investigated.

4.2.7.1 Molar concentration variation

The initial assumed concentration of 30 mmol was varied in an arithmetic progression from 30 – 300 mmol in steps of 30 mmol, resulting in an increased reactant mass, it should also be noted that the reaction volume remained constant at 50 ml. The reactant mass required for each new molar concentration was calculated as per the following example for 300 mmol:

From Equation 58, replace 30 mmol with 300 mmol:

$$30\times 10^{-2}\, mol\ l^{-1} = \frac{4.714\times 10^{-3}\, x\ mol\, g^{-1}}{0.05\, l}$$

Equation 60

Hence, x = 3.182 g, and the required mass of DETA, is, therefore, 0.5155 g.

These sets of calculations were used to determine the reactant masses for all amines (small and polymeric) used to prepare BIAS samples with varied molar concentrations (Table 4-6):

Table 4-6: Reagent masses for synthesis of BIAS with varied molar concentrations.

Sample code	Amine (g)	Silica Precursor (g)	Vol. of HCl (ml)	Yield (g)	Amine-silica Yield (%)
DETA_2-2	0.103	0.636	7.26	0.179	63.2
DETA_3-3	0.155	0.955	11.00	0.287	67.5
DETA_4-4	0.206	1.273	14.15	0.402	71.0
DETA_10-10	0.516	3.182	35.30	1.117	78.9
TETA_2-2	0.108	0.636	7.10	0.189	65.5
TETA_3-3	0.163	0.955	10.50	0.309	71.3
TETA_4-4	0.217	1.273	14.10	0.405	70.2
TETA_10-10	0.542	3.182	35.00	1.242	86.0

4.2.7.2 Amine concentration variation

All primary assumptions were maintained, except the initial basis of a 1:1 Si:N ratio, which was varied. Working with X (Si):Y (N), where Y can vary arithmetically between 1 and 16, X is a constant that equals 1. Reagent masses for each ratio are presented in Table 4-7. For reference, a summary calculation is presented below, showing reagent mass required for a sample with Y = 2. Note; the mass for the silica precursor required is the same as that previously calculated in Equation 58;

$$Mols\ of\ solute = \frac{x}{2(103.1\, g\ mol^{-1})} = 4.85\times 10^{-3}\, x\ mol\ g^{-1}$$

Equation 61

Which equates to a required mass of DETA of 0.1031 g, i.e. twice the mass required for a 1:1 S:N ratio.

Table 4-7: Reagent masses for synthesising BIAS with varied amine concentration.

Sample code	Amine used (g)	Vol. of HCl used (ml)	Yield (g)	Amine-silica yield (%)
DETA_1-0.5	0.026	3.34	no ppt	n/a
DETA_1-0.75	0.039	3.60	0.057	44.4
DETA_1-2	0.103	4.75	0.034	17.6
DETA_1-4	0.206	6.72	0.068	23.1
DETA_1-8	0.412	10.70	0.083	16.5
DETA_1-16	0.825	19.60	0.083	9.0
TETA_1-0.1	0.006	3.00	no ppt	n/a
TETA_1-0.2	0.011	3.11	no ppt	n/a
TETA_1-0.3	0.017	3.14	milky	n/a
TETA_1-0.4	0.022	3.17	milky	n/a
TETA_1-0.5	0.027	3.26	0.032	26.9
TETA_1-0.75	0.041	3.38	0.053	40.3
TETA_1-2	0.108	4.40	0.069	34.8
TETA_1-4	0.216	6.07	0.066	21.6
TETA_1-8	0.432	9.55	0.076	14.6
TETA_1-16	0.864	16.55	0.081	8.5
PDADMAC_1-2	0.100	2.65	0.043	22.8
PDADMAC_1-3	0.150	2.67	0.083	34.4
PDADMAC_1-4	0.200	2.57	0.079	27.3
PDADMAC_1-5	0.250	2.63	0.117	34.2
PDADMAC_1-6	0.300	2.68	no ppt	n/a
PDADMAC_1-8	0.400	2.62	no ppt	n/a
PDADMAC_1-20	1.000	2.67	no ppt	n/a
TEPA_1-0.5	0.028	3.28	0.053	44.8
TEPA_1-0.75	0.043	4.40	0.069	51.9
TEPA_1-2	0.114	4.30	0.068	33.2
TEPA_1-4	0.227	5.81	0.077	24.3
TEPA_1-8	0.454	9.35	0.080	14.8
TEPA_1-16	0.909	15.90	0.084	8.4
B13P_1-2	0.131	5.40	0.054	24.5
B13P_1-4	0.262	8.00	0.069	19.7

4.2.7.3 Silica concentration variation

All primary assumptions were maintained, except the initial basis of a 1:1 Si:N ratio, which was varied. Working with X (Si):Y (N), where X varies arithmetically between 1 and 4 and, Y is a constant that equals 1, reagent masses for each ratio are

presented in Table 4-8. For reference, a summary calculation is presented below, showing reagent masses required for a sample with X = 4. Note, the mass of DETA required is the same as that previously calculated in Equation 59:

From Equation 55;

$$Mols\ of\ solute\ = \frac{x}{4(212.139\ g\ mol^{-1})} = 1.17\times10^{-3}\,x\ mol\ g^{-1}$$

Equation 62

$$30\times10^{-3}\,mol\,l^{-1}\ = \frac{1.17\times10^{-3}\,x\,mol\,g^{-1}}{0.05\,l}$$

Equation 63

which equates to a required mass of silica of 1.273 g.

Sample code	Amine Used (g)	Silica precursor used (g)	Vol. of HCl used (ml)	Yield (g)	Amine-silica Yield (%)
DETA_2-1	0.052	0.636	6.75	0.149	64.3
DETA_4-1	0.052	1.273	12.50	0.253	61.3
TETA_2-1	0.055	0.636	6.30	0.182	77.4
TETA_4-1	0.055	1.273	11.94	0.392	94.5
B13P_2-1	0.071	0.636	6.65	0.173	69.1
B13P_4-1	0.071	1.273	11.80	0.400	92.9
BPEI_2-1	0.050	0.636	6.80	0.218	94.9
BPEI_4-1	0.050	1.273	11.80	0.281	68.4
PAH_2-1	0.050	0.636	5.34	0.167	72.6
PAH_4-1	0.050	1.273	10.88	0.205	49.9

Table 4-8: Reagent masses for synthesising BIAS with varied silica concentration.

4.3 Synthetic overview for Amine In-situ Impregnated Silicas (AIIS)

The stability, regenerability and efficiency of AIIS as carbon capture sorbents were investigated. Here, unmodified silica was synthesised from the acid hydrolysis of a soluble alkali metal silicate, with the condensation of silica governed by both the reaction concentration and pH, as suggested by Taposikotoky and Dolui [127-129]; the produced material serves as a comparator to AIIS. AIIS was synthesised via a hybrid process based on both the wet impregnation method proposed by Wang *et al.*

[130] and the bio-inspired method (amine assimilated synthetic method) discussed in sections 4.2 and 4.5. Consequently, material synthesis was divided into two tranches, the first yielded unmodified silica particles, while the second yielded AIIS particles.

4.3.1 Determination of reactant mass for unmodified silica and AIIS

The amount of silica precursor required to synthesise a specific amount of unmodified silica was determined using the following assumptions:

- High initial solution concentration of 300 mmol (to increase the speed of silica aggregation from solution at near neutral pH).
- Reaction volume kept constant at 50 ml for comparability with BIAS samples.
- Starting Si:N ratio of 1:1.

From a starting concentration of 300 mmol, the masses of reagents required were calculated as shown previously (Equation 60).

4.3.2 Preparation of unmodified silica

3.182 g of $Na_2SiO_3.5H_2O$ (silica precursor) was dissolved in ~21.7 ± 2 ml of W_d; on complete dissolution, ~ 28.3 ± 2 ml of 1 M HCl was slowly added to the W_d/silica precursor mixture, with continuous stirring to ensure homogenous mixing. Addition of the acid reduced the pH of the solution from 13.00 ± 0.3 to close to neutral (7.00 ± 0.05). Formation of a sol-gel was observed as pH approached neutral, and polycondensation of silica was allowed to continue for ~5 min under continuous stirring, and at room temperature. After this time, the aggregated particles were removed from the solution by centrifugation and decanting (section 4.2.3), before washing with W_d (essential for Cl^- removal), collection and drying, as previously reported in section 4.2.5; dried silica particles were labelled as unmodified silica.

4.3.3 Overview of AIIS

DETA (Figure 4-1) was selected as the amine for AIIS preparation for the following reasons: it possesses unique chemical and physical properties including lower density compared with the other small molecule amines, short chain length and, most importantly, it exhibited fast sorption kinetics and relatively high capture capacities during CO_2 sorption analysis when used as an amine source for BIAS synthesis.

4.3.3.1 Preparation of AIIS

0.515 g DETA was weighed into a plastic vial and 20 ml of solvent (methanol) added. The mixture was shaken to ensure complete dissolution of both compounds (DETA is readily soluble in polar organic solvents) forming a homogenous solution, which was added to a pre-prepared silica sol-gel, as detailed in section 4.3.2**.** The composite mixture was stirred continuously for a predetermined time; 90 min was used as a standard stirring time, unless otherwise stated.

4.3.3.2 Drying process for AIIS

The slurry formed was poured into a ceramic crucible and placed in a vacuum oven; allowing both vacuum and elevated temperature contributes to drying. The oven was set to 358 K and a vacuum created, the sample was held under these conditions for 3 h, after which the vacuum was reduced and the sample removed and weighed (Figure 4-5), before labelling using the format amine S:N (D1-1). Samples were initially prepared on the basis of silica to nitrogen ratio of 1:1, allowing each atom of Si to react with one atom of N to give an optimised product, as mentioned previously. Ratios either side of equality were investigated to study the effect of relative concentration on materials development, and a similar process was used to calculate the reactant masses for all S:N ratios investigated.

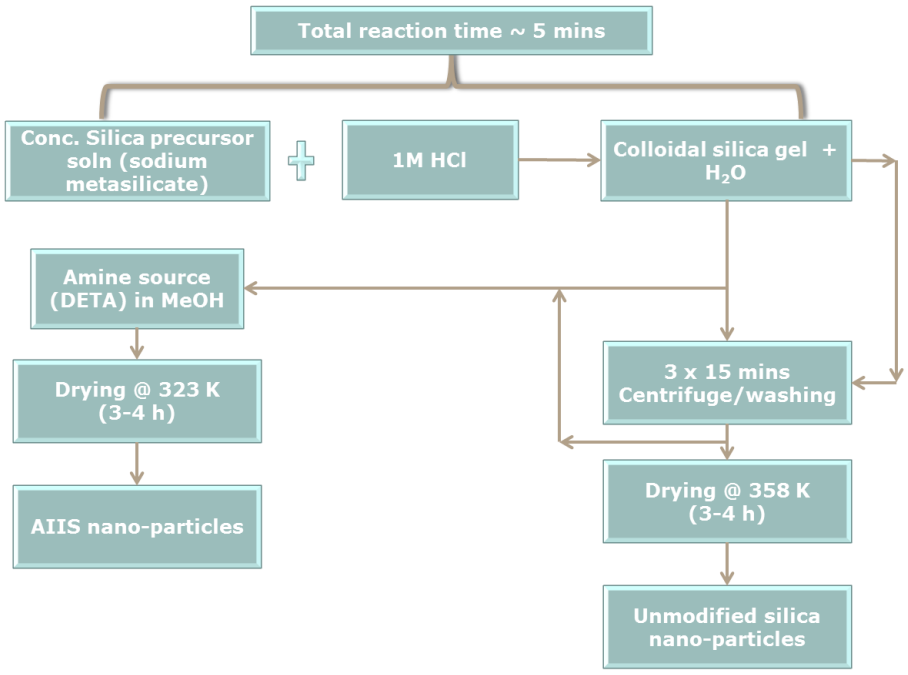

Figure 4-5: Synthesis flow diagram for AIIS nanoparticles prepared in this study**.**

4.4 Synthetic overview for nitrogen enriched Resorcinol and Formaldehyde (RF) organic and carbon xerogels

Nitrogen enriched RF xerogels were synthesised using a modified version of the polycondensation reaction of resorcinol and formaldehyde [131-133]. Melamine (M) was introduced to the process, as a nitrogen rich precursor, with the aim of incorporating basic nitrogen functionalities into the final sol-gel formed; this was expected to increase the CO_2 capture capacities of the materials produced [68, 70, 134]. Calculated required masses for R, F and M were dissolved in deionised water (W_d) and mixed thoroughly in the presence of a basic catalyst (most often sodium carbonate, Na_2CO_3). The solution formed was heated to a predetermined temperature in a sealed vessel, and allowed to gel, after which the water entrained in the hydrogel formed was exchanged for acetone via a solvent exchange process. Once complete, the hydrogels were dried under vacuum, with the final dried products called MRF organic xerogels. To produce carbon xerogels, the dried gels were pyrolysed at a predetermined temperature under an inert atmosphere. To study the effects of pore structure on CO_2 capture, the pyrolysed gels were subsequently physically activated using CO_2 as the activating agent.

4.4.1 Step by step MRF organic xerogel synthesis

MRF xerogels were synthesised by the catalysed endothermic, polycondensation, polymerisation reaction of the precursors (resorcinol and formaldehyde), W_d as the diluent, Na_2CO_3 as the basic catalyst and melamine as the nitrogen rich precursor (Figure 4-8). The reaction is proposed to follow a mechanism similar to that proposed for RF polymerization, according to the model proposed by the Lawrence Livermore laboratory [135] which occurs in two stages, the addition and polycondensation-polymerisation reactions of the Melamine Resorcinol and formaldehyde to form substituted resorcinol, or the hydroxymethyl derivative, with mono-, di-,and tri-substituted resorcinol being produced (Figure 4-6), this is followed by polycondensation -polymerisation of these intermediates to form growing oligomers, which subsequently make up the clusters that compose the gel structure (Figure 4-7).

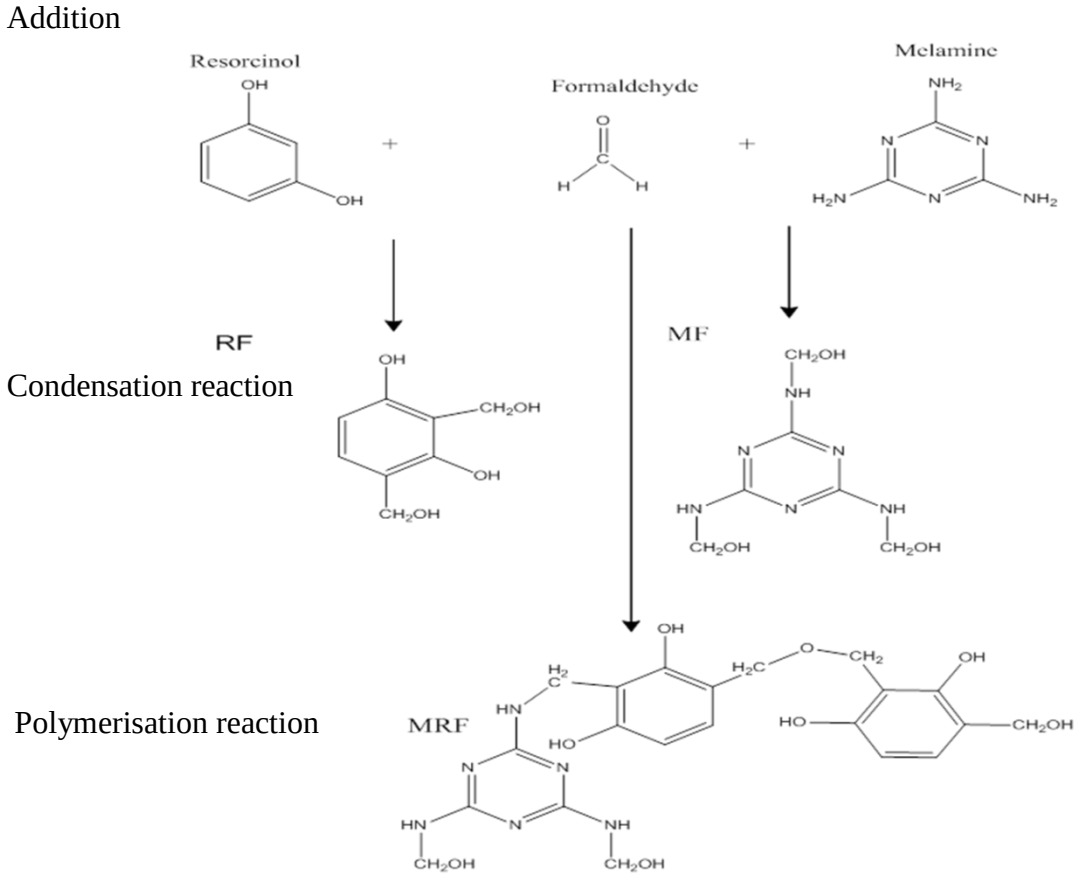

Figure 4-6: Proposed reaction mechanism for MRF xerogels (initial addition reaction, followed by polycondensation of MF and RF, then finally polymerisation/cross linkage of monomer particles).

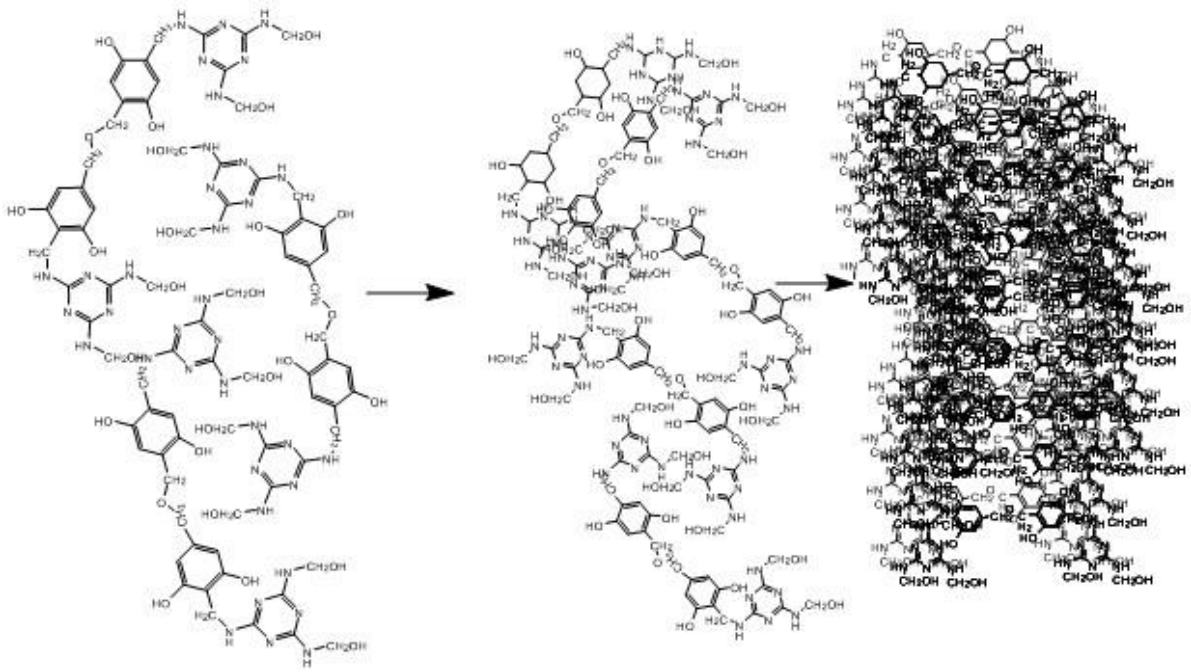

Figure 4-7: Proposed cluster growth of MRF monomers, assuming a similar mechanism to that model proposed by the Lawrence Livermore laboratory [135].

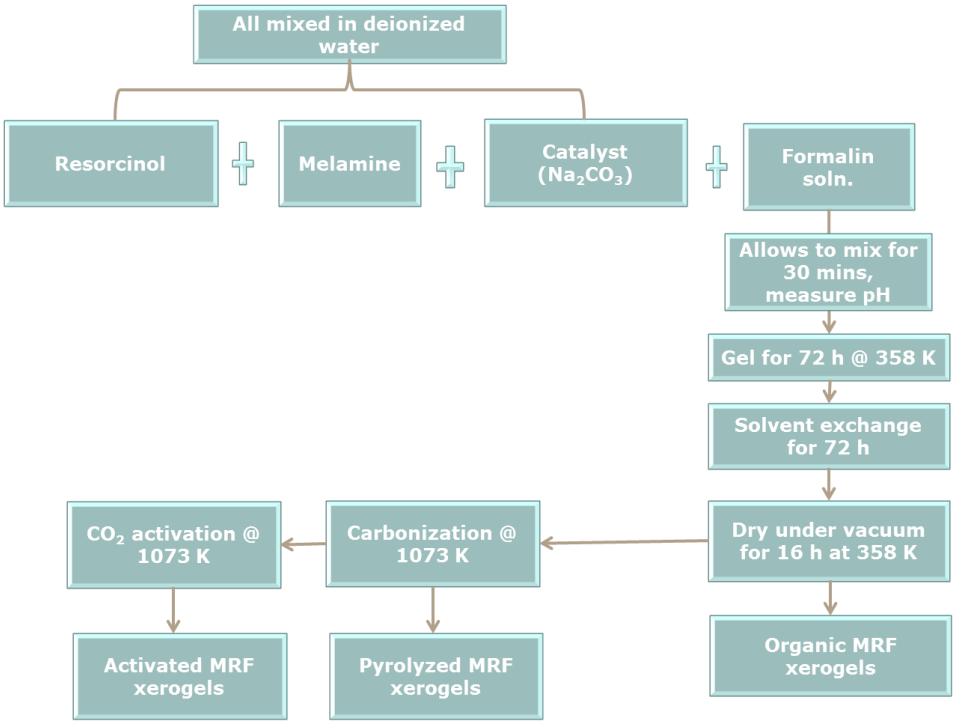

Figure 4-8: Synthesis flow diagram for MRF organic and carbon xerogels prepared in this study.

The following assumptions were made to determine the reagent masses required for synthesis:

- Total reaction volume of 60 ml.
- Solids content of 20% wt/vol (12 g).
- R/F ratio of 0.5.

All xerogels prepared in this study were labelled, C_R/C_wt%M X, where:

C = catalyst type

R/C = ratio of resorcinol to catalyst

wt% M = percentage of melamine in the total solid content of xerogel formed

X = P = pyrolysed, or X = A = activated.

For example Na_100_10% P, represents a material produced using a Na_2CO_3 catalyst, an R/C ratio of 100, M as 10% of the total solids, which has undergone pyrolysis.

4.4.1.1 Determination of reagent masses for preparing MRF xerogels (Na_100_10%A)

The masses of resorcinol, formaldehyde, sodium carbonate and melamine were determined from the initial assumed stoichiometry presented in Table 4-9

Table 4-9: Calculated masses of reactants for Na_100_10% synthesis

Reactants	Equiv. Mol	Equiv. Wt.	Percentage (%)	Predicted Wt. (g)
R	1.00	110.1	57.9	6.95
F	2.00	60.1	31.6	3.79
M	0.15	19.0	10.0	1.20
C	0.01	1.1	0.6	0.07
Total	3.16	190.3	100.0	12.00

The volume of formalin required was determined using the actual weight of resorcinol from Table 4-9:

$$weight\ of\ F(g) = \frac{(\%F \times wt.of\ R)}{\%R}$$

Equation 64

Hence, the weight of formaldehyde required was:

$$weight\ \ of\ F(g) = \frac{(31.56 \times 6.945)}{57.88} = 3.788\ g$$

Equation 65

Assuming the density of formalin to be 1.09 g ml^{-1}, and that formalin contains 37 wt% formaldehyde, the volume of formalin required was given as:

$$1\,ml\ \ formalin\ = 1.09\ g\ \ formalin = 0.37 \times 1.09 = 0.4033\ g\ \ formaldehyde$$

Equation 66

$$volume\ of\ \ formalin\ \ \ required\ \ (ml) = \frac{wt.F(g)}{0.4033\ g}$$

Equation 67

So, 3.788 g of formaldehyde is delivered by 9.39 ml of formalin. As formaldehyde has a density of 0.815 g ml^{-1}, this equates to a volume of 4.65 ml, hence methanol and water make up the remaining 4.74 ml, so an additional 5.26 ml of water would be required to make the total reaction volume up to the desired 60 ml. Different catalyst types were investigated, and the same calculations adopted for the

determination of reagent masses for a constant R/C ratio of 100, using the molar mass of the replacement catalyst in place of that for Na_2CO_3 (Table 4-10). This calculation was repeated for all xerogels produced; for xerogels containing no melamine, the initial formulation process was the same but melamine wt% was excluded, as shown in Table 4-11.

Table 4-10: Calculated reactant masses for xerogels synthesised using different catalysts (melamine (g) = 1.2 g).

Sample Code	R (g)	F (g)	C (g)	Formalin (ml)	Additional W_d (ml)
Na_2CO_3_100 (10%)	6.945	3.788	0.067	9.39	5.26
K_2CO_3_100 (10%)	6.932	3.781	0.087	9.37	5.26
Li_2CO_3_100 (10%)	6.958	3.795	0.047	9.41	5.25
Cs_2CO_3_100 (10%)	6.857	3.740	0.203	9.27	5.32
$(NH_4)_2CO_3$_100 (10%)	6.949	3.790	0.061	9.40	5.25

Table 4-11: Calculated reactant masses for RF gels synthesised without melamine.

Sample Code	R (g)	F (g)	C (g)	Formalin (ml)	Additional W_d (ml)
Na_2CO_3_10	7.310	3.987	0.704	9.89	5.01
Na_2CO_3_25	7.576	4.132	0.292	10.25	4.82
Na_2CO_3_50	7.670	4.183	0.148	10.37	4.76
Na_2CO_3_100	7.717	4.209	0.074	10.44	4.73
Na_2CO_3_200	7.741	4.222	0.037	10.47	4.71
Na_2CO_3_300	7.749	4.226	0.025	10.48	4.71
Na_2CO_3_500	7.755	4.230	0.015	10.49	4.70

4.4.1.2 Preparation of MRF xerogels (Na_100_10%_PA)

6.945 g of R was added to ~50 ml of W_d and stirred continuously until complete dissolution of R. 1.2 g of M was added to the R/W_d mixture and allowed to completely dissolve, before 0.067 g of C was also added. The whole mixture was then allowed to achieve complete dissolution under continuous mixing, using a magnetic stirrer. 9.39 ml of formalin solution was added to the M/R/F/C/W_d mixture (~5.26 ml of W_d was added to make the solution volume up to 60 ml) before continuous stirring for 30 min to ensure a homogenous mixture. After this time, a colour change was usually observed (clear to bright yellow/orange), at which point the pH was measured using a Hanna pH 20 bench-top meter equipped with a HI

1110B pH electrode probe. In order to ensure accurate pH measurements, the probe was calibrated with HANNA pH buffers (pH4 and pH10) prior to each synthetic run. The same synthetic steps were used in the preparation of different MRF xerogel compositions, and the masses required for each system are shown in Table 4-12.

Table 4-12: Calculated reactant masses of MRF gels synthesised in this study.

Sample Code	R (g)	F (g)	C (g)	M (g)	Formalin (ml)	Additional water (ml)
Na_2CO_3_50 (1%)	7.593	4.141	0.146	0.120	8.34	5.79
Na_2CO_3_100 (1%)	7.640	4.167	0.074	0.120	8.30	5.81
Na_2CO_3_300 (1.5%)	7.636	4.165	0.024	0.175	10.33	5.22
Na_2CO_3_500 (1.5%)	7.642	4.168	0.015	0.175	10.33	5.22
Na_2CO_3_10 (7%)	6.833	3.727	0.658	0.783	9.24	5.33
Na_2CO_3_25 (7%)	7.065	3.853	0.272	0.809	9.55	5.17
Na_2CO_3_50 (7%)	7.146	3.898	0.138	0.819	9.66	5.12
Na_2CO_3_100 (7%)	7.176	3.914	0.069	0.841	9.70	5.10
Na_2CO_3_300 (7%)	7.215	3.935	0.023	0.827	9.76	4.93
Na_2CO_3_500 (7%)	7.221	3.938	0.014	0.827	9.76	4.93
Na_2CO_3_50 (10%)	6.903	3.765	0.133	1.200	9.33	5.28
Na_2CO_3_50 (20%)	6.136	3.346	0.118	2.400	8.30	5.81
Na_2CO_3_50 (30%)	5.369	2.928	0.103	3.600	6.25	6.85
Na_2CO_3_50 (40%)	4.601	2.509	0.089	4.801	6.22	6.86
Na_2CO_3_50 (50%)	3.835	2.091	0.074	6.000	5.22	7.36
Na_2CO_3_100 (10%)	6.945	3.788	0.067	1.200	9.39	5.26
Na_2CO_3_100 (20%)	6.174	3.367	0.059	2.400	8.35	5.78
Na_2CO_3_100 (30%)	5.402	2.946	0.052	3.600	6.22	6.86
Na_2CO_3_100 (40%)	4.630	2.525	0.045	4.800	5.20	7.37
Na_2CO_3_100 (50%)	3.859	2.104	0.037	6.000	5.22	7.36

4.4.1.3 Gelation and polymerisation (curing) of MRF xerogels

After pH was recorded, the reaction vessel was sealed and placed in a conventional oven (Figure 4-3) set at 358 K ± 3 K. The elevated temperature used increased the rate of the polymerisation reaction, hence, reducing gelation time. Cluster formation and particle growth has been reported to start approximately an hour after gelation starts, as supported by observations by Cook and co-workers [135] where sol dynamic viscosity was seen to level off [135]. At this stage, the sol is in a colloidal form, constituting monomer particles, although, the characteristics of the final hard

gel, obtained after curing, composed of covalently cross-linked monomer particles, do not start to form until a few hours later and progress slowly afterwards [136]. As a result, the sol-gel was allowed to cure for 72 h before subsequent processing.

4.4.1.4 Solvent exchange of MRF xerogels

Solvent exchange is required, before sample drying, when an aqueous medium is used, to reduce the surface tension of the entrained solvent, hence, the possibility of material shrinkage; hence, the exchange solvent should have the following characteristics:

- Low surface tension
- Polar species
- Low boiling point

Acetone was used as it meets these desired characteristics, and it has been widely used in the literature as a good solvent exchange liquid for RF xerogel synthesis. After gelation and curing, the final cross-linked gel (hydrogel) was allowed to cool, and any surface water drained off. The hydrogel formed was broken into smaller pieces to increase the contact area with acetone. Initially, approximately twice the initial synthesis solution volume (2 x 60 ml) of acetone was added to the hydrogel and the mixture shaken vigorously (dependent on the strength of the hydrogel) to remove any surface water, before draining. 180 ml of acetone was then added to the hydrogel and the container sealed with paraffin tape to prevent loss of acetone to evaporation or spillage. Once tightly sealed, the vessel was placed on a shaker (Jencons lab-line incubator and shaker), set to 210 rpm, and allowed to solvent exchange for 72 h.

4.4.1.5 Drying conditions of MRF xerogels

Drying conditions influence the shrinkage and textural properties of the xerogels formed; hence, constant drying conditions were adopted and maintained throughout this study. After removal from the shaker, excess acetone was decanted, before the xerogels were placed in a vacuum oven (Townson and Mercer 1425-2) and heated at 358 K under vacuum for ~16 h, to ensure complete removal of all absorbed acetone/water.

4.4.2 Preparation of carbon xerogels

A selected, dried MRF xerogel was weighed into a ceramic boat and placed in a tube furnace (Carbolite tube furnace), before the furnace was sealed and argon (Ar) introduced at 200 cm^3 min^{-1}. After a delay of 30 min, to ensure atmospheric oxygen had been purged from the system, the xerogel was heated using a pyrolysis regime pre-determined from thermo-gravimetric analysis. Figure 4-9 shows the temperature time profile used for pyrolysis.

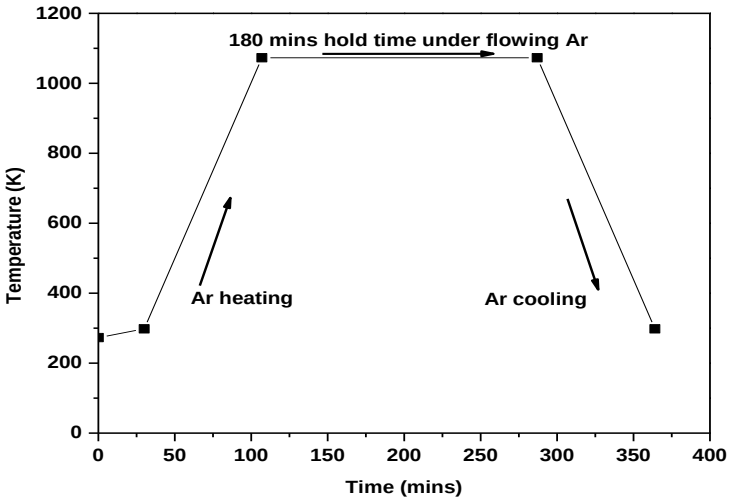

Figure 4-9: Temperature - time profile applied to the pyrolysis of MRF carbon xerogels produced in this study.

After cooling to room temperature, the final product was transferred to a sample vial, and labelled as an MRF carbon xerogel with reference to the original synthesis parameters.

4.4.3 Preparation of activated xerogels

Activation of MRF carbon xerogels was performed to investigate its effect on the textural, and CO_2 capture, proprieties of the xerogels. Conditions for activation were similar to those for pyrolysis, except, at the maximum heat treatment temperature of 1073 K, Ar was replaced with CO_2, again flowing at 200 cm^3 min^{-1}, and the system held under these conditions for a selected time interval (Figure 4-10). Samples were activated for either, 4, 8 or 12 h to also investigate the effect of hold time on the aforementioned properties. The final activated products were placed in sample bottles and designated as MRF activated carbon xerogels.

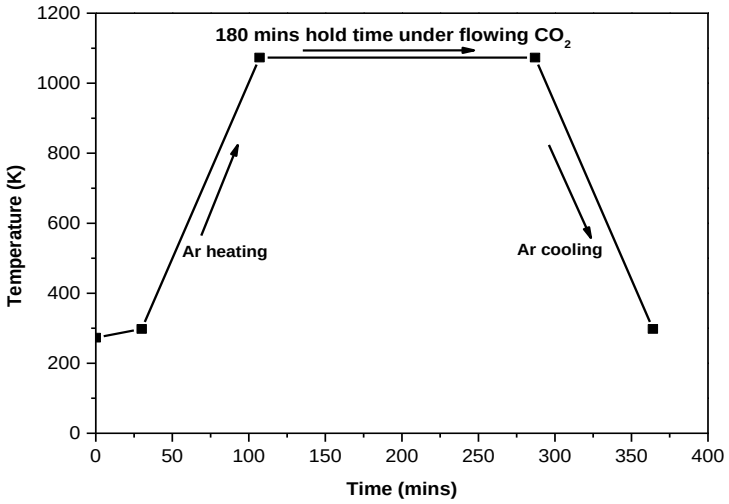

Figure 4-10: Temperature - time profile applied to the activation of MRF carbon xerogels produced in this study.

4.5 Synthetic overview for Ionic-liquid Impregnated Activated Carbons (IIAC)

Synthesis of the ionic liquids used in the preparation of IIAC was out-sourced to Imperial College London; four types of ionic liquids were synthesised and supplied (Figure 4-11):

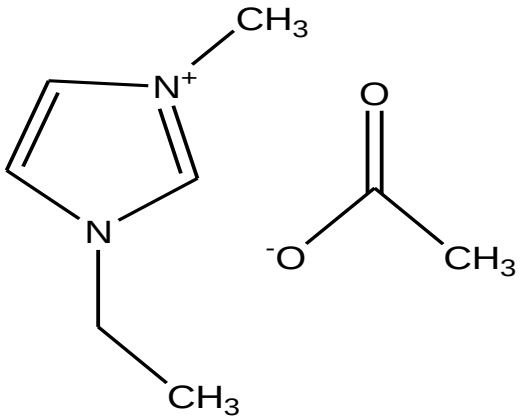

(a) Emim-OAc (1-ethyl-3-methylimidazolium acetate)

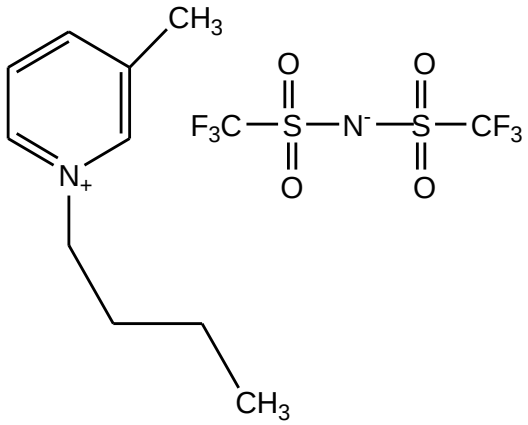

(b) **Bmpy-NTf_2 (1-butyl-3-methypridinium bis (trifluormethylsulfonyl) imide)**

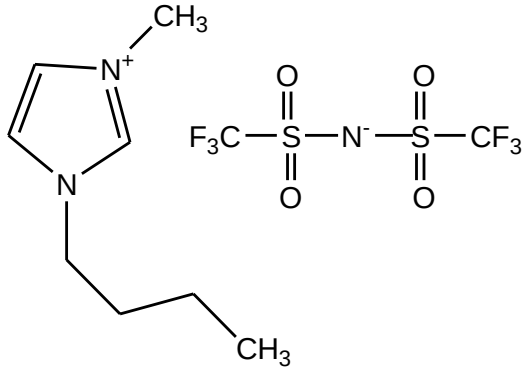

(c) Bmim-NTf_2 (1-butyl-3- methylimidazolium bis (trifluoromethylsulfonyl) imide)

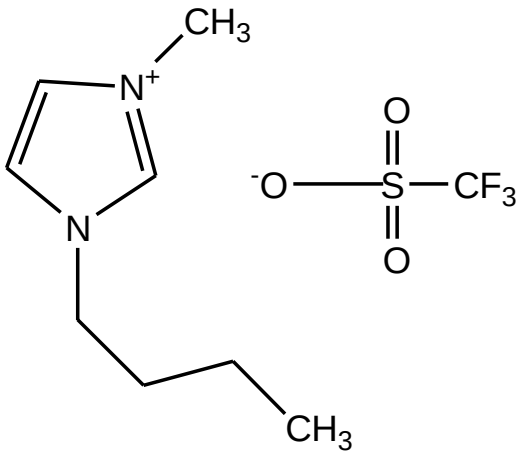

(d) Bmim-OTf (1-butyl-3- methylimidazolium trifluoromethanesulfonate)

Figure 4-11: Figures a-d represents ionic liquids used for IIAC synthesis in this study

Based on an extensive literature review, Bmim-NTf_2, was chosen as a possible candidate for impregnation trials as it has shown high CO_2 solubility, and the anion present in its structure is recognised as an excellent binder of CO_2 (ionic liquids that encompass CO_2-philic anionic species, such as carbonyl or fluorine, have shown increased CO_2 capacity) [137].

Three types of activated carbon, from two suppliers, were used in this study; prior to selection of the support material, all three were characterised and compared against standard requirements for support materials, with activated carbon pellets chosen as the overall support material of choice (refer to chapter 8 for standard requirements for support materials), carbon materials investigated were:

- Activated carbon pellets (Norit)
- Granular activated carbon (Sigma Aldrich)
- Activated carbon powder (Norit)

4.5.1 Synthesis of Bmim-NTf_2 impregnated activated carbon (pellet type)

Bmim-NTf_2 impregnated activated carbons were synthesised using a simplified version of the well-studied wet impregnation-vaporisation method [80, 138-141] (Figure 4-12). To prepare 50 wt% ionic liquid impregnated activated carbon, 50 g of Bmim-NTf_2 was dissolved in 20 ml HPLC grade dichloromethane (DCM), and the solution shaken for 30 s to ensure effective mixing of both liquids. 50 mg of activated carbon was placed in a glass vial and the Bmim-NTf_2/DCM mixture added, with the resulting mixture stirred using a magnetic stirrer for 2 h, after which time the solvent (DCM) was removed by placing the impregnation system in a vacuum oven heated to 358 K for 4 h. The percentage weight of Bmim-NTf_2 in the composite was determined from the weight change in the activated carbon before and after wet impregnation. Different ratios of Bmim-NTf_2 were used, and the samples labelled as AC_{form}(wt% Bmim-NTf_2). Where AC is activated carbon; form is the physical appearance of AC, in this case, pellets; and wt% Bmim-$NTf_{2\ is}$ the concentration of ionic liquid in the final product.

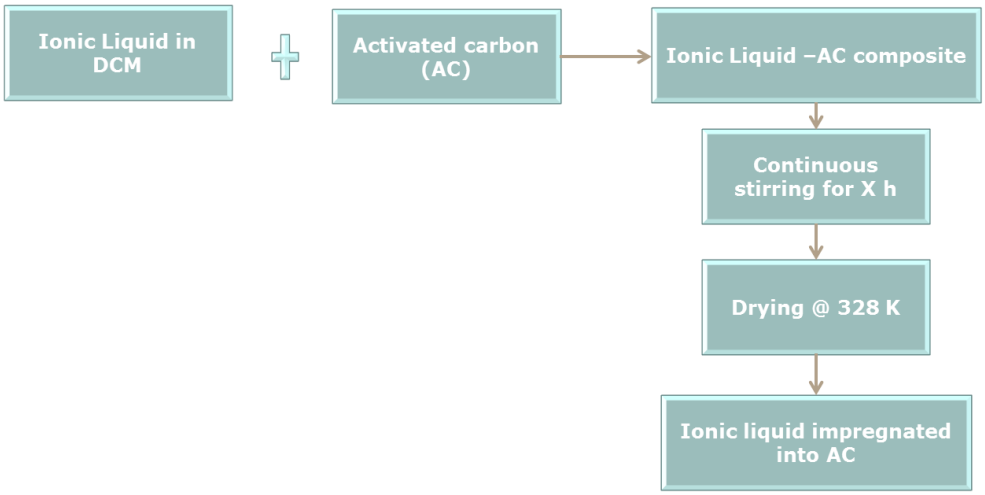

Figure 4-12: Synthesis flow diagram for IIAC samples prepared in this study.

Table 4-13: Bmim NTf_2 impregnated onto activated carbon pellets at different concentrations.

Sample code	IL used (g)	AC used (g)	dry (g)	Volatile losses (%)
AC	0.000	0.206	0.186	10.0
AC_10	0.023	0.203	0.193	14.4
AC_20	0.050	0.201	0.223	11.4
AC_30	0.087	0.203	0.263	9.2
AC_40	0.134	0.201	0.305	8.9
AC_50	0.201	0.201	0.379	5.5

4.6 Characterisation procedures

To develop an in-depth understanding of the characteristics (physical and chemical) of the materials synthesised in this study, it was essential to determine the porous properties (surface area, micro and meso-porosities, pore size distribution), surface functionalisation, morphologies, elemental compositions, thermal stabilities and, most importantly, CO_2 sorption characteristics of the different families of sorbents produced.

4.6.1 Porosity measurements by N_2 adsorption at 77 K

Porosity parameters of all samples prepared were determined via nitrogen sorption measurement using a Micromeritics Accelerated Surface Area Porosity (ASAP) 2420 analyser (Figure 4-13). Depending on the material to be analysed, ~40 mg or ~0.5 g of sample was weighed into a sample tube prior to placement on the ASAP analyser for outgassing and degassing. The outgas conditions involved reducing the pressure

from atmospheric to partial vacuum (5 mmHg/670 Pa), then to full vacuum (10 μmHg/1.33 Pa). Once at full vacuum, the temperature was raised from ambient to 323 K, held for 30 min, thus completing the outgas step. The degas step began by heating the sample from 323 to 383 K at 5 K min^{-1}, held for 2 h, before cooling to room temperature, backfilling with analysis gas before the sample tube was removed. After degas was complete, the sample tubes were reweighed and the new weights recorded (sample mass differences were attributed to adsorbed gases/volatiles). Sample tubes were transferred from the degas ports to the analysis ports for N_2 sorption analysis at 77 K. The ASAP was programmed to collect 40 data points in the range P/P^o = 0.001 to 1.0 for the adsorption branch and 30 points in the range P/P^o = 1 and 0.1 for the desorption branch.

Figure 4-13: Photograph of the Micromeritics Surface Area and Porosity Analyser (ASAP) 2420 used in this study.

4.6.2 CHN – O Elemental analysis

Selected samples were analysed for their percentage composition of carbon, hydrogen, nitrogen and oxygen. ~2 mg ± 0.5 mg of each selected sample was analysed and the data recorded using a CHNS/O analyser Series 11, E400, Perkin Elmer (Figure 4-14)

Figure 4-14: Photograph of the Perkin Elmer, model 2400 Series 11 CHNS/O analyser used in this study.

4.6.3 Fourier Transform Infrared Spectroscopy (FTIR)

To determine the surface functional groups present within the samples, IR analysis was performed on a small amount of each selected sample (~40 mg ± 10 mg), which was finely ground before analysis. A single reflection diamond/ZnSe ATR crystal on a ABB MB3000 FTIR laboratory spectrometer was used to collect IR spectra (Figure 4-15), scanning 32 times over a frequency of 600 – 4000 cm^{-1} at a resolution of 16 cm^{-1}.

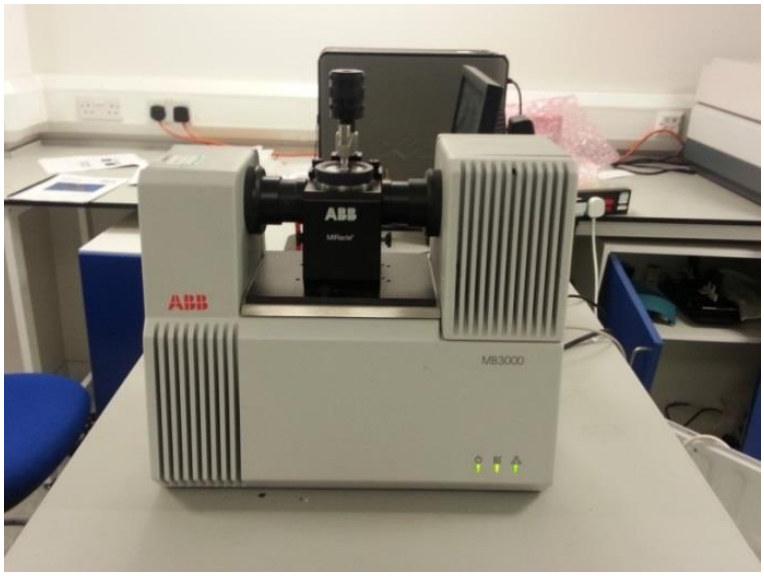

Figure 4-15: Photograph of the ABB MB3000 FTIR laboratory spectrometer used in this study.

4.6.4 Scanning Electron Microscopy (SEM)

Selected samples were examined via SEM to determine the effects of chemical modification on surface morphology and textural properties (particle size, pore volumes etc.). A Hitachi SU6600 Analytical variable pressure Field Emission SEM was used (Figure 4-16) and operated at 20 keV with a scan resolution of 500 nm and magnifications up to 250, 000 times were applied.

Figure 4-16: Photograph of the Hitachi SU6600 Analytical variable pressure Field Emission SEM analyser used in this study.

All samples were finely ground then gold coated prior to analysis; coating was undertaken to enhance the samples conductivity, because the quality of the micrographs taken can be affected by surface charge. The Edwards S150 sputter coater shown in Figure 4-17 was used as the gold coater.

Figure 4-17: Photograph of the Edwards S150 sputter coater used in this study.

4.6.5 Powder X-Ray Diffraction (PXRD)

The PXRD profiles of selected BIAS samples were recorded using a PANalytical X'Pert Powder X-ray diffractometer equipped with a Cu K α radiation source and measurements were taken at a scan rate of 0.2^{o} min^{-1} and a step size of 0.1^{o} (between $2\theta = 5 - 90$).

Figure 4-18: Photograph of the PANalytical X'Pert Powder X-ray diffractometer used in this study.

4.6.6 Thermo-Gravimetric Analysis (TGA)

Proximate analyses, thermal stabilities and decomposition profiles of selected materials prepared were acquired using a thermo-gravimetric analyser. Here, a Netzsch STA 449 Fl Jupiter combined TGA-DSC instrument was used and the operating parameters varied depending on the materials being characterised. An overview of the operating conditions for materials characterised using this device is presented below.

Figure 4-19: Photograph of the Netzsch STA 449 Fl Jupiter combined TGA-DSC instrument used in this study.

4.6.6.1 TGA for AIIS and BIAS particles

Approximately 5 ± 3 mg of sample was weighed into a platinum pan and placed on a microbalance, with a pre-weighed counterweight. The equipment was set up using air (50 ml min^{-1}) for combustion and N_2 (20 ml min^{-1}) as a protective gas. The heating regime used was from room temperature to 1273 K, at a heating rate of 5 K min^{-1}, before cooling to room temperature at 20 K min^{-1}. An isothermal step was included at the onset, to allow the system to equilibrate at ambient conditions for 10 min before the heating step commenced.

4.6.6.2 TGA for RF and MRF xerogels

Approximately 10 ± 3 mg of sample was weighed into a platinum pan and placed on a microbalance, with a pre-weighed counterweight. The equipment was set up to operate under flowing N_2 (50 ml min^{-1}), and an isothermal/purge step was included at the onset; here N_2 was used to purge any atmospheric oxygen within the system to prevent oxidative combustion which could result in an inaccurate thermo prolife of the sample. After a 20 min purge at ~298 K, the temperature was raised to 1273 K at a rate of 10 K min^{-1}, before cooling to room temperature following a similar regime to that described above.

4.6.7 CO_2 adsorption by gravimetric analysis

CO_2 sorption performances of the synthesised sorbents were determined using an Intelligent Gravimetric Analyser (IGA) supplied by Hiden Isochema Ltd, which uses

gravimetry to accurately measure the magnitude and dynamics of CO_2 sorption on a given sorbent [117]. ~35 ± 5 mg of sample was accurately weighed, before outgassing from 100 kPa to vacuum at a rate of 6 kPa min^{-1}. Once the IGA system equilibrated at vacuum, the sample was heated from room temperature to 393 K at a heating rate of 3 K min^{-1} using a fast response furnace. The sample was allowed to degas for 2 - 3 h depending on the material being analysed (BIAS, AIIS and MRF organic xerogels were held for 3 h, while MRF carbon xerogels and IIAC were held for 2 h). Degassing was employed to remove any physically adsorbed water and/or volatiles from the sorbent surface. After the sample had been effectively degassed (negligible mass change observed), the fast response furnace was replaced with a Grant water-bath pre-set to the desired (e.g. 333 K) temperature. Samples were typically cooled to, and held at, 333 K, before 99.9% CO_2 was introduced and the pressure increased from vacuum to the desired pressure step (10, 100 or 900 kPa) at 5 kPa min-1, and allowed to equilibrate at each pressure step. For desorption steps, the pressure was reduced from the final adsorption pressure point to the predetermined desorption pressure point, usually the inverse of the adsorption points. For a two point system (10 and 100 kPa), desorption began at 100 kPa, before evacuation to 10 kPa, followed by desorption to vacuum at a rate of 5 kPa min^{-1}. Once a sorption run was complete, the sample chamber was re-pressurised to atmospheric pressure and the sample removed and stored for further characterisation.

Figure 4-20: Photograph of the Hiden Isochema Intelligent Gravimetric Analyser (IGA) used in this study.

4.6.7.1 Vacuum swing CO_2 cycling (regeneration) studies

Here, Vacuum Swing Adsorption (VSA) was used for regeneration studies; a typical VSA cycle uses reduced pressure to shift the equilibrium position and cause desorption of adsorbed species, hence regeneration of the adsorbent [142]. Sample regeneration experiments were performed using the IGA system referred to in Section 4.6.7; here samples were analysed as detailed previously but, rather than single sorption steps, sequential steps were programmed into the IGA system depending on the number of sorption cycles required..

4.6.7.2 Micropore analysis of MRF activated carbon xerogels

Due to the problematic nature of characterising the microporous properties of carbon sorbents using N_2 adsorption at 77 K, CO_2 adsorption at 273 K was used and the data collected were analysed using the Dubinin Astakhov (DA) method. Data between partial pressures of 0.01 and 0.25 were analysed, as this is representative of the microporous range. The same analysis conditions were employed as detailed previously (section 4.6.7), and the adsorbate gas was again CO_2, with the water bath set to 273 K. To prevent the circulating media from freezing, a mixture of 20% ethylene glycol/80% water was used. After sample degas, a total of 30 pressure points were measured within the partial pressure range 0.01 and 0.258 (3 kPa and 900 kPa) and the data used to determine the pore size, surface area and pore size distribution of the materials investigated.

CHAPTER 5 (RESULTS AND DISCUSSION I)

BIO-INSPIRED AMINE SILICA (BIAS) FOR CO_2 CAPTURE

5 INTRODUCTION TO AMINE MODIFIED BIO-INSPIRED SILICA (BIAS) FOR CO_2 CAPTURE

In contrast to chemically synthesised silicas, which involve synthesis under harsh conditions (e.g. elevated temperatures and pressures) usually in either highly basic or acidic medias, Bio-Inspired Amine Silicas (BIAS) have been synthesised via routes inspired by the ability of diatoms to grow complex silica skeletons under green conditions (e.g. mild pH, ambient temperature) [143, 144]. Sumper *et al.* [145] showed that silica spheres can be condensed from a suite of cationic polypeptides, isolated from *diatomcylindrotheca fusiformis* in aqueous silicic acid in vitro [145]. Further research, showed that polyamines, and specially designed amine containing compounds, have the ability to condense silica, although, due to their limited self-assembly properties, it has been difficult to achieve homogenous structures in the nano range, with most structures ranging from poly-dispersed spheres to hexagonal platelets. The chemical behaviour of silica particles is determined by the hydroxyl groups, which are responsible for adsorptive properties, including adsorption of water, alcohols and amines; the reaction with amines make these useful support material for CO_2 capture [146]

The ease and ability to modify the surface of silicas, makes them suitable support materials for a variety of applications, including, in recent years, CO_2 capture; different silica based materials have been prepared over the years, and silica modified with amines have been shown to possess high affinities for CO_2 [93, 147-152]. Samanta *et al*. [29], carried out an extensive review on the current developments on CO_2 capture sorbents, concluding that amine functionalised sorbents (i.e. amine functionalised silicas) show promise for CO_2 capture from simulated flue gas conditions, however, they cautioned that more needs to be done, from bench through to pilot scale studies, before commercialisation of these materials is tenable.

Here, a novel method for the preparation of amine modified silica, as a CO_2 capture material, was developed, by a co-condensation functionalisation method. Here, silica is condensed via the acid hydrolysis method (Chapter 4), using a series of amines (small and large molecular amines) aimed at controlled incorporation of amine functionalities onto the condensed silica. So far, there has been no report of the use

of such techniques for CO_2 capture material development. This approach allows anchorage of the organic functionalities to the walls of the poly-condensed silica in a single step (Figure 5-1), allowing a greater degree of coverage and surface homogeneity of the organic functional groups; consequently eliminating pore blockage, as it is assumed that the organic functional groups are homogenously distributed compared to methods such as the wet impregnation (in situ-impregnation), as discussed in Chapter 6.

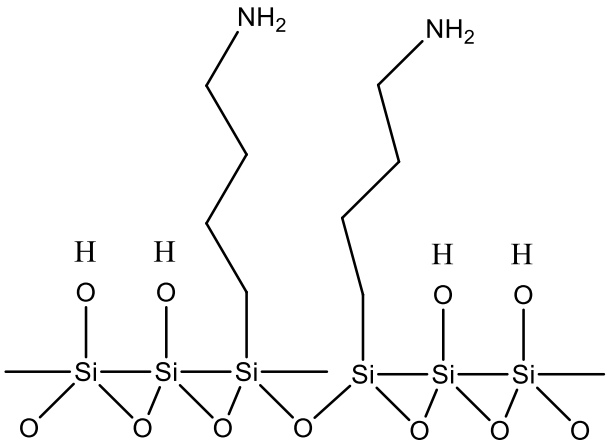

Figure 5-1: Proposed structure of amine modified bio-inspired silica prepared in this study

This chapter presents the results obtained from the preparation and characterisation of BIAS nanoparticles, as described in Chapters 3 and 4. Discussion of these results is structured into four sections; the first examines the validity of the synthesis method employed, using N_2 sorption at 77 K to determine textural parameters, e.g. BET specific surface area, pore volume and pore size distribution. The second deals with the optimisation of the synthetic parameters on sorbent performance, e.g. progressive amine modification, effect of reaction concentration, acid volume quantification etc. The third presents characterisation results for the synthesised materials, including functional groups, concentrations, elemental compositions, thermal stabilities, morphologies, porosities and the effect of these properties on material performances. While the final section examines sorbent regeneration, and the effect of process parameters, such as temperature, pressure and sample ageing on the sorbents CO_2 capture capacity and overall efficiency.

5.1 Repeatability studies on the synthetic routes used for BIAS production

To determine that the synthesis method adopted was repeatable, 10 BIAS nanoparticle samples, were prepared; 5 each using diethylenetriamine (DETA) and triethylenetetramine (TETA) as the amine source under otherwise identical synthetic conditions. The chemical properties, as determined by elemental analysis and CO_2 sorption analysis, and physical properties, as determined by textural parameters; evaluated by N_2 sorption at 77 K, were compared to establish synthetic repeatability, employing both standard and relative standard deviations as models for analysing process repeatability, lower values signify replicates are repeatable to a high accuracy, while higher values imply higher process error in replicates. Here, only BIAS samples prepared using the small molecular amines DETA and TETA are presented; BIAS samples prepared using polymeric amines, and small molecular amines TEPA and PEHA are presented in Appendix A.

5.1.1 Textural properties of BIAS repeat samples prepared using small molecular amines (DETA/TETA)

The textural properties, including BET specific surface area, BJH total pore volume and average pore size, of all samples prepared were determined using N_2 sorption at 77 K, with results presented in Table 5-1and Table 5-2; corresponding N_2 sorption isotherms and their relative pore size distributions are presented in Figure 5-2 and Figure 5-3. All repeats show similar sorption isotherms (Figure 5-2), classified as Type II [95], according to IUPAC classification, which implies indefinite multi-layer formation on the pore site after completion of the initial monolayer formation, indicative of sorbents with observed wide pore size distributions (Figure 5-3). The desorption branches varied depending on the hysteresis loop observed, according to Sing and co-workers [104], hysteresis loops recorded below the closure limits (partial pressures ~0.42), indicate irreversible changes, such as chemisorption or swelling of the sorbent during the adsorption step, this phenomenon was observed for some of the materials analysed here, hence, such behaviour is proposed as a plausible cause for the open-ended loops exhibited in the DETA 1-1 repeats.

Table 5-1: Textural parameters obtained for repeat preparations of DETA BIAS nanoparticles

Sample ID	S_{BET}	V_{TOTAL}	Pore size
	m^2g^{-1}	cm^3g^{-1}	nm
DETA_1-1A	30.0	0.05	26.4
DETA_1-1B	54.9	0.12	32.7
DETA_1-1C	37.9	0.10	33.4
DETA_1-1D	43.3	0.10	38.6
DETA_1-1E	30.3	0.08	39.9
Average	39.3	0.09	34.2
Standard dev	10.4	0.03	5.4
Relative Sdev	0.3	0.33	0.2

S_{BET}: surface area, V_{TOTAl}: total pore volume

Table 5-2: Textural parameters obtained for repeat preparations of TETA BIAS nanoparticles

Sample ID	S_{BET}	V_{TOTAL}	Pore size
	m^2g^{-1}	cm^3g^{-1}	nm
TETA_1-1A	33.9	0.15	25.2
TETA_1-1B	23.3	0.09	16.6
TETA_1-1C	46.2	0.24	26.1
TETA_1-1D	39.7	0.18	16.2
TETA_1-1E	45.4	0.18	16.6
Average	37.7	0.17	20.1
Standard dev	9.5	0.05	5.0
Relative Sdev	0.3	0.29	0.3

S_{BET}: surface area, V_{TOTAl}: total pore volume

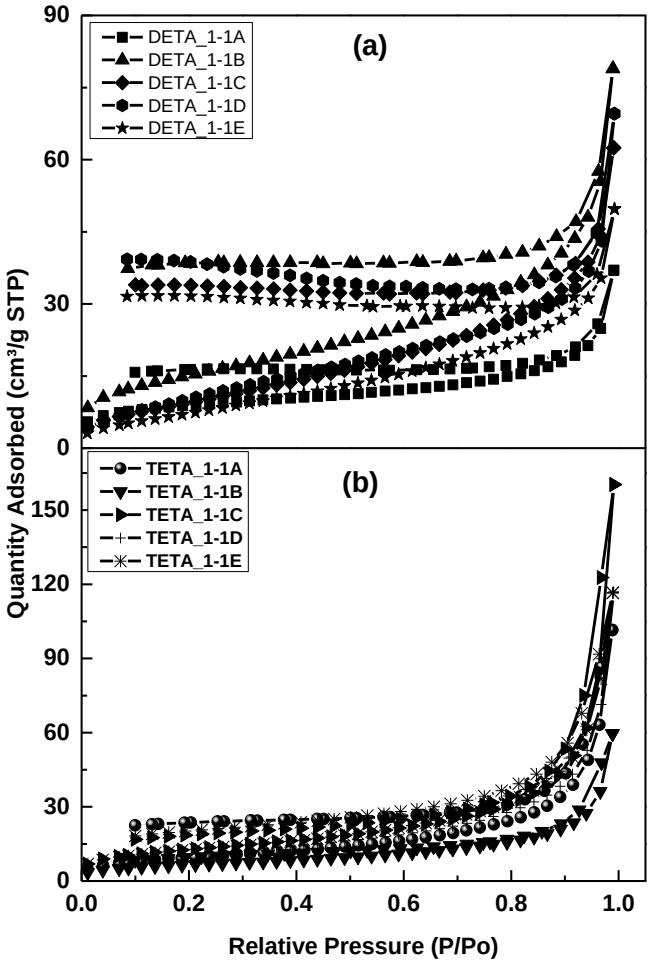

Figure 5-2: N_2 sorption isotherms for (a) DETA and (b) TETA BIAS repeats, measured at 77 K

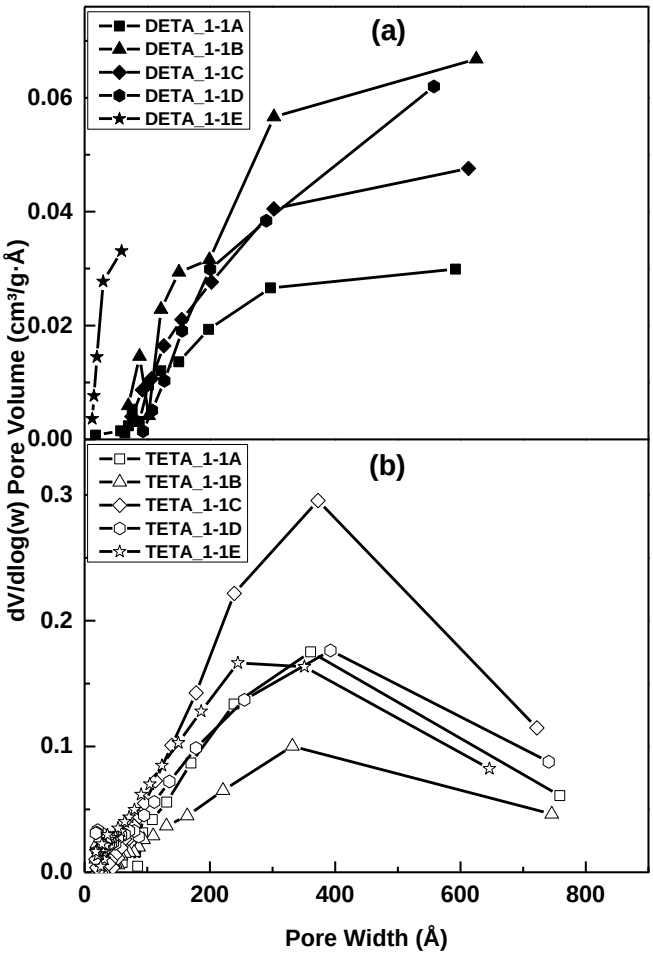

Figure 5-3**:** Pore size distributions obtained for (a) DETA and (b) TETA BIAS repeat samples.

The results presented in

Table 5-1 and Table 5-2, show little consistency within the synthetic process used, all properties, repeatable to a maximum ~33% relative standard deviation for both DETA and TETA BIAS nanoparticles. The variance observed, suggests that the materials produced are sensitive to minute variations within the synthesis method adopted, hence, repeatability within reduced error limits would be difficult and unpredictable. Elemental compositions and CO_2 sorption analyses were used to further probe the consistency of the synthesis process used.

5.1.2 Elemental analyses of DETA and TETA BIAS repeats

Ultimate analyses of BIAS repeat samples allowed N wt% to be used as an indicator of the repeatability of the chemical composition produced by the synthesis process adopted. Table 5-3 shows that, although the materials are texturally different, the chemical compositions are relatively consistent, although not entirely similar as DETA BIAS repeats show a repeatability of ~18% and TETA BIAS repeats ~13% relative standard deviation, respectively.

Table 5-3: Chemical properties for DETA and TETA BIAS repeat samples showing the N wt% from elemental analysis.

Sample ID	DETA BIAS repeats			TETA BIAS Repeats		
	wt% C	w% H	wt% N	wt% C	w% H	wt% N
1A	3.5	1.6	2.1	4.8	2	3.5
1B	2.7	1.2	2.1	4.4	1.5	3.1
1C	4	1.8	3.1	4.7	1.6	3.3
1D	2.7	1.6	2.6	4.7	1.4	3.2
1E	3.8	1.6	2.4	4.5	1.7	2.7
Average	3.3	1.6	2.5	4.6	1.6	3.2
Standard dev	0.6	0.2	0.4	0.2	0.2	0.3
Relative Sdev	0.2	0.1	0.1	0	0.1	0.1

5.1.3 CO_2 adsorption analyses for BIAS repeat samples

CO_2 capture capacities for the repeat samples were measured to determine synthetic consistency with regards sorption capacity as a key criterion for carbon capture materials. The results show only a slight variation in sorption capacity indicating that although repeat samples have a higher percentage error within the textural properties, both elemental analysis, which suggested similar nitrogen content and CO_2 uptakes (Table 5-4), as a consequence, were relatively similar, although more can be done to

improve the consistency of the synthetic route adopted, however, within this study, the large synthesis error was accepted as it did not sufficiently impact on the adsorption properties.

Table 5-4: CO_2 adsorption capacities for DETA and TETA bio-inspired silica repeats

Sample ID	DETA BIAS		TETA BIAS	
	CO_2 adsorption capacity (mmol g^{-1}) , 333 K			
	10 kPa	100 kPa	10 kPa	100 kPa
1A	0.297	0.849	0.206	0.535
1B	0.262	0.728	0.230	0.639
1C	0.256	0.807	0.189	0.563
1D	0.281	0.715	0.272	0.628
1E	0.310	0.690	0.234	0.701
Average	0.281	0.758	0.226	0.613
Standard dev	0.023	0.067	0.031	0.066
Relative Sdev	0.082	0.088	0.137	0.108

5.2 Effect of molar and amine concentration variations during synthesis

Once repeatability of the synthetic method adopted had been established, the effects of varying reagent concentrations were investigated; producing a series of materials with unique, dissimilar properties compared using N_2 sorption, elemental and CO_2 sorption analyses. Here, suites of DETA and TETA BIAS samples were prepared using silica to amine ratios in the range 1:0.1 to 1:16. Due to the similar trends observed, irrespective of amine used, on physical and chemical properties, only results for DETA BIAS samples have been presented here, with all other results presented in Appendix A, although, some complementing results from TETA are included for discussion as appropriate.

5.2.1 N_2 sorption analysis of amine varied DETA BIAS samples.

The textural properties of DETA BIAS samples, with varying amine contents, were determined by N_2 sorption at 77 K (Table 5-5). N_2 sorption isotherms and BJH desorption pore size distributions for the samples are shown in Figure 5-5. Despite the variation discussed previously, all trends were considered to be representative of the system changes, with only local magnitude affected by the deviation in sample production. A change in isotherm type was observed where the characteristic Type IV isotherm observed in DETA_1-0.2 gradually changes to a Type II isotherm, as

evident for DETA_1-0.33. This results because, as the concentration of amine is increased, BIAS nanoparticles of larger pores sizes are produced, hence, the resulting materials have broader pore size distributions, resulting in the transition from highly porous to non-porous materials, as can be seen from the gradual transition from Type IV to Type II sorption isotherms (Figure 5-4). The specific surface area (Table 5-5) reduces between DETA_1-02 and DETA_1-075; this is expected because of the formation of larger pores, although, after the initial reduction in surface areas, a plateauing was observed irrespective of the variation in Si:N ratio used; this plateau suggests that an optimized product was produced within the experimental parameters probed i.e., as DETA is incrementally added, there is eventually little or no further effect on the porous properties of the silica particles formed, either because (i) the BIAS nanoparticles are optimised, with the excess amine removed during washing or (ii) the synthetic process is self-limiting. A widening of the PSD (Figure 5-7) was observed, which suggests that larger particles are formed with incremental addition of DETA to the synthetic process, as represented by larger surface pore sizes and reduced surface area (Table 5-5)

Table 5-5: Textural characteristics of DETA loaded BIAS samples prepared

Sample ID	S_{BET}	V_{TOTAL}	Pore size
	m^2g^{-1}	cm^3g^{-1}	Nm
DETA_1-0.20	320.4	0.36	3.8
DETA_1-0.25	255.6	0.48	6.2
DETA_1-0.33	173.7	0.84	21.2
DETA_1-0.50	70.5	0.04	8.5
DETA_1-0.75	25.1	0.07	11.8
DETA_1-1	30.3	0.08	39.9
DETA_1-2	15.5	0.04	14.5
DETA_1-4	26.2	0.06	14.3
DETA_1-8	23.7	0.06	9.0
DETA_1-16	29.5	0.06	8.7

S_{BET}: surface area, V_{TOTAl}: total pore volume

A similar trend is observed with the total pore volume, with an initial increase from 0.36 – 0.84 cm^3 g^{-1}, between DETA_1-0.2 and DETA_1-0.33. Increased DETA loading outside this range showed no significant effect on pore volume. The significant reduction observed, is proposed to be the point of maximum saturation, after which, increased DETA concentration only serves to reduce the rate of silica

formation, thus allowing larger silica particles to form without considerable textural effects, supporting the earlier argument that, the BIAS nanoparticles were optimised, with the excess amine removed during washing.

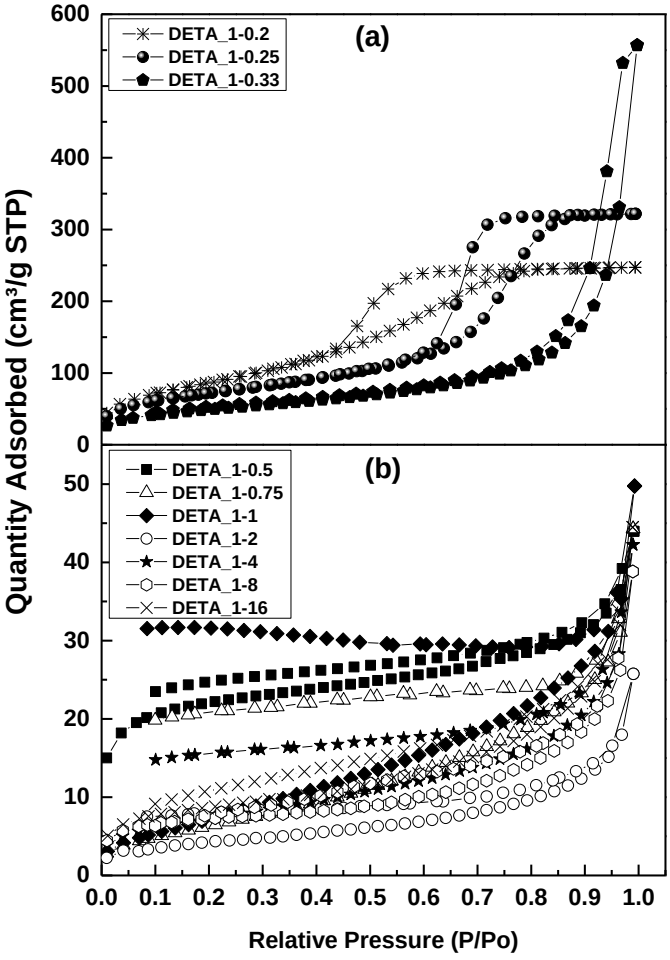

Figure 5-4**:** N_2 sorption isotherms for (a) loading of 1-0.2 and 1-0.33 and (b) loadings of 1-0.5 to 1-16 DETA loaded BIAS samples, prepared in this study.

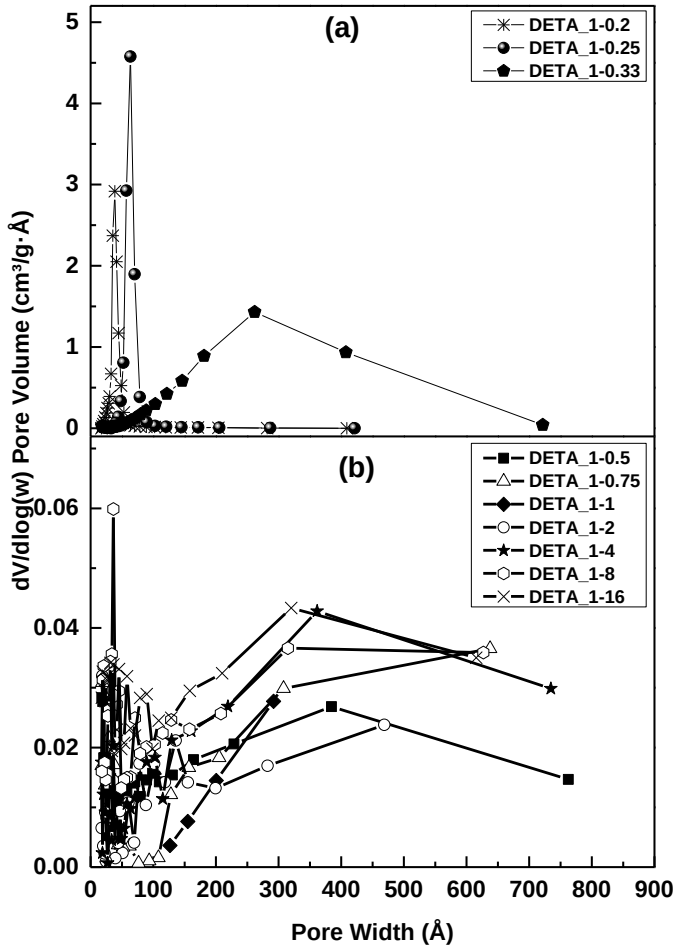

Figure 5-5: Pore size distributions for (a) loading of 1-0.2 and 1-0.33 and (b) loadings of 1-0.5 to 1-16 DETA loaded BIAS samples, prepared in this study

To further probe the effects of incremental DETA loading on the chemical properties of the samples prepared, elemental analyses were performed on DETA loaded BIAS samples. The results will provide further evidence to support either the formation of optimised particles or a self-limiting synthetic process occurring within the parameter space used.

The percentage composition of the organic constituents present in the prepared DETA loaded BIAS samples were determined by elemental analysis and the results are presented in Table 5-6; these show that the wt% of nitrogen is relatively similar for all samples, although some outliers were observed. For reference, TETA loaded BIAS samples are presented (

Table 5-7) and were consistent to within ~9% relative standard deviation. This negligible change over all samples analysed, suggests that increased amine loading has no corresponding effect on the quantity of available organics incorporated into the silica matrix during synthesis, again supporting the assumption that a saturation point exists.

Table 5-6: chemical properties for DETA loaded BIAS samples prepared in this study

Sample ID	Bio-inspired DETA loaded silica		
	wt% C	wt% H	wt% N
DETA_1-0.2	4.4	1.5	2.6
DETA_1-0.25	1.4	1.4	1.0
DETA_1-0.33	3.4	1.6	2.6
DETA_1-0.5	1.8	1.6	1.5
DETA_1-0.75	2.4	1.3	2.4
DETA_1-1	2.7	1.6	2.6
DETA_1-2	3.3	1.7	3.1
DETA_1-4	3.0	1.8	2.8
DETA_1-8	3.5	1.9	3.4
DETA_1-16	2.8	1.5	1.6

Table 5-7: chemical properties for TETA loaded BIAS samples prepared in this study

Sample ID	Bio-inspired TETA loaded silica		
	wt% C	wt% H	wt% N
TETA_1-0.25	4.5	1.9	3.3
TETA_1-0.5	4.8	1.9	3.4
TETA_1-0.75	3.8	1.9	3.3
TETA_1-1	4.8	2.0	3.5
TETA_1-2	5.3	2.2	4.1
TETA_1-4	5.8	2.1	4.0
TETA_1-8	4.5	1.9	3.3
TETA_1-16	4.8	1.9	3.4

5.2.2 N_2 sorption analysis of molar varied DETA and TETA BIAS samples prepared in this study

The textural properties of DETA and TETA BIAS samples prepared using varied molar concentration were determined by N_2 sorption at 77 K (Table 5-8 and Table 5-9). BJH desorption pore size distributions and N_2 sorption isotherms for the

samples are presented in Figure 5-7 and Figure 5-6, respectively. From the isothermal plots for the DETA and TETA BIAS series, they most closely fit Type II according to the IUPAC classification [95], which implies that there is indefinite multi-layer formation on the pore site after completion of initial monolayer formation; it is also indicative of sorbents with a wide pore size distribution, as supported by the pore size distributions presented in Figure 5-6.

Table 5-8: Textural parameters obtained for molar concentration varied TETA BIAS samples, produced in this study

Sample ID	S_{BET}	V_{TOTAL}	Pore size
	m^2g^{-1}	cm^3g^{-1}	nm
TETA_1-1	33.4	0.16	15.1
TETA_2-2	25.5	0.07	12.5
TETA_3-3	32.4	0.08	12.5
TETA_4-4	41.6	0.12	14.2
TETA_10-10	63.5	0.21	15.8

S_{BET}: surface area, V_{TOTAl}: total pore volume

Table 5-9: Textural parameters obtained for molar concentration varied DETA BIAS samples, produced in this study

Sample ID	S_{BET}	V_{TOTAL}	Pore size
	m^2g^{-1}	cm^3g^{-1}	nm
DETA_1-1	30.3	0.08	39.9
DETA_2-2	14.7	0.03	13.3
DETA_3-3	54.7	0.15	14.6
DETA_4-4	59.5	0.21	17.4
DETA_10-10	57.6	0.22	16.3

S_{BET}: surface area, V_{TOTAl}: total pore volume

Despite the noticeable increase in surface area and pore volume observed for increasing molar concentration, the relative similarities shown for the pore size distribution and N_2 sorption isotherms suggests that, variations in molarity have little or no effect on the final material texture, however, an increase in product mass was achieved as expected for increased reagent use (Appendix A). This scenario is similar to the earlier argument that an optimised reaction concentration exists, over which only slight increases in textural properties are observed, however, it should be noted that the silica to nitrogen ratio remains 1:1; hence, materials with similar characteristics would be expected. As stated above, an advantage of varying molar concentration was altering the product yield, with an increase from ~42% at

TETA_1-1 to > 85% for TETA_10-10; similar results were observed for DETA (~29% at DETA_1-1 to > 79% for DETA_10-10). Since similar textural properties were obtained, irrespective of molar concentration, it is advantageous to synthesise samples at higher molar concentrations, increasing yield without compromise of the sorbents physical characteristics. To further support scaled synthesis, chemical properties were determined using elemental analysis in conjunction with CO_2 capture potentials.

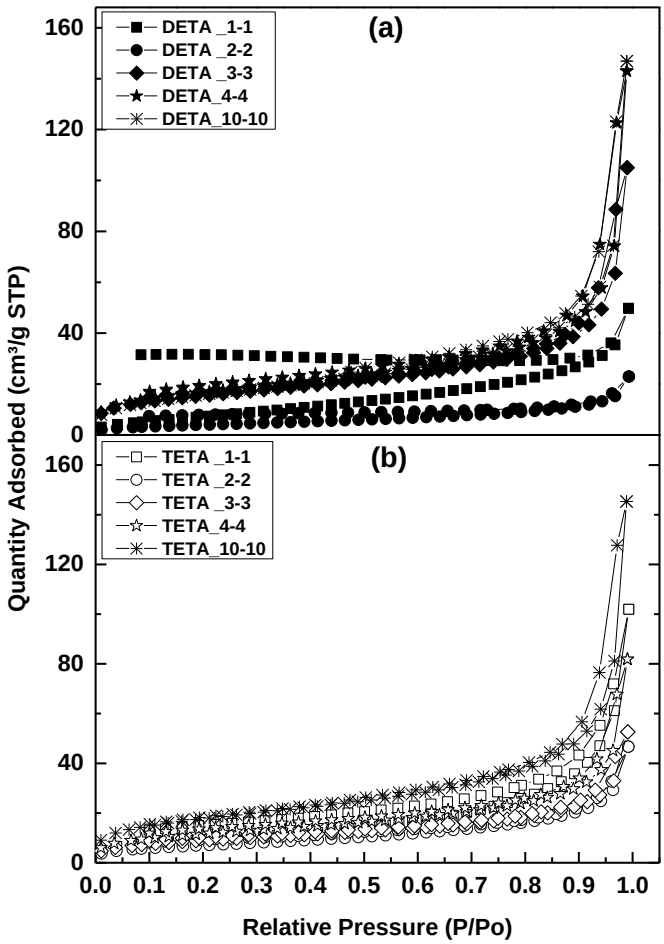

Figure 5-6: N_2 sorption isotherms for (a) DETA and (b) TETA molar concentration varied BIAS samples.

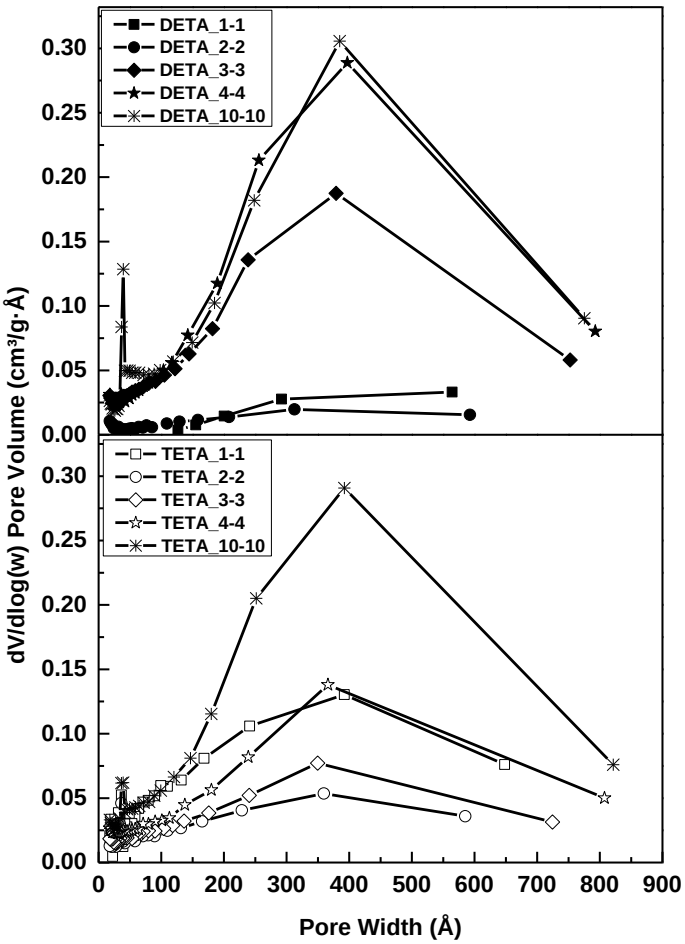

Figure 5-7: Pore size distributions for (a) DETA and (b) TETA molar concentrations varied BIAS samples, measured at 77 K

5.2.3 Elemental analyses of DETA and TETA molar concentration varied BIAS samples prepared in this study

Elemental analyses were performed on DETA and TETA molar concentration varied BIAS samples to determine the effect of increasing initial reaction concentration; the wt% of nitrogen was determined (Table 5-6 and

Table 5-7) and it was observed that, between DETA_1-1 and DETA_10-10, there was ~39% increase in the nitrogen content. A similar trend was observed for TETA molar concentration varied BIAS samples, where nitrogen content increased by ~18% between TETA_1-1 and TETA_10-10.

Table 5-10: Chemical properties for the molar concentration varied DETA BIAS samples prepared in this study

Sample ID	wt% C	wt% H	wt% N
DETA_1-1	2.7	1.6	2.6
DETA_2-2	3.2	1.9	2.7
DETA_3-3	3.3	1.6	2.8
DETA_4-4	4.2	2.0	3.4
DETA_10-10	4.3	2.8	3.6

Table 5-11: Chemical properties for the molar concentration varied TETA BIAS samples prepared in this study

Sample ID	wt% C	wt% H	wt% N
TETA_1-1	4.8	2.0	3.5
TETA_2-2	4.9	2.1	3.5
TETA_3-3	5.3	2.3	3.9
TETA_4-4	5.2	2.3	3.9
TETA_10-10	6.1	2.3	4.2

5.2.4 Effects of DETA and TETA molar concentration variations on CO_2 adsorption capacities on samples prepared in this study

CO_2 adsorption studies were performed to determine the effect of varying both molar and amine concentrations on the sorbents affinity for CO_2 at the pressure analysed (10 or 100 kPa). From Table 5-12, as molar concentration increases, equilibration time also increases (Appendix A), suggesting that CO_2 diffusion into the pores is restricted, either by diminished material integrity, or as the result of synthetic complications caused by increased poly-condensation of silica at high reaction concentrations affecting the final reaction pH, i.e. the surface charge of the sorbent and the degree of ionisation of adsorbate [153] causing a reduction in CO_2 diffusion. Although increased molarity increased nitrogen content slightly, this does not reflect on incremental increase in the materials total CO_2 capacity (Figure 5-8), as the estimated instantaneous capacities are similar. The increased interaction between the adsorbate and the adsorbent via nitrogen species, allowing increased adsorption to occur, does reflect slightly in the performance observed for 10 kPa, while, at 100 kPa, the effect of increased CO_2 diffusion into the pores is more prevalent. This is so because for physical adsorption processes, the extent of adsorption increases and

reduces with pressure; hence, the effect of surface chemistry on the overall sorption capacity becomes negligible as pressure increases.

Table 5-12**:** CO_2 adsorption capacities and equilibration times for molar concentration varied DETA BIAS nanoparticles

Sample ID	DETA BIAS		TETA BIAS	
	CO_2 adsorption capacity (mmol g^{-1}) , 333 K			
	10 kPa	100 kPa	10 kPa	100 kPa
1-1	0.163	0.535	0.206	0.535
2-2	0.214	0.484	0.280	0.553
3-3	0.213	0.448	0.329	0.570
4-4	0.190	0.412	0.393	0.617
10-10	0.323	0.511	0.302	0.566

Similar results were observed when the CO_2 adsorption capacities of amine varied BIAS samples were analysed, no significant effect on the materials affinity for CO_2 was observed (Table 5-13), with only slight variation in the equilibrium values, but similar total working capacities. It was originally anticipated that increasing the amine concentration during synthesis would increase the amine content in the materials, ultimately increasing the materials CO_2 capacity by incorporating more basic nitrogen groups during synthesis, but this was not the case, based on the present synthetic method adopted, as a maximum amount of amine could be incorporated into the silica structure, after which additional amine present only affected the physical properties.

Table 5-13: CO_2 adsorption capacity for amine loaded DETA and TETA BIAS nanoparticles

Sample	CO_2 capacity (mmol g^{-1})	CO_2 capacity (mmol g^{-1})
	10 kPa	100 kPa
DETA_1-0.25	0.108	0.338
DETA_1-0.5	0.163	0.471
DETA_1-1	0.163	0.535
DETA_1-2	0.214	0.552
DETA_1-4	0.221	0.589
DETA_1-8	0.236	0.594
DETA_1-16	0.101	0.432
TETA_1-0.25	0.194	0.422
TETA_1-0.5	0.223	0.523
TETA_1-1	0.206	0.535
TETA_1-2	0.262	0.640
TETA_1-4	0.171	0.494
TETA_1-8	0.275	0.660
TETA_1-16	0.226	0.590

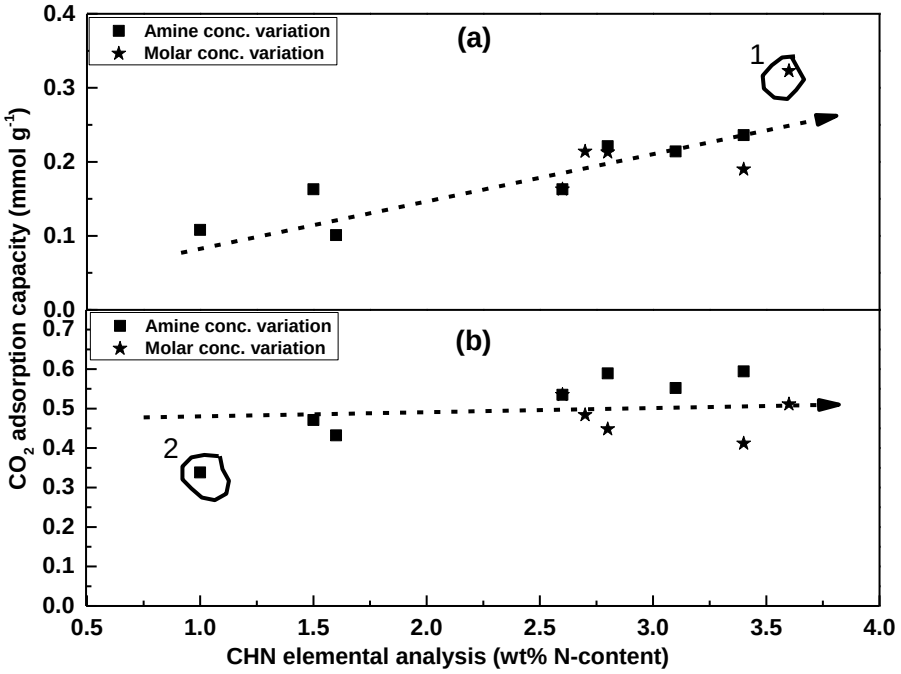

Figure 5-8: Effect of nitrogen content on CO_2 adsorption capacities of amine and concentration varied BIAS nanoparticles measured at 333 K ((a) 10 kPa and (b) 100 kPa, with 1 and 2 outliers)

5.3 Effects of amine modification on BIAS production

Once the material synthesis was proven to be consistent and reproducible with regard to adsorption behaviour, within the limits of this study, material optimisation was investigated and detailed characterisation performed with comparison to a calcined standard. Calcination was performed at 823 and 1027 K to effectively remove any amine incorporated into the silica structure, thus, serving as a reference point for future comparative studies. DETA_1-1 was synthesised on a large scale (500 ml) and used as a stock sample for analysis to ensure consistency of the characterisation techniques employed.

5.3.1 Effect of calcination on the textural properties on DETA_1-1 (500 ml)

Calcination was performed to investigate the influence of amine incorporation into the silica matrix on both the physical and chemical properties. N_2 sorption at 77 K was used to determine how the removal of amine affected the sorbents textural properties (Figure 5-9 and Table 5-14); there was no significant change observed for samples before and after calcination with similar isotherms and pore size distributions obtained and only the development of micropores at a calcination temperature of 823 K causing a marked increase in surface area and overall nitrogen adsorbed, suggesting that heat treatment to remove nitrogen functionalities did not necessarily affect the porous structure either because the energy required to break the bonds formed between both species is low or the nitrogen functionalities are distributed on the surface of the silica, hence, during heat treatment, they are readily removed. FTIR analysis was conducted before and after calcination to identify the functionalities present to further probe these proposed mechanisms.

Table 5-14: Effect of calcination on the textural properties of DETA 1-1 (500 ml)

Sample	S_{BET}	V_{TOTAL}	Pore size
	m^2g^{-1}	cm^3g^{-1}	nm
DETA 1-1_{cal} (823 K)	112.7	0.12	10.4
DETA 1-1_{cal} (1273 K)	20.4	0.06	16.1
DETA 1-1	25.9	0.07	13.2

S_{BET}: surface area, V_{TOTAl}: total pore volume

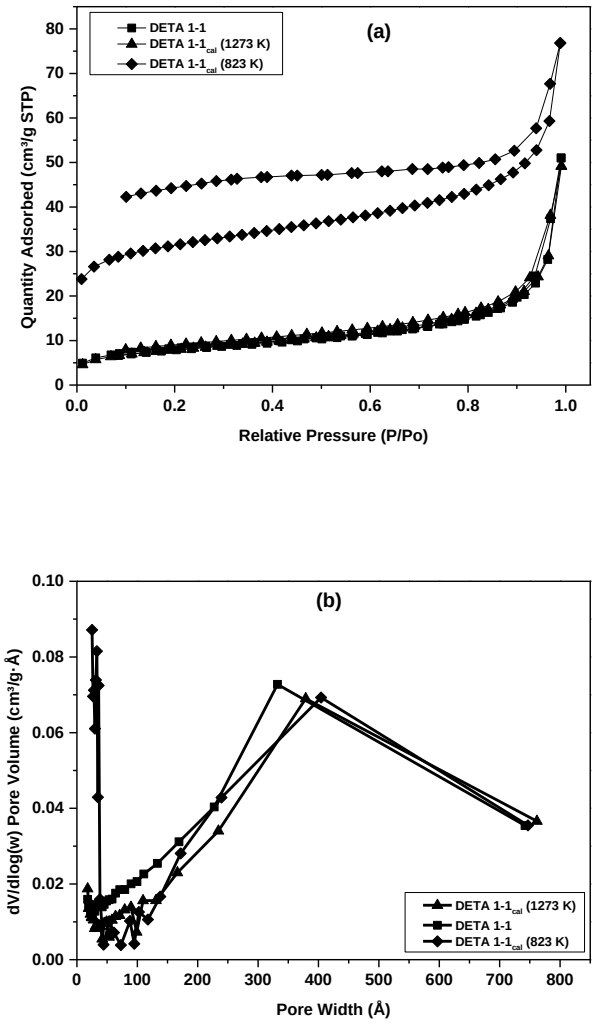

Figure 5-9: (a) N_2 sorption isotherms and (b) pore size distributions for calcined DETA 1-1 compared with DETA 1-1 BIAS samples.

5.3.2 Elemental analysis of DETA 1-1 (500 ml) and calcined DETA_1-1 (500 ml) samples prepared in this study

Ultimate analyses for calcined and as-synthesised DETA_1-1 (500 ml) were performed (Table 5-15). The data show that, upon calcination at temperatures up to 823 K, there is a significant decrease in the corresponding wt% of carbon, hydrogen and nitrogen, with ~95% of the amine incorporated into the silica matrix removed during calcination.

Table 5-15: Elemental analysis of DETA_1-1 (500 ml scale) and calcined DETA_1-1 (500 ml scale)

Sample ID	wt% C	wt% H	wt% N	CO_2 capacity (mmol g^{-1})	CO_2 capacity (mmol g^{-1})
				10 kPa	100 kPa
DETA_1-1	3.1	1.6	2.6	0.237	0.683
DETA_1-1_{cal}(823 K)	0.2	0.4	0.1	0.024	0.156

5.3.3 FTIR analysis of BIAS (TETA and DETA), DETA 1-1 (500 ml) and calcined DETA 1-1 (500 ml) samples prepared in this study

FTIR spectra for selected samples are presented in Figure 5-10, which shows absorption peaks at 798 and 1067 cm^{-1} representing Si-O-Si symmetric and asymmetric stretching vibrations, respectively; these indicate the presence of silica within the materials analysed. The peak observed at 957 cm^{-1} can be attributed to -Si-OH (silanol group), while peaks at 2330 and 2360 cm^{-1} represent the anti-symmetric stretching band of physisorbed CO_2 and the vibration of gaseous CO_2 [154], respectively. The presence of nitrogen functional groups within the synthesised material is indicated by absorption peaks at 1460, 1530 and 1634 cm^{-1}, with the peaks representing, -CH_2 scissoring mode, -NH_2 asymmetric and symmetric bending of the primary amines, respectively [118, 155].

Upon calcination, absorption peaks previously attributed to the presence of amines disappeared, leaving just the Si-O-Si peaks, which confirm that the nitrogen functional groups had been removed via calcination at the temperatures investigated.

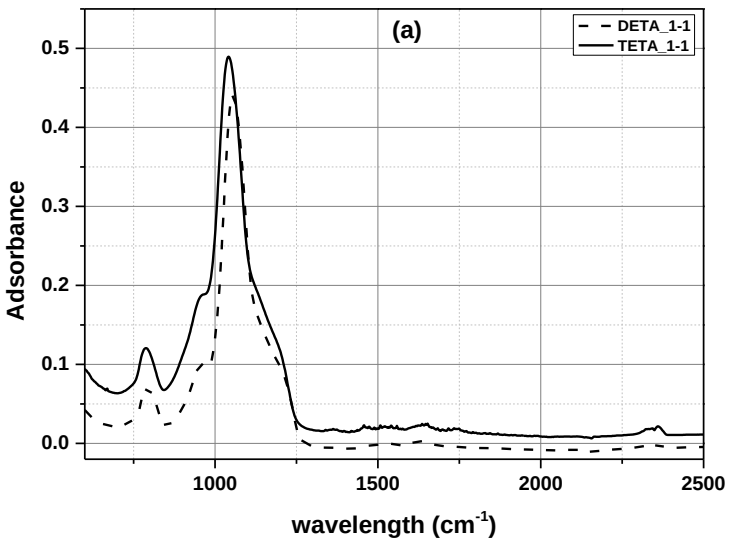

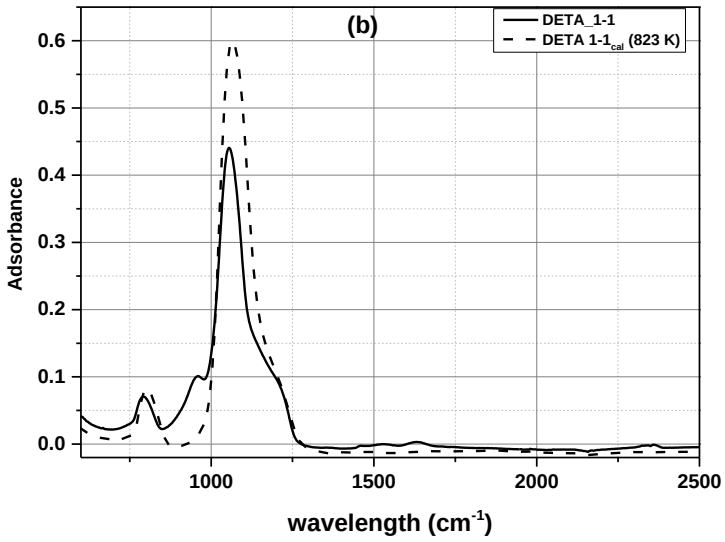

Figure 5-10: IR spectra for (a) DETA and TETA BIAS nanoparticles, and (b) DETA_1-1 and DETA_1-1_{cal} (823 K).

5.3.4 TGA and DSC analyses of DETA1-1 and TETA1-1 BIAS sample prepared in the study

Thermal stabilities of both DETA_1-1 and TETA_1-1 BIAS were investigated and typical traces are presented in Figure 5-11, showing the effect of elevated temperatures on the decomposition of the sorbents analysed. From the TGA plot (Figure 5-11), DETA_1-1 is seen to lose ~17 wt%, while TETA_1-1 loses ~16 wt%, and both losses are ascribed to the loss of physisorbed water, volatiles, amine and salinol groups. Three main mass losses were observed on the TGA and DSC profiles, the first step occurs within the temperature range of ambient to ~393 K (desorption of physisorbed water and/or volatiles e.g. atmospheric CO_2 [156]), the larger pore sizes of DETA_1-1 (Table 5-8) showed a higher wt% loss for this step compared to TETA_1-1 (Table 5-9) suggesting that the pores are more accessible to atmospheric contaminants (volatiles). The second step, between 433 and 559 K is due to the decomposition of molecular water and organic matter, while the final step, between 600 and 740 K, was principally due to the loss of organic materials, in this case DETA/TETA. Negligible mass loss was observed at temperatures above 960 K, suggesting that the decomposition of any organic matter present was complete. Both DETA and TETA BIAS samples exhibited good thermal stability within the lower temperature range used (≤ 400 K), before decomposition began, continuing even

after the boiling point of DETA (477 K) and TETA (538 K) up to 790 K, suggesting that although there was significant loss of organic groups at higher temperatures, a high thermal stability exists which provides a large working temperature range for the samples within an industrial context.

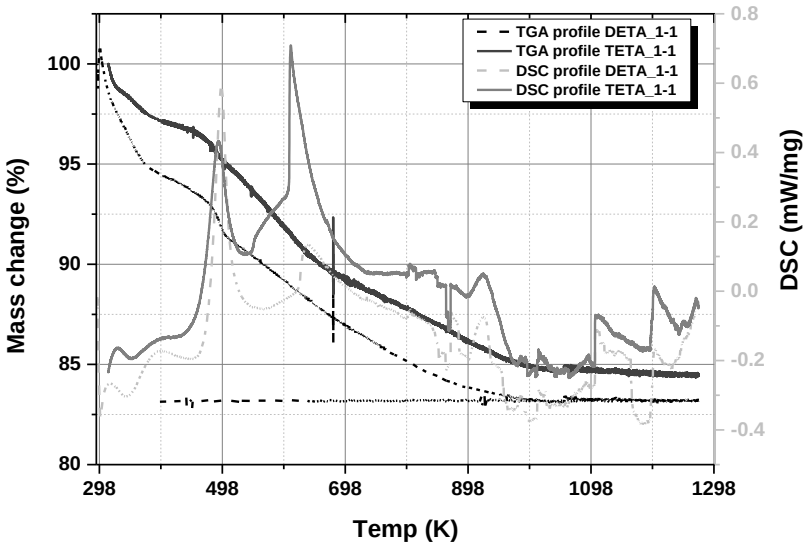

Figure 5-11: DSC-TGA thermographs of DETA and TETA BIAS samples (ambient to 1273 K).

5.4 CO_2 adsorption analysis on DETA_1-1 (500 ml) and calcined DETA_1-1 (500 ml) BIAS samples prepared in this study

CO_2 adsorption studies were performed using an IGA system, allowing both equilibrium uptakes and kinetic data to be evaluated. Isothermal measurements were conducted at 333 K (10 and 100 kPa). These conditions best simulate the process gases requiring remediation; flue gas desulfurisation produces a partial pressure of between 10 and 15 kPa CO_2 at a stream temperature of 333 – 348 K [157]. CO_2 sorption analysis was used to determine the effect of amine functionalisation on the sorbents CO_2 affinity. CO_2 capacities for both sorbents increased with pressure; however the calcined sorbents showed a reduced affinity for CO_2 when compared with the as-synthesised species.

The CO_2 sorption data presented in Table 5-15 indicate that CO_2 adsorption capacity increased with the presence of amine; the adsorption capacity of the calcined samples is attributed to the presence of silanol groups and/or the textural properties (physisorption). Incorporation of amine functionalities is expected to increase the

interaction of acidic CO_2 molecules with the basic sites ($-NH_2$) incorporated into the silica. In theory, CO_2 interacts with an amine via N-H···O hydrogen bonding or via an interaction between the N lone pair and the C atom of CO_2 molecule, thus increasing the number of available basic sites will in essence, increase the CO_2 adsorption capacity [158] and the CHN analysis and sorption results confirm such a trend; at low pressures, we propose that there is interaction between CO_2 and the sorbents surface functional groups allowing the basic sites to react with the acidic CO_2 to form a stable carbamate, according to the zwitterion mechanism presented in Equation 1 through to Equation 4, which is reversible by either heat or vacuum.

5.4.1 Effect of temperature on CO_2 adsorption on DETA 1-1 (500 ml) BIAS samples prepared in this study

Once the effect on amine functionalisation had been established, the effect of temperature on time limited adsorption capacity was investigated at temperatures between 313 and 373 K; for each isothermal run the sorbents are allowed to equilibrate for 60 min before outgassing to vacuum, and degas at 393 K to complete the desorption process, ensuring approximately the same initial mass before subsequent adsorption at the next temperature in the sequence is followed, results are shown in Figure 5-12. At 313 K, the CO_2 sorption capacity of DETA_1-1 was 0.30 mmol g^{-1} (10kPa) and 0.66 mmol g^{-1} (100 kPa), and the uptake was seen to increase with temperature until a highest CO_2 sorption capacity was reached at 353 K, capacities achieved were 0.42 mmol g^{-1} (10 kPa) and 0.86 mmol g^{-1} (100 kPa) at 353 K.

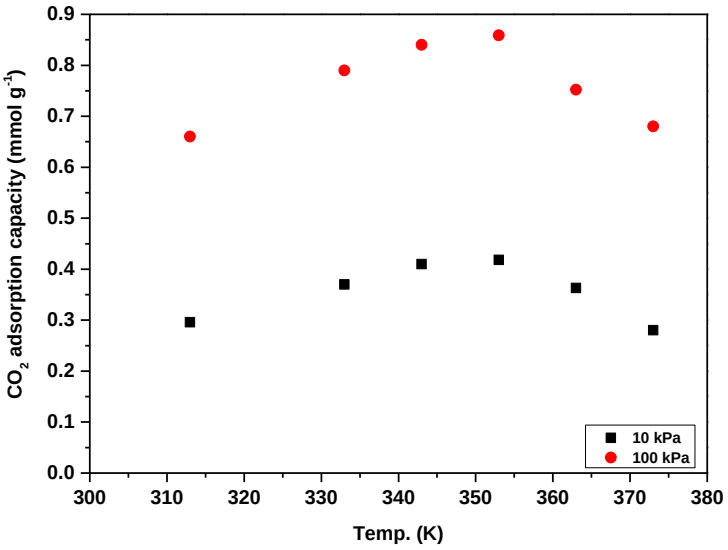

Figure 5-12: Effect of temperature on 60 min CO_2 adsorption capacities of DETA_1-1

Continued increase in temperature above 353 K, causes a drastic decrease in sorption capacity, with capacities as low as 0.28 mmol g^{-1} (10 kPa) and 0.68 mmol g^{-1} (100 kPa), recorded at 373 K. This suggests that within the temperature range 313 to 353 K, the diffusion of CO_2 in the organics sites within the silica matrix may be a sorption rate-control step with increasing temperature resulting in an increase in interactions with the number of accessible amine sites in the sorbent, thus, increased CO_2 sorption capacity. At temperatures higher than 353 K, thermodynamics may play a more important role, thus, resulting in decrease of the sorption capacity with increasing temperature, hence, a decreased sorption capacity ; similar results were achieved by Zhang *et al.* [153].

5.4.2 Ageing studies on the BIAS nanoparticles

It is essential that, not only should CO_2 capture materials be efficient and reusable, they should also be chemically and structurally stable over time, allowing for long term use. Here, ageing studies were performed to investigate the effects of time, storage and atmospheric conditions on BIAS samples. DETA_1-1 (500 ml) was used for a five month ageing study, N_2 sorption at 77 K was used to determine the effect of time on textural properties (Figure 5-13), while CO_2 sorption (333 K, and pressures up to 100 kPa) was used to investigate the influence of time on the sorbents CO_2 affinity. Figure 5-13 shows a slight reduction in the porous parameters within the time range investigated, of which the change in average pore volume was the

most significant, here a reduction of ~19% was observed between the first and the last samples analysed, the other parameters remained relatively unaffected over the time of analysis. CO_2 adsorption showed total capacity was relatively unchanged with only ≤ 1.0% variation between the first and fifth month. This suggests that the materials synthesised were not affected by time, storage or handling conditions over the time period studied, in terms of their CO_2 affinity, and the small changes in textural parameters had little effect on CO_2 uptake (Figure 5-13).

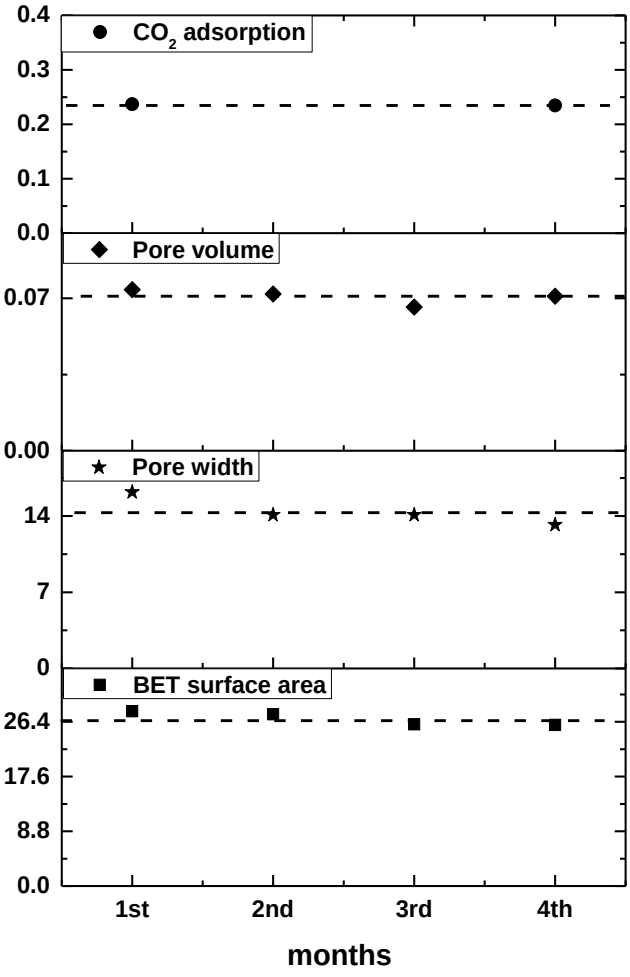

Figure 5-13: Textural properties and CO_2 adsorption data for DETA_1-1 analysed over a 5 month period.

5.4.3 Regeneration and cycling studies on DETA 1-1 (500 ml) BIAS nanoparticles

The commercial application of solid sorbents for CO_2 capture requires that adsorbents not only have high CO_2 capacity but a stable adsorption capacity with

repeated use, and constant adsorption-desorption performance for long-term use [146]. Regeneration of any sorbent involves the removal of the adsorbed species from its surface either by pressure, temperature or concentration swing desorption to restore the sorbent to its initial pristine state and to recover the desorbed species, or for general gas treatment by selective adsorption. In this study, Concentration Swing Adsorption (CSA) was used; adsorption-desorption cycling studies were carried out to determine the performance and stability of the sorbent over repeat use. The sample was exposed to 10% CO_2/90% N_2 for the adsorption step and for desorption, pure N_2 was used as purge gas; sorption was performed at 333 K (100 kPa) for 17 cycles with 60 min equilibration times between each sorption cycle, producing a CSA process method. Results show that the sorbent maintained a stable capacity up to 99% of the initial uptake over all cycles, only 11 cycles have been presented (Figure 5-14). Hence, displaying a stable and easily reversible CO_2 adsorption-desorption performance.

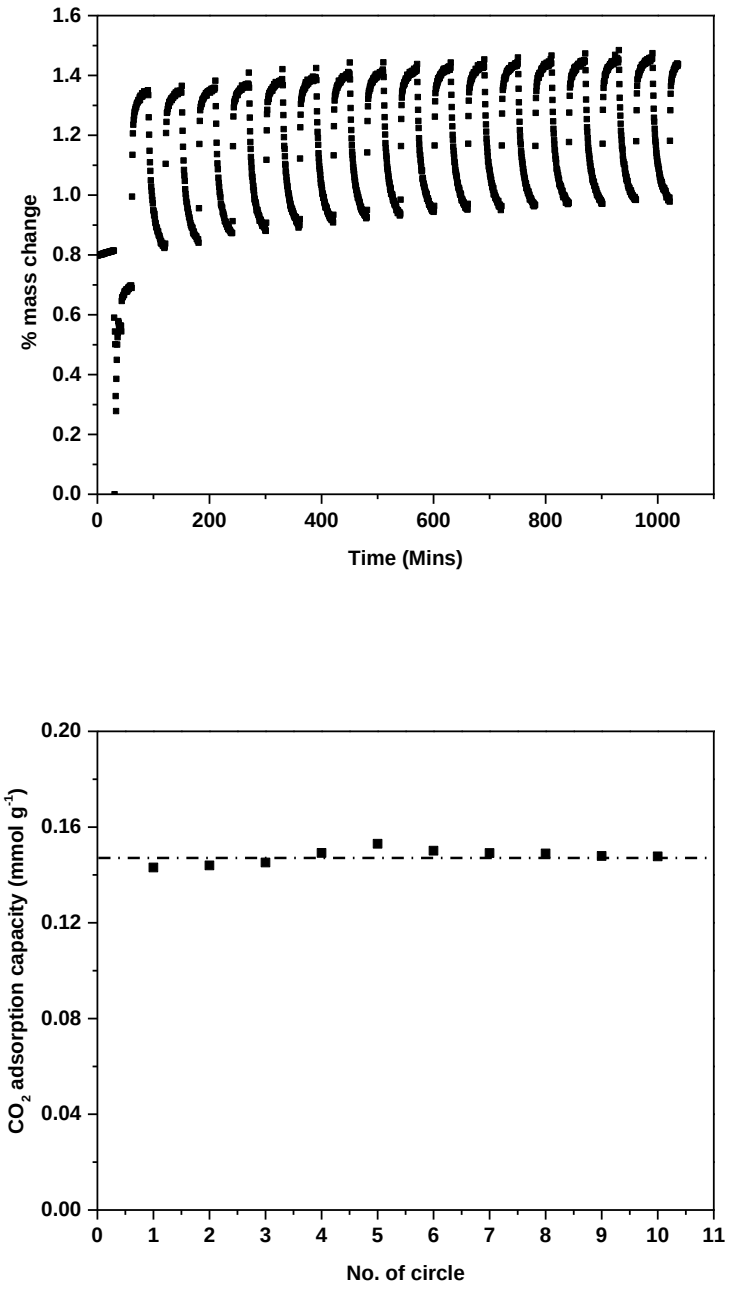

Figure 5-14: Cyclic studies using concentration swing adsorption (333 K, 100 kPa, 10% CO_2/90% N_2 and pure N_2)

5.5 Summary

In this chapter, Bio Inspired Amine Silica (BIAS) have been characterised, optimised and evaluated as novel materials capable of efficiently capturing CO_2 from flue gas streams at ambient conditions. Methods such as: N_2 adsorption analysis, CHN elemental analysis, TGA, FTIR, and most importantly, CO_2 sorption analysis were employed; the results and discussion section were divided into four sections. The

first section demonstrated consistency of the synthesis method employed, results indicated that samples were slightly reproducible, although a larger error was evident when compared with the other systems considered in this study; this is suspected to be due to the sensitive nature of the synthetic method chosen as slight variations within repeats (human errors, environmental errors and/or reaction chemistry), affected both the physical and chemical properties of the materials prepared. Although for subsequent analysis (Sections 5.3 and 5.4) a large quantity of DETA_1-1 was synthesised and analysis performed on the stock, allowing for effective comparison. Secondly, optimisation parameters for BIAS synthesis were discussed using N_2 adsorption at 77 K to evaluate how parameters, such as molar concentration and amine loading influenced the sorbents textural and chemical properties, with results suggesting that, although both parameters had little effect on the physical and chemical characteristics, increased molar concentration was preferred as it resulted in a marked improvement in material yield, increasing to > 85%. The third section discussed characterisation of the materials synthesised:

- Results from FTIR showed that new functional groups (basic amino groups) were incorporated into the silica structure (surface and pores) via the preparatory method adopted.
- Elemental analysis confirmed the presence of nitrogen within the as-synthesised BIAS nanoparticles, while TGA proposed an estimated working temperature range before DETA decomposition began.
- N_2 sorption results showed that, as DETA was progressively incorporated, there were no evident changes in textural properties, as supported by elemental analysis, which showed the incorporation of amine into the silica matrix reaches a maximum amount after which incremental addition of amines did not significantly affect the porous structure.

Finally, the effect of amine modification on CO_2 adsorption was investigated in the fourth section, with the general trend that the presence of nitrogen functional groups within the silica structure greatly improved the materials affinity for CO_2, when compared with its calcined counterpart, which was texturally more defined (large surface area and pore volumes). Ageing, sorbent regeneration studies and the effect

of temperature on the sorbent CO_2 capacity were also investigated and results reported indicate that time has little effect on both the materials texture and affinity for CO_2 while the overall CO_2 capture potential is influenced by both physical and chemical parameters.

CHAPTER 6 (RESULTS AND DISCUSSION II)

AMINE IN SITU-IMPREGNATED SILICA (AIIS) FOR CO_2 CAPTURE

6 INTRODUCTION TO AMINE IN SITU-IMPREGNATED SILICA (AIIS) FOR CO_2 CAPTURE

CO_2 capture and storage, especially from anthropogenic sources, is of critical importance in mitigating against the effects of greenhouse gases on global climate change [13, 17]. There is a growing interest in developing technologies for efficient capture and sequestration of large quantities of CO_2, which involves a three step process: capture from primary emission sources, transportation and, finally, sequestration or reuse. Capture of CO_2 involving the use of PCCC materials like, zeolites [160, 161], metal oxides, metal organic frameworks and activated carbons [161-164], is a developing technology which capitalises on key attributes, such as low energies of regeneration, high CO_2 selectivity over competing species present in flue gas streams and, most importantly, high sorption capacities coupled with fast process kinetics [163, 165]. Currently, research has focused on developing and/or improving CO_2 capture sorbents by loading aminosilanes/amines onto the materials porous structure as a promising strategy for sorbent design. To this end, two main methods have been used for material development. The most common and widely used approach involves the physical impregnation of a porous support with aminosilanes/amine species, while the second approach involves grafting and/or tethering aminosilanes/amines onto a support material, which itself must have a large surface area [73, 134, 162, 166].

To date, amine modification has been shown to increase CO_2 adsorption capacities, as amines have a high affinity for CO_2, hence, a large array of different types of primary, secondary, hindered, polymeric and silane amines have been grafted and or wet impregnated on mesoporous supports to increase CO_2 capacity; Wang *et al.* [167] reported CO_2 adsorption capacities of ~2.1 mmol g^{-1} (348 K, 100 kPa) for silica gels impregnated with ≤ 30% polyethyleneimine (PEI), Zhang *et al.* [168] impregnated tetraethylenepentamine (TEPA) on disordered mesoporous silica (≤ 60 wt% TEPA) with CO_2 capacities ~3.7 mmol g^{-1} (328 K, 100 kPa) [168], and Heydari-Gorji [162] reported adsorption capacities of ~4.7 mmol g^{-1} for 55 wt% PEI impregnated on pore-expanded MCM-41 (348 K, 100 kPa) [162]. Although useful in-terms of CO_2 adsorption capacity, these approaches all suffer similar disadvantages i.e. the use of toxic chemicals during synthesis of the support material and/or during the impregnation process itself, as amines do not covalently anchor to

silica, there is the problem of amine leaching over repeated use. There is also the issue of synthetic complexity (multi-pot processes), which makes industrial scale up uneconomical, hence it is imperative to develop materials that are simple to make (single pot processes), cost effective (cheap and easily sourced starting materials) [134, 169] and efficient (meets the required sorbent specification).

In this study, a new route for the preparation of amine modified silica, as a CO_2 capture material, was developed; diethylenetriamine (DETA) was in situ-impregnated into aggregated silica formed from the polycondensation of sodium metasilicate pentahydrate (Section 0) and the effects of amine (DETA) inclusion on both the physical and chemical properties of the prepared materials were investigated. A reaction mechanism has been proposed for the reaction between the silica gel and the amine during in-situ impregnation utilising the fact that, as previously mentioned in Chapter 2 section 2.3.1.4.2, silanol groups have shown the ability to form hydrogen bonding with Lewis bases. Hydrogen bonds can be represented as X-H····Y, where X is the oxygen atom from the silanol group and Y is any σ or д electron donor site. The silanol groups act as proton donors and can either form homo-intermolecular type H-bonds, i.e. hydrogen bonding between adjacent groups on the silica surface in which one group acts as proton donor, the other as proton acceptor, or hetero-intermolecular type H-bonds (Figure 6-1), i.e. hydrogen bonding with different species, in our case DETA (Figure 6-2);

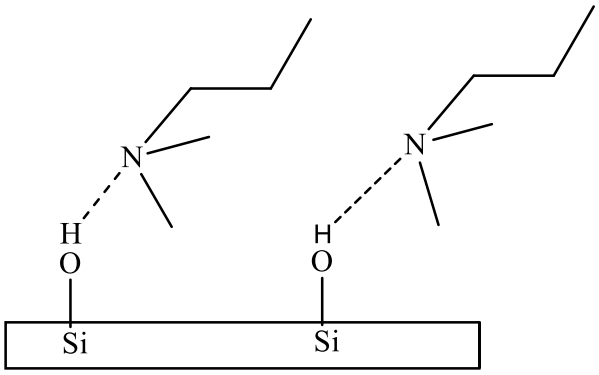

Figure 6-1: Hetero-intermolecular H-bonding between surface silanol group and amine specie.

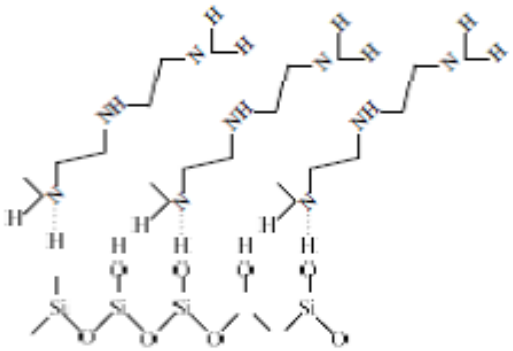

Figure 6-2: Proposed adsorbed mechanism of DETA on SiO_2 surface by H-bonding

This chapter presents the results obtained from the preparation and characterisation of Amine In situ Impregnated Silica (AIIS), as described in Chapters 3 and 4. Discussion of these results is structured into three sections; the first examines the validity of the synthesis method employed, using N_2 sorption at 77 K to determine parameters e.g. BET specific surface areas, pore volumes and pore sizes. The second examines the important characterisation results, such as functional groups present, elemental compositions, thermal stabilities, morphologies, porosities and how these properties influence material characteristics. The final section presents results from CO_2 adsorption analysis and sorbent regeneration studies, and also examines how process parameters, such as pressure and temperature, affect CO_2 capacity and overall efficiency of the synthetic method adopted.

6.1.1 Repeatability studies on synthesis method for the production AIIS nanoparticles.

To determine the repeatability of the synthesis method adopted, 6 samples, 3 each of AIIS and unmodified silica nanoparticles were prepared under otherwise identical synthetic conditions. N_2 sorption at 77 K was used to probe the textural similarities, while elemental analysis evaluated the repeatability of the elemental composition of the aforementioned materials.

6.1.2 Textural properties of AIIS and unmodified silica repeat samples prepares in this study.

The textural properties, including BET specific surface area, BJH total pore volume and average pore size of all samples prepared were determined by N_2 sorption measurements at 77 K, with results presented in Table 6-1 and Table 6-2, and Figure 6-3 and Figure 6-4. All repeats showed similar sorption isotherms, classified as Type IV, according to the IUPAC classification [95], pore size distributions, and Type H2 hysteresis loops.

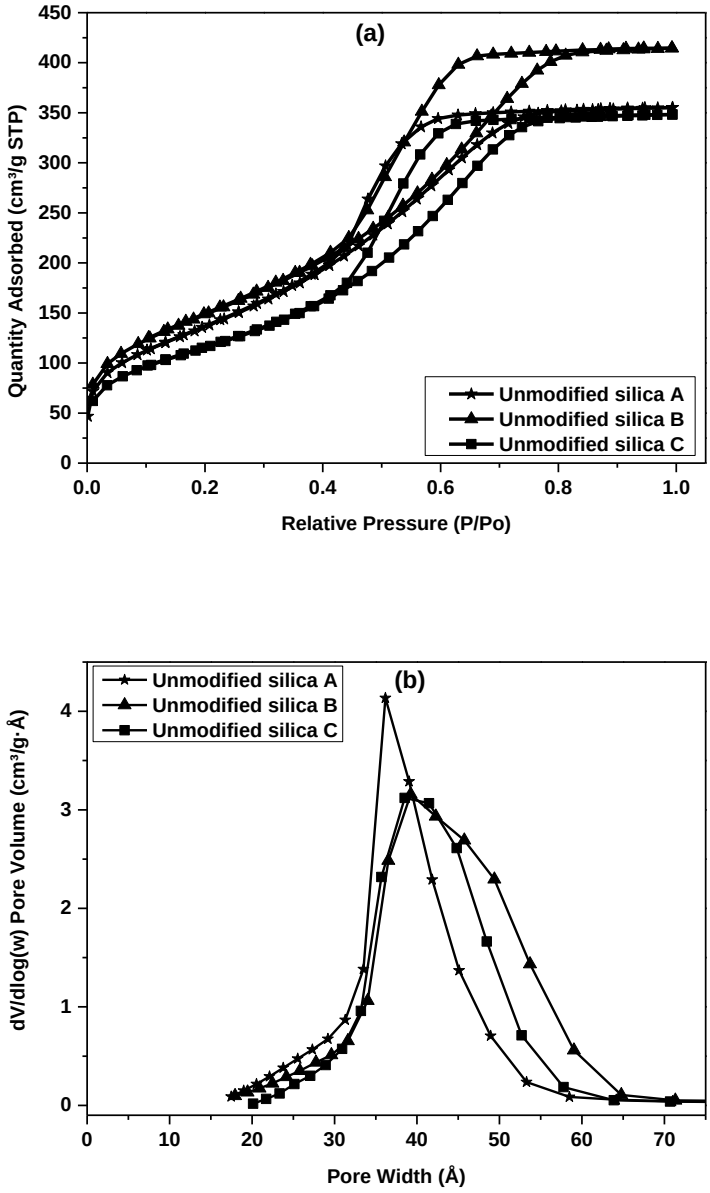

Figure 6-3: (a) N_2 sorption isotherms and (b) pore size distributions for unmodified silica prepared in this study.

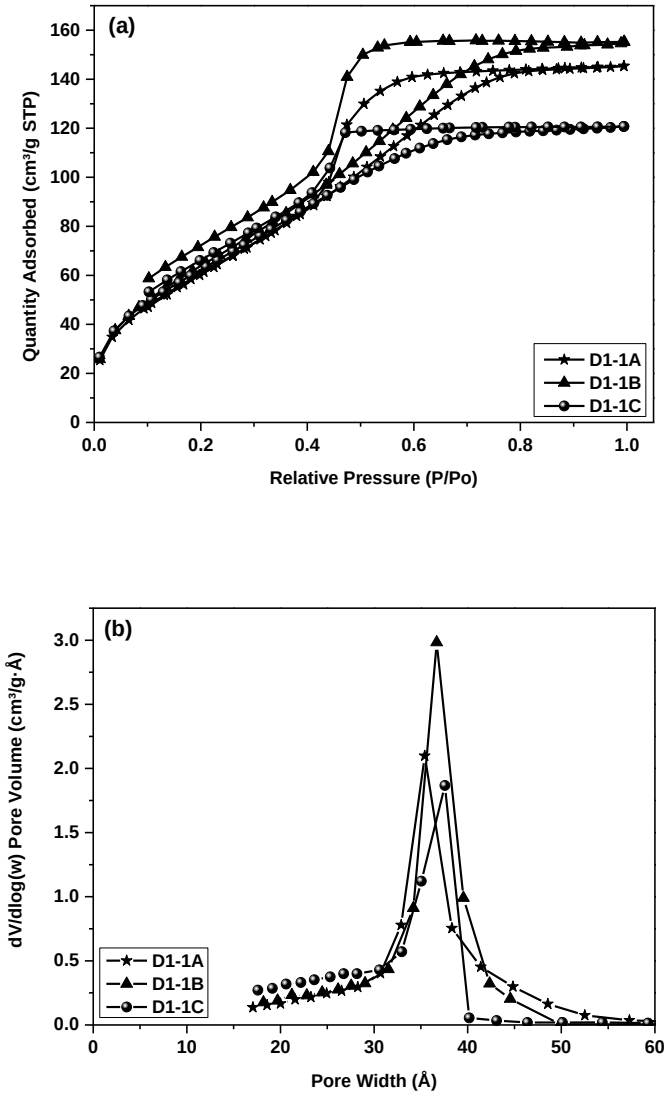

Figure 6-4: (a) N_2 sorption isotherms and (b) pore size distributions for D1-1 AIIS repeats prepared in this study.

Table 6-1: Textural parameters obtained for unmodified silica repeats prepared in this study.

Sample	S_{BET}	V_{TOTAL}	Pore size
	m^2g^{-1}	cm^3g^{-1}	Nm
Unmodified silica A	509.1	0.54	3.6
Unmodified silica B	546.0	0.64	4.0
Unmodified silica C	423.9	0.54	4.0
Average	493.0	0.60	3.9
Standard dev	62.6	0.10	0.2
Relative Sdev	0.1	0.17	0.1

S_{BET}: surface area, V_{TOTAl}: total pore volume

Table 6-2: Textural parameters obtained for D1-1 AIIS repeats, prepared in this study

Sample	S_{BET}	V_{TOTAL}	Pore size
	m^2g^{-1}	cm^3g^{-1}	nm
D1-1A	237.9	0.23	3.9
D1-1B	250.8	0.24	3.2
D1-1C	242.2	0.19	2.9
Average	243.6	0.20	3.3
Standard dev	6.6	0.03	0.5
Relative Sdev	0.0	0.2	0.2

S_{BET}: surface area, V_{TOTAl}: total pore volume

These results, demonstrate acceptable levels of consistency in the synthetic process used for the preparation of both unmodified and AIIS nanoparticles, with all porosity parameters, repeatable to a maximum of ~15% relative standard deviations for the AIIS repeats and ~17% for the unmodified silica repeats.

6.1.3 Elemental analysis for AIIS repeats prepared in this study

The N wt% of AIIS repeats, derived from ultimate analysis of the prepared samples was used as an indicator to investigate repeatability of the synthesis process. Table 6-4 shows that, although the materials are slightly texturally different with relative standard deviations ~15%, estimated for the BET surface area determined from N_2 sorption at 77 K, N wt% in AIIS (D1-1) showed consistency, with repeatability within ~8%. Hence, the synthesis method adopted, gave reproducible materials that show consistency in both porosity and elemental composition.

Table 6-3: Elemental analysis for D1-1 AIIS repeats, prepared in this study

Sample ID	AIIS (D1-1)		
	wt% C	wt% H	wt% N
D1-1A	17.6	6.0	13.0
D1-1B	18.7	6.7	12.7
D1-1C	15.2	4.3	11.2
Average	17.2	5.7	12.3
Standard dev	1.8	1.2	1.0
Relative Sdev	0.1	0.2	0.1

6.2 Effects of amine modification on AIIS production

Once repeatability of the synthesis method adopted was established, within acceptable levels of accuracy, the effects of varying the amount of DETA loaded during the in situ impregnated synthetic process on both the physical and chemical properties were investigated on the unmodified silica and D1-1AIIS.

6.2.1 N_2 sorption analysis of the unmodified and DETA in situ-impregnated silica nanoparticles prepared in this study

The effects of incremental DETA loading on the physical properties were investigated and the textural properties determined using N_2 sorption at 77 K. Table 6-4 summarises the textural properties of AIIS nanoparticles synthesised, a reduction in the sorbents textural properties was observed as the concentration of DETA increased; this is common and has been widely reported in the literature [146, 168, 170-172]. Although, D1-1 showed a deviation from the trend exhibited by the other samples, this is suspected to be the consequence of DETA forming a greater number of interactions with the silica surface silanol groups, than being deposited within the silica pores, hence, reducing associated pore blocking. Figure 6-5 and Table 6-4 show how DETA loading contributes to the partial filling of the pores, inferred from the significantly reduced amount of N_2 adsorbed, and the associated pore volume, when compared with the unmodified silica. These observations, suggest that DETA has been progressively loaded into the porous structure via in situ-impregnation, in agreement with observations by other workers studying amine loaded silica with high organic content.

Table 6-4: Surface areas, pore volumes, and average pore diameters for samples prepared within this study

Sample	[Si]:[N]	S_{BET} m^2g^{-1}	V_{TOTAL} cm^3g^{-1}	Pore size nm
Unmodified silica	n/a	546.0	0.64	4.0
D8-1	1:0.125	312.9	0.36	3.6
D4-1	1:0.25	179.5	0.20	3.6
D2-1	1:0.5	134.1	0.15	3.4
D1-1	1:1	250.8	0.24	3.3

S_{BET}: surface area, V_{TOTAl}: total pore volume

N_2 sorption isotherms of all five sorbents show similar shapes, categorized as Type IV in the IUPAC classification [95] (Figure 6-5a). The similarities in isotherm shape,

suggest that the overall porous structure of the silica was not affected by in situ-impregnation with DETA, while Type H2 [99] hysteresis loops were observed between $0.46 \leq P/P^o \leq 0.9$, signifying the presence of mesopores [173, 174]. The hysteresis phenomenon occurs because adsorbed fluids have different meniscus when they adsorbed and desorbed. Here, the probable reason for reducing hysteresis phenomena is that of pore filling by the amines specie during in situ impregnation.

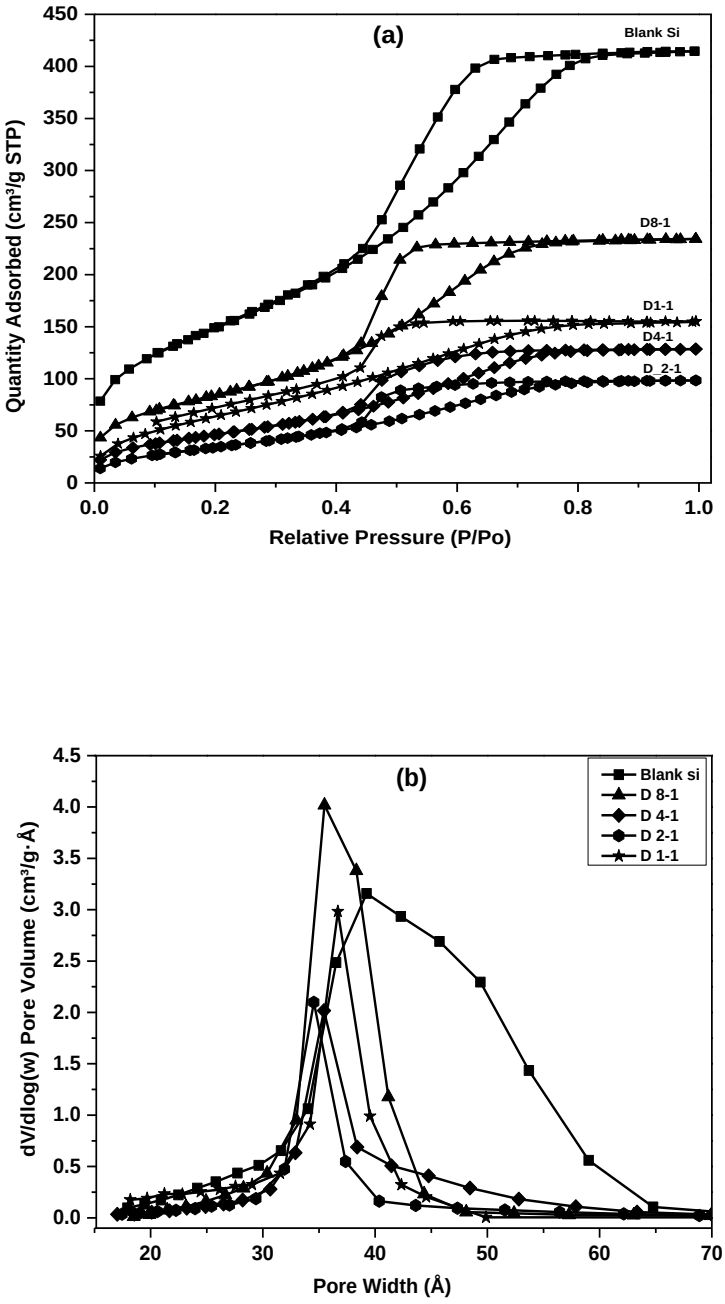

Figure 6-5: (a) N_2 sorption isotherms (b) pore size distributions of unmodified silica and AIIS samples prepared in this study

From the pore size distribution presented in Figure 6-5b, it is clear that the sorbents all show relative uniform pore sizes with the pore size curves showing a decrease in peak height and peak value with no obvious change in the shape of the distribution curve, suggesting that, although the pore volume and average pore size decrease with in situ impregnation, the pore structure was retained [170].

6.2.2 FTIR analysis of the unmodified and DETA in situ-impregnated silica particles prepared in this study

D1-1 was selected as a representative of the prepared AIIS nanoparticles (Figure 6-6) to identify new functionalities present when compared with unmodified silica.

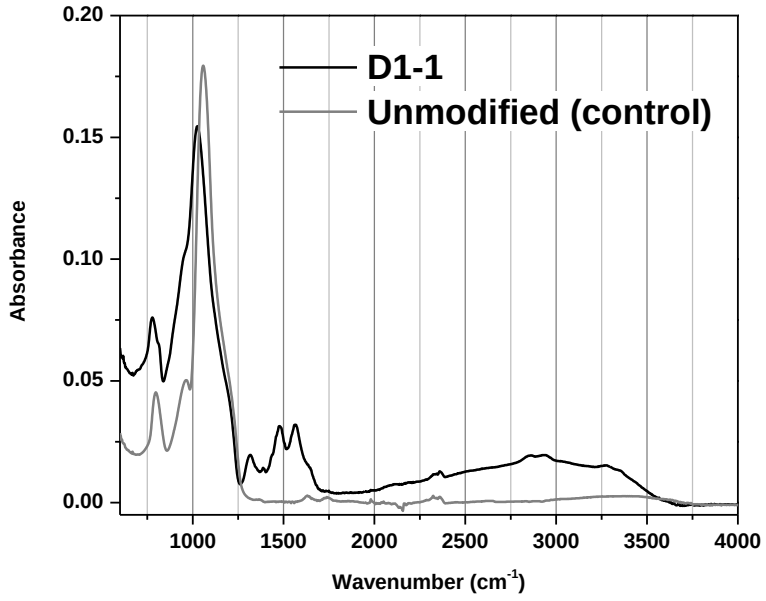

Figure 6-6: IR spectra for D1-1 and unmodified silica synthesised in this study

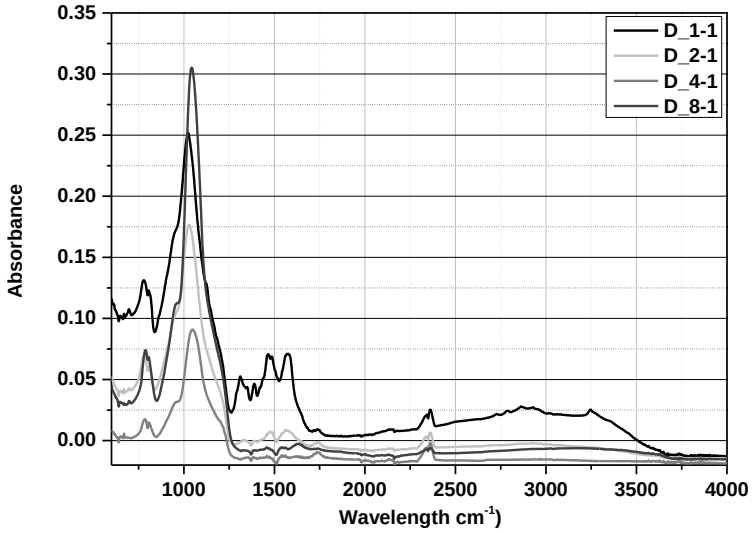

Figure 6-7: IR spectra for all AIIS samples prepared

From Figure 6-6, the FTIR spectrum of D1-1 shows several additional absorption peaks compared with that for unmodified silica, which were ascribed to the bonds resulting from DETA molecules (-NH_2 and C-N). Both samples show absorption peaks at 1065 and 795 cm^{-1}, corresponding to Si-O-Si asymmetric and symmetric stretching vibrations respectively. On in situ-impregnation with DETA, further peaks at 2300 – 2350 cm^{-1} (anti-symmetric stretching band of physisorbed CO_2 or vibration of gaseous CO_2 both arising from air) [150] were observed; absorption bands at 2969 cm^{-1} (C-H bond) and a broad band at 3280 – 3370 cm^{-1} (representing the asymmetric and symmetric stretching modes of -NH_2 groups as well as –OH vibration from adsorbed water and silanol groups) were also observed. These results suggest that some of the O-H flexing vibrations of the silanol groups were replaced by N-H stretching vibrations of amine groups, indicating that amine groups were successfully incorporated into the silica matrix [26]. This hypothesis was further supported by observation of skeletal vibrations of the NCOO absorption peaks at 1320 cm^{-1}, probably due to the reaction between the sorbent and atmospheric CO_2, according to the zwitterion mechanism [41, 167], where amines reacts with CO_2 to form a carbamate [155] (Figure 6-8).

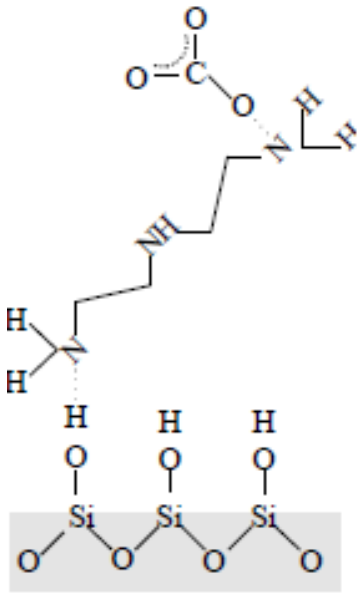

Figure 6-8: Proposed reaction mechanism between CO_2 and AIIS nanoparticles

IR spectra for selected samples are presented in Figure 6-7, to demonstrate the effect that DETA in situ impregnation had on peak intensity of the new functionalities incorporated via the synthetic route chosen; bands attributed to the presence of amino functional groups are observed and become more distinct with increasing DETA concentration from D8-1 to D1-1, suggesting that more amino functional groups are incorporated with increased DETA loadings.

6.2.3 Ultimate analyses (elemental) of unmodified silica and AIIS nanoparticles prepared in this study

Ultimate analyses of AIIS and unmodified silica nanoparticles were performed to determine the effectiveness of the synthetic process with regards nitrogen wt% incorporated into the modified silica, with unmodified silica serving as a reference material. From Table 6-5, the wt% nitrogen present was seen to increase with increased DETA loading, as was expected, with loadings of ~31.17% DETA successfully in situ-impregnated D1-1.

Table 6-5: Elemental analysis and CO_2 adsorption capacities (10 and 100 kPa) for unmodified silica and AIIS samples prepared in this study.

Sample	wt% C	wt% H	wt% N	wt% Amine	Amine Conc. (mmol g^{-1})	CO_2 capacity at 10 kPa (mmol g^{-1})	CO_2 capacity at 100 kPa (mmol g^{-1})
Unmodified silica	trace	trace	trace	trace	trace	0.14	0.53
D1-1	18.7	6.7	12.7	31.2	9.08	1.14	1.78
D2-1	10.6	3.2	7.4	18.1	5.28	0.56	0.92
D4-1	6.0	3.2	4.5	10.9	3.18	0.35	0.70
D8-1	4.1	3.0	2.6	6.3	1.82	0.37	0.74

On plotting the wt% amine added against the wt% nitrogen derived from ultimate analysis (Figure 6-9), results, showed a linear correlation existed between amine loading and the subsequent wt% of amine present in the in situ-impregnated sorbent. This gave an indication that the desired quantity of amine functionality within the silica framework could be controlled and/or estimated prior to CHN analysis, provided the pore volume was not exhausted. The reliability of this correlation was tested to allow for its use as a predictive tool in estimating the wt% nitrogen from reaction concentration.

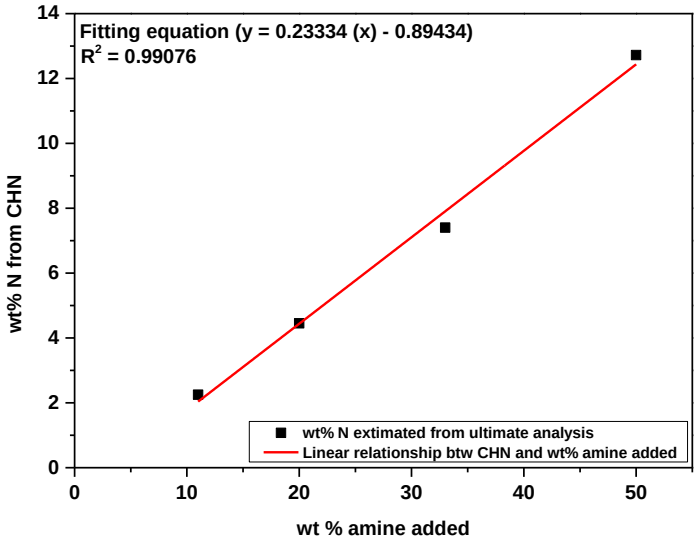

Figure 6-9: Predictive tool for estimating the wt% N pre-ultimate analysis using the linear fit between wt amine added and wt% nitrogen from CHN.

D5-1 and D7-1 were synthesised with amine loadings of 16.67 and 12.5 wt%, respectively; the correlation tool and elemental analysis were used to determine the

wt% N. Results showed that, from elemental analysis, wt% N for the prepared D5-1 sample was 3.6, while the correlation estimated a wt% N of 3.7. Similar accuracy was observed when the wt% nitrogen in D7-1 was estimated (~2.5 wt%)

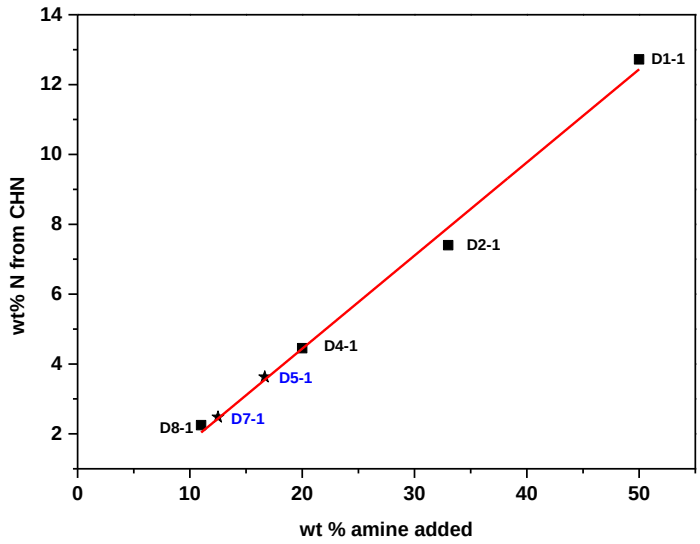

Figure 6-10: Correlation of amine loading with wt% of amine in situ-impregnated within the silica framework for materials synthesised in this study.

Knowledge of this relationship allows for the quantitative prediction of the reagents required for synthesising predetermined nitrogen content within the support materials, with accuracies of ~95% achieved.

Major factors influencing AIIS development, is the volume of acid used during synthesis and the quantity of DETA needed to in situ impregnate a predefined amount of nitrogen functionality onto the sorbent, as previously discussed.

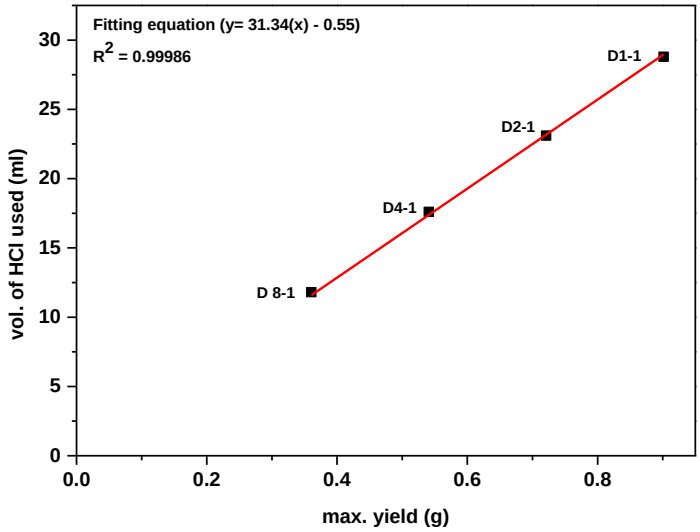

Figure 6-11: The correlation between volume of acid needed and the calculated max yield

From work undertaken on bio inspired amine silica (BIAS), a similar linear correlation exists between maximum silica yield and the volume of acid used to adjust the pH to neutral (7.00 +/- 0.05) during the acid hydrolysis step (Figure 6-11); subsequent analyses show the correlation to have an accuracy of 95 ± 4%. With the increased synthetic control offered by these two correlations, sorbents can be tailored to specification (N-content) and demand (quantity).

6.2.4 SEM analysis of the unmodified and DETA in situ-impregnated silica particles

Surface morphology was studied using Scanning Electron Microscopy (SEM) (Figure 6-12) and particles can be observed as pseudo-spherical in shape but aggregated with non-uniform sizes. The micrographs for both samples are relatively similar suggesting that, upon in situ-impregnation, the samples maintain the original morphology of the unmodified silica, insinuating that the amine does not necessarily coat the external silica surface during impregnation but fills the pore spaces during synthesis, as also comfirmed from N_2 sorption analysis (Figure 6-5). SEM analysis shows that the porous structure of silica is maintained, however, the presence of DETA appears to cause the particles to be more tightly packed with less visible voids, and greater agglomeration of smaller particles to form larger nano-sized particles is also observed.

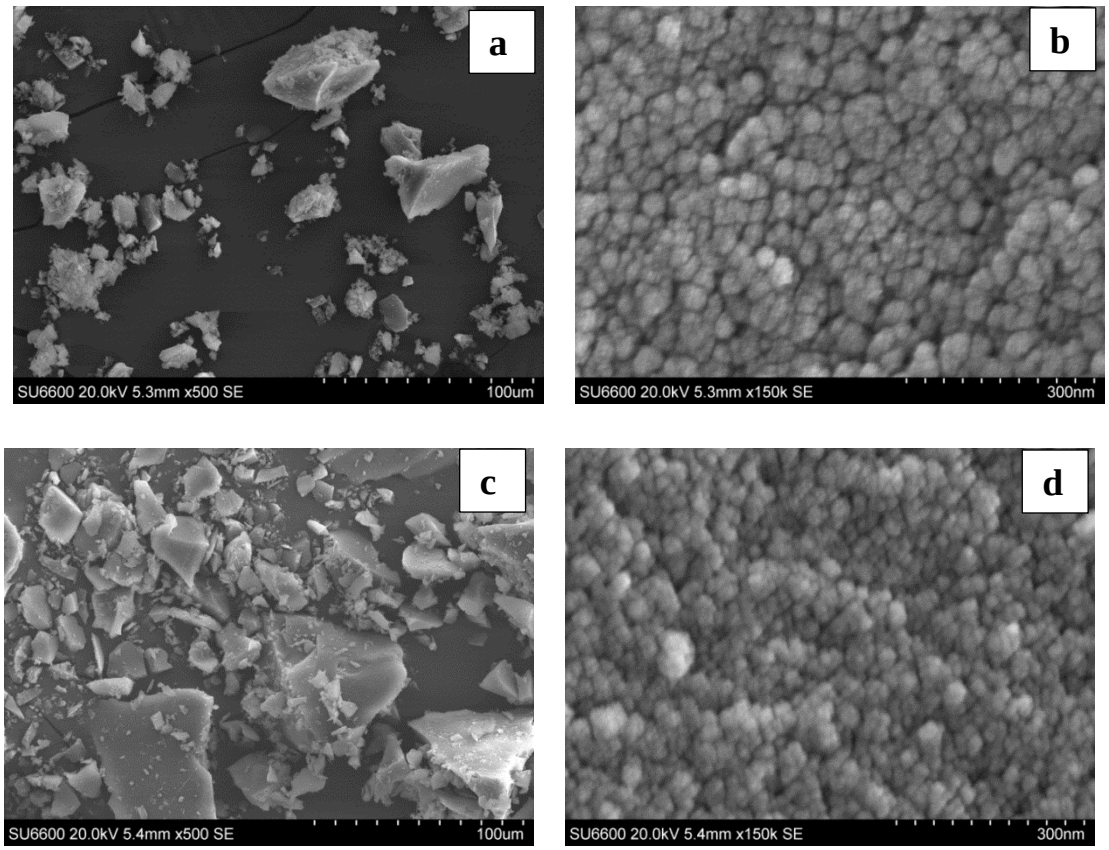

Figure 6-12: SEM images of unmodified (a + b) and D1-1 (c + d) AIIS samples prepared in this study

6.2.5 TGA and DSC analyses of unmodified silica and AIIS nanoparticles prepared in this study

Thermal analyses were conducted on D1-1 and unmodified silica (Figure 6-13), the calorimetric curve for the D1-1 shows one endothermic peak and three exothermic peaks. The initial weight loss, between 295 and 450 K, is ascribed to desorption of physisorbed water and/or volatiles e.g. atmospheric CO_2 [151]. The first two exothermic peaks, observed at 553 and 690 K, are due to the decomposition of molecular water and organic materials present, in this case DETA. The final exothermic peak, at 1073 K, is due to the decomposition of the remaining silanol groups present in the materials, the intensity and mass loss at this stage suggests that the amount of silanol present in the sample was not significant. The thermographs also show that the unmodified silica demonstrates good thermal stability in the temperature range analysed (298 – 1273 K) indicating no significant loses other than those ascribed to H_2O and silanol groups (loss occurs at all temperature). With regards thermal stability, D1-1 showed good thermal stability within the lower temperature ranges, up to 400 K, before decomposition began, continuing even after

the boiling point of DETA (477 K) up to 790 K, which suggests that although there was significant loss of organic groups at higher temperatures, the material can be used at temperatures up to 400 K.

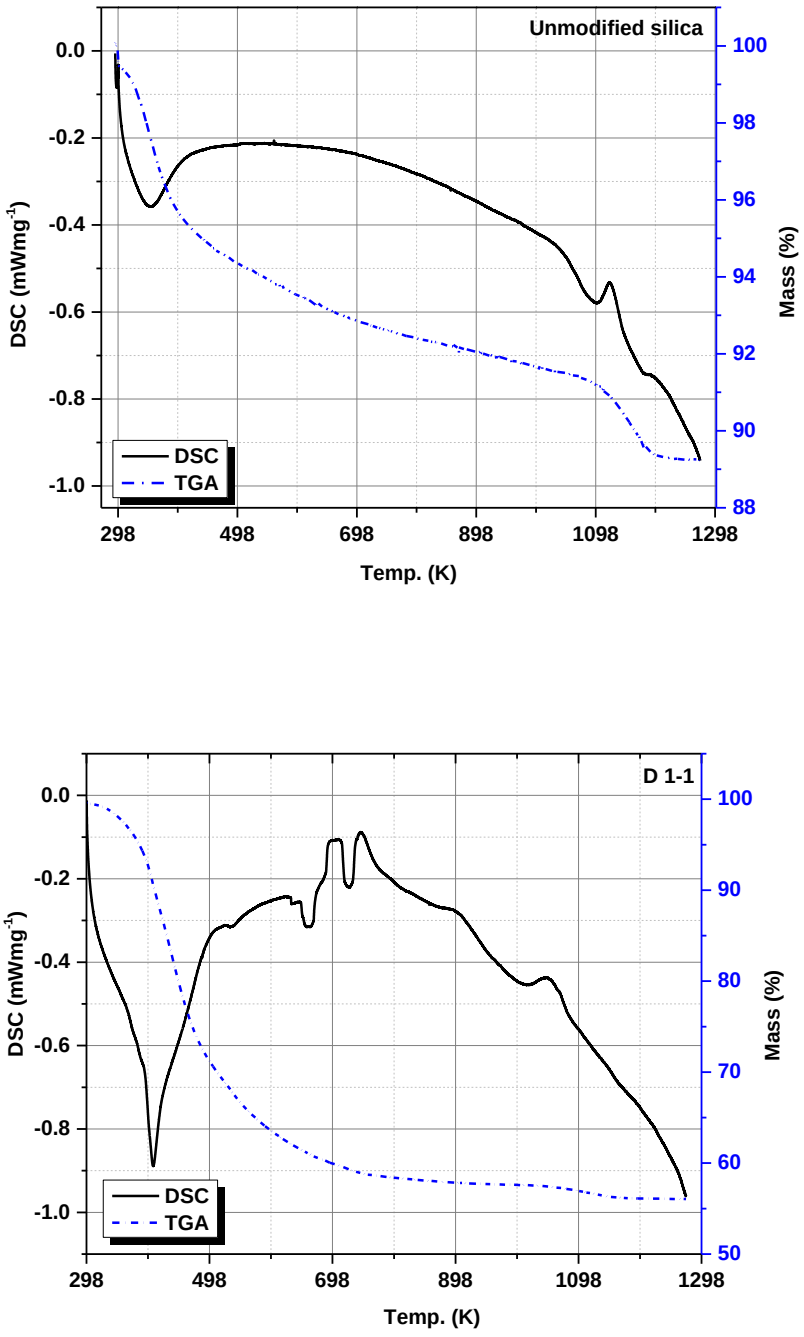

Figure 6-13: DSC-TGA thermographs of unmodified silica and D1-1 in the temperature range of ambient to 1273 K

6.3 CO_2 adsorption studies

CO_2 uptakes, with respect to pressure, were studied using an IGA system, allowing both equilibrium masses and kinetic data to be evaluated. Isothermal measurements were conducted at 333 K for 10 and 100 kPa respectively These conditions best simulate the process gases requiring remediation; flue gas desulfurisation produces a partial pressure of between 10 and 15 kPa CO_2 at a stream temperature of 333 – 348 K [175].

6.3.1 Effect of DETA in situ impregnation (wt% nitrogen) on CO_2 adsorption capacity

To investigate the effect of increasing DETA concentration on the final silica nanoparticles formed, loadings of up to 50% DETA were used within the initial reaction mixture and CO_2 adsorption studies performed on both unmodified and AIIS nanoparticles, allowing the effect of amine impregnation on sorbent CO_2 affinity to be studied. The CO_2 adsorption data, shown in Table 6-5, indicates that CO_2 capacity increases with increasing amine content, while the adsorption capacity of unmodified silica is attributed to the presence of silanol groups on the silica surface and/or the sorbents textural properties. Impregnation with amine functionalities is expected to increase the interaction of acidic CO_2 molecules with the basic sites ($-NH_2$) incorporated into the silica [26, 144, 162, 172]. In theory, an increasing number of basic sites will increase the CO_2 adsorption capacity [176] and the CHN analysis and sorption results confirm such a trend; however, a caveat of a minimum wt% amine exists (10 ± 3%) before a significant influence on CO_2 capacity is observed. As other parameters, such as surface silanol groups and a sorbents porous structure, act to normalize any contributions from the basic nitrogen groups present, it is necessary that, for there to be a notable influence on the overall CO_2 capture capacity of the material, there is good accessibility of the acidic CO_2 to the basic nitrogen groups and a significant quantity of such groups present in the material.

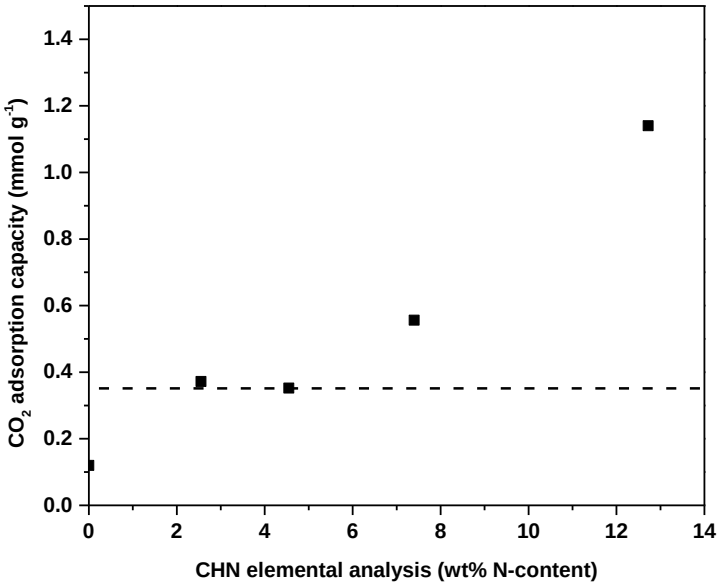

Figure 6-14: Effect of nitrogen content on CO_2 adsorption capacities on AIIS nanoparticles measured at 333 K and 100 kPa.

6.3.2 Regeneration studies of the unmodified and DETA in situ-impregnated silica by vacuum swing adsorption

The commercial application of solid sorbents for post combustion carbon capture, requires that the materials not only have high CO_2 capacities and selectivities but also stable sorption capacities with repetitive cycling [29, 146]. Here, Vacuum Swing Adsorption (VSA) was used [142]; a typical VSA cycle uses reduced pressure to shift the equilibrium position and cause desorption of adsorbed species and regeneration of the sorbent [146]. The adsorption pressure was set at 100 kPa and desorption at vacuum (0.1 kPa) then, a 60 min VSA cycle programme was performed for D1-1 at 333 K, allowing analysis over 21 cycles. Figure 6-15 shows that the CO_2 capacity reduces after the first cycle but remains fairly constant thereafter, reducing by only ~5% over the latter 20 cycles. The initial loss in capacity (~0.54 mmol g^{-1}) is attributed to the strong interaction between CO_2 and the sorbent which is not overcome by simple evacuation, complete regeneration is achieved using elevated temperature (393 K), but for this study, VSA was used for consistency of regeneration process. This retained uptake forms the new zero for adsorption and reproducible sorption behavior was observed for all subsequent cycles.

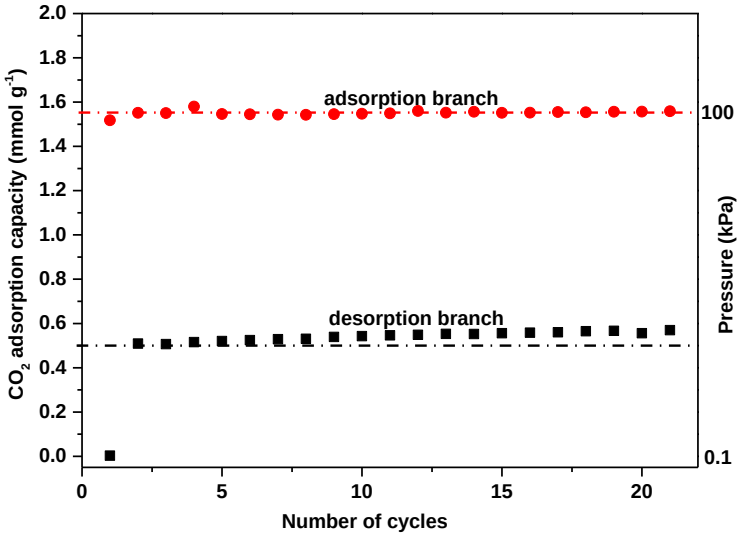

Figure 6-15: CO_2 adsorption-desorption runs on D1-1 at 333 K and 100 kPa (60 min per cycle)

6.4 Summary

The aim of this chapter was to analyse findings from the characterisation and optimisation studies conducted on Amine In situ Impregnated Silica (AIIS) as suitable sorbents for efficiently capturing CO_2 from flue gas at ambient conditions. To characterise samples prepared, methods such as: N_2 adsorption, CHN elemental analysis, TGA, SEM, FTIR and, most importantly, CO_2 sorption analysis were used; while to optimise the synthesis process, different predictive methods were adopted; the volume of acid needed and, to a large extent, the degree/quantity of amine functionalisation, were predicted using a linear correlation between amine loading and the subsequent wt% of amine present in the in situ-impregnated sorbents. The results were divided into three main sections: the first demonstrated the consistency of the synthesis method employed, with results indicating that the synthetic method was controllable and consistent with samples reproducible to a level of ~94%. Secondly, the characterisation methods discussed previously (Chapters 3-4) were used to characterise the materials synthesised:

- Results from FTIR showed that new functional groups (basic amino groups) were incorporated into the silica structure via the preparatory method adopted and as the concentration of DETA incorporated into the silica increased so did the peak intensity from the IR spectra obtained.

- Elemental analysis confirmed the presence and quantity of nitrogen within the AIIS nanoparticles, while TGA proposed an estimated working temperature range for CO_2 capture before DETA decomposition began.
- SEM micrographs showed similarities in pore structure between the modified and unmodified silica samples, this suggests the synthesis method adopted did not necessarily affect the porous structure.
- Results from N_2 sorption, showed that, as DETA was progressively added onto silica via the in situ-impregnation method, the textural properties reduced as expected until 50 wt%, most likely to be because of incomplete pore filling during impregnation.

The final section, looked at the effect of amine modification on CO_2 adsorption, and the general consensus was that the presence of nitrogen functional groups within the silica structure greatly improved the materials affinity for CO_2, when compared with unmodified silica, which was texturally superior (larger surface area and pore volume), although it possessed negligible CO_2 capture capacity.

CHAPTER 7 (RESULTS AND DISCUSSION III)

NITROGEN ENRICHED RESORCINOL FORMALDEHYDE GELS FOR CO_2 CAPTURE.

7 INTRODUCTION TO NITROGEN ENRICHED RESORCINOL FORMALDEHYDE GELS FOR CO_2 CAPTURE

Activated carbon (AC) has been extensively studied for carbon capture because of its large surface area, microporous nature, thermal/chemical stability and fast sorption kinetics [65, 177]. Current research has shown that the affinity of AC to adsorb CO_2 can be improved by modifying the surface chemistry of the carbon matrix by incorporating heteroatoms, such as nitrogen, to enhance specific adsorbate-adsorbent interactions, nitrogen within the carbon matrix can cause an increase in the number of basic groups and can also change the charge distribution on the graphene layers [66, 69, 70, 178]. Various methods have been proposed for the incorporation of these basic nitrogen functionalities within the carbon structure, including; surface coating [179, 180], use of nitrogen rich precursors within the synthesis step [134, 169, 178, 181] and post–synthetic ammonia treatment [132, 134]. However, improved sorption capacities are not guaranteed when employing these techniques because of selectivity issues, hence, it is necessary that, coupled with improved sorption, modified materials also demonstrate a marked improvement in the sorbents affinity for CO_2 when placed in a competing environment [182]. These requirements underpin the work needed to develop materials that are simple to make, cost effective [132, 183] and efficient. This chapter presents the results obtained from the preparation and characterisation of nitrogen enriched resorcinol formaldehyde (RF) organic and carbon xerogels, as described in Chapters 3 and 4. Discussion of these results is structured into three sections; the first looks at the validity of the synthesis method employed, using BET specific surface area and porosity data to evaluate synthesis repeatability. The second examines the characterisation results, including surface functional groups, elemental compositions, thermal stabilities, morphologies, porosities, and how these properties influence the overall characteristics of the materials. While the third section presents results from CO_2 adsorption and sorbent regeneration studies, with an overview of how parameters, such as temperature and pressure, influence the sorbents CO_2 capture capacity and overall efficiency.

7.1 Optimisation of nitrogen enriched (Melamine) Resorcinol Formaldehyde (MRF) xerogels

7.1.1 Effect of catalyst type on MRF xerogels formed

As discussed in Section 4.4.1.2, the amount and type of catalyst used in the gel making process influences the textural and morphological properties of the final material; from the literature, sodium carbonate (Na_2CO_3) is the most common catalyst used, acting as a base during the polymerisation reaction between resorcinol and formaldehyde. Na_2CO_3 influences the creation of ionized resorcinol by hydrogen abstraction from one of the two OH groups present in the resorcinol ring. The ionized site then acts as a site for monomer growth, hence, the final structure and properties of the gel formed depend mainly on the overall amounts of catalyst added during synthesis [184]. The ratio of resorcinol (R) to catalyst (C_t) (R/C_t) was used as an indication of the quantity of catalyst present within the gel mixture; increasing ratios indicated decreased catalyst quantities, and for decreased ratios, the reverse case. Generally, gels formed using low R/C_t ratios gave rise to dense gels [182] with smaller particles and pore sizes, and the reverse is observed for gels formed with higher R/C_t ratios [94, 114, 185-187].

Torres *et al*. [186] employed five different Group I carbonate catalysts to study the effect of catalyst on the textural properties of the final gels [136, 186], a similar approach was adopted here to investigate and justify the use of Na_2CO_3 as the catalyst of choice for MRF synthesis. Torres *et al.*[186], stated that the gelation time increased with cation size (i.e. moving down Group I from lithium to caesium), and that this favoured the aggregation of primary particles into clusters, which developed gels with larger pore sizes and volumes. Table 7-1, shows that, for the first three catalysts chosen, (lithium, sodium and potassium carbonate) there was no significant impact on the textural properties of the materials produced, only a slight increase in the average pore size and total pore volume working down the series. However, the use of caesium carbonate caused significant changes, including a drastic reduction in the surface area, related to the larger pore sizes, although, in contrast, the total pore volume was considerable larger. These observations were in agreement with work carried out by Torres *et al.* [186], where Na_2CO_3 was adopted as the catalyst of choice for two main reasons: the first was that, Na_2CO_3 is the most widely reported alkaline catalyst used for RF polymerisation, and the second is that, with regards to

textural properties of the gels formed in comparison to other Group I catalysts, there was no significant change in porosity. N_2 sorption measurements at 77 K for the gels prepared in this study, support this observation as Li, K and Na cations show similar isotherms (Type IV [95]) and narrow pore size distributions, with Cs cations a notable exception in the series. Similar observation have been made by co-workers for non-modified gels [188, 189].

Table 7-1: Textural characteristics of organic aerogels made with different catalysts prepared in this study

Sample	S_{BET} m^2g^{-1}	V_{TOTAL} cm^3g^{-1}	V_{MIC} cm^3g^{-1}	Pore size nm
Li_2CO_3_100 (10%)	461.5	0.67	0.03	6.2
Na_2CO_3_100 (10%)	432.7	0.68	0.03	6.7
K_2CO_3_100 (10%)	434.3	0.76	0.03	7.6
Cs_2CO_3_100 (10%)	194.6	1.44	0.03	38.1

S_{BET}: surface area, V_{TOTAl}: total pore volume. V_{MIC}: micropore volume.

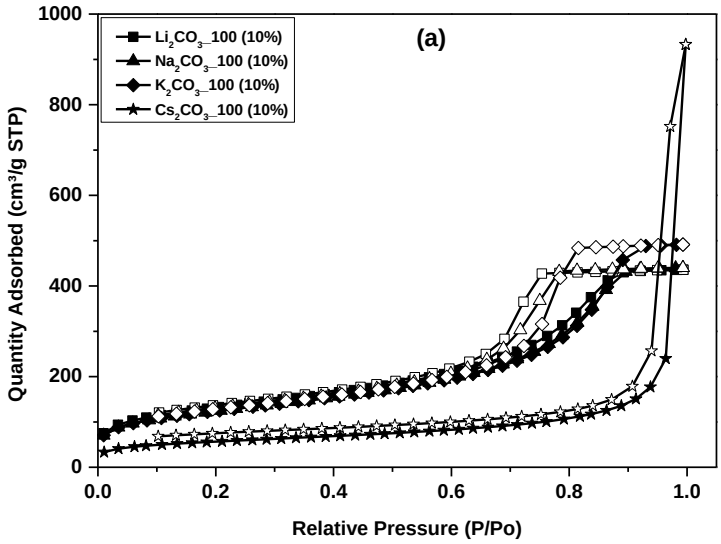

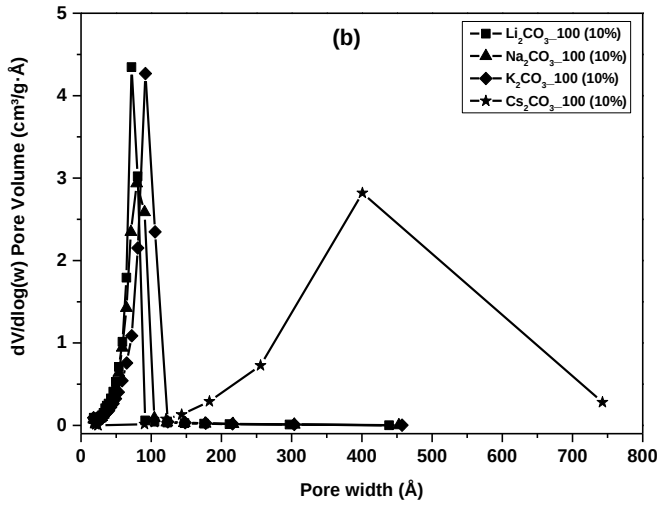

Figure 7-1: (a) N_2 sorption isotherms and (b) BJH desorption pore size distributions for organic MRF aerogels made with different catalysts, measured at 77 K.

7.1.2 Effect of R/C_t ratio on the textural properties of organic xerogels

The R/C_t ratio was varied within the modified gel synthesis to determine the most suitable ratio for the preparation of MRF xerogels. R/C_t ratios between 10 and 500 were investigated using porosity data derived from N_2 sorption analysis at 77 K, Table 7-2 shows the textural characteristics of the various R/C_t ratios investigated. As R/C_t ratio increased from 10 to 500, average pore sizes were observed to increase, resulting in increased pore volumes. An initial increase in surface area was observed between R/C_t 10 – 200, followed by a decrease after R/C_t 300, this is because of the alteration of the pH by changing the R/C_t ratio. Generally, increasing the basic catalyst concentration decreases particle size, reduces pore size and increases surface area. Conversely, above a certain pH, a reduction of the pore volume and surface area is observed which is attributed to increased shrinkage, during drying and pyrolysis, caused by a lack of cross-linking [190].

Table 7-2: Textural characteristics of organic aerogels made with different R/C_t ratios prepared in this study.

Sample	S_{BET} m^2g^{-1}	V_{TOTAL} cm^3g^{-1}	V_{MIC} cm^3g^{-1}	Pore size nm	pH
Na_2CO_3_10	n/a	n/a	n/a	n/a	7.80
Na_2CO_3_25	27.8	0.02	0.01	1.8	7.62
Na_2CO_3_50	416.7	0.23	0.03	2.4	7.45
Na_2CO_3_100	530.8	0.35	0.05	2.9	7.31
Na_2CO_3_200	556.1	0.60	0.04	4.4	7.17
Na_2CO_3_300	520.8	0.84	0.04	7.2	6.92
Na_2CO_3_500	345.5	0.99	0.02	13.4	6.62

S_{BET}: surface area, V_{TOTAl}: total pore volume. V_{MIC}: micropore volume.

Sorption isotherms, and the respective pore size distributions, are presented in Figure 7-2; at R/C_t ratios below 50, the quantity of N_2 adsorbed was minimal and, as already mentioned, the surface area and pore volumes were relatively low compared to the higher R/C_t ratios used. The significant reduction in the porous properties resulted from the lack of cross-linkage within the gel structure, caused by the short gelation times associated with low R/C_t. As R/C_t increases, the amount of catalyst decreases while the gelation time increases, this results in the formation of larger particle sizes, which consequently pack less closely increasing the pore volumes and surface areas observed [191, 192].

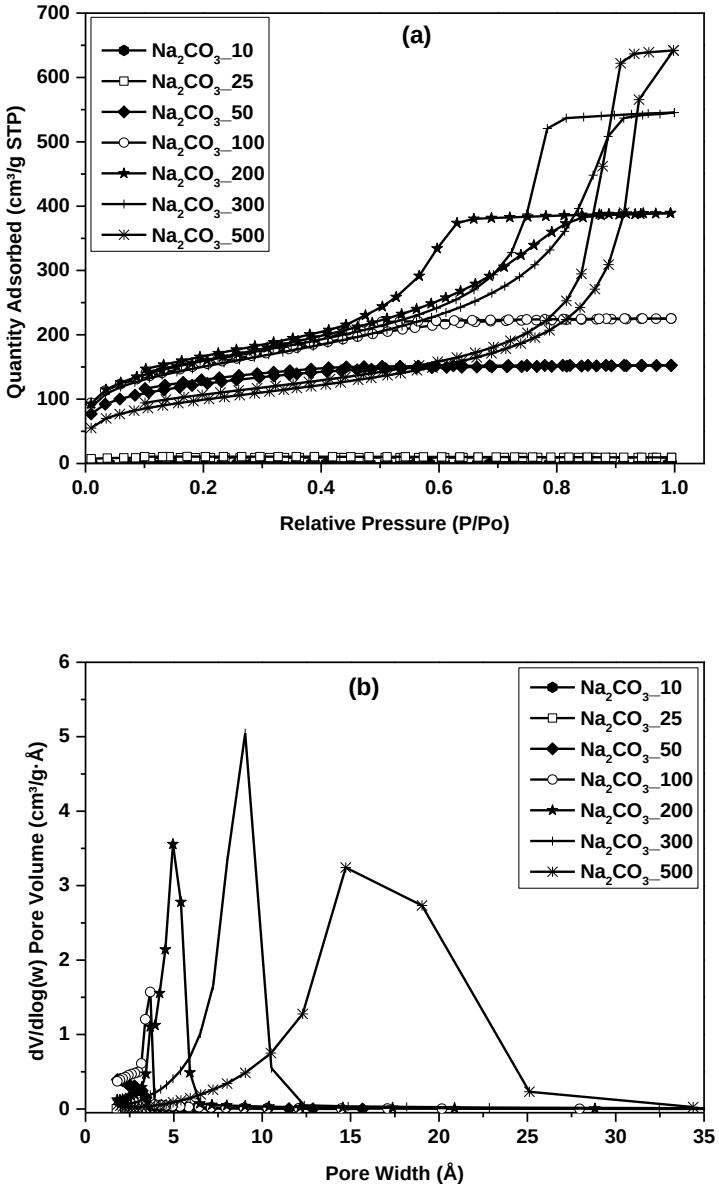

Figure 7-2: (a) N_2 sorption isotherms and (b) pore size distributions for organic xerogels made with different R/C_t ratios, measured at 77 K.

From the N_2 sorption isotherms (Figure 7-2), all R/C_t ratios show typical Type IV [95] isotherm behaviour indicative of materials consisting mainly of mesopores, the hysteresis loop was seen to progress from Type H2 [99] (R/C_t 50 – 300) to Type H1 [99] (R/C_t 500). The change in hysteresis type is the result of increased mesopore formation observed for larger R/C_t ratios, which causes a decrease in surface area and micropore volume. It should also be noted that increasing the R/C_t ratio reduces the pH of the reactant solution, which, in turn, increases the gelation time; as mentioned in Section 7.1.2. If pH is too low, precipitation occurs, while, if the pH is

too high, condensation is hindered, hence, a high enough pH is needed to promote polycondensation, suggesting that a threshold value may exist that will accommodate the pH drop during MRF gel preparation, resulting from the addition of melamine to the reaction before the need for acid stabilisation is required but not high enough that clusters have little or no time to grow and coalesce before gelation occurs. Hence, an R/C_t ratio of 100 was chosen as the ideal ratio, and subsequently used in the preparation of future MRF xerogels. Previous studies on the effect of pH on RF gel formation have maintained that the initial sol pH is a critical factor in controlling gel properties with the initial sol pH controlling the extent of the condensation reaction between R and F [193]; too high a pH in the initial sol (low R/C_t ratios), hinders the condensation reaction and too low a pH (high R/C_t ratios), hampers the formation of R anions (refer to Figure 7-2).

7.1.3 Repeatability studies on synthesis method for MRF xerogels production.

To determine that the synthesis method adopted was repeatable, 8 samples, four each of Na_2CO_3_100 (7%) and Na_2CO_3_100 (10%), were prepared under identical synthesis conditions. The chemical (final pH) and textural properties of the materials formed were then compared to evaluate synthetic repeatability employing both standard deviation and relative standard deviations as models for analysing process repeatability, with lower values signifying replicates are repeatable to a high accuracy, while higher values imply higher process errors in replicates.

Table 7-3: Textural parameters obtained for repeat preparations of Na_100 (7%) xerogels prepared in this study

Sample	S_{BET} m^2g^{-1}	V_{TOTAL} cm^3g^{-1}	V_{MIC} cm^3g^{-1}	Pore size nm	pH
Na_100 (7%) A	491.4	0.595	0.027	4.9	7.24
Na_100 (7%) B	502.0	0.595	0.028	4.8	7.25
Na_100 (7%) C	487.5	0.583	0.026	4.8	7.23
Na_100 (7%) D	501.9	0.531	0.031	4.2	7.24
Average	495.7	0.576	0.028	4.7	7.24
Standard Dev	7.4	0.030	0.003	0.3	0.01
Relative Sdev	0.0	0.053	0.091	0.1	0.00

S_{BET}: surface area, V_{TOTAl}: total pore volume. V_{MIC}: micropore volume.

Table 7-4: Textural parameters obtained for repeat preparations of Na_100 (10%) xerogels prepared in this study.

Sample	S_{BET} m^2g^{-1}	V_{TOTAL} cm^3g^{-1}	V_{MIC} cm^3g^{-1}	Pore size nm	pH
Na_100 (10%) A	432.7	0.681	0.028	6.7	7.23
Na_100 (10%) B	409.3	0.632	0.026	6.5	7.28
Na_100 (10%) C	401.5	0.613	0.023	6.6	7.26
Na_100 (10%) D	412.8	0.668	0.024	6.8	7.13
Average	414.1	0.648	0.025	6.6	7.23
Standard Dev	13.3	0.032	0.002	0.1	0.07
Relative Sdev	0.0	0.049	0.090	0.0	0.01

S_{BET}: surface area, V_{TOTAl}: total pore volume. V_{MIC}: micropore volume.

The results presented in Table 7-3 and

Table 7-4 demonstrate the consistency of the synthetic process, with textural parameters: BET specific surface area, total pore volume and average pore size, of all repeats, repeatable to within ~7 and 5% for Na_100 (7%) and Na_100 (10%), respectively. The N_2 sorption isotherms and pore size distributions obtained are presented in Figure 7-3 and Figure 7-4; and it is evident that the plots show near identical distributions.

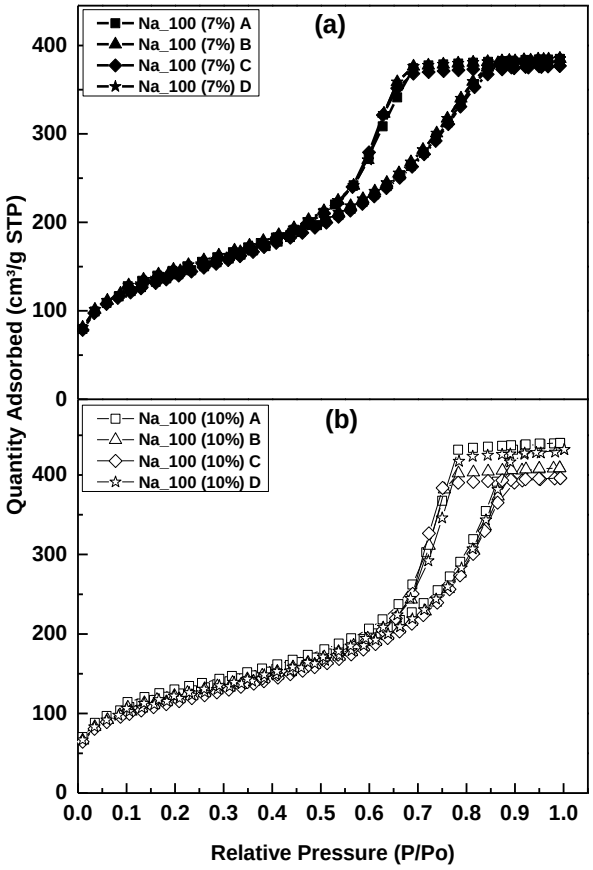

Figure 7-3: N_2 sorption isotherms for (a) Na_100 (7%) and (b) Na_100 (10%) repeats

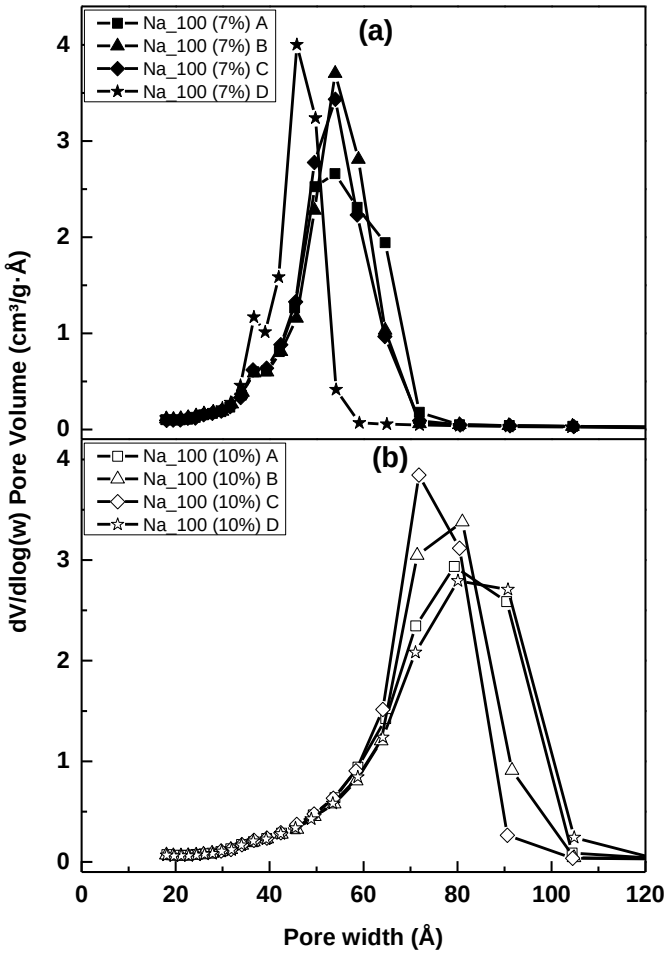

Figure 7-4: Pore size distributions for (a) Na_100 (7%) and (b) Na_100 (10%) repeats

7.2 Effects of Melamine enrichment on RF xerogel production

Once repeatability of the synthetic method had been established, the effects of melamine addition to the textural characteristics of MRF xerogels were investigated using N_2 sorption measurements, SEM microscopy, FTIR and CHN/O elemental analysis.

7.2.1 N_2 sorption analysis on MRF xerogels

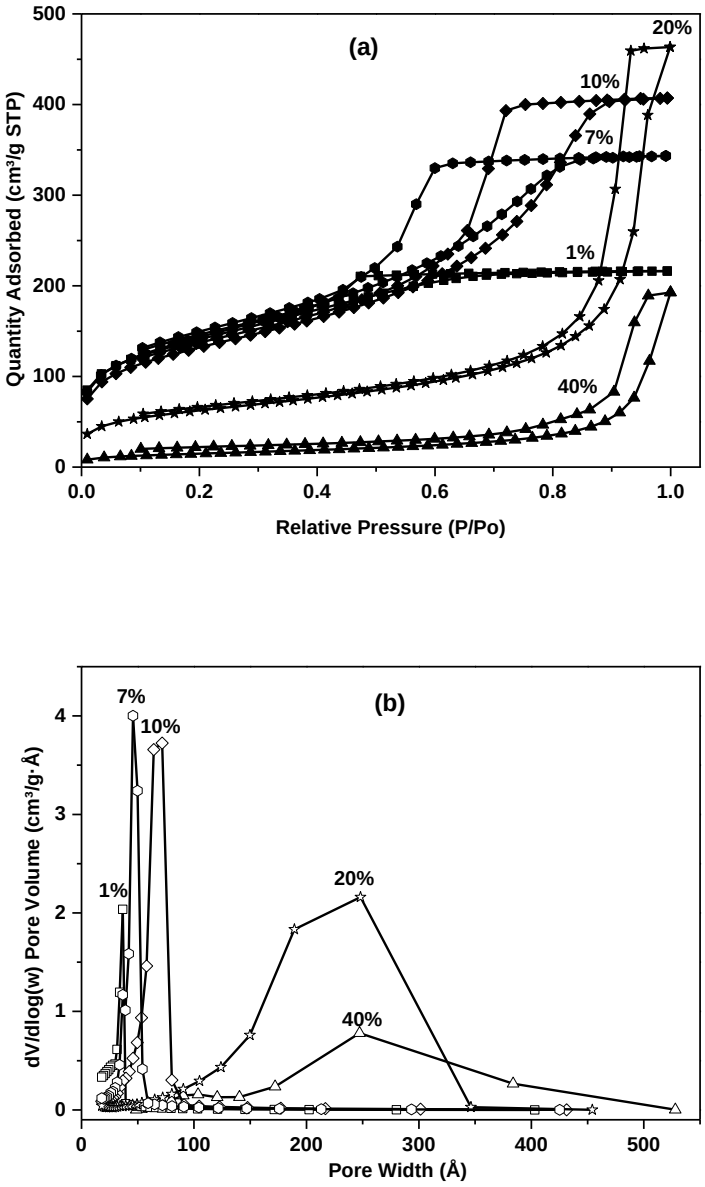

Figure 7-5: (a) N_2 sorption isotherms and (b) pore size distributions for organic xerogels made with different melamine wt%, measured at 77 K.

As melamine wt% increased, the degree of cross-linking decreased; during normal synthesis the pH is altered by decreasing amount of catalyst, although the R/C_t molar ratio is maintained, the effect is similar to that of higher R/C_t ratios (lower pH) explained in Section 7.1.2., hence, as pH decreases with increasing melamine concentration, the number of resorcinol anions decreases and this diminishes the formation of hydroxymethyl derivatives, this favours condensation, with the obtained clusters weakly branched (decreased cross-linkage) with a decreased number of

particles formed (reduced surface area) and increased particle sizes (Figure 7-12 and Figure 7-13) [190]. Type H2 [99] hysteresis loops were observed for xerogels up to 10 wt% melamine, indicating the presence of mesoporosity and a complex interconnected pore structure with narrow pore openings. Samples prepared at > 10 wt% melamine exhibited Type H1 loops [99], which are indicative of a narrow distribution of cylindrical pores. Capillary condensation in the mesopores increases from P/P_o ~0.45 to ~0.75, while the isotherms show limited multi-layer formation, corresponding to complete filling of the capillaries as P/P_o tends to unity;

Table 7-5: Textural characteristics of organic xerogels made with different wt% melamine prepared in this study.

Sample	S_{BET}	V_{TOTAL}	V_{MIC}	Pore size
	m^2g^{-1}	cm^3g^{-1}	cm^3g^{-1}	nm
Na_100 (0%)	515.4	0.35	0.05	2.9
Na_100 (1%)	489.9	0.34	0.04	2.9
Na_100 (7%)	487.5	0.58	0.03	4.8
Na_100 (10%)	432.7	0.68	0.03	6.7
Na_100 (20%)	216.1	0.72	0.02	16.0
Na_100 (40%)	52.4	0.30	n/a	20.3

Na – Na_2CO_3(catalyst), 100 – R/C_t ratio

S_{BET}: surface area, V_{TOTAl}: total pore volume. V_{MIC}: micropore volume.

Table 7-5 summarises the textural properties of MRF organic xerogels synthesised using Na_2CO_3 R/C_t 100; as expected, the BJH average pore width increases with increasing melamine content, from ~2.9 nm at 0 wt% to ~20.3 nm at 40 wt%. The BET surface area of the xerogels with < 7 wt% melamine show no significant trend with melamine content, but as the melamine content increases to 40 wt% from ~7%, there is a marked reduction in surface area, by ~90%, which can be attributed to either the partial filling of the pores with melamine or the effect of reduced cross linking, resulting from reduced pH, discussed previously. Generally, the pore size distribution widens with pore radius shifting to larger values as the amount of catalyst decreases, there is an increase in pore volume with no increase in surface area, and this is likely due to the formation of larger pores.

7.2.2 FTIR analysis of MRF xerogels

MRF sorbents were characterised using FTIR to determine surface functionalities present, with comparison to non-modified gels to indicate those groups attributable

to the addition of melamine to the synthetic method. The effect of melamine on the xerogels prepared was analysed using two approaches, the first approach was solely to identify new functional groups present in the gels as a result of melamine being added to the synthesis route, while the second approach, evaluated how the increase in melamine content affected the presence of these identified functional groups.

The FTIR spectra for Na_100 (0%), Na_100 (40%), and melamine (99% purity) are shown in Figure 7-6, demonstrating new bands incorporated via melamine enrichment. The spectra for both Na_100 (0%) and Na_100 (40%) exhibit peaks at similar positions, which are identified as resulting from the functional groups present. Peaks observed at 1092 and 1220 cm^{-1} can be ascribed to the associated C-O-C stretching vibrations of methylene ether bridges between resorcinol molecules formed during polycondensation. The absorption band at 1604 cm^{-1} is assigned to the aromatic ring of resorcinol, while absorption bands at 2942 and 1463 cm^{-1} are associated with -CH- stretching and scissoring vibrations in both spectra [191, 194].

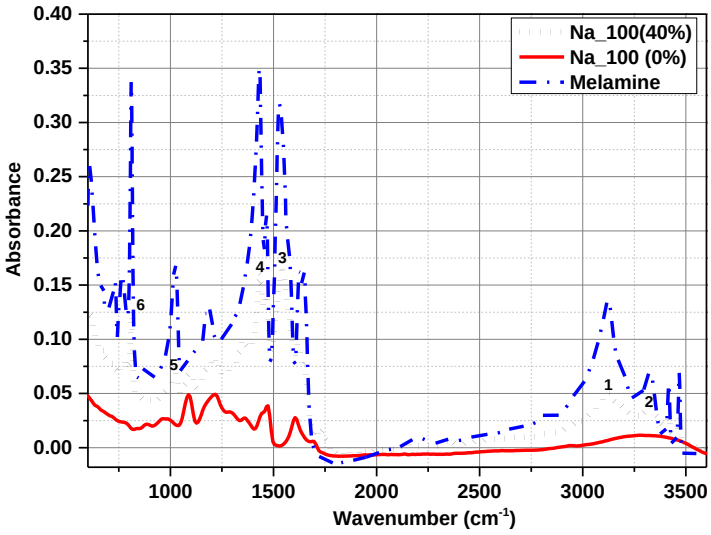

Figure 7-6: FTIR spectra for Na_100, Na_100 (40%) and melamine

Six comparable, defined peaks are observed in both the FTIR spectra of Na_100 (40%) and that for melamine; by contrast, the reference material Na_100 (0%) does not exhibit peaks at 3469, 3420, 3346, 3136, 1549, 1436, 1021, and 811 cm^{-1}, which are ascribed to the modes detailed in Table 7-6 [191, 194].

Table 7-6: New absorption bands present in Na_100 (40%) [191, 194].

Absorption mode	Absorption band (cm^{-1})
bending vibration of triazine ring	811
C-N stretch of the primary amines	1021
semicircle stretching vibrations of the triazine ring	1436
quadrant stretching vibrations of the triazine ring	1541
symmetric stretching vibration of the triazine ring	3136
asymmetric NH_2 stretching vibration	3346
N-H stretching	3419, 3469

The influence of melamine content on the strength of the new peaks, identified as resulting from the inclusion of melamine, was studied. All MRF Na_100 organic xerogels analysed showed the 8 peaks detailed in Table 7-6, as melamine content increases, bands at 784 and 811 cm^{-1}, attributable to the bending vibration of the triazine ring, become stronger. The development of the band at 1541 cm^{-1} (stretching vibrations of the triazine ring) increases in strength with increasing melamine content, as do the N-H in plane deformation (1604 cm^{-1}) and symmetric stretching (3417 cm^{-1}) bands, while the decrease in intensity of the peak at 1474 cm^{-1} (CH_2-scissor vibration and CH_3-flexural vibration) is ascribed to a reduced degree of crosslinking. Such groups are considered basic species capable of acting as Lewis bases to interact with acidic gases [194].

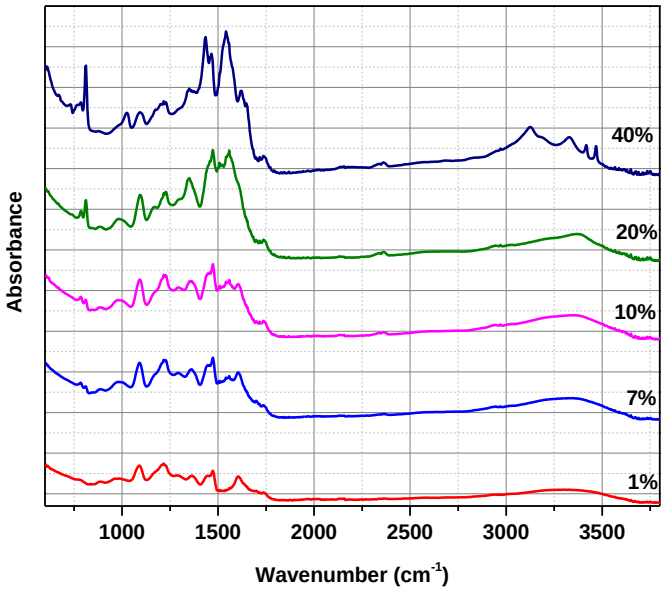

Figure 7-7: FTIR spectra for MRF Na_100 (1 – 40%) organic xerogels synthesised in this study

7.2.3 Ultimate analysis of MRF organic and carbon xerogels

The ultimate analyses of the MRF organic and activated xerogels were determined by elemental analysis and the results are presented in Table 7-7. The results show that the percentage nitrogen in the MRF structure, indicating the development of nitrogen functionalities within the organic xerogels, increases with melamine content. Upon carbonisation at 1073 K, the nitrogen content showed a reduction of ~64% of the total nitrogen content in the corresponding organic xerogel analysed, as thermal degradation of surface species occurred, except for Na_100 (1%), where activation/carbonisation had no effect on the nitrogen content. It is also worth noting that the percentage carbon increased upon carbonisation; this is attributed to bond decomposition (C-O and C-H) in the form of CO_2 and H_2 and other volatiles leaving behind a more densely packed, high carbon content material.

Table 7-7: Chemical properties for the MRF Na_100 (1 – 40%) organic and carbon xerogels prepared in this study

Sample	wt% M wet basis	Organic xerogels				Carbon xerogels				% N retained after pyrolysis
		C	H	N	O	C	H	N	O	
		wt% C	wt% H	wt% N	wt% O	wt% C	wt% H	wt% N	wt% O	
Na_100(1%)	1.2	60.6	5.2	0.8	33.5	90.5	1.0	0.8	7.7	100.0
Na_100(7%)	7.6	57.9	5.6	5.0	31.5	86.9	1.3	1.8	10.0	35.5
Na_100(10%)	11.1	58.0	5.1	7.4	29.5	88.7	0.9	2.6	7.8	35.1
Na_100(20%)	21.6	54.2	5.1	14.4	26.4	80.2	1.7	4.9	13.2	34.0
Na_100(40%)	36.6	49.1	5.0	24.4	21.5	82.9	1.1	8.7	7.4	35.7

7.2.4 TGA analysis of melamine enriched organic RF xerogels

Thermal stability of MRF xerogels was investigated and typical traces are shown in Figure 7-8. The thermo-graphs indicate sample stability at temperatures up to 575 K, during which period, physically adsorbed water and residual acetone is lost [190], followed by the elimination of molecular water, from the methylol groups of formaldehyde and hydroxyl groups of resorcinol, with a final mass loss due to degradation of the organic constituents (triazine rings from melamine); the observed thermal stability demonstrates a large working temperature range for the samples within an industrial context.

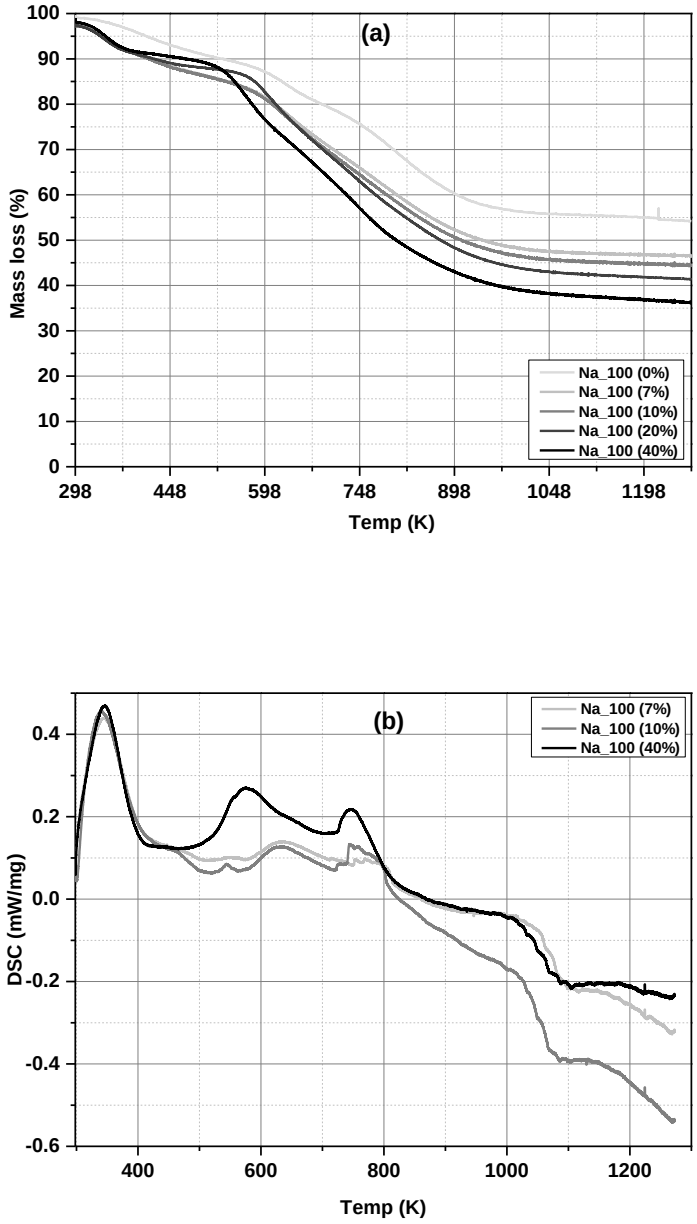

Figure 7-8: (a) TGA thermographs showing wt% loss with increasing temperature and (b) DSC curves showing the decomposition profile of the MRF xerogels prepared.

Thermal gravimetric analysis was also used to determine the optimal pyrolysis conditions required for production of MRF carbons, from Figure 7-8, it can be seen that all samples analysed showed negligible mass loss after 1073 K, although the overall total mass lost varied, depending on the wt% melamine used during MRF synthesis. This suggests that a temperature of 1073 K would be suitable for carbonisation; to verify that higher temperatures were not required for pyrolysis/carbonisation, three comparative temperatures (1073, 1173 and 1273 K) were chosen that fall within the region of negligible mass change. According to

Maria *et al.* [195], chemical and physical activation leads to increased micropore volumes and specific surface areas without any alteration of a materials mesoporosity. However, when chemical activation is used, there is a marked increase in the volume of micropores without an appreciable contribution from mesoporosity (development of narrow microporosity); whereas the opposite is true for physical activation, where significant widening of the narrow micropore is observed. In this study, only physical activation methods were employed (Section 4.4.3).

7.2.4.1 The effect on pyrolysis temperature on porous sturture of MRF carbon xerogels

The data obtained for the textural parameters of Na_100 (20%) MRF carbon xerogels produced in this study are shown in Table 7-8, while N_2 adsorption isotherms and corresponding pore size distributions are shown in Figure 7-9.

Table 7-8: Textural properties for Na_100 (20%) xerogels pyrolyzed at different temperatures

Sample	Temp. K	S_{BET} m^2g^{-1}	S_{micro} m^2g^{-1}	V_{MIC} cm^3g^{-1}	Pore size nm
Na_100 (20%)A	1073	515.4	341.2	0.18	14.0
Na_100 (20%)B	1172	413.7	259.9	0.13	14.5
Na_100 (20%)C	1273	363.3	208.9	0.11	14.7

S_{BET}: surface area, V_{TOTAl}: total pore volume. V_{MIC}: micropore volume.

As pyrolysis temperature was increased, the micropore area is seen to decrease, from 341.2 m^2 g^{-1} at 1073 K to 208.9 m^2 g^{-1} at 1273 K, this is due to the effect of carbonisation temperature on the micropores (< 2nm) (diminishing pore volume causes the samples surface area to be reduced). From Figure 7-9, all isotherms obtained show similar shapes (Type IV), which indicate the presence of micro- and mesopores, however, the sample pyrolysed at 1073 K showed a higher quantity of N_2 adsorbed [196].

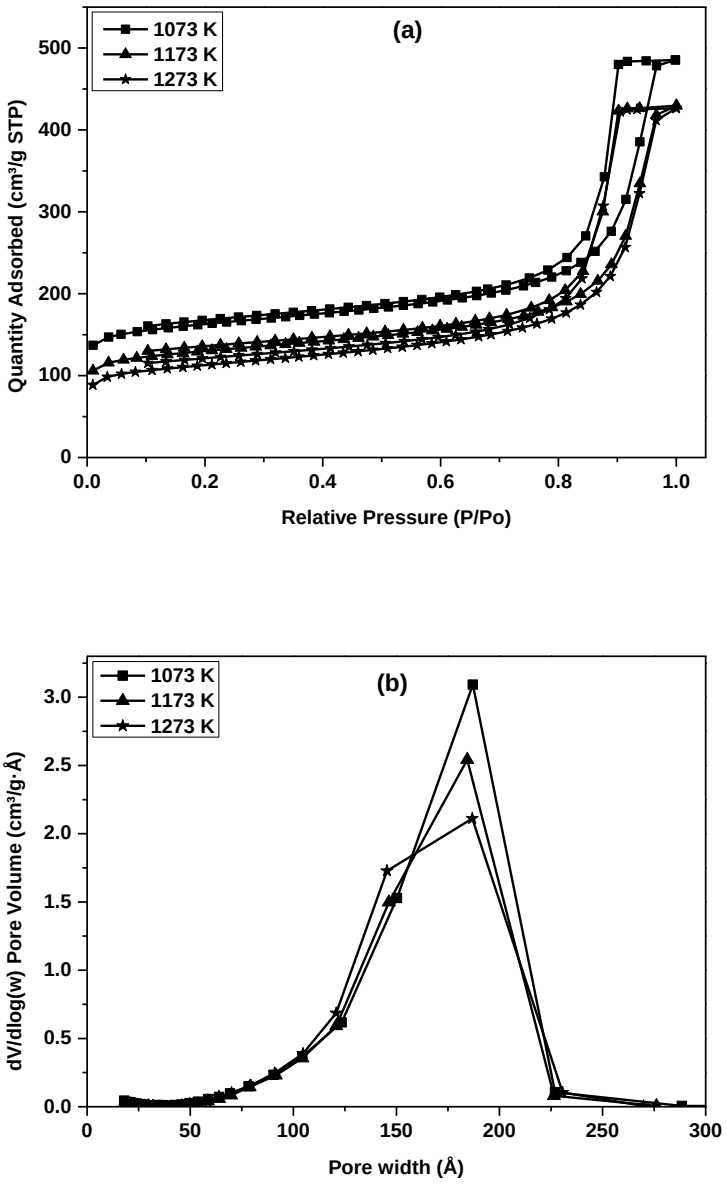

Figure 7-9: (a) N_2 sorption isotherms and (b) pore size distributions for Na_100 (20%)P carbon xerogels pyrolysed at different temperatures

The isotherms obtained suggest the presence of microporosity with significant uptake at low relative pressures, the relatively gradual increase in the amount of N_2 adsorbed over of the relative pressures of 0.2 – 0.8 indicates the presence of mesopores while the sudden sharp increase in amount adsorbed as the relative pressure approaches unity is caused by condensation in the larger mesopores, as well as within and between the carbon particles formed during carbonisation. The BJH pore size distribution shows a peak at ~18 nm, which reduces in volume with increased carbonisation temperature, directly observed as a loss of the sorbents pore volume

(Table 7-8). Considering the negligible change in average pore diameter and detrimental reduction in pore volume, 1073 K was chosen as the most suitable temperature for carbonisation of the organic xerogels prepared.

7.2.4.2 Effect of pyrolysis and activation on textural properties of the MRF carbon xerogels

Table 7-9 show the textural characteristics of the pyrolysed and activated MRF xerogels.

Table 7-9: Textural characteristics of pyrolysis and activated xerogels at 1073 K

Sample	S_{BET}	V_{TOTAL}	V_{MIC}	Pore size
	m^2g^{-1}	cm^3g^{-1}	cm^3g^{-1}	nm
Na_100 (1%)_P	94.7	0.05	0.04	n/a
Na_100 (7%)_P	535.0	0.41	0.15	3.7
Na_100 (10%)_P	591.8	0.54	0.16	4.7
Na_100 (20%)_P	514.8	0.73	0.18	13.3
Na_100 (40%)_P	396.2	0.43	0.16	13.0
Na_100 (1%)_A	329.3	0.18	0.12	2.6
Na_100 (7%)_A	611.5	0.43	0.20	3.5
Na_100 (10%)_A	671.1	0.58	0.20	4.6
Na_100 (20%)_A	764.7	0.95	0.27	11.5
Na_100 (40%)_A	646.8	0.65	0.28	15.0

S_{BET}: surface area, V_{TOTAl}: total pore volume. V_{MIC}: micropore volume.

It is commonly accepted that pyrolysis, activation conditions, treatment time, treatment temperature, precursor properties and structure all affect the porous structure of the resulting pyrolysed or activated carbon xerogel. Here, carbonisation (pyrolysis) was performed to enrich the carbon content in the organic xerogel (Table 7-7) by creating and ordering the carbon structure, while activation acted to improve microporosity, resulting in the formation of a well-developed and easily accessible pore network with relatively larger surface areas (Table 7-9).

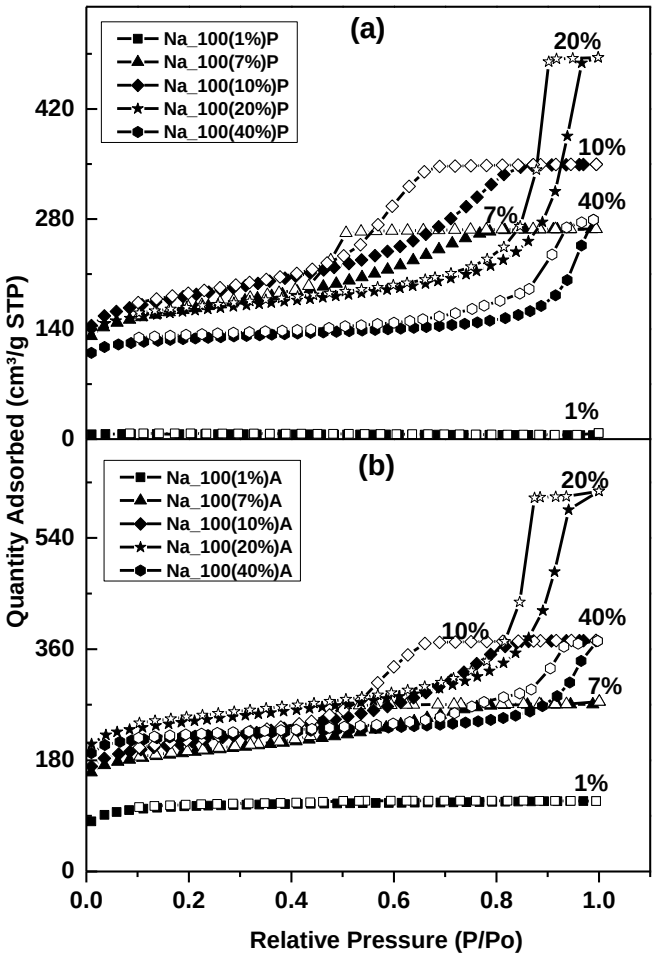

Figure 7-10: N_2 sorption isotherms for (a) pyrolysed MRF c xerogels and (b) activated MRF xerogels, produced in this study.

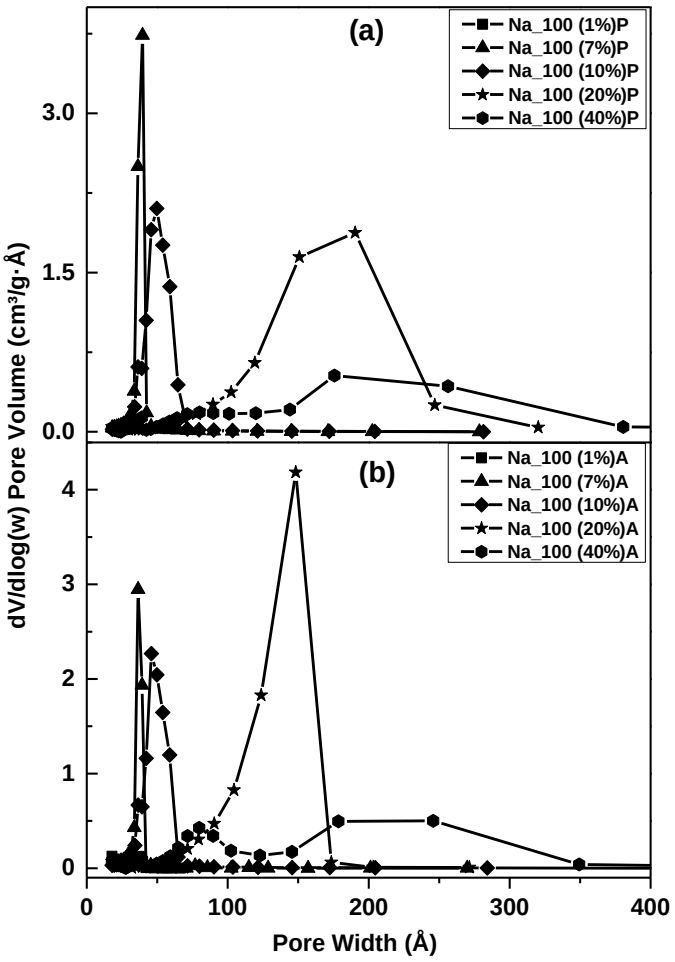

Figure 7-11: Pore size distributions for (a) pyrolysed MRF xerogels and (b) activated MRF xerogels, produced in this study

Adsorption isotherms obtained for both the carbonised and activated xerogels are relatively similar in shape, however, an obvious difference is seen in the quantity of N_2 adsorbed. Isotherms are of Type I [95] for both carbonised and activated 1% samples, while all other samples showed Type IV [95] behaviour, indicating the development of both micro and meso-porosity.

7.2.5 SEM analysis for the organic xerogels

Figure 7-12 and Figure 7-13 (A - F) show the cross-sectional SEM images for both the organic and carbon MRF gels synthesised at $R/C_t = 100$, with varying melamine contents, increasing from 0 – 40 wt% melamine in the final gel, at magnifications of 100 and 50 k). It can be seen that the MRF xerogels consist of interconnected microspheres, which exist as single particles or aggregates, creating a range of

macropores in both the organic and carbon xerogels. This allows easy gas diffusion through the channels, which can be beneficial for CO_2 sorption processes, since macropores provide low resistance pathways for diffusion into the porous structure; the material would also require micropores, as demonstrated in Figure 7-12 and Figure 7-13, for adsorbing the diffused CO_2. Aggregation of microspheres was observed to increase with increasing melamine content, indicating an increase in particle size as a consequence [25, 197].

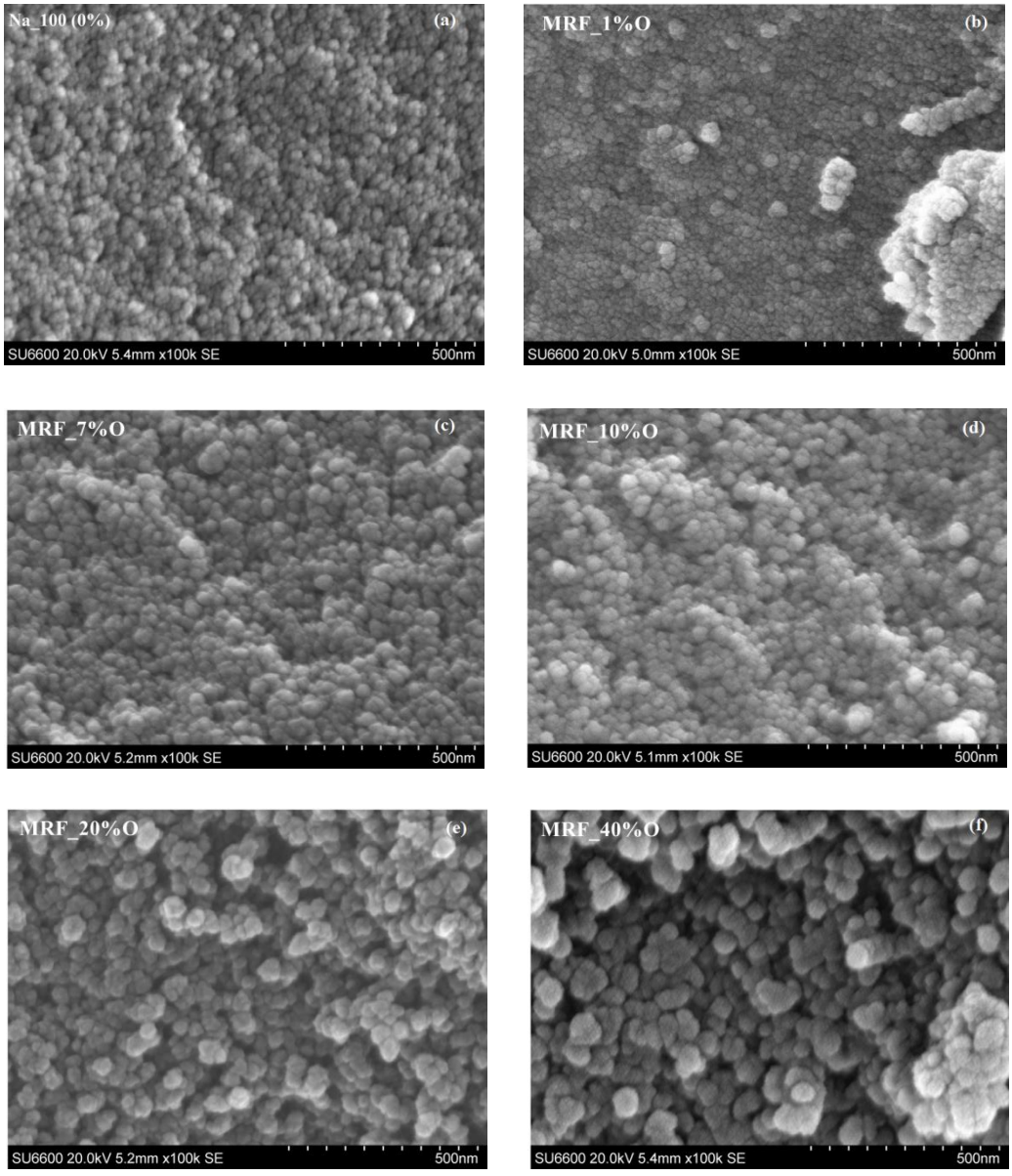

Figure 7-12: SEM images of (a) organic unmodified RF xerogels and (b-f) organic MRF xerogels with magnifications of 100 k

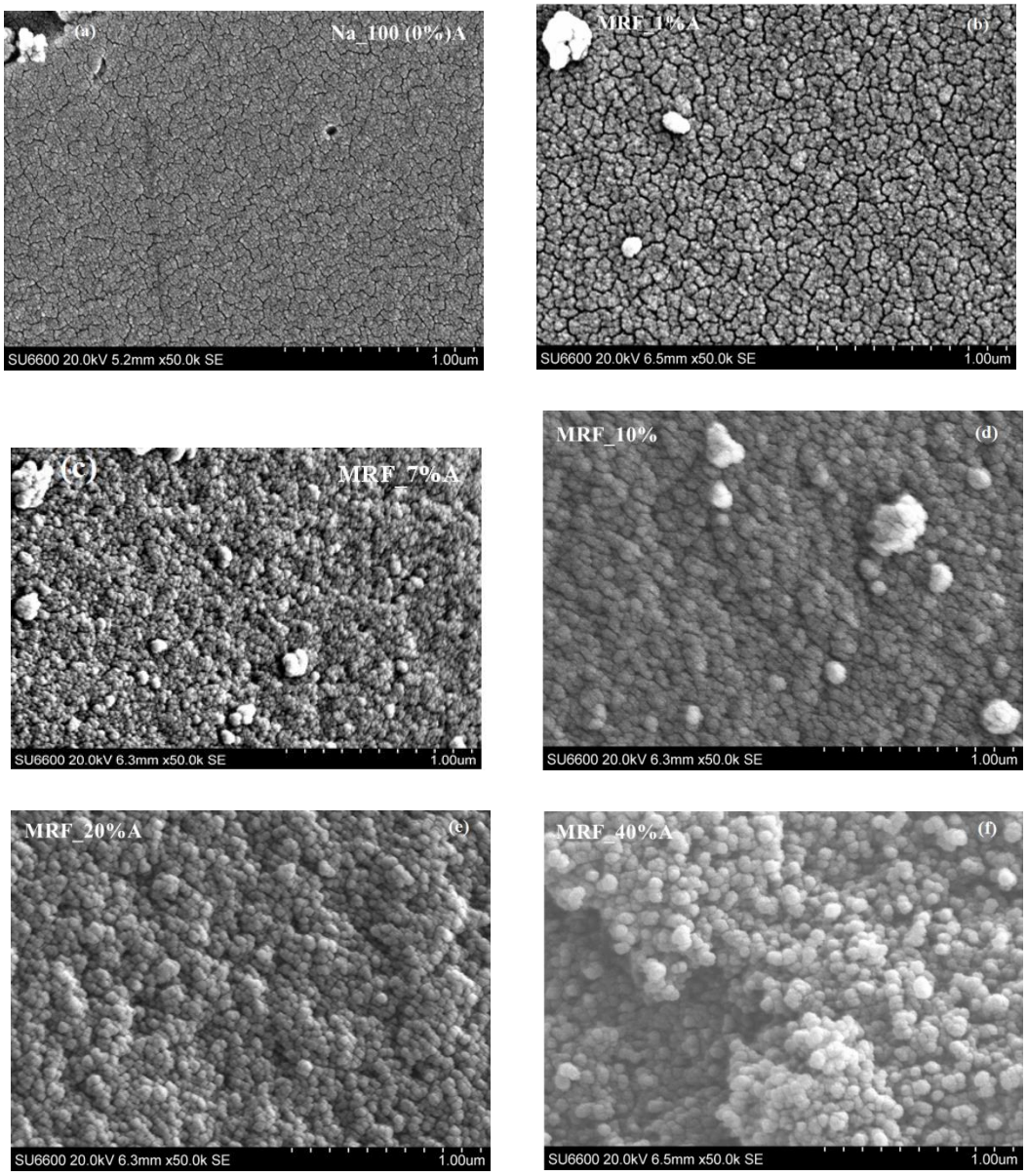

Figure 7-13: SEM images of (a) activated unmodified RF xerogels and (b-f) activated MRF xerogels with magnifications of 50 k

7.3 CO_2 Adsorption analysis on MRF xerogels

CO_2 adsorption on MRF xerogels, synthesised at R/C_t = 100, with different melamine contents, increasing from 1 – 40 wt%, was performed on both the organic and carbon xerogels produced. Temperatures of 298 and 333 K, and pressures between 10 and 900 kPa, were used to investigate the influence that melamine addition had on the sorbents CO_2 capacities. CO_2 sorption performances for the synthesised sorbents were determined using an Intelligent Gravimetric Analyser (IGA) supplied by Hiden Isochema Ltd, which uses gravimetry to accurately measure the magnitude and dynamics of gas/vapour sorption on a given sorbent

[117] (section 3.8.1). Selected samples were analysed in triplicate to demonstrate that CO_2 adsorption capacities were reproducible, and cycling studies further confirmed consistency of results. Table 7-10 and Table 7-11 present the CO_2 data obtained for all MRF organic and carbon xerogels prepared in this study. The maximum pressure used at temperatures investigated, corresponds to a relative pressure of 0.27, hence, full pore filling may not be expected but all systems are significantly below the total pore volume available assuming an adsorbed phase density for CO_2 of 1.023 g cm^{-3} [198, 199], however it is notable that the isotherm for 1% loading is the same as the uptake expected for complete filling of the micropore volume, with no plateau evident, indicating that microporosity does not solely control CO_2 adsorption.

Table 7-10: CO_2 adsorption capacity for MRF organic xerogels at 298 and 333 K, measured at 10, 100 and 900 kPa

Sample	CO_2 adsorption capacity (mmol g^{-1}) at 10 kPa		CO_2 adsorption capacity (mmol g^{-1}) at 100 kPa		CO_2 adsorption capacity (mmols g^{-1}) at 900 kPa	
	298 K	333 K	298 K	333 K	298 K	333 K
Na_100 (1%)	0.260	0.101	1.088	0.608	3.740	2.756
Na_100 (7%)	0.332	0.127	1.201	0.673	4.080	2.969
Na_100 (10%)	0.345	0.129	1.181	0.668	3.934	2.891
Na_100 (20%)	0.367	0.124	1.140	0.670	3.500	2.680
Na_100 (40%)	0.168	0.055	0.567	0.339	2.273	1.835

Table 7-11: CO_2 adsorption capacity for MRF carbon xerogels at 298 and 333 K, measured at 10, 100 and 900 kPa

Sample	CO_2 adsorption capacity (mmol g^{-1}) at 10 kPa		CO_2 adsorption capacity (mmol g^{-1}) at 100 kPa		CO_2 adsorption capacity (mmols g^{-1}) at 900 kPa	
	298 K	333 K	298 K	333 K	298 K	333 K
Na_100 (1%)	0.511	0.209	1.970	1.154	5.507	4.245
Na_100 (7%)	0.817	0.368	2.627	1.602	5.971	4.952
Na_100 (10%)	0.918	0.407	2.820	1.808	6.558	5.161
Na_100 (20%)	0.900	0.410	2.977	1.798	6.923	5.136
Na_100 (40%)	0.962	0.433	3.732	1.921	8.071	6.406

7.3.1 Effect of melamine content on CO_2 adsorption capacity of MRF Na_100 xerogels

A reference material was used to investigate how progressive nitrogen enrichment of MRF xerogels affects the CO_2 adsorption capacity, using Na_100 (0%) as the control material. From Figure 7-14, it can be seen that there was a slight dependence of CO_2

capture capacity on micropore volume, which is to be expected, as the presence of micropores in carbons has been attributed to the adsorption of CO_2 [200, 201].

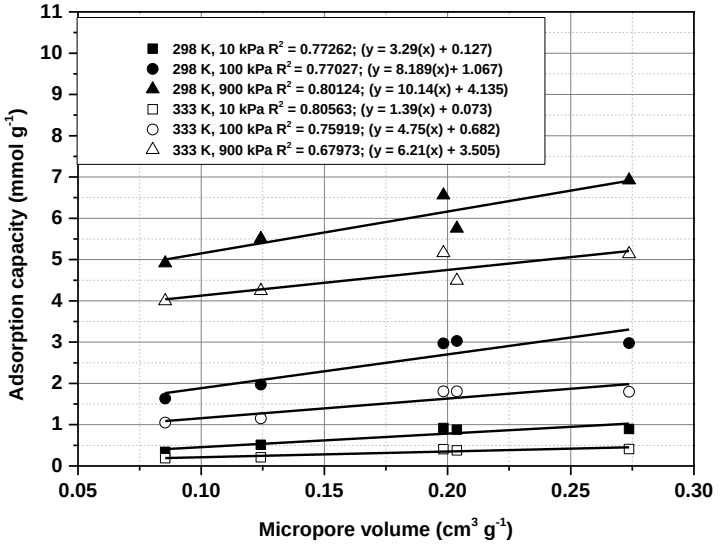

Figure 7-14: Relationship between micropore volume and CO_2 adsorption capacity measured at different temperatures and pressures for activated Na_100 series (0-40 wt% melamine).

CO_2 adsorption capacities consistently increased with increasing wt% melamine, irrespective of test conditions, which may be due to either the increased micropore volume or increased nitrogen content (Figure 7-15), determined previously from CHN analysis. Pevida *et al.*[66], amongst other authors [16, 68, 146, 202-205], reported that the CO_2 capacities of modified carbons (activated and impregnated anthracite) were not solely dependent on textural properties but also the presence of basic nitrogen groups [146]. In order to distinguish the role of N-content on overall CO_2 capture capacity, the direct dependence on CO_2 sorption capacity is evaluated for both the organic and carbon xerogels prepared (Figure 7-15). For the organic xerogels, the CO_2 capture mechanism was mainly driven by physisorption, as sorption capacity reduced with decreasing surface area, whereas, on activation, the role of N-content was more significant, and an increasing trend was observed (Figure 7-15b). This is either because of increased accessibility of CO_2 to the nitrogen functionalities embedded within the pores, as a result of rearrangement of the porous network during activation, or the availability of active basic sites on the sorbents surface. Although, the exact types of basic sites present on the carbon surface was not covered within the scope of this project, their confirmed presence provides a

plausible explanation for the marked increased in CO_2 capacity observed for increased N-content.

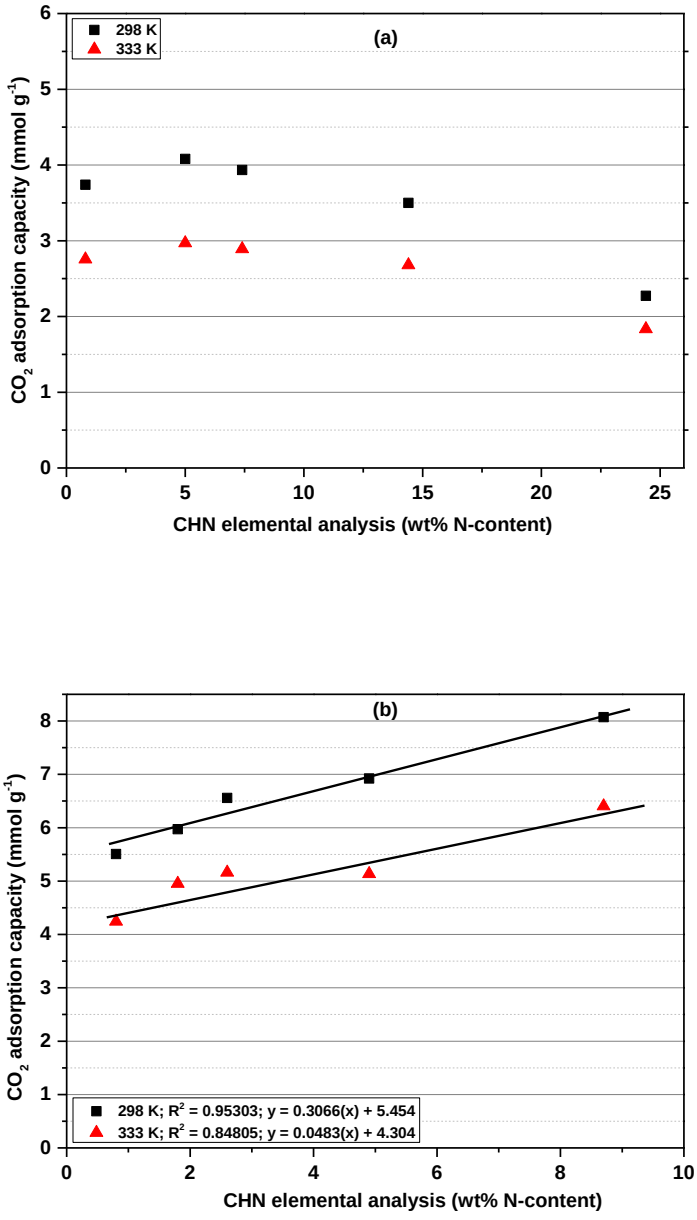

Figure 7-15: Effect of nitrogen content on CO_2 adsorption capacities on (a) organic and (b) carbon xerogels measured at 298 and 333 K, 900 kPa.

To evaluate the influence of basic nitrogen groups incorporated into the structure of the materials prepared in this study, carbon based materials with similar textural properties and negligible nitrogen contents were compared. Commercial activated carbon (AC) (S_{BET} = 577 m^2 g^{-1}, V_T = 0.614 cm^3g^{-1}) supplied by Norit, graphite nanofibers (GNFs) (S_{BET} = 567 m^2 g^{-1}, V_T = 0.708 cm^3g^{-1} [206]), ordered

mesoporous carbon (S_{BET} = 798 m^2 g^{-1}, V_T = 0.870 cm^3g^{-1} [67]) and activated resorcinol formaldehyde carbon xerogel (S_{BET} = 225 m^2 g^{-1}, V_T = 0.123 cm^3g^{-1}, prepared in situ) were used for CO_2 adsorption comparative purposes (Figure 7-16a).

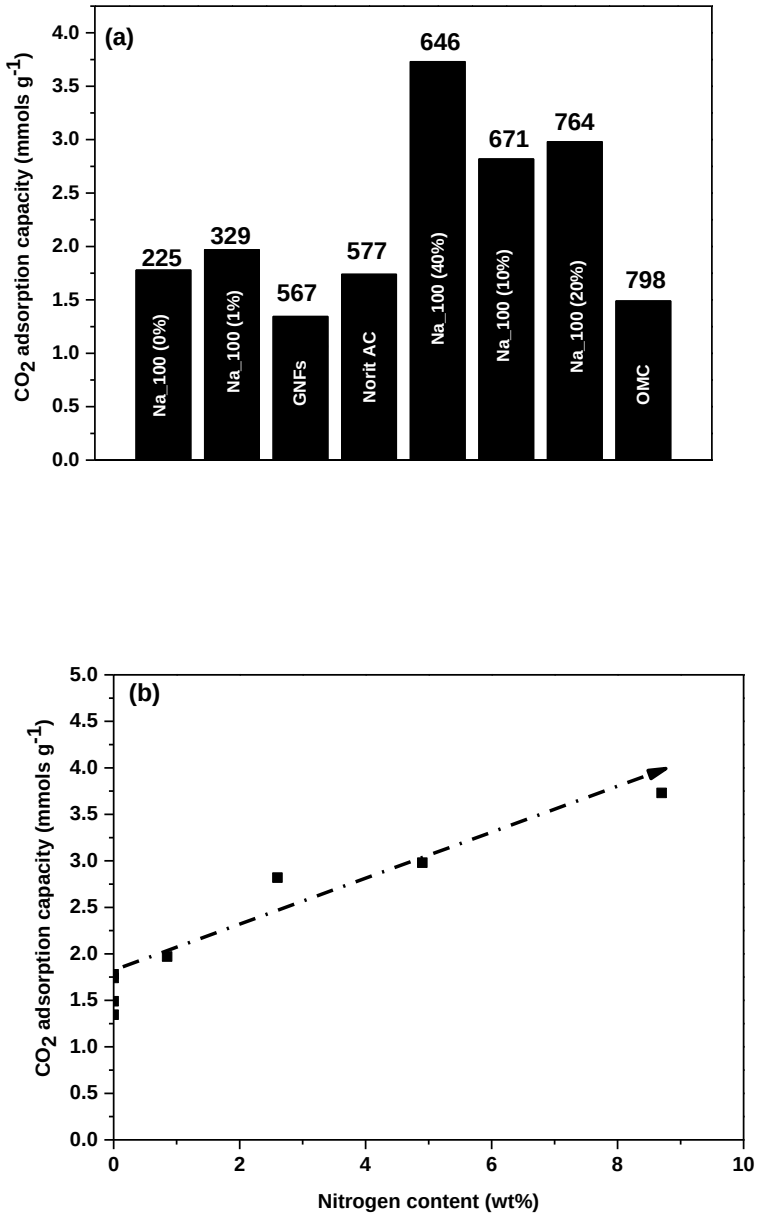

Figure 7-16: Comparative plot showing the influence of (a) surface area and (b) nitrogen content on CO_2 adsorption capacity of sorbents with varying surface areas measured at 100 kPa and 298 K

All comparative materials had negligible nitrogen content and similar textural properties, except for Na_100 (0%)A, which had significantly lower BET surface area and pore volume. Assuming the quantity of CO_2 adsorbed can be deconvoluted into adsorption resulting from the presence of micropores (physisorption), and separately, the

presence of melamine (nitrogen content), Figure 7-16b indicates that as nitrogen content increases, so does the overall CO_2 capacity, supporting the theory that the presence of basic nitrogen groups leads to improved adsorption of acidic gases, such as CO_2. The interdependence of melamine content and CO_2 adsorption capacity was further demonstrated when the adsorption pressure was increased (Figure 7-17). Na_100 (40%)A shows the highest CO_2 adsorption capacity of all materials prepared, despite lower S_{BET} and V_T compared to Na_100 (20%)A, the presence of ~9% nitrogen, after activation, is suggested to account for the significantly improved adsorption capacity.

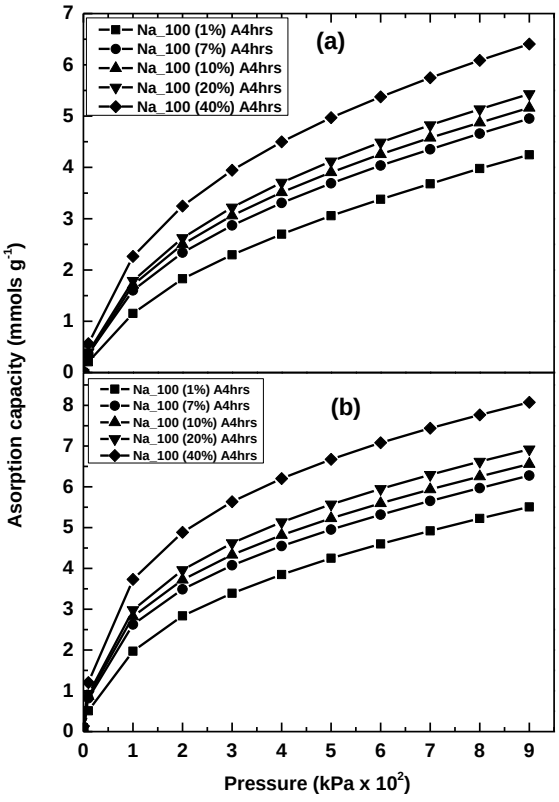

Figure 7-17: CO_2 adsorption isotherm of MRF activated carbon xerogels at (a) 333 K and (b) 298 K

7.3.2 Effect of textural properties on CO_2 adsorption capacity of the organic and carbon xerogels

Textural parameters, including pore volume, surface area and pore size, were used to determine the suitability of a sorbent for CO_2 capture. The molecular size of CO_2 is 0.36 nm [207], and only pores < 5 times the adsorbate size (i.e. ≤ 1.5 nm) have been reported to be effective for CO_2 capture by physisorption at atmospheric pressure

[178, 208]. From Table 7-10, the CO_2 adsorption capacity (10 kPa and 298 K) for the MRF Na_100 organic xerogels analysed, increased progressively between Na_100 (1 – 20%), from 0.260 – 0.367 mmol g^{-1}, before a reduction to 0.168 mmol g^{-1} at 40 wt% (Table 7-10). Considering the surface area obtained for these samples (Table 7-5), it is evident that the capture capacities of the sorbents were not solely related to the surface area. It is suspected that pore blocking, by saturation of the porous structure, melamine resulted in the decrease observed for its CO_2 capture capability. The same was observed when MRF Na_100 carbon xerogels were analysed, CO_2 adsorption capacity increased slightly with surface area, then at Na_100 (40%), there was a marked increase in CO_2 capacity, although, there was a decrease in surface area and pore volume because CO_2 capture performance of porous carbons depends heavily on the presence of narrow micropores (< 1.5 nm), which have a high adsorption potential that enhances the adsorption of CO_2 molecules. On the other hand, it has been observed by several authors [66], [67], [70], [68], [134], [26] that the presence of basic nitrogen groups leads to improved adsorption of acidic CO_2. This could be due to the strong pole–pole interactions between the large quadrupole moment of CO_2 molecules [209] and the polar sites associated with nitrogen groups coupled with the sample porosity [68]. These results suggest that the large CO_2 uptake by Na_100 (40%)A is due to a combination of both the narrow microporosity and the high nitrogen content (Table 7-7). This supports the argument that, not only the textural properties play a part in CO_2 capture, giving credence to the initial suggestion that the capture of CO_2 occurred by two mechanisms, one involving basic nitrogen functional groups, and, the other, the microporous nature of the sorbent [201], [68].

7.3.3 Effect of temperature on CO_2 adsorption capacity of MRF xerogels

The influence of temperature on adsorption capacity was determined by using different analysis temperatures (273, 298 and 333 K) for CO_2 adsorption on Na_100 (40%)A, at pressures between 10 and 900 kPa. All sorbents analysed showed a reduced CO_2 adsorption capacity with increasing temperature, with the highest capacity recorded at 273 K. This behaviour is typical for physisorption processes, which can be identified as the dominant mechanism for adsorption in the carbon series investigated, and occurs because the increase in temperature increases both the molecular diffusion of CO_2 into the porous structure and the surface adsorption

energy [210], hence, the adsorbed CO_2 becomes unstable resulting in desorption of the adsorbed species. A reported example is where CO_2 sorption capacity of mesoporous carbon (IBN9-NCl-A) reduced with temperature, with adsorption capacity reducing from 2.5 – 0.1 mmol g^{-1} (273 – 328 K). As physisorption is an endothermic process, the thermodynamics of the system resulted in a reduced CO_2 capacity with increasing temperature [70, 208].

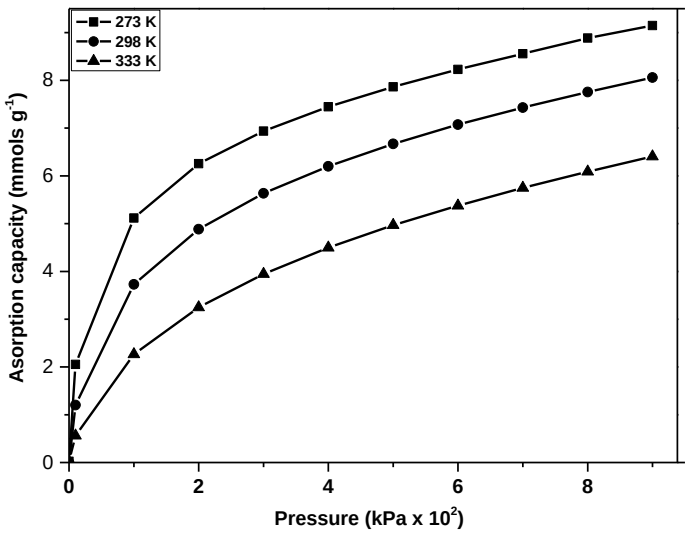

Figure 7-18: CO_2 adsorption isotherm of Na_100 (40%)A at different temperatures (273, 298 and 333 K),

7.3.4 Regeneration studies for MRF organic and carbon xerogels

As well as high CO_2 adsorption capacity, a stable cyclic performance is also of critical importance when evaluating the performance of sorbents for CO_2 capture. It is essential that adsorbents not only have high CO_2 capacity but also that a stable sorption capacity exists during repetitive cycling, with constant adsorption-desorption performance over long-term use [26, 211]. For cycling/regeneration, two main techniques exist; temperature swing adsorption and pressure/vacuum swing adsorption, considering the effects of temperature on amino groups present and the overall process cost, VSA was adopted; moreover, when CO_2 is recovered at sub-ambient pressures, VSA is seen as a more prospective method for CO_2 capture from flue gas [142]. Here, Vacuum Swing Adsorption (VSA) was used for regeneration studies; a typical VSA cycle uses reduced pressure to shift the equilibrium position and cause desorption of adsorbed species, hence regeneration of the adsorbent [142].

Adsorption-desorption cycling studies were performed on Na_100 (40%)A, to determine the performance and stability of the sorbent during repeated use. The sample was exposed to pure CO_2 at 298 K at two pressure extremes, 100 kPa and vacuum, for 30 cycles with a 60 min equilibration time between cycles. ~87% CO_2 adsorption was achieved within the first 30 min, while equilibrium adsorption was achieved at ~38 min, the reverse is the case for the desorption branch, although, dependent on the rate at which pressure is admitted into the adsorption chamber, this determined the kinetics of the sorption process; here pressure was admitted at a rate of 5 kPa min^{-1}. Faster sorption kinetics can be achieved by increasing the admittance rate; hence, making the sorbent ideal in an industrial context. Also, results obtained show that the sorbent maintained a stable capacity, up to 99.9 % of the initial uptake, over 30 cycles, indicating a stable and easily reversible CO_2 adsorption-desorption performance

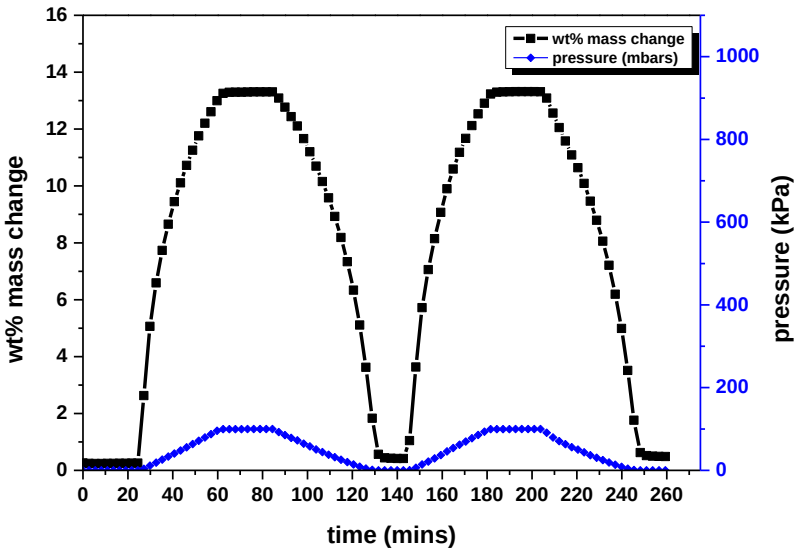

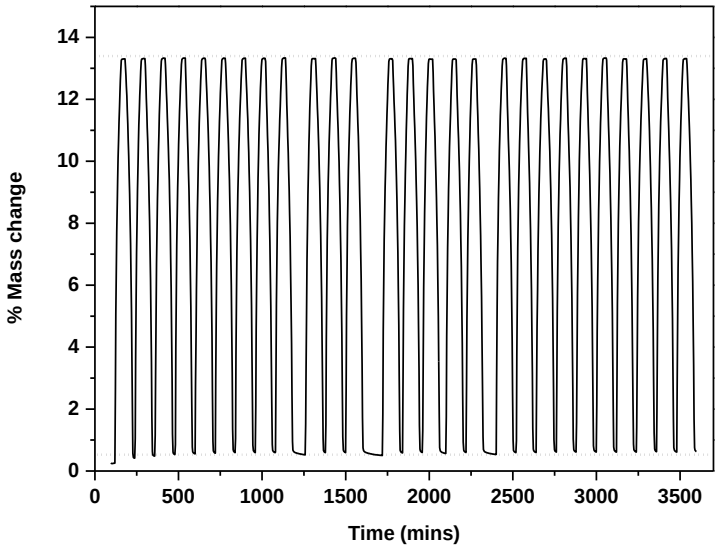

Figure 7-19: 60 min sorption **c**yclic studies on activated Na_100 (40%)A carbon xerogel using vacuum swing adsorption at 298 K, and measured at atmospheric pressure.

7.4 Summary

In this chapter, an optimized Melamine Resorcinol Formaldehyde (MRF) organic and carbon xerogel has been characterised and evaluated as a CO_2 capture adsorbent. The chapter detailed results on effects of synthesis parameters, characterisation of materials and adsorption studies. Firstly, the optimised conditions for MRF synthesis were discussed using N_2 adsorption at 77 K to evaluate how parameters, such as catalyst type and R/C_t ratio, influenced the sorbents porous structure. Results suggested that Na_2CO_3 was the most suitable catalyst and a R/C_t of 100 was determined to be the most effective ratio. This was supplemented by repeatability studies to investigate consistency of the synthesis method chosen; results indicated that samples were reproducible to a level of ~96%. Secondly, the characterisation methods discussed previously (Chapters 3-4) were used to characterise the materials synthesised:

- Results from FTIR show that new functional groups were incorporated into the xerogels via the preparatory method adopted.
- Elemental analysis confirmed the presence of nitrogen within the as-synthesised xerogels (organic and carbon), while TGA proposed an estimated

working temperature range, as well as the optimum carbonisation temperature.

- SEM analysis, showed factors like pH, gel time, quantity of melamine etc.to influence particle size.

Lastly, CO_2 adsorption studies were performed, which showed that increasing nitrogen content increases CO_2 adsorption capacity, with overall CO_2 capture potential influenced by both physical parameters, e.g. BET surface area, pore volume and pore sizes etc., and chemical parameters, e.g. nitrogen content, although process factors such as temperature and pressure, also influenced the sorbents overall efficiency as a CO_2 capture sorbent.

CHAPTER 8 (RESULTS AND DISCUSSION IV)

ACTIVATED CARBON IMPREGNATED WITH IONIC LIQUID FOR CO_2 CAPTURE

8 INTRODUCTION TO ACTIVATED CARBON IMPREGNATED WITH IONIC LIQUID FOR CO_2 CAPTURE

Continued focus by the international community on mitigating against climate change has increased the attention for the design of alternative technologies to reduce the effects of over reliance on fossil fuels. Present methods of CO_2 capture, such as absorption, adsorption, membrane separation etc., concentrate efforts on developing sorbents that are highly selective, and have high capture capacities, because efficient CO_2 capture materials require these traits. Currently, materials like activated carbon, zeolites and molecular sieves possess such characteristics, making them suitable for CO_2 capture, although, activated carbons hold an advantage over similar materials, as they are relatively cheap, easy to prepare and possess well-developed micro-meso porous structures, allowing for a vast array of industrial applications [65, 67, 177, 211].

As a result, activated Carbons (AC) have been extensively studied for carbon capture as a consequence of their large surface areas, microporous natures, thermal and chemical stabilities and fast sorption kinetics [65]. Research into surface modification of AC has shown that the CO_2 sorption capacity of AC can be increased by introducing nitrogen functional groups into their structure [66, 67, 180]. Methods used to incorporate basic amine functionalities within the carbon structure are similar to those mentioned in Chapter 7. Conventionally, nitrogen rich amines are generally used as nitrogen fixing agents in the modification of AC, here preliminary studies have been conducted using a nitrogen containing, high CO_2 solubilising ionic liquid, as the nitrogen precursor for incorporation onto AC, adopting the well-established wet impregnation method. Houshmand and co-workers [179] reported that basic nitrogen groups (amines) can be grafted unto AC using two distinct methodologies. The first was a direct synthetic method, here, the presence of the amine groups from the ionic liquid, condense with carboxyl groups on AC to generate surface amide groups [179]; as activated carbon contains surface carboxyl groups resulting from oxidation with concentrated nitric acid (~70%) at elevated temperatures [212]; the second method was termed the indirect synthetic method, where a linking agent serves as a bridge between the surface carboxyl groups and the amine groups of the ionic liquid.

So far, the use of ionic liquids has shown to be an attractive alternative for CO_2 capture because of their unique properties i.e. negligible volatilities, high thermal stabilities and tuneable chemical properties (task specific). It is, therefore, imperative to develop materials that are simple to make, cost effective [134, 169] and efficient; here, preliminary studies on the facile preparation and characterisation of task specific ionic liquids, wet impregnated on a micro/meso-porous AC with comparable CO_2 capacity, at ambient conditions and pressures up to 100 kPa have been reported. Bmim-NTf_2 (1-buty-3- methylimidazolium bis (trifluoromethylsulfonyl) imide) was used as the nitrogen enriching agent, with AC pellets as the support material, achieving loadings up to 50 wt% Bmim-NTf_2.

This chapter presents results acquired from preliminary studies carried out on preparation and characterisation of Ionic-liquid Impregnated Activated Carbon (IIAC) as described in Chapters 3 and 4. Discussion of these results is structured into two sections; the first section examines the effects that wet impregnation had on the textural properties of the support material, while the second section looks at the CO_2 adsorption results obtained, and the effect of process parameters such as temperature and pressure were also analysed.

8.1 Textural properties of IIAC

The influence of Bmim-NTf_2 impregnation on the textural characteristics of the support material was investigated by analysing the textural properties, including BET specific surface area, BJH total pore volume and average pore size of all samples prepared using N_2 sorption at 77 K, with results presented in Table 8-1 and Figure 8-2; the corresponding N_2 sorption isotherms and pore size distributions are presented in Figure 8-1. All isotherms were classified as Type I [95] in accordance with the IUPAC classification [95] (Figure 8-1a) and exhibit Type H2 [99] hysteresis loops, according to the BDDT method [93], at relative pressures between ~0.433 and ~0.888, which are associated with capillary condensation of nitrogen in the mesopores. The Type I nature of the isotherms with a majority of the nitrogen adsorbed at relative pressure below 0.1 implies that the AC is composed of mainly micropores. The pristine AC exhibited a high N_2 uptake with a maximum of 536.4 $cm^3\ g^{-1}$ at P/Po = 0.99, and corresponding BET and BJH parameters of surface area = 1387.2 $m^2\ g^{-1}$, total pore volume = 0.83 $cm^3\ g^{-1}$ and average pore width = 2.8 nm.

Table 8-1 summarises the textural properties of IIAC samples prepared, with a reduction in the sorbents textural properties observed as the concentration of Bmim-NTf_2 was increased; this is common and has been widely reported in the literature [146, 168, 170-172]. Here, the quantity of N_2 adsorbed reduced significantly, from 536.4 cm^3 g^{-1} for pristine condition to ≤5.3 cm^3 g^{-1} at 50 wt%, suggesting that, Bmim-NTf_2 has been progressively loaded into the porous structure via the chosen synthetic routed adopted. This is in agreement with observations by other workers studying amine loaded carbon with high organic content [146, 168, 170-172].

Table 8-1: Textural parameters obtained for pristine and Bmim-NTf_2 impregnated activated carbons, prepared in this study.

Sample ID	S_{BET} m^2g^{-1}	S_{MIC} m^2g^{-1}	V_{TOTAL} cm^3g^{-1}	V_{MIC} cm^3g^{-1}	Pore size nm
AC (0%)_control	1387.2	406.2	0.83	0.21	2.8
AC (10%)	1081.3	266.5	0.65	0.14	2.8
AC (20%)	736.1	111.5	0.47	0.05	2.9
AC (30%)	451.6	28.5	0.29	0.01	2.9
AC (40%)	140.1	0.0	0.11	0.00	3.2
AC (50%)	5.1	0.0	0.01	0.00	4.2

S_{BET}: surface area, V_{TOTAl}: total pore volume. V_{MIC}: micropore volume.

Wang *et al.* [80] reported that when amino acid functionalised 1-ethyl-3-methylimidazolium lysine ([EMIN][Lys]) was immobilised into porous poly(methyl methacrylate) (PMMA) at concentrations up to 58 wt%, the BET surface area and BJH pore volume reduce from 547 m^2 g^{-1} and 1.34 cm^3 g^{-1} at pristine condition to 0.77 m^2 g^{-1} and 0.01 cm^3 g^{-1} [80]. With similar observations reported by Xinlong Yan *et al.* [213], for SBA-15 modified with amines (polyethyleneimine) up to 50 wt% [213]. These similar observations, reported by other authors, support the findings presented here, that incremental addition of Bmim-NTf_2 to pristine AC gradually fills the pores and sometimes blocks them, thus, restricting nitrogen access into the pores at the liquid nitrogen temperature (steric hindrance of nitrogen diffusion into the pores).

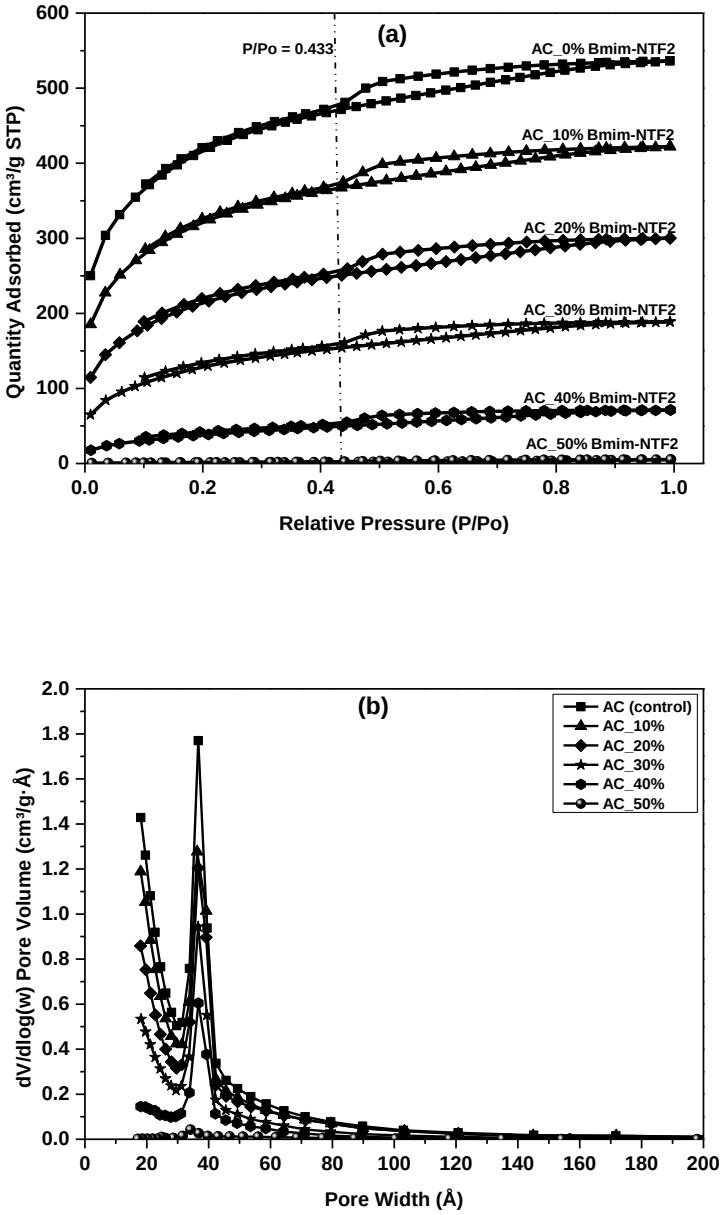

Figure 8-1: (a) N_2 sorption isotherms at 77 K and (b) pore size distributions for Bmim-NTf_2 progressively impregnated onto pristine AC (10-50 wt%).

Figure 8-1, shows that the samples have narrow PSDs with a majority of pores concentrated at ~4 nm, indicative of relatively uniform pore sizes, although, on modification with Bmim-NTf_2, a decrease in the PSD peak was observed, however, there was no notable change in the shape of the distribution. This suggests that, although changes to the pore volume and average pore size were observed, no obvious changes to the pore structure occurred during modification [175].

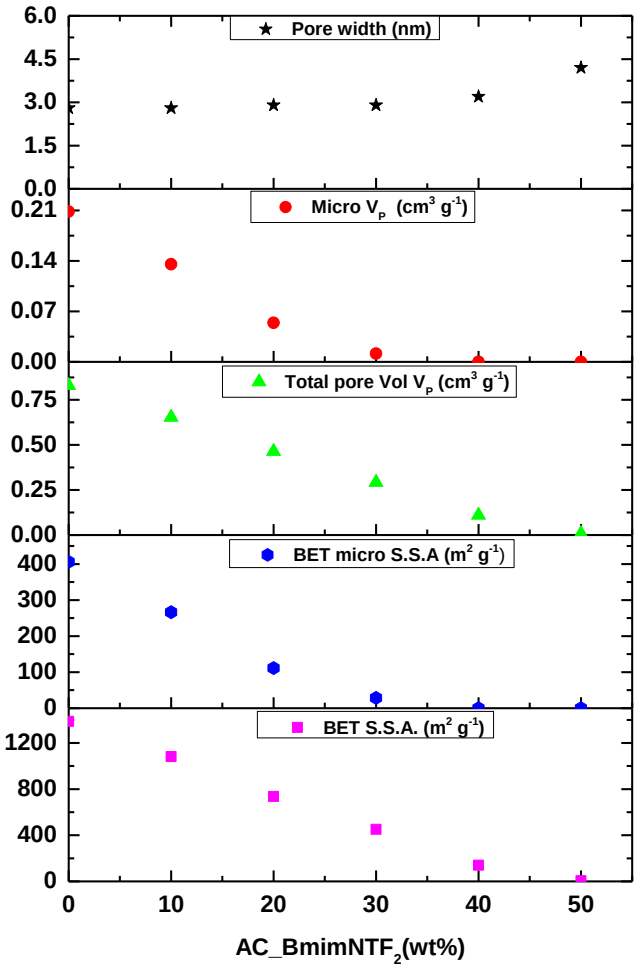

Figure 8-2: Textural parameters for Bmim-NTf_2 progressively impregnated onto pristine AC (10-50 wt%)

8.2 CO_2 adsorption analysis on IIAC

CO_2 adsorption studies were performed using an intelligent gravimetric system, with isothermal measurements conducted at 298 and 333 K (10 and 100 kPa) for the IIAC samples (support and Bmim-NTf_2 impregnated sorbents ≤50 wt%). CO_2 sorption data (Figure 8-3), indicates that CO_2 adsorption capacities at the pressures investigated (10 and 100 kPa), reduced with increased modification, due to the compromised textural properties (Figure 8-2). Due to the physical and chemical properties of the sorbents, the CO_2 capture capacity can be attributed to two mechanisms; the textural property and the other, the available basic nitrogen functional groups, both suspected to take place simultaneously, with physisorption resulting from the sorbents textural properties, and the latter, related to the nitrogen content (amino functional groups)

within the modified material. To determine the effects of modification, the BET surface area was normalised to compare CO_2 capture capacity per unit surface area. The overall CO_2 capacity increased from 0.00138 mmol m^{-2} at pristine condition to 0.0467 mmol m^{-2} at 50 wt% impregnation (333 K, 10 kPa) and from 0.00072 to 0.0345 mmol m^{-2} (333 K, 100 kPa) for pristine and 50 wt% Bmim-NTf_2 respectively. It was estimated that > 48 times increase in utilisation of the available surface was observed at 50 wt% Bmim-NTf_2, suggesting that the presence of the ionic liquid impregnated within the AC improved the sorbents CO_2 affinity and this increase was observed at all concentrations analysed. Also, as temperature increased from 298 to 333 K, utilisation of CO_2 capacity per unit area increased from ~34 to ~48 times when the pristine AC was compared to the 50 wt% Bmim-NTf_2 impregnated AC sample.

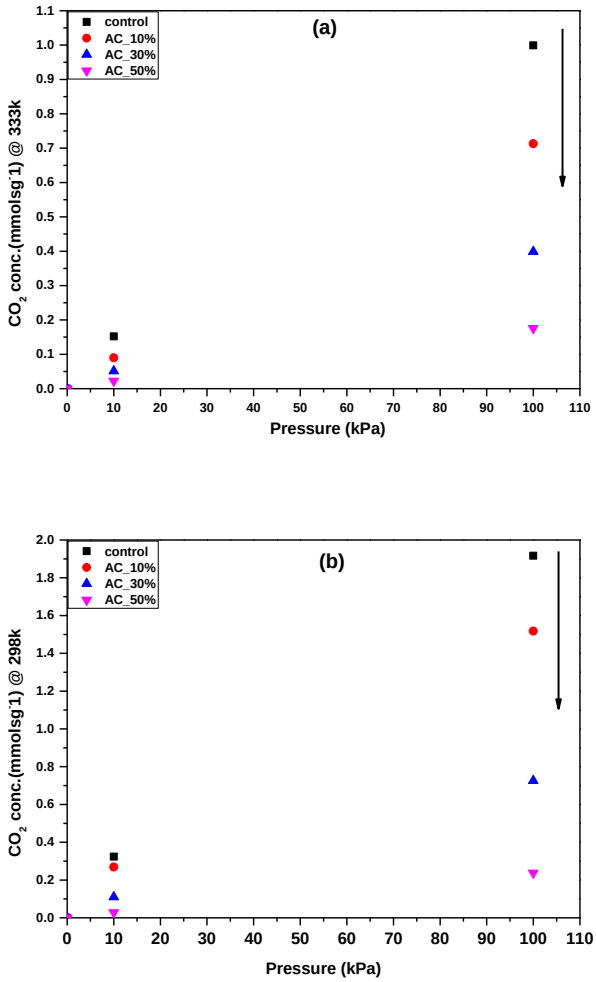

Figure 8-3: CO_2 adsorption isotherms for Bmim-NTf_2 impregnated AC at (a) 298 K and (b) 333 K, measured at 10 and 100 kPa respectively.

8.3 Effect of temperature on CO_2 adsorption on the AC samples

The effect of temperature on the adsorption capacity of the Bmim-NTf_2 impregnated AC was investigated, with results showing that the adsorption capacity of pristine AC reduced by ~48% between 298 – 333 K; while, Bmim-NTf_2 loadings of 10, 30 and 50% reduced by ~48, 45, 26%, respectively. This suggests that, as temperature and ionic liquid (Bmim-NTf_2) loadings increased, the net reduction in CO_2 capacity resulting from increased temperature reduces. This observation supports previous findings that not only the physical properties (for physisorption, adsorption capacities reduce with temperature) of the sorbent is responsible for CO_2 capture but Bmim-NTf_2 impregnation provides basic functional groups that enhance the sorbent surface, providing specific adsorption sites for CO_2 [160] .

8.4 Summary

Preliminary studies were carried out on the preparation of Ionic-liquid Impregnated Activated Carbon (IIAC) using a conventional wet impregnation method. To characterise the materials prepared, methods such as N_2 and CO_2 sorption analysis were used. The chapter details results on effects of synthesis parameters, materials characterisation and CO_2 adsorption studies. Firstly, the effect of modification on the sorbents textural property was discussed using N_2 sorption at 77 K, followed by the effect of modification on CO_2 adsorption. From initial results obtained, it was observed that ionic liquid impregnation resulted in decreased textural properties (surface area, pore size and pore volume) of AC when compared with its pristine form; this correlates with the literature [179, 212, 214, 215] and has been interpreted as pore blockage resulting from functional groups attached on the surface of AC. So far, CO_2 adsorption studies conducted on impregnated AC samples, suggests that two adsorption mechanisms are predominantly responsible for the sorbents total CO_2 capacities, ,with both mechanisms assumed to occur simultaneously; one dependent on the sorbents porous structure (surface area, pore size and volume), while the other is influenced by the sorbents chemical properties i.e. the amino functionality (nitrogen content) of the modified sorbent.

CHAPTER 9

CONCLUSIONS

9 OVERVIEW

This study has evaluated the current technologies and materials available for CO_2 capture, subsequently investigating a suite of novel alternative materials, prepared using simple synthetic methods, capable of efficiently capturing CO_2 from flue gas. Detailed preparation, characterisation and optimisation of these materials have been presented, with preparatory methods focused on increasing the nitrogen content during material syntheses via various synthetic routes; this is because, from literatures presented, nitrogen enrichment of porous materials have been shown to significantly improve their affinity to adsorb CO_2. Adsorbents prepared were characterised for individual physical and chemical properties, using, scanning electron microscopy, thermo-gravimetric analysis, infrared spectroscopy, elemental analyses and N_2 sorption at 77 K. Gravimetric methods were employed for CO_2 sorption capacities; with analysis were conducted under varying analysis conditions i.e. different temperatures and pressures.

In attempting to discuss key findings and conclusions, it was necessary to give consideration to the main research aims and objectives (Chapter 1, Section 1.2) and the overall goal of this study; conclusions presented are with reference to the research objectives, which were to:

9.1 Employ a simple synthetic approach:

In this study, three synthetic routes were adopted for adsorbent preparation, including a co-synthetic method, adopted for the preparation of bio-inspired amine silica and melamine resorcinol and formaldehyde xerogels, a wet impregnation method for ionic-liquid impregnated activated carbon and, finally, an in situ impregnation method used for amine in-situ impregnated silica synthesis. These routes present a facile and rapid material synthesis routes, demonstrated to produce bio-inspired amine silica and amine in-situ impregnated silica nanoparticles in only 7 hours, presenting a significant achievement when compared with similar amine modified silica based materials [146, 159, 162] which can take in excess of 3 days for complete material preparation. In addition, work conducted in this study demonstrates that the synthesis methods adopted were efficient at producing reproducible nitrogen rich materials, which have shown promise as CO_2 capture materials. Although material costing and environmental impact assessments were not

conducted, consideration of synthesis time, reaction conditions (neutral pH, ambient temperature), synthetic steps and precursor costs favours bio-inspired amine silica and amine in-situ impregnated silica as plausible alternatives to conventional silica based CO_2 capture adsorbents, which utilise toxic starting materials and include multi-step processes. For melamine resorcinol formaldehyde carbon xerogels, initial preparations mimicked the sol gel methodology, with a timescale of ~ 7 days for complete materials synthesis; however, preliminary results from optimisation studies performed here have shown that materials with similar physical properties can be prepared within a third of the synthesis time (i.e. ~ 2 days), providing substantial savings with regards to costs and material turnover.

9.2 Study the effect of amine modification on CO_2 capture capacity:

The effect of basic nitrogen functional groups on the CO_2 capture capacities of different materials have been extensively discussed, and findings in this study are similar to those reported in the literature, confirming that the presence and availability of such groups increases the affinity of a material for CO_2 by providing anchor sites, adhering the CO_2 molecules via either an acid–base interaction, a quadrupole interaction, or hydrogen bond formation. Improved sorption capacities are especially prevalent at low CO_2 partial pressures, as in the case of flue gases containing ~10 -15 % CO_2. For comparative studies, and to deconvolute the effect of nitrogen content, on CO_2 capture capacities of materials prepared, evaluation of results was made in relation to individual nitrogen free species, with results indicating that the presence of basic nitrogen functional groups increased a sorbents CO_2 capacity. The underlying mechanism for enhancement was material specific, e.g. for amine in-situ impregnated silica and bio-inspired amine silica nanoparticles, amine active sites and CO_2 form ammonium carbamate, in anhydrous conditions, on the amine-modified sorbent following a zwitterionic mechanism. Finally, increased nitrogen content would, therefore, be expected to increase CO_2 sorption capacity, as observed for both amine in-situ impregnated silica and melamine resorcinol formaldehyde samples analysed, however for bio-inspired amine silica, nitrogen content did not increase markedly, hence, for comparative reasons, the effect of nitrogen inclusion into the silica matrix was tested against its calcined form, results confirm that the presence of nitrogen within the silica matrix increased the materials CO_2 affinity.

9.3 Investigate sorbent regeneration/cycling studies:

The regeneration and/or cycling of the prepared materials were carried out using either temperature or vacuum swing adsorption, depending on individual materials, but for commercial application is it necessary that the regenerative technique employed must be one with reduced energy penalties. Within the range of analysis conditions considered within the scope of this work, all prepared materials showed effective and stably reversible CO_2 adsorption, with efficiencies of ~ 99% achieved for melamine resorcinol formaldehyde samples cycled over a 60 minute adsorption-desorption cycle, using vacuum swing adsorption; this suggests that adsorption of CO_2 on basic active sites is mainly controlled by weak van der Waals interactions, which are easily reversed by vacuum. In contrast, the amine in-situ impregnated silica nanoparticle samples tested showed an initial reduction in capacity after the first cycle, owing to the strong (acid-base) interaction between CO_2 and the basic amine groups, which is not overcome by vacuum alone; however, when the sorption capacity was recalibrated with a new baseline value adopted, only ~5% of the capture capacity was lost over 11 cycles, although not significant, for long term use, thermal regeneration would be beneficial. It is also noteworthy that bio-inspired amine silica samples when thermally regenerated i.e. when the effect of temperature on CO_2 sorption capacity was investigated, exhibited complete reversible CO_2 adsorption-desorption over all cycles investigated. Finally, thermal stabilities were investigated, using conditions similar to those employed for regeneration, to determine amine stability during regenerative processes; findings showed that amines were significantly stable at the analysis temperatures and up to $\leq$ 400 K for bio-inspired amine silica and amine in-situ impregnated silica nanoparticles, and $\leq$ 600 K for MRF xerogels, respectively.

In conclusion, individual materials have been presented, and the related material syntheses extensively investigated, with preparatory methods focused on tailoring the nitrogen content via various synthetic routes. It has been shown that nitrogen enrichment and the textural characteristics of a material play an important part in its overall CO_2 capture potential [26, 144, 162, 172]. The results show that melamine resorcinol formaldehyde carbon xerogels and amine in-situ impregnated silica nanoparticles are the most promising of the materials investigated, although further research into the effects of the extent of functionalisation is required to potentially

incorporate greater weight contributions into the materials prepared, which could impact on CO_2 uptake as required for efficient carbon capture.

Table 9-1: Summary of physical, chemical and regeneration properties for the best performing materials produced from each category of materials investigated.

Best material in category	Characterisation techniques						
	BET S.S.A ($m^2 g^{-1}$)	CHN (Nwt%)	CO_2 sorption (333 K)		Regeneration cycles	Cycle efficiency (%)	Synthesis time (hr)
			10 kPa	100 kPa			
DETA 1-1	25.9	2.6	0.237	0.683	11	99	~6
D1-1	250.8	12.7	1.141	1.783	21	95	~7
Na_100 (40%)A	646.8	8.7	0.433	1.921	30	99	~160

CHAPTER 10

RECOMMENDATIONS FOR FUTURE WORK

10 FUTURE WORK

This chapter details proposed future work for all the materials prepared in this study; as there are several areas within this project that require additional investigation; also, coupled with this proposed future work, alternative uses of some of the materials prepared in this study have been recommended. The chapter is divided into four sections; each covering an individual material investigated with proposals on areas not already covered within the scope of this work.

Future work on Bio Inspired Amine Silica (BIAS):

- Scale up of the production of the BIAS nanoparticles above the 500 ml scale to investigate the repeatability of the proposed scale up parameters.
- Fine tune the synthesis process to improve sorbent repeatability by either controlled pH or the use of an automated synthesis process to eliminate human error.
- Further studies on small molecular amines with longer amine chains like hexaethyleneheptamine (HEHA), note that pentaethylenehexamine (PEHA) was the longest chain analysed so far.
- Study of BIAS samples as alternative materials for other industrial processes e.g. drug delivery systems and water treatment.
- Investigate the effect that humid conditions have on the overall efficiency of the BIAS nanoparticles when in a competing environment with water vapour, and also the sorbents tolerance to flue gas contaminants (NO_x and SO_x).
- Selectivity studies using Ideal Adsorbed Solution Theory (IAST) should be carried out on pure streams to predict how selective BIAS would adsorb CO_2 over N_2 in a competing environment. It is a common method for evaluating gas selectivity based on pure gas adsorption results, a predictive model that does not require any mixture data and is independent of the actual model of physical adsorption.

Further work on Amine In situ-Impregnated Silica (AIIS):

- Investigate other amine types suitable for use via in situ-impregnation technique e.g. polymeric amines (poly-allylamine hydrochloride (PAH),

branched polyethyleneimine (BPEI), melamine) longer chain small molecular amines e.g. pentaethylenehexamine (PEHA), tetraethylenepentamine (TEPA

- Further study on sorbent regeneration i.e. the use of concentration swing adsorption instead of vacuum swing adsorption to avoid the 5% loss in overall capacity recorded after the first 20 cycles analysed.
- Investigate the effect that humid conditions have on the overall efficiency of the AIIS nanoparticles when in a competing environment with water vapour and also the sorbents tolerance to flue gas contaminants (NO_x and SO_x).
- Selectivity studies using *IAST* should be carried out on pure streams to predict how selective AIIS would adsorb CO_2 over N_2 in a competing environment.

Further work on Nitrogen enriched Resorcinol Formaldehyde (RF) organic and carbon xerogels:

- Optimisation studies on the preparation method to reduce overall preparation time, looking at shortened gelation and solvent exchange times, although, preliminary results have been presented in Appendix C.
- Further study on activation of the xerogels produced, with chemical activation proposed to determine its effect on microporous properties of the carbon xerogels formed and how this would influence material efficiency for CO_2 capture.
- Investigate the nitrogen functional groups present by X-ray photoelectron spectroscopy (XPS) before and after pyrolysis, and activation, of the prepared xerogels to determine the nature of the nitrogen functionalities present.
- Selectivity studies using *IAST* should be carried out on pure streams to predict how selective MRF xerogels would adsorb CO_2 over N_2 in a competing environment.

Further work on Ionic-liquids Impregnated Activated Carbons (IIAC):

- Investigate alternative ionic liquids suitable for wet impregnation on AC with special emphasis on CO_2 affinity of the proposed ionic liquids.
- Research methods of encapsulating ionic liquids in a one step process, and also by a synthetic route capable of modifying the support material without compromising the textural properties.

10.1 Results from preliminary work undertaken related to future work recommendations

Preliminary investigations carried out on materials prepared but not contained within the body of research reported.

Fine tuning of the synthesis process to improve BIAS repeatability with reduced associated error; five unique synthetic approaches were proposed:

- Run 1 – Vigorous stirring of the reaction solution until silica aggregation begins, reaction was continued for 1 min before the reaction was terminated (pH ≈ 8.58).
- Run 2 – Normal synthesis used but aggregated amine silica was washed once instead of the standard three times (pH = 7.05)
- Run 3 – Normal synthesis was employed but reaction was terminated as soon as silica aggregation commenced (pH ≈ 8.89).
- Run 4 – Vigorous stirring until aggregation, then run was terminated (pH ≈ 9.55).
- Run 5 – vigorous stirring until pH ≈ 7.00 was attained.

The results from these preliminary tests suggest that there is a higher degree of repeatability using runs 3 and 5, although, more investigations are required to rule out any uncertainty and improve the synthesis repeatability (Appendix A).

Scaled up production of the bio inspired amine silica to investigate the reliability of the proposed scale up parameters

It is essential that, for commercialisation, the synthetic process can be scaled up to produce optimized materials while using predetermined amounts of reagents; so far, scale up parameters have been tested for samples produced on 50 ml and 500 ml scales (DETA BIAS samples only) with considerable degrees of accuracy achieved (> 95%). Other amine sources can be compared and, where possible, larger production scales can be adopted to further validate the proposed scale up parameters.

Amine in situ-impregnated silica

An alternative solvent for use in the in situ-impregnation technique for preparing AIIS samples was investigated, with water used instead of methanol; N_2 sorption, elemental and CO_2 sorption at 333 K (10 and 100 kPa) analyses (Appendix B) were used to characterise the samples produced and also to serve as a comparison to materials prepared using methanol. Initial results showed some comparable properties i.e. N-content, although CO_2 capacities were significantly reduced when water was used as the solvent. SEM could be used to show if changes in morphology influence the CO_2 capacity with regards CO_2 diffusivity within the pores.

Nitrogen enriched resorcinol formaldehyde organic and carbon xerogels

Is it essential that, not only should the synthesis process by simple, it should also be cheap and efficient and, so far in this study, we have shown that using the standard synthesis method proposed by Pekala [132] produces sorbents that are efficient, cheap, simple and can be produced to scale. Although, sorbent preparation is in excess of 8 days start to finish, with an additional day each for carbonisation and activation. Preliminary studies have shown that materials with similar characteristics (textural properties and N-content) can be synthesised in 3 days with an extra day needed for carbonisation and activation (Appendix C), hence, allowing reduced production costs and increased material throughput. It is, therefore, beneficial that more work be carried out to investigate the long term effects of altering the synthesis process and a detailed cost benefit analysis carried out.

Investigation of the plateau at lower CO_2 adsorption pressure (100 kPa) for MRF carbon xerogels

Detailed study of the plateau observed for the MRF samples would be beneficial in understanding why there was a maximum CO_2 adsorption capacity observed at 10 and 100 kPa, even though, from the CHN analysis carried out, the nitrogen content within the carbon xerogel continued to increase with increasing melamine content. It would also be beneficial to use techniques that can provide greater understanding regarding the chemical structure of MRF organic and carbon xerogels, as well as the mechanism of CO_2 adsorption. X-ray photoelectron spectroscopy (XPS), for

example, could provide chemical bonding information of the blank materials (RF organic and carbon xerogels) and the melamine doped counterparts.

Finally, the use of alternative nitrogen rich precursors e.g. ammeline and ammelide; where the presence of the hydroxyl group in the triazine ring increases the solubility of the precursor in basic media would allow for their increased incorporation into the final gel formed. Melamine, was restricted to concentrations ≤ 40 wt% due to solubility issues, hence, ammeline and/or ammelide, as nitrogen enriching agents, are proposed to increase nitrogen contents of the suite of materials obtainable (i.e. > 40 wt%).

Ionic liquids (ILs) WET impregnated onto activated carbons

An alternative to wet impregnation is encapsulation of the ionic liquid within the aggregated silica. Preliminary studies have been conducted, which show that the synthesis is feasible, although not reported within this work; it would be a plausible alternative to the wet impregnation method which was adopted, to show that ionic liquids can be impregnated within a porous medium in a single step synthetic method.

11 REFERENCES

[1] Ball DW. Physical Chemistry Handbook; Brooks and Cole; Second edition, **2002**

[2] Biello D. 400 PPM: Carbon Dioxide in the Atmosphere Reaches Prehistoric Levels. Retrieved May. **2013**;19:**2013**.

[3] Metz B, Davidson O, De Coninck H, Loos M, Meyer L. IPCC special report on carbon dioxide capture and storage. Prepared by Working Group III of the Intergovernmental Panel on Climate Change. IPCC, Cambridge University Press: Cambridge, United Kingdom and New York, USA. **2005**;4.

[4] Solomon, S., D. Qin, M. Manning, Z. Chen, M. Marquis, K.B. Averyt, M. Tignor and H.L. Miller. Climate change IPCC Fourth Assessment Report. The Physical Science Basis. Cambridge university press; **2007**.

[5] National Resource Defence Council (NRDC). Concequences of global warming. http://www.nrdc.org/globalwarming/fcons/fcons1.asp; **2014**.

[6] Prentice I, Farquhar G, Fasham M, Goulden M, Heimann M, Jaramillo V, et al. The carbon cycle and atmospheric carbon dioxide. **2001**.

[7] Arrhenius S. XXXI. On the influence of carbonic acid in the air upon the temperature of the ground. The London, Edinburgh, and Dublin Philosophical Magazine and Journal of Science. **1896**;41(251):237-76.

[8] Keeling CD. The concentration and isotopic abundances of carbon dioxide in the atmosphere. Tellus. **1960**;12(2):200-3.

[9] Callendar GS. On the amount of carbon dioxide in the atmosphere. Tellus. **1958**;10(2):243-8.

[10] Bray J. An analysis of the possible recent change in atmospheric carbon dioxide concentration. Tellus. **1959**;11(2):220-30.

[11] Berger A. The effect of greenhouse gases on climate. Proceedings of the Conference on Future Energy Systems and Technology for CO_2 Abatement; Antwerp, Belgium, **2002** p. 18-9.

[12] Raynaud D, Jouzel J, Barnola J, Chappellaz J, Delmas R, Lorius C. The ice record of greenhouse gases. Science-New York then Washington DC. **1993**;259:926.

[13] Mitchell JF. The “greenhouse” effect and climate change. Reviews of Geophysics. **1989**;27(1):115-39.

[14] Zhang C, Song W, Sun G, Xie L, Wang J, Li K, et al. CO_2 capture with activated carbon grafted by nitrogenous functional groups. Energy & Fuels. **2013**;27(8):4818-23.

[15] Rojey A, Torp T. Capture and geological storage of CO_2: an overview. Editions technip 27 Rue Ginoux, 75737 Paris 15, France **2005**.

[16] Quéré CL, Andres RJ, Boden T, Conway T, Houghton R, House JI, et al. The global carbon budget 1959–2011. Earth System Science Data. **2013**;5(1):165-85.

[17] Morrissey WA, Justus JR. Global climate change. Congressional Research Service, Library of Congress, Resources, Science, and Industry Division; updated 2001

[18] Carapellucci R, Milazzo A. Membrane systems for CO_2 capture and their integration with gas turbine plants. Proceedings of the Institution of Mechanical Engineers, Part A: Journal of Power and Energy. **2003**;217(5):505-17.

[19] United Nations Framework Convention on Climate Change (UNFCCC). **1992**.

[20] Schipper ELF. Conceptual History of Adaptation in the UNFCCC Process. Review of European Community & International Environmental Law. **2006**;15(1):82-92.

[21] De Chazournes LB. Kyoto Protocol to the United Nations Framework Convention on Climate Change. UN’s Audiovisual Library of International Law (http://untreaty un org/cod/avl/ha/kpccc/kpccc html). **1998**.

[22] Act CC. Elizabeth II. Chapter 27. her Majesty’s Stationery office, London, UK **2008**.

[23] Department of energy and climate change, 2013 UK Greenhouse Gas Emissions, Final Figures. Statistical release. **2014**.

[24] Olivier JG, Janssens-Maenhout G, Peters JA. Trends in global CO_2 emissions: 2012 report: PBL Netherlands Environmental Assessment Agency; **2012.**

[25] Pevida C, Drage T, Snape CE. Silica-templated melamine–formaldehyde resin derived adsorbents for CO_2 capture. Carbon. **2008**;46(11):1464-74.

[26] Samanta A, Zhao A, Shimizu GKH, Sarkar P, Gupta R. Post-combustion CO_2 Capture Using Solid Sorbents–A Review. Industrial & Engineering Chemistry Research. **2012**.

[27] Gibbins J, Chalmers H. Preparing for global rollout: A [] developed country first'demonstration programme for rapid CCS deployment. Energy Policy. **2008**;36(2):501-7.

[28] EIA U. Annual energy outlook 2013. US Energy Information Administration, Washington, DC. **2013**.

[29] Samanta A, Zhao A, Shimizu GKH, Sarkar P, Gupta R. Post-Combustion CO_2 Capture Using Solid Sorbents: A Review. Industrial & Engineering Chemistry Research. **2011**;51(4):1438-63.

[30] Sjostrom S, Krutka H. Evaluation of solid sorbents as a retrofit technology for CO_2 capture. Fuel. **2010**;89(6):1298-306.

[31] Yang H, Xu Z, Fan M, Gupta R, Slimane RB, Bland AE, et al. Progress in carbon dioxide separation and capture: A review. Journal of Environmental Sciences. **2008**;20(1):14-27.

[32] Kanniche M, Gros-Bonnivard R, Jaud P, Valle-Marcos J, Amann J-M, Bouallou C. Pre-combustion, post-combustion and oxy-combustion in thermal power plant for CO_2 capture. Applied Thermal Engineering. **2010**;30(1):53-62.

[33] Luby P, Susta MR. Exploring the many carbon capture options. Power. **2007**;151(4).

[34] Davidson RM. Post-combustion carbon capture from coal fired plants: solvent scrubbing: IEA Clean Coal Centre London; **2007**.

[35] Rubin ES, Rao AB, Berkenpas MB. Development and application of optimal design capability for coal gasification systems: Carnegie-Mellon University; **2007**.

[36] Figueroa JD, Fout T, Plasynski S, McIlvried H, Srivastava RD. Advances in CO_2 capture technology. The US Department of Energy's carbon sequestration program. International Journal of Greenhouse Gas Control. **2008**;2(1):9-20.

[37] Qiu H, Lv L, Pan B, Zhang Q, Zhang W. Critical review in adsorption kinetic models. Journal of Zhejiang University-Science A. **2009**;10(5):716-24.

[38] Gielen D. The Future Role of CO_2 Capture and Storage Results of the IEA-ETP Model.International energy agancy, report number EET/2003/04 Paris November. **2003**.

[39] Danckwerts P. The reaction of CO_2 with ethanolamines. Chemical Engineering Science. **1979**;34(4):443-6.

[40] Donaldson TL, Nguyen YN. Carbon dioxide reaction kinetics and transport in aqueous amine membranes. Industrial & Engineering Chemistry Fundamentals. **1980**;19(3):260-6.

[41] Caplow M. Kinetics of carbamate formation and breakdown. Journal of the American Chemical Society. **1968**;90(24):6795-803.

[42] Zhang X, Zhang C-F, Liu Y. Kinetics of absorption of CO_2 into aqueous solution of MDEA blended with DEA. Industrial & Engineering Chemistry Research. **2002**;41(5):1135-41.

[43] Arnold D. CO_2 can be produced from flue gas. Oil Gas J;(United States). **1982**;80(47).

[44] Rochelle GT. Amine scrubbing for CO_2 capture. Science. **2009**;325(5948):1652-4.

[45] Agency IE. Biofuels for transport: an international perspective: International Energy Agency, Organisation For Economic Co-Operation And Developmen (OECD); **2004**.

[46] Figueroa JD, Fout T, Plasynski S, McIlvried H, Srivastava RD. Advances in CO_2 capture technology. The U.S. Department of Energy's Carbon Sequestration Program. International Journal of Greenhouse Gas Control. **2008**;2(1):9-20.

[47] Bai H, Yeh AC. Removal of CO_2 Greenhouse Gas by Ammonia Scrubbing. Industrial & Engineering Chemistry Research. **1997**;36(6):2490-3.

[48] Gal E. Ultra cleaning combustion gas including the removal of CO_2. World Intellectual Property, Patent WO. **2006**;2006022885.

[49] Knuutila H, Svendsen HF, Anttila M. CO_2 capture from coal-fired power plants based on sodium carbonate slurry; a systems feasibility and sensitivity study. International Journal of Greenhouse Gas Control. **2009**;3(2):143-51.

[50] Hatch Jr T, Pigford R. Simultaneous absorption of carbon dioxide and ammonia in water. Industrial & Engineering Chemistry Fundamentals. **1962**;1(3):209-14.

[51] Koutinas AA, Yianoulis P, Lycourghiotis A. Industrial scale modelling of the thermochemical energy storage system based on $CO_2 + 2NH_3 \leftrightarrow NH_2COONH_4$ equilibrium. Energy Conversion and Management. **1983**;23(1):55-63.

[52] Brooks L, Audrieta L, Bluestone H, Jofinsox WC. Ammonium carbamate. Inorganic Syntheses, Wiley online library, Volume 2. **1946**:85-6.

[53] Siriwardane RV, Robinson C, Shen M, Simonyi T. Novel Regenerable Sodium-Based Sorbents for CO_2 Capture at Warm Gas Temperatures. Energy & Fuels. **2007**;21(4):2088-97.

[54] Baciocchi R, Storti G, Mazzotti M. Process design and energy requirements for the capture of carbon dioxide from air. Chemical Engineering and Processing: Process Intensification. **2006**;45(12):1047-58.

[55] Mahmoudkhani M, Keith DW. Low-energy sodium hydroxide recovery for CO_2 capture from atmospheric air. Thermodynamic analysis. International Journal of Greenhouse Gas Control. **2009**;3(4):376-84.

[56] Rao AB, Rubin ES, Keith DW, Granger Morgan M. Evaluation of potential cost reductions from improved amine-based CO_2 capture systems. Energy Policy. **2006**;34(18):3765-72.

[57] Wilcox J. Carbon capture: Springer, New York Dordrecht Heidelberg London; **2012**.

[58] Hart A, Gnanendran N. Cryogenic CO_2 capture in natural gas. Energy Procedia. **2009**;1(1):697-706.

[59] Bredesen R, Jordal K, Bolland O. High-temperature membranes in power generation with CO_2 capture. Chemical Engineering and Processing: Process Intensification. **2004**;43(9):1129-58.

[60] Li S, Falconer JL, Noble RD. SAPO-34 membranes for CO_2/CH_4 separation. Journal of Membrane Science. **2004**;241(1):121-35.

[61] Olajire AA. CO_2 capture and separation technologies for end-of-pipe applications . A review. Energy. **2010**;35(6):2610-28.

[62] Ruthven DM. Principles of adsorption and adsorption processes: John Wiley & Sons; **1984**.

[63] Khatri RA, Chuang SS, Soong Y, Gray M. Thermal and chemical stability of regenerable solid amine sorbent for CO_2 capture. Energy & Fuels. **2006**;20(4):1514-20.

[64] Ruthven DM. Principles of adsorption and adsorption processes. John wileyand sons, New york; **1984**.

[65] Roop CB, Meenakshi G. Activated carbon adsorption. CRC PressTaylor & Francis Group, NW, FL. **2005**.

[66] Plaza MG, Pevida C, Arenillas A, Rubiera F, Pis JJ. CO_2 capture by adsorption with nitrogen enriched carbons. Fuel. **2007**;86(14 SPEC. ISS.):2204-12.

[67] Pevida C, Plaza M, Arias B, Fermoso J, Rubiera F, Pis J. Surface modification of activated carbons for CO_2 capture. Applied Surface Science. **2008**;254(22):7165-72.

[68] Sevilla M, Valle-Vigón P, Fuertes AB. N-Doped Polypyrrole-Based Porous Carbons for CO_2 Capture. Advanced Functional Materials. **2011**;21(14):2781-7.

[69] Bezerra DP, Oliveira RS, Vieira RS, Cavalcante Jr CL, Azevedo DC. Adsorption of CO_2 on nitrogen-enriched activated carbon and zeolite 13X. Adsorption. **2011**;17(1):235-46.

[70] Hao GP, Li WC, Qian D, Lu AH. Rapid Synthesis of Nitrogen-Doped Porous Carbon Monolith for CO_2 Capture. Advanced Materials. **2010**;22(7):853-7.

[71] Llewellyn P. Adsorption by Powders and Porous Solids (Second Edition). Oxford: Academic Press **2014**, p. 529-64.

[72] Wei J, Shi J, Pan H, Zhao W, Ye Q, Shi Y. Adsorption of carbon dioxide on organically functionalized SBA-16. Microporous and Mesoporous Materials. **2008**;116(1–3):394-9.

[73] Liang Z, Fadhel B, Schneider CJ, Chaffee AL. Adsorption of CO_2 on mesocellular siliceous foam iteratively functionalized with dendrimers. Adsorption. **2009**;15(5-6):429-37.

[74] Zeleňák V, Badaničová M, Halamová D, Čejka J, Zukal A, Murafa N, et al. Amine-modified ordered mesoporous silica: Effect of pore size on carbon dioxide capture. Chemical Engineering Journal. **2008**;144(2):336-42.

[75] Hoffmann F, Cornelius M, Morell J, Fröba M. Silica-based mesoporous organic–inorganic hybrid materials. Angewandte Chemie International Edition. 2006;45(20):3216-51.

[76] Welton T. Room-temperature ionic liquids. Solvents for synthesis and catalysis. Chemical Reviews. **1999**;99(8):2071-84.

[77] Wasserscheid P, Keim W. Ionic liquids-new" solutions" for transition metal catalysis. Angewandte Chemie. **2000**;39(21):3772-89.

[78] Blanchard LA, Gu Z, Brennecke JF. High-pressure phase behavior of ionic liquid/CO_2 systems. The Journal of Physical Chemistry B. **2001**;105(12):2437-44.

[79] Anthony JL, Anderson JL, Maginn EJ, Brennecke JF. Anion effects on gas solubility in ionic liquids. The Journal of Physical Chemistry B. **2005**;109(13):6366-74.

[80] Wang X, Akhmedov NG, Duan Y, Luebke D, Hopkinson D, Li B. Amino acid-functionalized ionic liquid solid sorbents for post-combustion carbon capture. ACS applied materials & interfaces. **2013**;5(17):8670-7.

[81] Thiruvenkatachari R, Su S, An H, Yu XX. Post combustion CO_2 capture by carbon fibre monolithic adsorbents. Progress in Energy and Combustion Science. **2009**;35(5):438-55.

[82] Howard H, Jerry M, Alan H Advanced Post-Combustion CO_2 Capture, Clean Air Task Force. **2009**.

[83] Sircar S. Pressure swing adsorption. Industrial & Engineering Chemistry Research. **2002**;41(6):1389-92.

[84] Skarstrom c. patent 2,944,627, Skarstrom method and apparatus for fractionating gaseous mixtures by adsorption; July **1960**.

[85] Tarka T, Ciferno J, Gray M, Fauth D. CO_2 capture systems using amine enhanced solid sorbents.

[86] F. Rouquerol, J. Rouquerol, Sing K. Adsorption by Powders and Porous Solids - Principles, Methodology and Applications: Academic Press; **1999**.

[87] Masel RI. Principles of adsorption and reaction on solid surfaces. **1996**.

[88] Do Duong D. Adsorption analysis: equilibria and kinetics: Imperial College Press; London SW7 2BT; **1998**.

[89] Gregg SJ, Sing KSW, Salzberg H. Adsorption surface area and porosity. Journal of The Electrochemical Society. **1967**;114(11):279C-C.

[90] Young DM, Crowell AD. Physical adsorption of gases. Butterworths press; **1962**.

[91] Corporation MI. Gas Adsorption Theory; http://www.micromeritics.com/repository/files/gas_adsorption_theory_poster.pdf; **2014**.

[92] The recommendations for the characterization of porous solids. Pure and applied chemistry. **1994**;66(8):1739-58.

[93] Brunauer S, Deming LS, Deming WE, Teller E. On a Theory of the van der Waals Adsorption of Gases. Journal of the American Chemical Society. **1940**;62(7):1723-32.

[94] Brunauer S, Emmett PH, Teller E. Adsorption of Gases in Multimolecular Layers. Journal of the American Chemical Society. **1938**;60(2):309-19.

[95] Sing KS. Reporting physisorption data for gas/solid systems with special reference to the determination of surface area and porosity (Recommendations 1984). Pure and applied chemistry. **1985**;57(4):603-19.

[96] Fletcher A. Porosity and sorption behaviour. Internet site: http://www. staff. ncl. ac. uk/aj fletcher **2006**.

[97] De Boer J, Everett D, Stone F. The structure and properties of porous materials. Butterworths, London. **1958**;10:68.

[98] De Boer J, Lippens B, Linsen B, Broekhoff J, Van den Heuvel A, Osinga TJ. The t-curve of multimolecular N_2 adsorption. Journal of Colloid and Interface Science. **1966**;21(4):405-14.

[99] Burgess CG, Everett DH, Nuttall S. Adsorption hysteresis in porous materials. Pure and applied chemistry. **1989**;61(11):1845-52.

[100] Dr. Vladimar Ponec, Dr. Zlatko Knor, Cerny DS. Adsorption on Solids. Butterworth & co; Czechoslovakia: **1974**.

[101] Klobes P, Meyer K, Munro RG. Porosity and specific surface area measurements for solid materials: US Department of Commerce, Technology Administration, National Institute of Standards and Technology; **2006**.

[102] Arenas JP, Crocker MJ. Recent Trends in Porous Sound-Absorbing Materials. Sound & Vibration. **2010**;44(7):12-8.

[103] Ponec V, Knor Z, Černý S, Smith D, Adams N. Adsorption on solids: Butterworths London; **1974**.

[104] Rouquerol J, Rouquerol F, Llewellyn P, Maurin G, Sing KS. Adsorption by powders and porous solids: principles, methodology and applications: Academic press; Oxford UK, **2013**.

[105] Langmuir I. The adsorption of gases on plane surfaces of glass, mica and platinum. Journal of the American Chemical Society. **1918**;40(9):1361-403.

[106] Lippens BC, de Boer JH. Studies on pore systems in catalysts: V. The t method. Journal of Catalysis. **1965**;4(3):319-23.

[107] Polanyi M. The Potential Theory of Adsorption. Science. **1963**;141(3585):1010-3.

[108] Polanyi M. Section III. Theories of the adsorption of gases. A general survey and some additional remarks. Introductory paper to section III. Transactions of the Faraday Society. **1932**;28:316-33.

[109] Gil A, Grange P. Application of the Dubinin-Radushkevich and Dubinin-Astakhov equations in the characterization of microporous solids. Colloids and Surfaces A: Physicochemical and Engineering Aspects. **1996**;113(1–2):39-50.

[110] Boushehri A, Bzowski J, Kestin J, Mason E. Equilibrium and transport properties of eleven polyatomic gases at low density. Journal of physical and chemical reference data. **1987**;16(3):445-66.

[111] Marsh H, Rand B. The characterization of microporous carbons by means of the Dubinin-Radushkevich equation. Journal of Colloid and Interface Science. **1970**;33(1):101-16.

[112] Huber U, Stoeckli F, Houriet J-P. A generalization of the Dubinin-Radushkevich equation for the filling of heterogeneous micropore systems in strongly activated carbons. Journal of Colloid and Interface Science. **1978**;67(2):195-203.

[113] Robinson JW, Frame EMS, Frame GM, Skelly Frame EM, Frame Ii GM. Undergraduate Instrumental Analysis, 6th Edition; **2005**.

[114] Barrett EP, Joyner LG, Halenda PP. The Determination of Pore Volume and Area Distributions in Porous Substances. I. Computations from Nitrogen Isotherms. Journal of the American Chemical Society. **1951**;73(1):373-80.

[115] Griffiths P, De Haseth JA. Fourier transform infrared spectrometry: John Wiley & Sons; **2007**.

[116] Roberts BF. A procedure for estimating pore volume and area distributions from sorption isotherms. Journal of Colloid and Interface Science. **1967**;23(2):266-73.

[117] Benham M, Ross D. Experimental determination of absorption-desorption isotherms by computer-controlled gravimetric analysis. Z Phys Chem NF. **1989**;163:S25-S32.

[118] Smith BC. Fundamentals of Fourier transform infrared spectroscopy: CRC press; USA, **2011**.

[119] Kalantar-zadeh K, Fry B. Nanotechnology-enabled sensors: Springer; **2007**.

[120] Ewing GW. Analytical instrumentation handbook: CRC Press; USA, **1997**.

[121] Ryland AL. X-ray diffraction. Journal of Chemical Education. **1958**;35(2):80.

[122] Cole H. Bragg's law and energy sensitive detectors. Journal of Applied Crystallography. **1970**;3(5):405-6.

[123] Jenkins R, Snyder R. Introduction to X-ray powder diffractometry: John Wiley & Sons; **2012**.

[124] Gabbott P. Principles and applications of thermal analysis: John Wiley & Sons; **2008**.

[125] Menczel JD, Prime RB. Thermal analysis of polymers, fundamentals and applications: John Wiley & Sons; New Jersey and Canada **2009**.

[126] Belton DJ, Patwardhan SV, Annenkov VV, Danilovtseva EN, Perry CC. From biosilicification to tailored materials: Optimizing hydrophobic domains and resistance to protonation of polyamines. Proceedings of the National Academy of Sciences. **2008**;105(16):5963-8.

[127] Mathew L, Narayanankutty SK. Synthesis and characterization of nanosilica. International conference on advances in polymer technology; p. 279.

[128] Horacio E. The Colloid Chemistry of Silica: Developed from a Symposium Sponsored by the Division of Colloid and Surface Chemistry, at the 200th National Meeting of the American Chemical Society, Washington, DC, August 26-31, **1990**.

[129] Kotoky T, Dolui SK. Synthesis and Characterisation of Polyvinyl alcohol (PVA)/Silica Hybrid Composites Derived Through the Sol-Gel Method in Aqueous Medium: Effect of Acid Content, Silica Content and Viscosity of

PVA on the Dispersion Characteristics of Silica and the Physical Properties of the Composites. Journal of Sol-Gel Science and Technology. **2004**;29(2):107-14.

[130] Wang X, Ma X, Xu X, Sun L, Song C. Mesoporous-molecular-sieve-supported Polymer Sorbents for Removing H2S from Hydrogen Gas Streams. Top Catal. **2008**;49(1-2):108-17.

[131] Pekala R, Kong FM. Resorcinol-formaldehyde aerogels and their carbonized derivatives. Abstracts of papers of the American Chemical Society: 1155 16th St, NW, Washington, DC **2003**; p. 113.

[132] Pekala R. Organic aerogels from the polycondensation of resorcinol with formaldehyde. Journal of Materials Science. **1989**;24(9):3221-7.

[133] Pekala RW. Low density, resorcinol-formaldehyde aerogels. Google Patents **1989**.

[134] Xing W, Liu C, Zhou Z, Zhang L, Zhou J, Zhuo S, et al. Superior CO_2 uptake of N-doped activated carbon through hydrogen-bonding interaction. Energy & Environmental Science. **2012**;5(6):7323-7.

[135] Cook R, Letts S, Overturf III G, Lambert S, Wilemski G, Schroen-Carey D. Final Report UCRL-LR-105821-97-1. Lawrence Livermore National Laboratory, Livermore, CA. **1997**.

[136] Al-Muhtaseb SA, Ritter JA. Preparation and properties of resorcinol–formaldehyde organic and carbon gels. Advanced Materials. **2003**;15(2):101-14.

[137] Muldoon MJ, Aki SN, Anderson JL, Dixon JK, Brennecke JF. Improving carbon dioxide solubility in ionic liquids. The Journal of Physical Chemistry B. **2007**;111(30):9001-9.

[138] Ren J, Wu L, Li B-G. Preparation and CO_2 sorption/desorption of N-(3-aminopropyl) aminoethyl tributylphosphonium amino acid salt ionic liquids supported into porous silica particles. Industrial & Engineering Chemistry Research. **2012**;51(23):7901-9.

[139] Zhang Z, Wu L, Dong J, Li B-G, Zhu S. Preparation and SO_2 sorption/desorption behavior of an ionic liquid supported on porous silica particles. Industrial & Engineering Chemistry Research. **2009**;48(4):2142-8.

[140] Gray M, Hoffman J, Hreha D, Fauth D, Hedges S, Champagne K, et al. Parametric study of solid amine sorbents for the capture of carbon dioxide†. Energy & Fuels. **2009**;23(10):4840-4.

[141] Li B, Jiang B, Fauth DJ, Gray ML, Pennline HW, Richards GA. Innovative nano-layered solid sorbents for CO_2 capture. Chemical Communications. **2011**;47(6):1719-21.

[142] Webley PA, Xiao P, Zhang J. Recovery of carbon dioxide from flue gas streams by vacuum swing adsorption. **2005**.

[143] Bäuerlein E. Biomineralization of Unicellular Organisms: An Unusual Membrane Biochemistry for the Production of Inorganic Nano- and Microstructures. Angewandte Chemie International Edition. **2003**;42(6):614-41

[144] Halas NJ. Nanoscience under Glass: The Versatile Chemistry of Silica Nanostructures. ACS Nano. **2008**;2(2):179-83.

[145] Kröger N, Deutzmann R, Sumper M. Polycationic peptides from diatom biosilica that direct silica nanosphere formation. Science. **1999**;286(5442):1129-32.

[146] Liu S-H, Wu C-H, Lee H-K, Liu S-B. Highly stable amine-modified mesoporous silica materials for efficient CO_2 capture. Top Catal. **2010**;53(3-4):210-7.

[147] Yan X, Zhang L, Zhang Y, Qiao K, Yan Z, Komarneni S. Amine-modified mesocellular silica foams for CO_2 capture. Chemical Engineering Journal. **2011**;168(2):918-24.

[148] Samanta A, Zhao A, Shimizu GK, Sarkar P, Gupta R. Post-combustion CO_2 capture using solid sorbents: a review. Industrial & Engineering Chemistry Research. **2011**;51(4):1438-63.

[149] Gök Ö, Özcan AS, Özcan A. Adsorption kinetics of naphthalene onto organo-sepiolite from aqueous solutions. Desalination. **2008**;220(1-3):96-107.

[150] Aziz B, Hedin N, Bacsik Z. Quantification of chemisorption and physisorption of carbon dioxide on porous silica modified by propylamines: Effect of amine density. Microporous and Mesoporous Materials. **2012**;146):42-9.

[151] Bhagiyalakshmi M, Park SD, Cha WS, Jang HT. Development of TREN dendrimers over mesoporous SBA-15 for CO_2 adsorption. Applied Surface Science. **2010**;256(22):6660-6.

[152] Zhang X, Zhang X, Dong H, Zhao Z, Zhang S, Huang Y. Carbon capture with ionic liquids: overview and progress. Energy & Environmental Science. **2012**;5(5):6668-81.

[153] Zhang Z, Ma X, Wang D, Song C, Wang Y. Development of silica-gel-supported polyethylenimine sorbents for CO_2 capture from flue gas. AIChE Journal. **2012**;58(8):2495-502.

[154] Ma X, Wang X, Song C. "Molecular Basket" Sorbents for Separation of CO_2 and H2S from Various Gas Streams. Journal of the American Chemical Society. **2009**;131(16):5777-83.

[155] Stuart B. Infrared spectroscopy; Fundenmental and application.Wiley Online Library; **2004**.

[156] Xu X, Song C, Andresen JM, Miller BG, Scaroni AW. Novel Polyethylenimine-Modified Mesoporous Molecular Sieve of MCM-41 type as High-Capacity Adsorbent for CO_2 Capture. Energy & Fuels. **2002**;16(6):1463-9.

[157] Dao DS, Yamada H, Yogo K. Large-Pore Mesostructured Silica Impregnated with Blended Amines for CO_2 Capture. Industrial & Engineering Chemistry Research. **2013**;52(38):13810-7.

[158] Vaidhyanathan R, Iremonger SS, Shimizu GKH, Boyd PG, Alavi S, Woo TK. Direct Observation and Quantification of CO_2 Binding within an amine-functionalized nanoporous solid. Science, **2010**;330(6004):650-3

[159] Aziz B, Zhao G, Hedin N. Carbon Dioxide Sorbents with propylamine groups−silica functionalized with a fractional factorial design approach. Langmuir. **2011**;27(7):3822-34

[160] Bezerra D, Oliveira R, Vieira R, Cavalcante C, Jr., Azevedo DS. Adsorption of CO_2 on nitrogen-enriched activated carbon and zeolite 13X. Adsorption. **2011**;17(1):235-46.

[161] Arenillas A, Rubiera F, Parra JB, Ania CO, Pis JJ. Surface modification of low cost carbons for their application in the environmental protection. Applied Surface Science. **2005**;252(3):619-24.

[162] Heydari-Gorji A, Belmabkhout Y, Sayari A. Polyethylenimine-Impregnated Mesoporous Silica: Effect of Amine Loading and Surface Alkyl Chains on CO_2 Adsorption. Langmuir. **2011**;27(20):12411-6.

[163] Qi G, Wang Y, Estevez L, Duan X, Anako N, Park A-HA, et al. High efficiency nanocomposite sorbents for CO_2 capture based on amine-functionalized mesoporous capsules. Energy Enviromental Science. **2010**;4(2):444-52.

[164] Wang HC, Lu C, Bai H, Hwang JF, Lee HH, Chen W, et al. Pilot-scale production of mesoporous silica-based adsorbent for CO_2 capture. Applied Science. **2012**.

[165] Sayari A, Belmabkhout Y, Serna-Guerrero R. Flue gas treatment via CO_2 adsorption. Chemical Engineering Journal. **2011**;171(3):760-74.

[166] Chen C, Yang S-T, Ahn W-S, Ryoo R. Amine-impregnated silica monolith with a hierarchical pore structure: enhancement of CO_2 capture capacity. Chemical Communications. **2009**;0(24):3627-9.

[167] Wang K, Shang H, Li L, Yan X, Yan Z, Liu C, et al. Efficient CO_2 capture on low-cost silica gel modified by polyethyleneimine. Journal of Natural Gas Chemistry. **2012**;21(3):319-23.

[168] Zhang X, Zheng X, Zhang S, Zhao B, Wu W. AM-TEPA Impregnated Disordered Mesoporous Silica as CO_2 Capture Adsorbent for Balanced Adsorption–Desorption Properties. Industrial & Engineering Chemistry Research. **2012**;51(46):15163-9.

[169] Wang D, Sentorun-Shalaby C, Ma X, Song C. High-Capacity and Low-Cost Carbon-Based "Molecular Basket" Sorbent for CO_2 Capture from Flue Gas. Energy & Fuels. **2010**;25(1):456-8.

[170] Zhao Y, Shen Y, Bai L. Effect of chemical modification on carbon dioxide adsorption property of mesoporous silica. Journal of Colloid and Interface Science. **2012**;379(1):94-100.

[171] Goeppert A, Czaun M, May RB, Prakash GS, Olah GA, Narayanan S. Carbon dioxide capture from the air using a polyamine based regenerable solid adsorbent. Journal of the American Chemical Society. **2011**;133(50):20164-7.

[172] Wang K, Shang H, Li L, Yan X, Yan Z, Liu C, et al. Efficient CO_2 capture on low-cost silica gel modified by polyethyleneimine. Journal of Natural Gas Chemistry. **2012**;21(3):319-23.

[173] Duan G, Zhang C, Li A, Yang X, Lu L, Wang X. Preparation and characterization of mesoporous zirconia made by using a poly (methyl methacrylate) template. Nanoscale Research Letters. **2008**;3(3):118-22.

[174] Condon JB. Surface area and porosity determinations by physisorption: measurements and theory: Elsevier; **2006**.

[175] Zhao Y, Shen Y, Bai L, Ni S. Carbon dioxide adsorption on polyacrylamide-impregnated silica gel and breakthrough modeling. Applied Surface Science. **2012**;261:708-16.

[176] Zhang C, Song W, Sun G, Xie L-J, Wang J, Li K, et al. CO_2 capture with activated carbon grafted by nitrogenous functional groups. Energy & Fuels. Amerciacan Chemical Society; **2013**.

[177] Sircar S, Golden TC, Rao MB. Activated carbon for gas separation and storage. Carbon. **1996**;34(1):1-12.

[178] Zhao Y, Zhao L, Yao KX, Yang Y, Zhang Q, Han Y. Novel porous carbon materials with ultrahigh nitrogen contents for selective CO_2 capture. Journal of Materials Chemistry. **2012**;22(37):19726-31.

[179] Houshmand A, Daud W, Lee M-G, Shafeeyan M. Carbon Dioxide Capture with Amine-Grafted Activated Carbon. Water Air Soil Pollut. **2012**;223(2):827-35.

[180] Shafeeyan MS, Daud WMAW, Houshmand A, Shamiri A. A review on surface modification of activated carbon for carbon dioxide adsorption. Journal of Analytical and Applied Pyrolysis. **2010**;89(2):143-51.

[181] Bhown AS, Freeman BC. Analysis and status of post-combustion carbon dioxide capture technologies. Environmental science & technology. **2011**;45(20):8624-32.

[182] Mayer S, Pekala R, Kaschmitter J. The aerocapacitor: An electrochemical double-layer energy-storage device. Journal of The Electrochemical Society. **1993**;140(2):446-51.

[183] Tamon H, Ishizaka H, Mikami M, Okazaki M. Porous structure of organic and carbon aerogels synthesized by sol-gel polycondensation of resorcinol with formaldehyde. Carbon. **1997**;35(6):791-6.

[184] Pekala R, Alviso C, Kong F, Hulsey S. Aerogels derived from multifunctional organic monomers. Journal of non-crystalline solids. **1992**;145:90-8.

[185] Lu X, Arduini-Schuster M, Kuhn J, Nilsson O, Fricke J, Pekala R. Thermal conductivity of monolithic organic aerogels. Science. **1992**;255(5047):971-2.

[186] Morales-Torres S, Maldonado-Hodar FJ, Perez-Cadenas AF, Carrasco-Marin F. Textural and mechanical characteristics of carbon aerogels synthesized by polymerization of resorcinol and formaldehyde using alkali carbonates as basification agents. Physical Chemistry Chemical Physics. **2010**;12(35):10365-72.

[187] ElKhatat AM, Al-Muhtaseb SA. Advances in Tailoring Resorcinol-Formaldehyde Organic and Carbon Gels. Advanced Materials. **2011**;23(26):2887-903.

[188] Taylor SJ. Monitoring the Gelation Mechanism of Resorcinol-Formaldehyde Xerogels. PhD Thesis; **2014**.

[189] Anderson L. The Effect of the Catalyst on the Porous Properties of Resorcinol-Formaldehyde Xerogels. PhD Thesis; **2013**.

[190] Job N, Pirard R, Marien J, Pirard J-P. Porous carbon xerogels with texture tailored by pH control during sol–gel process. Carbon. **2004**;42(3):619-28.

[191] Stuart B. Infrared spectroscopy: Wiley Online Library; 2005.

[192] Chen WC, Wu SY, Liu HP, Chang CH, Chen HY, Chen HY, et al. Identification of melamine/cyanuric acid-containing nephrolithiasis by infrared spectroscopy. Journal of clinical laboratory analysis. **2010**;24(2):92-9.

[193] Lin C, Ritter JA. Effect of synthesis pH on the structure of carbon xerogels. Carbon. **1997**;35(9):1271-8.

[194] Hummel DO, Scholl. Infrared Analysis of Polymers, Resins and Additives: An Atlas. Vol. 1. Plastics, Elastomers, Fibers and Resins: Wiley; **1969**.

[195] Contreras MS, Páez CA, Zubizarreta L, Léonard A, Blacher S, Olivera-Fuentes CG, et al. A comparison of physical activation of carbon xerogels with carbon dioxide with chemical activation using hydroxides. Carbon. **2010**;48(11):3157-68.

[196] Martín-Martínez JM, Torregrosa-Maciá R, Mittelmeijer-Hazeleger MC. Mechanisms of adsorption of CO_2 in the micropores of activated anthracite. Fuel. **1995**;74(1):111-4.

[197] Vishnyakov A, Ravikovitch PI, Neimark AV. Molecular Level Models for CO_2 Sorption in Nanopores. Langmuir. **1999**;15(25):8736-42.

[198] Cazorla-Amoros D, Alcaniz-Monge J, de le Casa-Lillo M.A., Linares-Solano A. Carbon dioxide as an adsorptiove to characterise carbon molecular sieves and activated carbons. Langmuir. **1998**;14:4589-96.

[199] Cazorla-Amorós D, Alcaniz-Monge J, De la Casa-Lillo M, Linares-Solano A. CO_2 as an adsorptive to characterize carbon molecular sieves and activated carbons. Langmuir. **1998**;14(16):4589-96.

[200] Wei J, Zhou D, Sun Z, Deng Y, Xia Y, Zhao D. A Controllable Synthesis of Rich Nitrogen-Doped Ordered Mesoporous Carbon for CO_2 Capture and Supercapacitors. Advanced Functional Materials. **2013**;23(18):2322-8.

[201] Martín CF, Plaza MG, Pis JJ, Rubiera F, Pevida C, Centeno TA. On the limits of CO_2 capture capacity of carbons. Separation and Purification Technology. **2010**;74(2):225-9.

[202] Chandra V, Yu SU, Kim SH, Yoon YS, Kim DY, Kwon AH, et al. Highly selective CO_2 capture on N-doped carbon produced by chemical activation of polypyrrole functionalized graphene sheets. Chemical Communications. **2012**;48(5):735-7.

[203] Gutiérrez MC, Carriazo D, Ania CO, Parra JB, Ferrer ML, del Monte F. Deep eutectic solvents as both precursors and structure directing agents in the synthesis of nitrogen doped hierarchical carbons highly suitable for CO_2 capture. Energy & Environmental Science. **2011**;4(9):3535-44.

[204] Maroto-Valer MM, Tang Z, Zhang Y. CO_2 capture by activated and impregnated anthracites. Fuel Processing Technology. **2005**;86(14):1487-502.

[205] Saha D, Deng S. Adsorption equilibrium and kinetics of CO_2, CH_4, N_2O, and NH_3 on ordered mesoporous carbon. Journal of Colloid and Interface Science. **2010**;345(2):402-9.

[206] Meng L-Y, Park S-J. Effect of heat treatment on CO_2 adsorption of KOH-activated graphite nanofibers. Journal of Colloid and Interface Science. **2010**;352(2):498-503.

[207] Kurniawan Y, Bhatia SK, Rudolph V. Simulation of binary mixture adsorption of methane and CO_2 at supercritical conditions in carbons. AIChE Journal. **2006**;52(3):957-67.

[208] Drage T, Kozynchenko O, Pevida C, Plaza M, Rubiera F, Pis J, et al. Developing activated carbon adsorbents for pre-combustion CO_2 capture. Energy Procedia. **2009**;1(1):599-605.

[209] Buckingham A. Molecular quadrupole moments. Q Rev Chemical Society. **1959**;13(3):183-214.

[210] Drage TC, Arenillas A, Smith KM, Pevida C, Piippo S, Snape CE. Preparation of carbon dioxide adsorbents from the chemical activation of urea–formaldehyde and melamine–formaldehyde resins. Fuel. **2007**;86(1–2):22-31.

[211] Adib F, Bagreev A, Bandosz TJ. Effect of pH and Surface Chemistry on the Mechanism of H_2S Removal by Activated Carbons. Journal of Colloid and Interface Science. **1999**;216(2):360-9.

[212] Pittman C, He G-R, Wu B, Gardner S. Chemical modification of carbon fiber surfaces by nitric acid oxidation followed by reaction with tetraethylenepentamine. Carbon. **1997**;35(3):317-31.

[213] Yan X, Zhang L, Zhang Y, Yang G, Yan Z. Amine-Modified SBA-15: Effect of Pore Structure on the Performance for CO_2 Capture. Industrial & Engineering Chemistry Research. **2011**;50(6):3220-6.

[214] Gorgulho HF, Mesquita JP, Gonçalves F, Pereira MFR, Figueiredo JL. Characterization of the surface chemistry of carbon materials by potentiometric titrations and temperature-programmed desorption. Carbon. **2008**;46(12):1544-55.

[215] Marcoux L, Kim T-W, Bilodeau S, Kleitz F. Functionalized mesoporous organic-inorganic hybrids through pore surface-restricted post-polymerization. Studies in Surface Science and Catalysis. **2007**;170:1836-42.

12 APPENDIX

12.1 Appendix A

Table 12-1: CO_2 adsorption capacity and equilibration times for molar concentration varied TETA BIAS nanoparticles

Sample	Equilibration Times (mins)	CO_2 capacity (mmols g^{-1})	Equilibration Times (mins)	CO_2 capacity (mmols g^{-1})
	10 kPa		100 kPa	
TETA_1-1	230	0.206	191	0.535
TETA_2-2	484	0.280	600	0.553
TETA_3-3	1600	0.329	817	0.570
TETA_4-4	2880	0.393	777	0.617
TETA_10-10	612	0.302	2400	0.566

Table 12-2: Textural parameters obtained for repeat preparations of TEPA BIAS nanoparticles

Sample ID	S_{BET}	V_{TOTAL}	Pore size
	m^2g^{-1}	cm^3g^{-1}	nm
TEPA_1-1A	35.7	0.08	11.3
TEPA_1-1B	21.0	0.04	9.9
TEPA_1-1C	24.2	0.07	12.2
TEPA_1-1D	18.1	0.05	11.2
TEPA_1-1E	28.1	0.07	13.7
Average	25.4	0.06	11.7
Standard dev	6.8	0.02	1.4
Relative Sdev	0.3	0.33	0.1
% Relative sdev	26.8	33.33	12.0

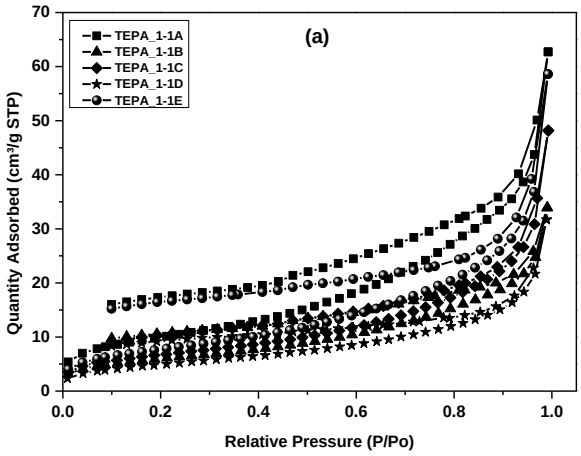

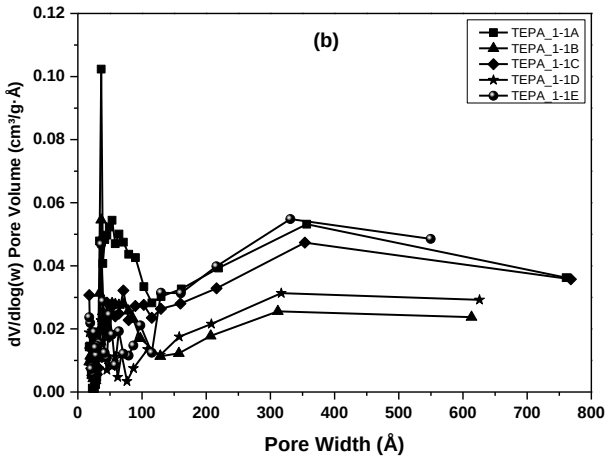

Figure 12-1: (a) N_2 sorption isotherms and (b) pore size distributions for TEPA BIAS repeat samples.

Table 12-3: Chemical properties for TEPA BIAS repeat samples from elemental analysis

Sample ID	Bio-inspired TEPA loaded silica		
	wt% C	wt% H	wt% N
TEPA_1-1A	6.5	2.2	4.0
TEPA_1-1B	6.6	2.2	4.5
TEPA_1-1C	6.2	2.1	3.6
TEPA_1-1D	6.3	2.0	4.2
TEPA_1-1E	6.5	2.4	3.8
Average	6.4	2.2	4.0
Standard dev	0.2	0.1	0.3
Relative Sdev	0.0	0.1	0.1
% Relative sdev	3.1	4.5	7.8

Table 12-4: Textural parameters obtained for repeat preparations of PEHA BIAS nanoparticles

Sample ID	S_{BET}	V_{TOTAL}	Pore size
	m^2g^{-1}	cm^3g^{-1}	nm
PEHA_1-1A	29.8	0.08	12.2
PEHA_1-1B	29.9	0.07	11.6
PEHA_1-1C	27.5	0.05	8.3
PEHA_1-1D	32.2	0.10	15.4
PEHA_1-1E	37.3	0.09	9.9
Average	31.3	0.08	11.5
Standard dev	3.7	0.02	2.7
Relative Sdev	0.1	0.25	0.2
% Relative sdev	11.8	25.00	23.5

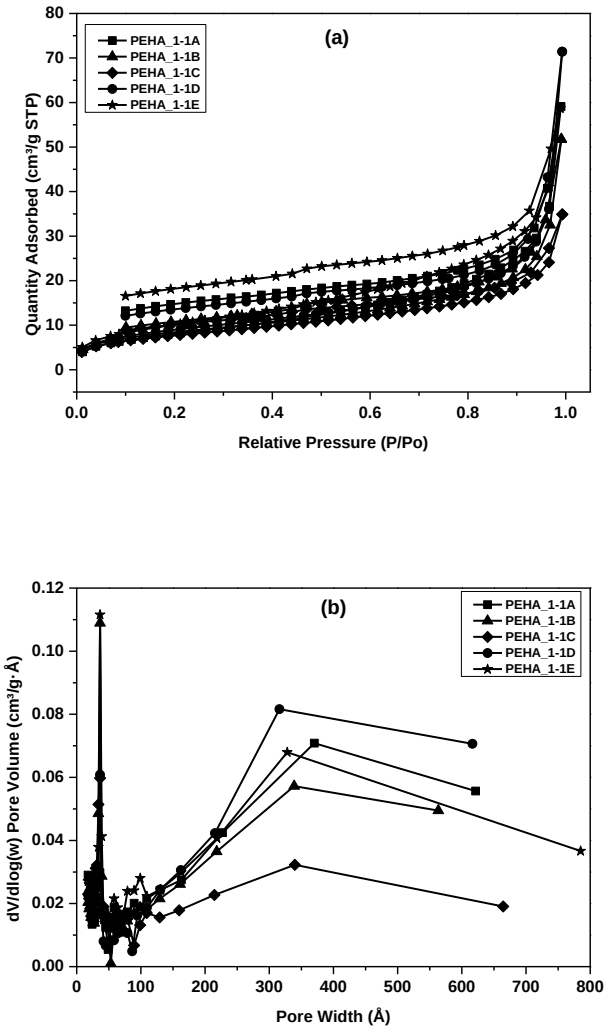

Figure 12-2: (a) N_2 sorption isotherms and (b) pore size distributions for PEHA BIAS repeat samples.

Table 12-5: Chemical properties for PEHA BIAS repeat samples from elemental analysis.

Sample ID	Bio-inspired TEPA loaded silica		
	wt% C	wt% H	wt% N
PEHA_1-1A	8.9	3.0	5.4
PEHA_1-1B	8.2	2.6	4.8
PEHA_1-1C	8.0	2.6	5.2
PEHA_1-1D	8.2	2.5	5.2
PEHA_1-1E	8.2	2.6	5.3
Average	8.3	2.7	5.2
Standard dev	0.3	0.2	0.2
Relative Sdev	0.0	0.1	0.0
% Relative sdev	3.6	7.4	3.8

Table 12-6: CO_2 adsorption capacities for TEPA and PEHA BIAS repeats

Sample ID	TEPA BIAS		PEHA BIAS	
	CO_2 adsorption capacity (mmol g^{-1}) , 333 K			
	10 kPa	100 kPa	10 kPa	100 kPa
1A	0.337	0.725	0.375	0.740
1B	0.322	0.722	0.313	0.680
1C	n/a	n/a	0.400	0.819
1D	n/a	n/a	0.353	0.755
1E	n/a	n/a	n/a	n/a
Average	0.330	0.723	0.360	0.748
Standard dev	0.010	0.003	0.037	0.057
Relative Sdev	0.030	0.004	0.103	0.076
% Relative sdev	3.030	0.415	10.278	7.620

Table 12-7: Textural characteristics of TEPA loaded BIAS samples prepared

Sample ID	S_{BET}	V_{TOTAL}	Pore size
	m^2g^{-1}	cm^3g^{-1}	nm
TEPA_1-1	29.8	0.08	12.2
TEPA_1-2	25.2	0.09	13.6
TEPA_1-4	28.0	0.09	12.1
TEPA_1-8	32.9	0.10	11.8
TEPA_1-16	30.2	0.07	10.1
Average	29.2	0.09	12
Standard dev	2.8	0.01	1.3
Relative Sdev	0.1	0.11	0.1
% Relative sdev	9.6	11.11	10.8

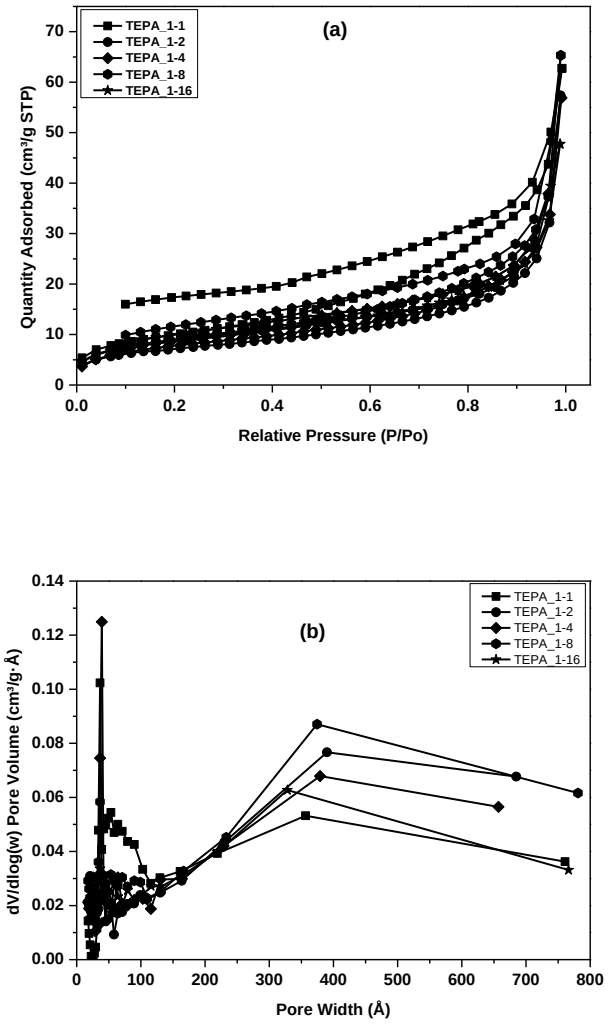

Figure 12-3: (a) N_2 sorption isotherms and (b) pore size distributions for TEPA loaded BIAS samples, prepared in this study.

Table 12-8: Chemical properties for TEPA loaded BIAS samples prepared in this study

Sample ID	Bio-inspired TEPA loaded silica		
	wt% C	wt% H	wt% N
TEPA_1-0.5	6.0	2.3	3.7
TEPA_1-0.75	6.4	2.4	4.0
TEPA_1-1	6.2	2.1	3.6
TEPA_1-2	6.2	2.3	3.9
TEPA_1-4	6.5	2.0	3.7
TEPA_1-8	6.7	2.5	4.3
TEPA_1-16	6.2	2.4	3.9
Average	6.3	2.3	3.9
Standard dev	0.2	0.2	0.2
Relative Sdev	0.0	0.1	0.1

% Relative sdev	3.2	8.7	5.1

Table 12-9: CO_2 adsorption capacity for amine loaded TEPA BIAS nanoparticles

Sample	CO_2 capacity (mmol g^{-1})	CO_2 capacity (mmol g^{-1})
	10 kPa	100 kPa
TEPA_1-0.5	0.134	0.453
TEPA_1-1	0.337	0.725
TEPA_1-2	0.279	0.659
TEPA_1-4	0.287	0.682
TEPA_1-8	0.264	0.660
TEPA_1-16	0.230	0.600

Table 12-10: Textural characteristics of amines used in BIAS production

Sample ID	S_{BET}	V_{TOTAL}	Pore size
	m^2g^{-1}	cm^3g^{-1}	nm
B3A	20.1	0.05	10.4
B13P	48.1	0.18	16.3
BPEI	100.4	0.22	5.4
PAH	153.0	0.81	18.1

Table 12-11: CO_2 adsorption capacity for other amines used in BIAS production

Sample ID	CO_2 adsorption capacity (mmol g-1) , 333 K	
	10 kPa	100 kPa
B3A	0.256	0.590
B13P	0.250	0.615
BPEI	0.587	0.962
PAH	0.302	0.675

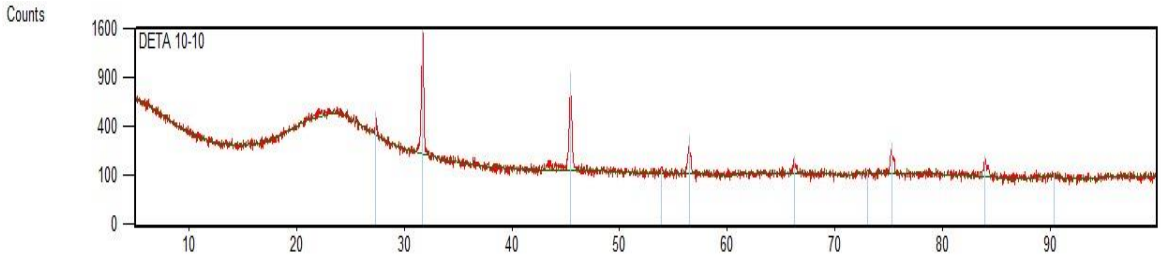

Figure 12-4: XRD patterns for DETA 10-10 BIAS sample prepared in this study

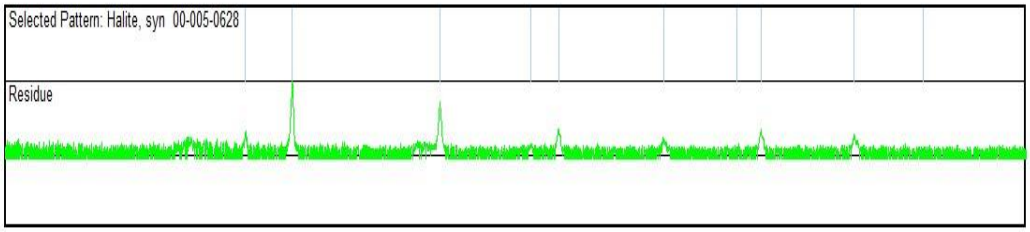

Figure 12-5: XRD patterns for DETA 10-10 BIAS sample prepared in this study showing peaks indicating the presence of NaCl.

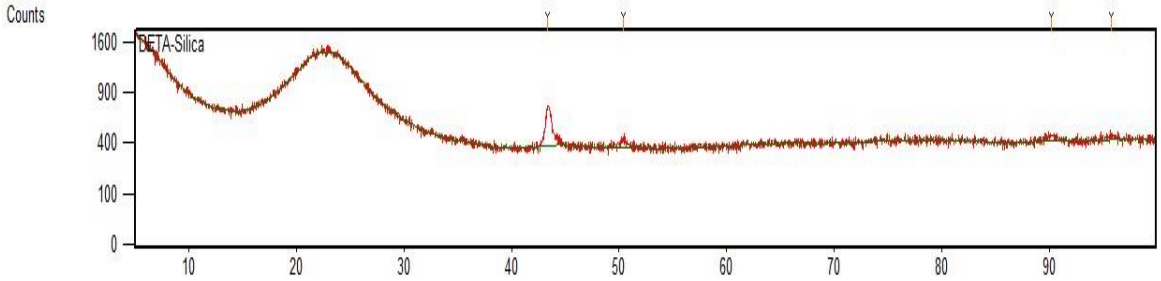

Figure 12-6: XRD patterns for DETA 1-1 BIAS sample prepared in this study showing peaks indicating the presence of NaCl is either absent or negligible.

12.2 Appendix B

Table 12-12: Textural parameters obtained for D1-1 (H_2O) repeats prepared in this study.

Sample ID	S_{BET}	V_{TOTAL}	Pore size
	m^2g^{-1}	cm^3g^{-1}	nm
D1-1A	198.9	0.28	4.3
D1-1B	189.3	0.28	4.4
D1-1C	202.4	0.33	4.7
D1-1D	201.0	0.35	5.2
Average	197.9	0.31	4.7
Standard dev	5.9	0.04	0.4
Relative Sdev	0.0	0.13	0.1
% Relative sdev	3.0	12.90	8.5

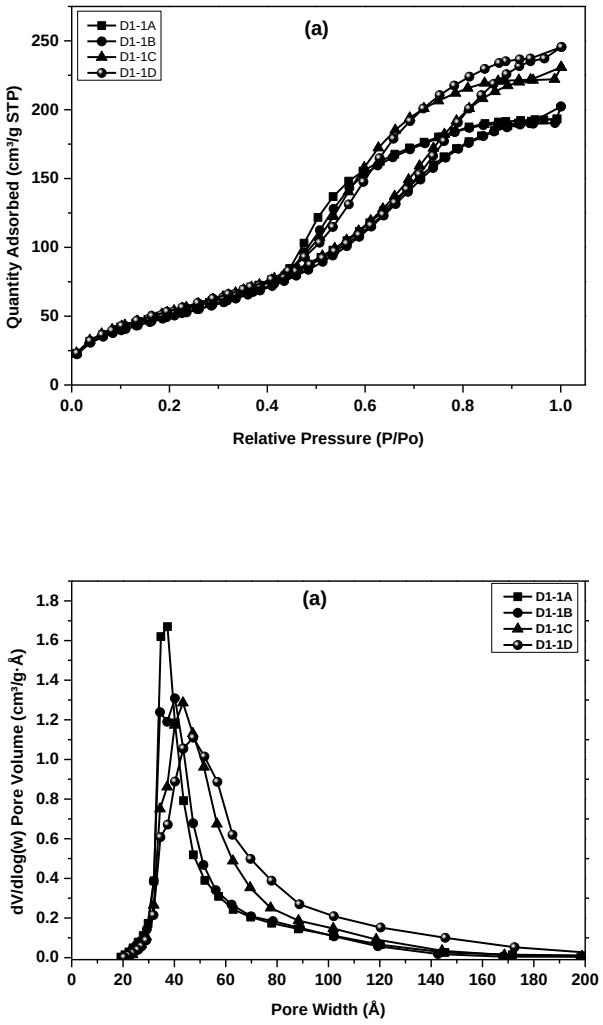

Figure 12-7: (a) N_2 sorption isotherms and (b) pore size distributions for D1-1 (H_2O) AIIS repeats prepared in this study.

Table 12-13: Textural parameters obtained for PAH (P1-1) and BPEI (B1-1) AIIS prepared in this study.

Sample ID	S_{BET}	V_{TOTAL}	Pore size
	m^2g^{-1}	cm^3g^{-1}	nm
B1-1	0.1	n/a	15.2
P1-1	14.9	n/a	2.7

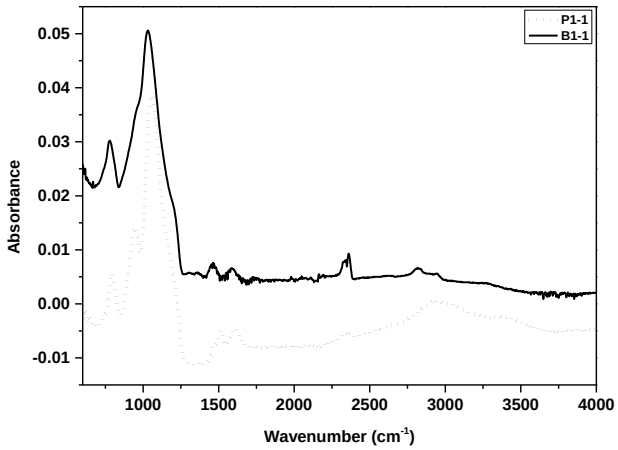

Figure 12-8: FTIR spectra for PAH (P1-1) and BPEI (B1-1) AIIS samples xerogels synthesised in this study

12.3 Appendix C

Table 12-14: Textural characteristics of additional pyrolysis and activated xerogels at 1073 K, prepared in this study.

Sample ID	S_{BET}	S_{MIC}	V_{TOTAL}	V_{MIC}	Pore size
	m^2g^{-1}	m^2g^{-1}	cm^3g^{-1}	cm^3g^{-1}	nm
Na_300 (0%)A	877.1	540.8	0.8	0.28	5.6
Na_300 (7%)A	602.4	436.4	0.55	0.22	8.1
Na_500 (0%)A	808.2	520.6	1.10	0.27	11.0
Na_500 (7%)A	665.9	496.2	0.47	0.26	4.5

Table 12-15: Textural characteristics of organic xerogels made with different wt% melamine prepared in this study, ($R/C_t = 50$).

Sample ID	S_{BET}	S_{MIC}	V_{TOTAL}	Pore size
	m^2g^{-1}	m^2g^{-1}	cm^3g^{-1}	nm
Na_50 (0%)	416.9	115.3	0.25	2.4
Na_50 (1%)	410.5	121.1	0.23	2.4
Na_50 (7%)	466.9	79.1	0.29	2.7
Na_50 (10%)	483.5	74.4	0.33	2.9
Na_50 (20%)	391.3	38.5	0.41	4.0
Na_50 (40%)	134.6	12.8	0.67	19.6

Table 12-16: Textural characteristics of pyrolysed xerogels made with different wt% melamine prepared in this study, ($R/C_t = 50$).

Sample ID	S_{BET}	S_{MIC}	V_{TOTAL}	V_{MIC}	Pore size
	m^2g^{-1}	m^2g^{-1}	cm^3g^{-1}	cm^3g^{-1}	nm
Na_50 (0%)P	5.0	n/a	n/a	n/a	n/a
Na_50 (7%)P	6.7	n/a	n/a	n/a	n/a
Na_50 (10%)P	12.9	12.6	0.01	0.01	2.2
Na_50 (20%)P	98.1	86.8	0.06	0.04	3.2
Na_50 (40%)P	373	292.2	0.39	0.15	12

Table 12-17: Textural characteristics of Na_100 (20%) pyrolysed at different times.

Sample ID	S_{BET}	S_{MIC}	V_{TOTAL}	V_{MIC}	Pore size
	m^2g^{-1}	m^2g^{-1}	cm^3g^{-1}	cm^3g^{-1}	nm
Na_100 (20%)_30mins	514.8	340.6	0.73	0.18	13.3
Na_100 (20%)_60mins	512.0	332.0	0.78	0.17	14.1
Na_100 (20%)_180mins	498.2	316.3	0.69	0.16	11.8
Average	508.3	329.6	0.7	0.2	13.1
Standard dev	8.9	12.3	0.0	0.0	1.2
Standard err	5.1	7.1	0.0	0.0	0.7
relative standard err	1.0	2.2	3.6	3.4	5.2

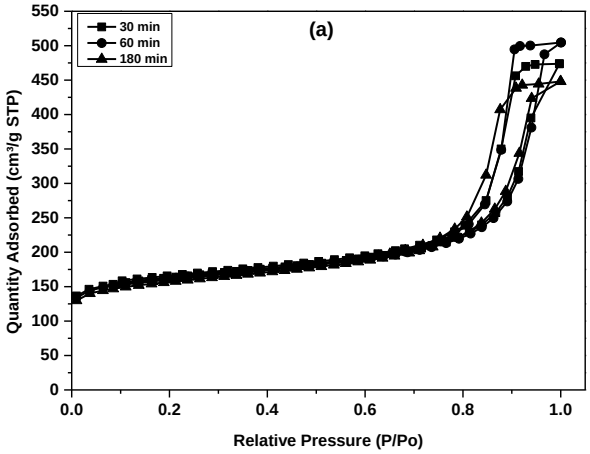

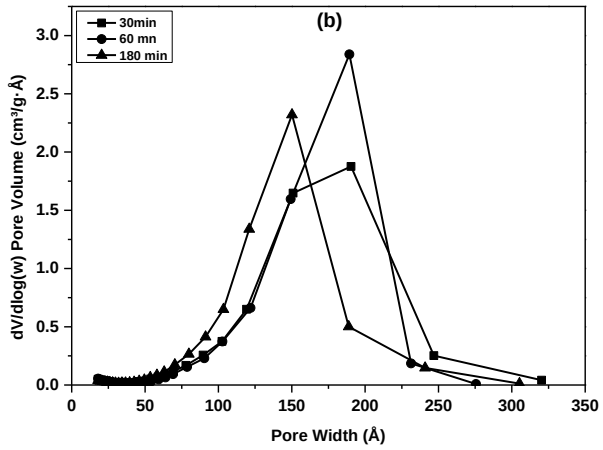

Figure 12-9: N_2 sorption isotherms and (b) pore size distributions for Na_100 (20%) pyrolysed at different times.

Table 12-18: CO_2 adsorption capacity for pyrolyzed MRF carbon xerogels (Na_100 (20%)P) at different times measured at 298 and 333 K (10 - 100 and kPa).

Sample	CO_2 adsorption capacity (mmols g^{-1}) at 10 kPa		CO_2 adsorption capacity (mmols g^{-1}) at 100 kPa	
	298 K	333 K	298 K	333 K
Na_100 (20%)_30mins	0.883	0.392	2.657	1.662
Na_100 (20%)_60mins	0.806	0.344	2.532	1.550
Na_100 (20%)_180mins	0.893	0.402	2.668	1.679

12.3.1 Optimization runs

Table 12-19: Effect of drying method applied (oven dried) on the textural parameters, measured using N_2 at 77 K

Sample ID	S_{BET}	V_{TOTAL}	Pore size
	m^2g^{-1}	cm^3g^{-1}	nm
Na_100 (7%)	471.0	0.64	5.4
Na_100 (10%)	357.2	0.71	7.3

Samples were prepared following the standard synthetic route (i.e. 3 days gel time, 3 days solvent exchange), but instead of vacuum dried, samples were dried in a conventional over (Figure 4-3) for 3 h.

Table 12-20: Effect of solvent exchange on the textural parameters, measured using N_2 at 77 K

Sample ID	S_{BET}	V_{TOTAL}	Pore size
	m^2g^{-1}	cm^3g^{-1}	nm
Na_100 (7%)	364.0	0.37	3.8
Na_100 (10%)	336.6	0.51	5.8

Samples were prepared adopting a different route, i.e. 3 days gel time, no solvent exchange, the vacuum dried 16 h.

Table 12-21: Effect of solvent exchange time frame on the textural parameters, measured using N_2 at 77 K

Sample ID	S_{BET}	V_{TOTAL}	Pore size
	m^2g^{-1}	cm^3g^{-1}	nm
Na_100 (7%)_1-0	391.4	0.42	3.9
Na_100 (7%)_1-1	432.7	0.43	3.9
Na_100 (7%)_1-2	473.7	0.57	4.8
Na_100 (7%)_1-3	449.0	0.54	4.7
Na_100 (10%)_1-0	411.2	0.51	5.6
Na_100 (10%)_1-1	375.3	0.57	6.2
Na_100 (10%)_1-2	438.5	0.66	6.4
Na_100 (10%)_1-3	402.4	0.60	6.1

Samples were prepared adopting a different route, i.e. 1 days gel time and the increased the level of solvent exchange from none to 3 days, then vacuum dried 16 h.

Table 12-22: Effect of pyrolysis on gels solvent exchange with different time frame on the textural parameters, measured using N_2 at 77 K

Sample ID	S_{BET}	S_{MIC}	V_{TOTAL}	V_{MIC}	Pore size
	m^2g^{-1}	m^2g^{-1}	cm^3g^{-1}	cm^3g^{-1}	nm
Na_100 (7%)_2-1	512.1	295.3	0.38	0.15	3.6
Na_100 (7%)_2-2	539.0	303.2	0.41	0.16	4.7
Na_100 (7%)_2-3	550.3	312.4	0.41	0.16	3.7

Samples made using different degree of solvent exchange were pyrolysed to determine the effect solvent exchange had on the final carbon xerogel produced.

12.4 Appendix D: Paper manuscript to be submitted to the Journal for Carbon

Synthesis and characterization of Melamine doped Resorcinol Formaldehyde (MRF) xerogels for CO_2 capture

Esegboria Obhielo and Ashleigh J. Fletcher*,

Department of Chemical and Process Engineering, University of Strathclyde, Glasgow G1 1XJ, UK

**To whom correspondence should be addressed. E-mail: ashleigh.fletcher@strath.ac.uk*

Abstract

Nitrogen enriched carbon xerogels were prepared using a modified version of traditional resorcinol-formaldehyde sol-gel chemistry, including melamine, a nitrogen rich precursor to produce Melamine-Resorcinol-Formaldehyde (MRF) xerogels at levels up to 40 wt% melamine added to the initial reaction concentration, retaining up to 9% nitrogen upon carbonization and activation. The solid monoliths formed were subsequently pyrolyzed, and physically activated, to enhance the textural properties; the effects of nitrogen enrichment on texture, morphology, and surface chemistry were probed using nitrogen adsorption and spectroscopic methods, with the observed trends collated with CO_2 adsorption capacities of the sorbents. Carbon capture performances were evaluated at pressures up to 900 kPa, and temperatures of 298 K and 333 K; CO_2 adsorption was shown to be influenced by both the microporous nature of the material, and by the nitrogen content of the synthesized sorbent. Nitrogen enriched RF gels showed high thermal stabilities with capacities up to 164.5 mgCO_2/g sorbent (3.73 mmol g^{-1}, 298 K) obtained for the maximum melamine loading achievable (40 wt%), and facile regeneration without evident loss of CO_2 adsorption capacity. The results suggest new strategies towards carbon capture materials synthesis.

1. Introduction

Current estimates suggest that over 85% of World energy demand is supplied by fossil fuels, contributing ~40% of total CO_2 emissions, mainly from coal-fired plants [1]. Increased utilization of fossil fuels has seen anthropogenic emissions rise by ~30% when compared to pre-industrialization levels [2, 3], and the Intergovernmental Panel on Climate Change (IPCC) have reported strong evidence

* Telephone +44(0)1415482431; E-mail: ashleigh.fletcher@strath.ac.uk

issues of toxicity, as well as the corrosive nature and cost of the reagents required, hence these materials are unfeasible for large scale implementation.

Carbons have been extensively studied for carbon capture, as a consequence of their large surface areas, microporous natures, thermal and chemical stabilities, fast sorption kinetics and the ease of functionalization of the graphene basal planes, incorporating heterogeneity. Nitrogen enrichment of carbon materials has been used to improve their adsorption capacity with respect to acidic CO_2, and methods to incorporate basic amine functionalities within carbons include surface coating [14-17], use of nitrogen rich precursors within syntheses [18-22], and post–synthetic ammonia treatments [23, 24]. Improving the adsorption capacity with such methods is not guaranteed, as there can be issues associated with selectivity, as flue gas contains < 15% CO_2, with the balance mainly N_2. Hence, it is essential that, coupled with improved sorption, modified materials also demonstrate a marked improvement in their affinity for CO_2 when placed in a competing environment [21].

It is, therefore, imperative to develop materials that are simple and cost effective to make [25, 26] and efficient to use; here, we report the facile preparation of a suite of nitrogen enriched micro/meso-porous carbon materials that show high CO_2 capacities, at ambient conditions and pressures up to 900 kPa. Melamine was used as the nitrogen rich precursor, in the synthesis of Melamine-Resorcinol-Formaldehyde (MRF) xerogels, at levels up to 40 wt% melamine added to the initial reaction concentration, retaining up to 9 wt% nitrogen upon carbonization and activation. The materials exhibited high CO_2 sorption capacities under static conditions with high stabilities, and facile regeneration with negligible loss of CO_2 capacity.

2. Experimental

2.1 Synthesis of organic xerogels

The previously reported synthetic route for production of Resorcinol-Formaldehyde (RF) sol-gels [27] was modified to include a nitrogen rich precursor, melamine (M), to produce a suite of MRF xerogels with varying wt% of nitrogen. A total solids content of 20% wt/vol, in 60 ml total reaction volume was used, i.e. total solids mass was kept constant at 12 g for all syntheses; resorcinol (4–8 g) and melamine (0.12–4.8 g) were dissolved in deionised water (54 ± 2 ml) and mixed thoroughly in the presence of sodium carbonate (45–76 mg Na_2CO_3, basic catalyst)

in a glass vial under continuous stirring, via a magnetic stirrer. Upon complete dissolution, formaldehyde (2–5 g) was added in the form of formalin solution, and the mixture stirred for 30 min to allow homogeneous mixing. The pH of the resulting solution was recorded before heating to 358 K in a sealed vessel for 72 h to produce a gel. Once gelled, any water present was exchanged with acetone via solvent exchange for a further 72 h, after which the solid gel was dried under vacuum and labelled Na_100(X%), where X represents the wt% of melamine added.

2.2 Production of carbon xerogels

~0.7 ± 0.05 g of the selected dried MRF xerogel was weighed into a ceramic boat and placed in a tube furnace (Carbolite MTF 12/38/250) under a continuous flow of argon (Ar) at 200 cm^3 min^{-1}. The furnace was purged for 30 min before heating from room temperature to 1073 K (10 K min^{-1}), held for 180 min, after which the furnace was cooled to room temperature and the sample removed and reweighed. Mass losses were subsequently calculated for all samples. The final products were labelled Na_100(X%)P where P represents pyrolyzed, and X represents the wt% of melamine added.

2.3 Production of activated carbon xerogels

The activation procedure followed a similar format to pyrolysis, however, for activation, when the system had reached 1073 K, the flow of gas was switched from Ar to CO_2 (200 cm^3 min^{-1}). The samples were held at 1073 K under CO_2 for 4 h; once the dwell time had elapsed, the flow was switched back to Ar and the system allowed too cool to room temperature. The resulting product was removed, reweighed and labelled as Na_100(X%)A where A represents activated, and X represents the wt% of melamine added.

2.4 Characterization methods

All samples were analyzed in their as-synthesized forms unless stated. ***Surface Area Determination -*** samples were outgassed at vacuum and heated at 383 K for 2 h to remove any physically adsorbed water or volatile gases, then subsequently analyzed using N_2 sorption at 77 K on a Micrometrics ASAP 2420 analyzer. Surface areas were determined by the BET method [28], pore sizes and pore volumes were estimated using the BJH method [29]. ***Elemental Analysis*** – sample compositions were determined using a CHNS-O analyzer (Series 11, E400, Perkin Elmer). ***Surface Functionalities*** – finely ground samples were analyzed using an ABB MB3000 Fourier Transform Infrared Spectroscopy (FTIR) laboratory

spectrometer (32 scans at a frequency of 600–4000 cm^{-1}, resolution 16 cm^{-1}). ***Surface Morphology*** – samples were finely ground, gold coated and analyzed using a Hitachi SU6600 analytical variable pressure field emission Scanning Electron Microscope, operating at 20 keV with a scan resolution of 500 nm, to probe surface texture and particle size. ***Thermal Stability and Proximate Analysis*** – thermal stability was determined using a Netzsch STA 449 FI Jupiter combined Thermal Gravimetric Analyzer (TGA)/Differential Scanning Calorimeter (DSC), programmed from ambient temperature (~295 K) to 1273 K, at 10 K min^{-1}, under flowing N_2 at 50 ml min^{-1}.

2.5 CO_2 sorption measurements

CO_2 sorption performance of synthesized sorbents was determined using an Intelligent Gravimetric Analyzer (IGA) supplied by Hiden Isochema Ltd., which uses gravimetry to accurately measure the magnitude and dynamics of gas/vapour sorption on a given sorbent [30]. ~35 ± 5 mg of a selected sample was accurately weighed into a sample holder and loaded into the system, before outgassing at vacuum and heated to 393 K, at 3 K min^{-1}, held for 2 h to remove any physically adsorbed water and volatiles from the sorbent surface. Samples were subsequently cooled to room temperature before heat and holding at a measurement temperature of either 298 K or 333 K. 99.9% CO_2 was introduced to the degassed sample and the pressure increased from vacuum to the desired pressure step (in the range of 900 kPa as desired) at 5 kPa min^{-1}. The system was allowed to equilibrate at each set pressure before progression to the next desired step in the static pressure sequence. Vacuum swing sorption measurements were performed using pure a CO_2 stream (99.9%), at 298 K, to determine sample cyclability up to 100 kPa.

3. Results and discussion

3.1 Materials Characterization

Thermal stability of MRF samples was investigated, and a typical trace is shown in Figure 1, clearly showing the sample (Na_100(20%)) to be stable up to 575 K, during which period, physically adsorbed water and residual acetone is lost, before the elimination of molecular water, in the form of the hydroxymethyl groups from formaldehyde and hydroxyl groups within resorcinol, and a loss due to degradation of organic constituents (triazine rings from melamine). The observed

thermal stability demonstrates a large working range for the samples in an industrial context.

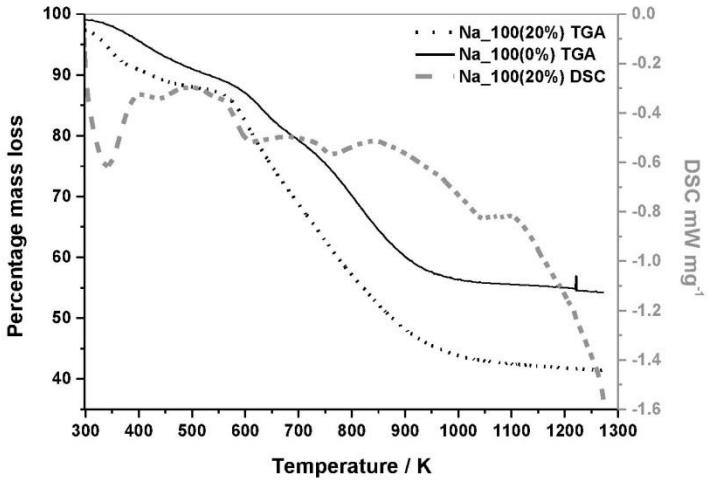

Figure 1: Thermal stability and decomposition profile of Na_100(0 and 20%) organic xerogel

The amount of melamine present in MRF xerogels was determined using elemental analysis and comparison of this profile with one obtained for an RF xerogel made without the addition of melamine Na_100(0%), showed both systems exhibit similar shapes for their decomposition profiles, with pronounced mass loss about 600 K, which correlates with the sublimation temperature of melamine (~598 K) as observed previously [19]. A notable difference in wt% mass loss exists between the two samples, larger for Na_100(20%), and this is attributable to the decomposition of melamine and the magnitude of the difference relates to the wt% of melamine in the xerogel determined by CHN analysis. Table 1 presents the results derived from ultimate analysis of the organic and pyrolyzed xerogels. While the organic xerogels retained 100% of the nitrogen available from the melamine precursor, it was observed that during pyrolysis, ~64% of the total nitrogen content was lost, except in the case of Na_100(1%), where, pyrolysis did not affect the nitrogen content.

Table 1: Chemical properties and CO_2 adsorption data for the MRF Na_100(1 – 40%) xerogels

Sample	wt% M wet basis	Organic xerogels				Carbon xerogels				% N retained after pyrolysis
		C	H	N	O	C	H	N	O	
		wt%C	wt%H	wt%N	wt%O	wt%C	wt%H	wt%N	wt%O	
Na_100(1%)	1.2	60.6	5.2	0.8	33.5	90.5	1.0	0.8	7.7	100.0
Na_100(7%)	7.6	57.9	5.6	5.0	31.5	86.9	1.3	1.8	10.0	35.5
Na_100(10%)	11.1	58.0	5.1	7.4	29.5	88.7	0.9	2.6	7.8	35.1
Na_100(20%)	21.6	54.2	5.1	14.4	26.4	80.2	1.7	4.9	13.2	34.0
Na_100(40%)	36.6	49.1	5.0	24.4	21.5	82.9	1.1	8.7	7.4	35.7

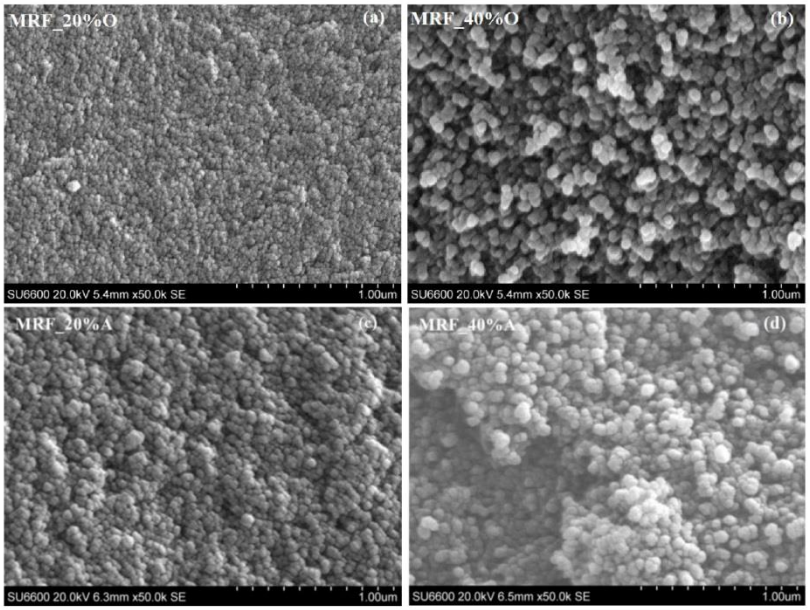

Figure 2: SEM images of (a) Na_100(20%), (b) Na_100(40%), (c) Na_100(20%)P and (d) Na_100(20%)P MRF xerogels synthesized in this study

Figure 2 shows cross-sectional SEM images for both the organic and carbon xerogels of Na_100(20%) and Na_100(40%), at magnifications of 50 k. All samples presented, consist of interconnected microspheres, which exist as single particles or aggregates creating a range of macropores in the organic and carbon xerogels, thus allowing easy gas diffusion. This should be beneficial for a CO_2 sorption process, since the macropores provide low resistance pathways for diffusion into the porous

structures, while the micropores provide additional adsorption capacity to adsorb the diffused CO_2. Aggregation of microspheres was seen to increase with increasing melamine content, indicating that increasing melamine content leads to increased pore sizes as a consequence of increased gelling time [31, 32].

FTIR spectra obtained for the series of MRF Na_100 organic xerogels (Figure 3) show that, as melamine content increases, bands at 784 cm^{-1} and 811 cm^{-1}, attributable to the bending vibration of the triazine ring, become stronger. The development of the band at 1541 cm^{-1} (stretching vibrations of the triazine ring) increases in strength with increasing melamine content, as do the N-H in plane deformation (1604 cm^{-1}) [18] and symmetric stretching (3417 cm^{-1}) [33] bands, while the decrease in intensity of the peak at 1474 cm^{-1} (CH_2-scissor vibration and CH_3-flexural vibration) is ascribed to a reduced degree of crosslinking [34, 35]. Such groups are considered basic species capable of acting as Lewis bases to interact with acidic gases [36].

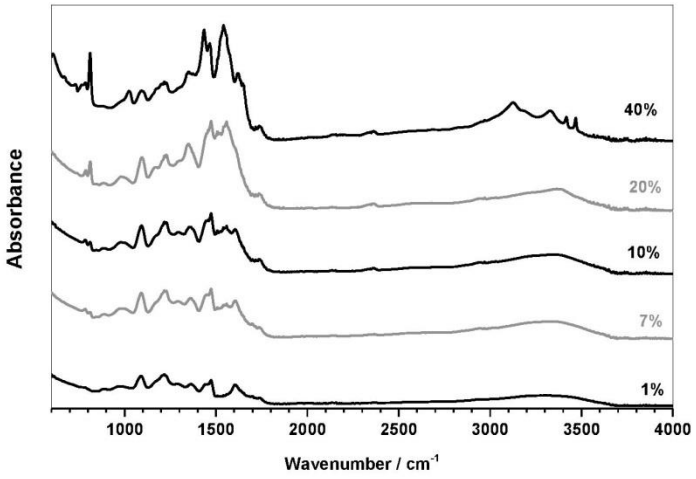

Figure 3: FTIR spectra for MRF Na_100(0-40%) organic xerogels synthesized in this study

Textural characteristics were determined using N_2 sorption measurements and the isotherms obtained can all be classified as Type IV [37] (Figure 4). As melamine wt% increases, the degree of cross-linking is expected to decrease, and this is reflected in the textural properties of the samples. Hysteresis is evident for all isotherms obtained, and the Type H1 loops observed indicate the presence of

mesoporosity [38], with cylindrical pores, for all samples. Capillary condensation in the mesopores increases from P/P_o ~0.45 to ~0.75, while the isotherms show limited multi-layer formation, corresponding to complete filling of the capillaries that is complete as P/P_o tends to unity.

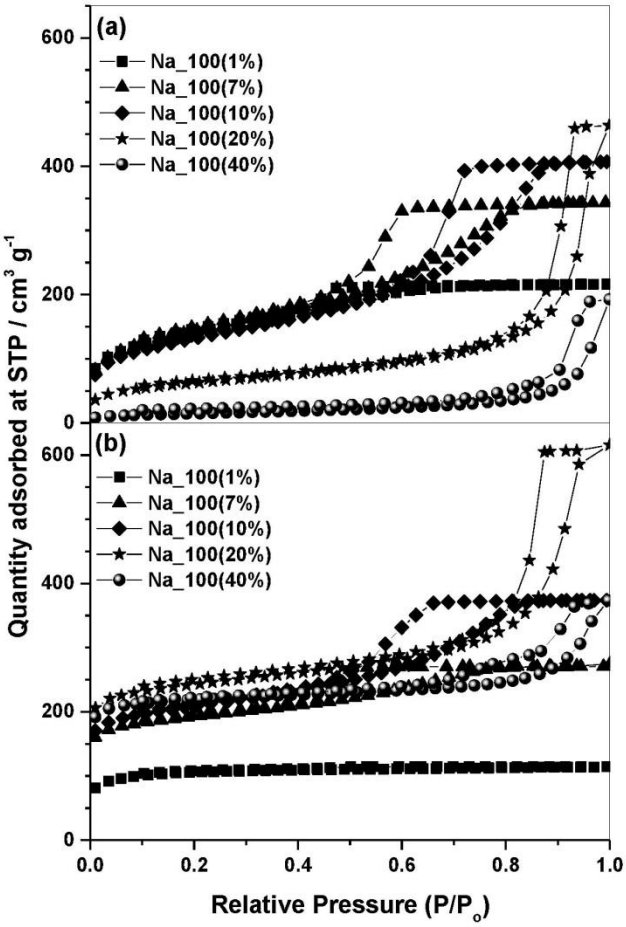

Figure 4: N_2 sorption isotherms (77 K) for MRF Na_100(1-40%) (a) organic and (b) carbon xerogels synthesized in this study

Table 2 summarises the textural properties of the MRF Na_100 organic and carbon xerogels; as expected, the BJH average pore width increases with increased melamine content, from ~2.9 nm (1 wt%) to ~20.3 nm (40 wt%) for the organic gels with a similar trend observed for the carbon gels, ~2.6 nm (1 wt%) to 15.0 nm (40 wt%). For all samples there is a decrease in average pore diameter on carbonization, in contrast to the mesopore widening observed for previous melamine

doped materials, which was ascribed to the inhomogeneity of melamine within the sample, this difference may be due to improved mixing during synthesis or, as there is little difference in the mesopore distribution on carbonization, the introduction of increased microporous character decreases the average pore diameter obtained. The BET surface areas of the organic samples with < 10 wt% melamine showed no significant differences but as melamine content increased further, up to 40 wt%, there is a marked reduction in surface area, by almost 90% (organic gel), attributed to either partial filling of the pores with melamine or poor crosslinking, coupled with increased particle sizes. Whereas, carbonization of the carbon xerogels results in an increase in surface area because, as carbonization progresses, linkages between aromatic carbon rings are broken, allowing the structure to reorganise and re-aggregate, this causes increased crosslinking, which results in increased micropore volumes and enhanced surface areas, while the collapse of the pore walls from elevated carbonization temperatures (pyrolysis and activation) allows new micropores to form.

Table 2: Textural properties of MRF Na_100(1-40%) organic and carbon xerogels synthesized in this study

	S_{BET} ($m^2 g^{-1}$)[§]		V_{TOTAL} ($cm^3 g^{-1}$)[†]		V_{MIC} ($cm^3 g^{-1}$)[*]		Average pore size (nm)[‡]	
	Organic	Carbon	Organic	Carbon	Organic	Carbon	Organic	Carbon
Na_100(1%)	490	329	0.335	0.177	0.040	0.124	2.9	2.6
Na_100(7%)	509	612	0.531	0.425	0.032	0.204	4.2	3.5
Na_100(10%)	500	671	0.717	0.578	0.038	0.198	6.1	4.6
Na_100(20%)	216	765	0.717	0.953	0.019	0.274	16.0	11.5
Na_100(40%)	52	647	0.298	0.647	0.002	0.277	20.3	15.0

[§] Determined from BET analysis.
[†] Determined from total uptake at $P/P_o \sim 1$.
[*] Determined from t-plot.
[‡] Determined from BJH method.

3.2 CO_2 Adsorption analysis

The effect of adsorption temperature on CO_2 capture was investigated by determining, the CO_2 adsorption characteristics of the MRF carbon xerogels prepared at different temperatures (298 and 333 K), at pressures from 0 to 900 kPa, as shown in Figure 5. The maximum pressure used at 298 K corresponds to a relative pressure of 0.27, hence, full pore filling may not be expected but all systems are significantly below the total pore volume available assuming an adsorbed phase

density for CO_2 of 1.023 g cm^{-3} [39], however it is notable that the isotherm for 1% loading is the same as the uptake expected for complete filling of the micropore volume with no plateau evident, indicating that microporosity does not solely control CO_2 adsorption. The observed decrease in CO_2 adsorption capacity, with temperature, was expected due to the exothermic character of physisorption, where both the molecular diffusion rate and the surface adsorption energy, increase with temperature [40].

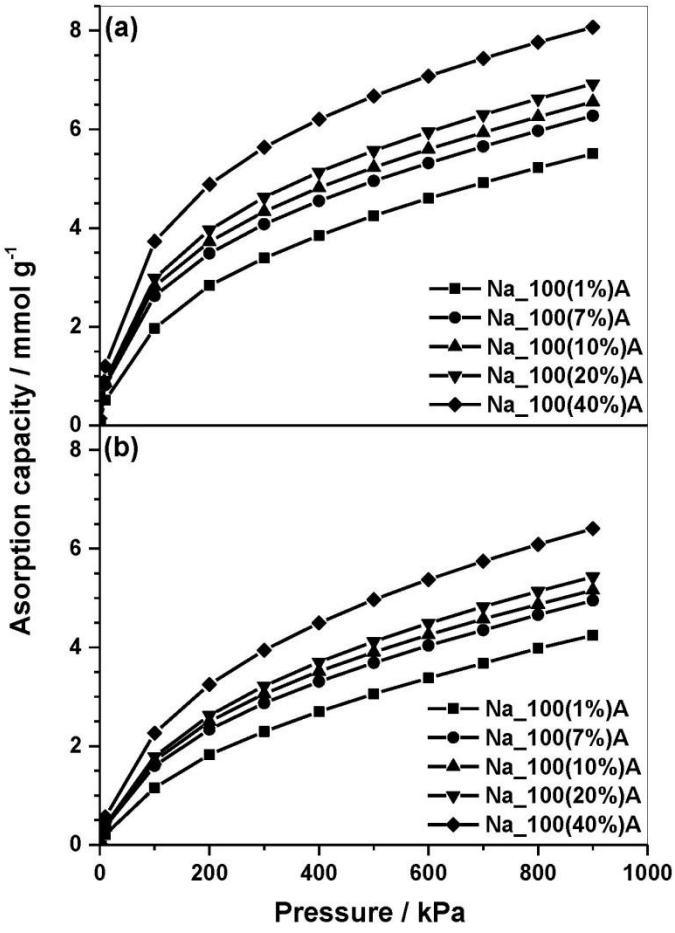

Figure 5: CO_2 adsorption isotherms for MRF activated carbon xerogels synthesized in this study at (a) 298 K and (b) 333 K

The isosteric enthalpies of adsorption (ΔH_i) were calculated at constant surface coverage using the Clausius-Clapeyron equation, and exothermic values were obtained for all systems under all pressures; as shown in Figure 6, ΔH_i decreased with increasing surface coverage. The values obtained for CO_2 adsorption were in the range 15 - 37 $kJmol^{-1}$, with a limiting isosteric enthalpy of ~43 $kJmol^{-1}$ at zero surface coverage, the limiting value at higher surface coverage compares favourably with the enthalpy of vaporization of CO_2 (15.3 $kJmol^{-1}$). The high heats of adsorption, especially at low surface coverage, are attributable to interactions between the acidic CO_2 molecules and the Lewis basic nitrogen functionalities; the values agree with those observed by Wei *et al.*[19], who observed a similar decrease in ΔH_i with increasing CO_2 uptake, suggesting that a limiting heat of adsorption exists for the interaction of melamine and CO_2 irrespective of material loading.

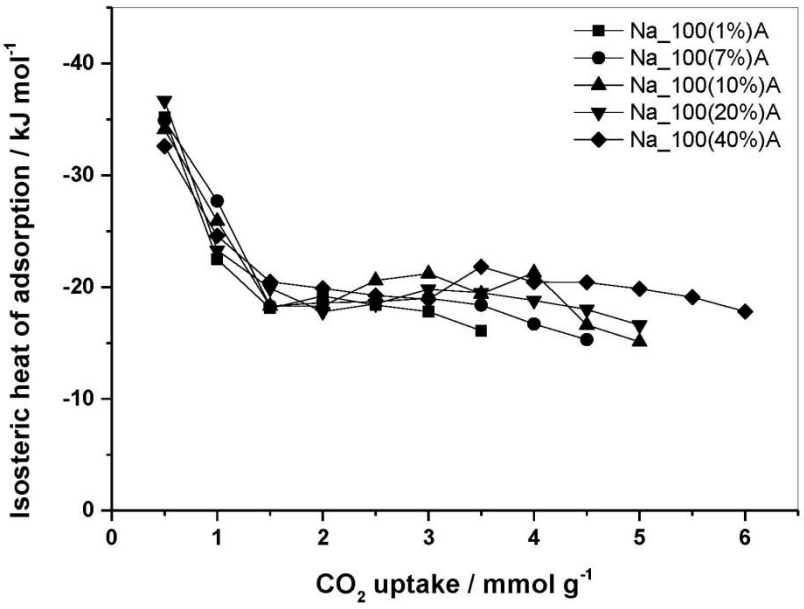

Figure 6: Isosteric heats of adsorption for CO_2 on carbon xerogels synthesized in this study.

CO_2 adsorption capacities were observed to increase with increasing wt% melamine, for both temperatures studied, which may be due to either the increased micropore volume or increased nitrogen content, determined previously from CHN analysis. Mercedes *et al.* [36] amongst other authors [18-20, 41, 42], reported that

CO_2 capacities of modified carbons (activated and impregnated anthracite) were not solely dependent on textural properties but also the presence of basic nitrogen groups [36]. To evaluate the influence of basic nitrogen groups incorporated into the structure of materials prepared, carbon based materials with similar textural properties, surface areas and total pore volumes were used as comparators: activated resorcinol formaldehyde carbon xerogel prepared in-house (225 $m^2 g^{-1}$, 0.12 $cm^3 g^{-1}$), graphite nanofibers (GNFs) (567 $m^2 g^{-1}$, 0.71 $cm^3 g^{-1}$) [43], commercial activated carbon (AC) (577 $m^2 g^{-1}$, 0.61 $cm^3 g^{-1}$) manufactured by Norit, and ordered mesoporous carbon (798 $m^2 g^{-1}$, 0.87 $cm^3 g^{-1}$) [44].

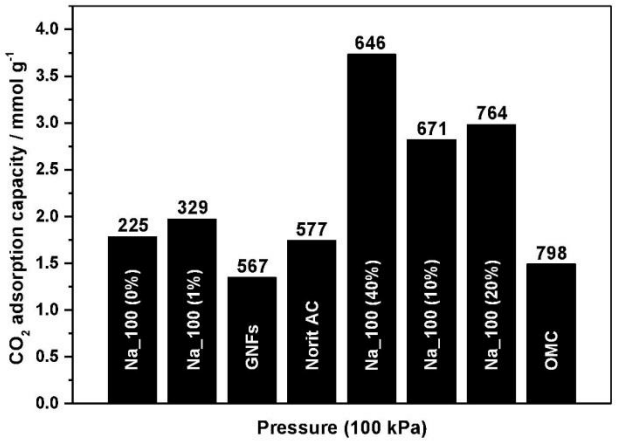

Figure 7: Comparative CO_2 adsorption capacities showing influence of increasing nitrogen content, (100 kPa, 298 K)

All comparative materials had negligible nitrogen content and similar textural properties with the quantity of CO_2 adsorbed, attributed to the presence of micropores (physisorption), allowing the role of melamine (nitrogen content) to be determined. Overall CO_2 capacity increased with increasing nitrogen content, supporting the theory that the presence of basic nitrogen groups leads to improved adsorption of acidic gases, such as CO_2. Figure 5 shows the CO_2 adsorption isotherms (up to 900 kPa at 298 and 333 K) of the five MRF sample prepared, with CO_2 capture capacity at 10, 100 and 900 kPa observed to increase as follows:

Na_100(40%)A > Na_100(20%)A > Na_100(10%)A > Na_100(7%)A > Na_100(1%)A

This is consistent with increasing nitrogen content (Table 1); however, it is important to consider both the effect of nitrogen content and the contribution to uptake from the micropores. Figure 5, and the corresponding textural data given in Table 2, show CO_2 capacity to increase with surface area until Na_100(40%)A, where a decrease in surface area does not correspond to a marked reduction in CO_2 capacity, the reverse was actually observed for the sample in question; all sorbents showed an increase in CO_2 capacity as pressure increased and it is notable that the uptake for 10% loading is significantly greater than that for 7%, despite the close values for the micropore volumes of the two samples, an analogous trend is observed for 20% and 40% loadings. This indicates that microporosity does not control CO_2 adsorption alone, hence, the ability to increase both microporous character and nitrogen content in tandem provides an attractive route to CCS materials development.

As well as high CO_2 adsorption capacity, a stable cyclic performance is critically important when evaluating the ultimate performance of sorbents for CO_2 capture. For cycling/regeneration, two main techniques exist; temperature swing adsorption and pressure/vacuum swing adsorption, considering the effects of temperature to amino groups present and the overall process cost, VSA was adopted, moreover, when CO_2 is recovered at sub-ambient pressures, VSA is seen as a more prospective method for CO_2 capture from flue gas [45]. Adsorption-desorption cycling study was performed to determine the performance and stability of the best performing sorbent with respect to capacity, under repeated use. The sample was exposed to pure CO_2, at 298 K, two pressure extremes, 100 kPa and vacuum, for 30 cycles with 60 min equilibration between cycles.

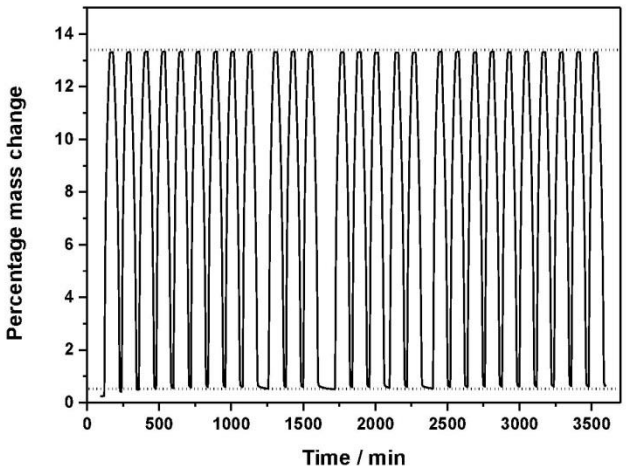

Figure 8: Cyclic studies using vacuum swing adsorption of CO_2 at 298 K on Na_100(40%)A synthesized in this study

~87% CO_2 adsorption was achieved within the first 30 min, while equilibrium adsorption was achieved at ~38 min, the reverse is the case for the desorption branch, although, dependent on the rate at which pressure is admitted into the adsorption chamber, this determined the kinetics of the sorption process; here pressure was admitted at a rate of 5 kPa min^{-1}. Faster sorption kinetics can be achieved by increasing the admittance rate; hence, making the sorbent ideal in an industrial context. Also, results obtained show that the sorbent maintained a stable capacity, up to 99.9% of the initial uptake, over 30 cycles, indicating a stable and easily reversible CO_2 adsorption-desorption performance

4. Conclusion

Melamine was successfully used as a nitrogen rich precursor for the preparation of nitrogen enriched resorcinol formaldehyde (MRF) activated carbon xerogels. A suite of materials were prepared with varying melamine concentrations to investigate the influence of increasing nitrogen content on the physical and chemical properties of the materials. Produced, CO_2 uptake capacities were not solely governed by surface area and/or micropore volume, but were also influenced by the nitrogen content of the materials. CO_2 uptake capacities up to 164.5 mg g^{-1} (3.73 mmol g^{-1}) sorbent at 298 K and 100 kPa, were achieved, and results from adsorption-desorption cycling showed that, after 30 cycles, the sorbent maintained

up to 99.9% of its original capacity, notably reaching 87% total adsorption capacity after 30 min. These nitrogen enriched carbon materials show potential for CO_2 capture from power plant flue gas as they possess high and stable adsorption capacities coupled with fast adsorption kinetics. Further research into the effect of the extent of functionalization on the aromatic precursor may allow greater weight contributions to be incorporated into the polymer matrix i.e. > 40 wt%, hence, the final carbon product, potentially increasing uptake.

Acknowledgements: EO thanks the University of Strathclyde for financial support.

References

[1] Carapellucci R, Milazzo A. Membrane systems for CO_2 capture and their integration with gas turbine plants. Proceedings of the Institution of Mechanical Engineers, Part A: Journal of Power and Energy. 2003;217(5):505-17.

[2] Tang Z, Zhang Y, Maroto-Valer MM. Study of the CO_2 adsorption capacities of modified activated anthracites. Preprints of Papers- American Chemical Society, Division of Fuel Chemistry. 2004;49(1):308.

[3] Keeling CD, Whorf TP. Atmospheric CO_2 records from sites in the SIO air sampling network. Trends: a compendium of data on global change. 2004.

[4] McCarthy JJ. Climate change 2001: impacts, adaptation, and vulnerability: contribution of Working Group II to the third assessment report of the Intergovernmental Panel on Climate Change: Cambridge University Press; 2001.

[5] Climate Change. IPCC Fourth Assessment Report. The Physical Science Basis. 2007.

[6] Zhang X, Zhang X, Dong H, Zhao Z, Zhang S, Huang Y. Carbon capture with ionic liquids: overview and progress. Energy & Environmental Science. 2012;5(5):6668-81.

[7] Plaza M, Pevida C, Arenillas A, Rubiera F, Pis J. CO_2 capture by adsorption with nitrogen enriched carbons. Fuel. 2007;86(14):2204-12.

[8] Chaffee AL, Knowles GP, Liang Z, Zhang J, Xiao P, Webley PA. CO_2 capture by adsorption: Materials and process development. International journal of greenhouse gas control. 2007;1(1):11-8.

9. Drage T, Kozynchenko O, Pevida C, Plaza M, Rubiera F, Pis J, et al. Developing activated carbon adsorbents for pre-combustion CO_2 capture. Energy Procedia. 2009;1(1):599-605.

10. Hicks JC, Drese JH, Fauth DJ, Gray ML, Qi G, Jones CW. Designing adsorbents for CO_2 capture from flue gas-hyperbranched aminosilicas capable of capturing CO_2 reversibly. Journal of the American Chemical Society. 2008;130(10):2902-3.

11. Choi S, Drese JH, Eisenberger PM, Jones CW. Application of amine-tethered solid sorbents for direct CO_2 capture from the ambient air. Environmental science & technology. 2011;45(6):2420-7.

12. Ello AS, Yapo JA, Trokourey A. N-doped carbon aerogels for carbon dioxide (CO_2) capture. African Journal of Pure and Applied Chemistry. 2013;7(2):61-6.

13. Liang Z, Fadhel B, Schneider CJ, Chaffee AL. Stepwise growth of melamine-based dendrimers into mesopores and their CO_2 adsorption properties. Microporous and Mesoporous Materials. 2008;111(1):536-43.

14. Pevida C, Plaza M, Arias B, Fermoso J, Rubiera F, Pis J. Surface modification of activated carbons for CO_2 capture. Applied Surface Science. 2008;254(22):7165-72.

15. Hao GP, Li WC, Qian D, Lu AH. Rapid Synthesis of Nitrogen-Doped Porous Carbon Monolith for CO_2 Capture. Advanced Materials. 2010;22(7):853-7.

16. Wei J, Zhou D, Sun Z, Deng Y, Xia Y, Zhao D. A Controllable Synthesis of Rich Nitrogen-Doped Ordered Mesoporous Carbon for CO_2 Capture and Supercapacitors. Advanced Functional Materials. 2013;23(18):2322-8.

17. Chandra V, Yu SU, Kim SH, Yoon YS, Kim DY, Kwon AH, et al. Highly selective CO_2 capture on N-doped carbon produced by chemical activation of polypyrrole functionalized graphene sheets. Chemical Communications. 2012;48(5):735-7.

18. Zhao Y, Zhao L, Yao KX, Yang Y, Zhang Q, Han Y. Novel porous carbon materials with ultrahigh nitrogen contents for selective CO_2 capture. Journal of Materials Chemistry. 2012;22(37):19726-31.

19. Xing W, Liu C, Zhou Z, Zhang L, Zhou J, Zhuo S, et al. Superior CO_2 uptake of N-doped activated carbon through hydrogen-bonding interaction. Energy & Environmental Science. 2012;5(6):7323-7.

20. Bhown AS, Freeman BC. Analysis and status of post-combustion carbon dioxide capture technologies. Environmental science & technology. 2011;45(20):8624-32.

21. Wang D, Ma X, Sentorun-Shalaby C, Song C. Development of carbon-based “molecular basket” sorbent for CO_2 capture. Industrial & Engineering Chemistry Research. 2012;51(7):3048-57.

22. Chen C, Son W-J, You K-S, Ahn J-W, Ahn W-S. Carbon dioxide capture using amine-impregnated HMS having textural mesoporosity. Chemical Engineering Journal. 2010;161(1):46-52.
23. Wang K, Shang H, Li L, Yan X, Yan Z, Liu C, et al. Efficient CO_2 capture on low-cost silica gel modified by polyethyleneimine. Journal of Natural Gas Chemistry. 2012;21(3):319-23.
24. Pekala R. Organic aerogels from the polycondensation of resorcinol with formaldehyde. Journal of Materials Science. 1989;24(9):3221-7.
25. Brunauer S, Emmett PH, Teller E. Adsorption of Gases in Multimolecular Layers. Journal of the American Chemical Society. 1938;60(2):309-19.
26. Barrett EP, Joyner LG, Halenda PP. The Determination of Pore Volume and Area Distributions in Porous Substances. I. Computations from Nitrogen Isotherms. Journal of the American Chemical Society. 1951;73(1):373-80.
27. Benham M, Ross D. Experimental determination of absorption-desorption isotherms by computer-controlled gravimetric analysis. Z Phys Chem NF. 1989;163:S25-S32.
28. Al-Muhtaseb SA, Ritter JA. Preparation and properties of resorcinol–formaldehyde organic and carbon gels. Advanced Materials. 2003;15(2):101-14.
29. ElKhatat AM, Al-Muhtaseb SA. Advances in Tailoring Resorcinol-Formaldehyde Organic and Carbon Gels. Advanced Materials. 2011;23(26):2887-903.
30. Hummel DO, Scholl. Infrared Analysis of Polymers, Resins and Additives: An Atlas. Vol. 1. Plastics, Elastomers, Fibers and Resins: Wiley; 1969.
31. Stuart B. Infrared spectroscopy: Wiley Online Library; 2005.
32. Pierotti R, Rouquerol J. Reporting physisorption data for gas/solid systems with special reference to the determination of surface area and porosity. Pure Appl Chem. 1985;57(4):603-19.
33. Burgess CG, Everett DH, Nuttall S. Adsorption hysteresis in porous materials. Pure and Applied chemistry. 1989;61(11):1845-52.
34. Drage TC, Arenillas A, Smith KM, Pevida C, Piippo S, Snape CE. Preparation of carbon dioxide adsorbents from the chemical activation of urea–formaldehyde and melamine–formaldehyde resins. Fuel. 2007;86(1–2):22-31.
35. Maroto-Valer MM, Tang Z, Zhang Y. CO_2 capture by activated and impregnated anthracites. Fuel Processing Technology. 2005;86(14):1487-502.
36. Sevilla M, Valle-Vigón P, Fuertes AB. N-Doped Polypyrrole-Based Porous Carbons for CO_2 Capture. Advanced Functional Materials. 2011;21(14):2781-7.
37. Gutiérrez MC, Carriazo D, Ania CO, Parra JB, Ferrer ML, del Monte F. Deep eutectic solvents as both precursors and structure directing agents in the synthesis of nitrogen doped

hierarchical carbons highly suitable for CO_2 capture. Energy & Environmental Science. 2011;4(9):3535-44.

38. Quéré CL, Andres RJ, Boden T, Conway T, Houghton R, House JI, et al. The global carbon budget 1959–2011. Earth System Science Data. 2013;5(1):165-85.

39. Saha D, Deng S. Adsorption equilibrium and kinetics of CO_2, CH_4, N_2O, and NH_3 on ordered mesoporous carbon. Journal of Colloid and Interface Science. 2010;345(2):402-9.

40. Webley PA, Xiao P, Zhang J, editors. Recovery of carbon dioxide from flue gas streams by vacuum swing adsorption. The 2005 Annual Meeting; 2005.

12.5 Appendix E: Paper manuscript to be submitted to the Journal for CO2 Utilization

New method for preparing amine in situ-impregnated silicas for CO_2 capture

Esegboria Obhielo, Siddharth V. Patwardhan, Ashleigh J. Fletcher[*],

Department of Chemical and Process Engineering, University of Strathclyde, Glasgow G1 1XJ, UK

[*]*To whom correspondence should be addressed. E-mail: ashleigh.fletcher@strath.ac.uk*

Abstract

The implementation of carbon dioxide (CO_2) capture methods using solid sorbents is reliant on the development of low cost sorbents with high CO_2 selectivity, simple synthesis routes and high CO_2 capture capacities. In this study, we present a new method for synthesizing silica modified with amines. Here, silica modified with diethylenetriamine (DETA) have been synthesized, characterized and evaluated as CO_2 capture sorbents, showing significant sorption capacities and selectivities under ambient pressure, at 333 K. Our novel approach involves the synthesis of amine in situ-impregnated silicas (AIIS) via aggregation of pre-condensed silica using DETA during the acid hydrolysis of soluble alkali metal silicates under neutral conditions. Unmodified silica was synthesized to serve as a control sorbent, allowing the effect of in situ-impregnation on CO_2 adsorption capacity and textural properties to be determined. As-synthesized sorbents were characterized and CO_2 adsorption isotherms were measured to determine CO_2 adsorption characteristics. The results showed that the capacities of AIIS were improved under the adsorption conditions investigated. Capacities up to 1.78 mmol g^{-1} were achieved (333 K, 100 kPa), and regenerative studies show negligible reduction in adsorption capacity, whilst a high CO_2/N_2 molar selectivity was sustained (up to 53 at 10 kPa). These AIIS indicate a route to novel sorbents for CO_2 capture, which have the advantage of stable capacities at above ambient temperatures.

Keywords: diethylenetriamine, polycondensation, selectivity, adsorption, sorbent.

1. Introduction

The increased utilization of fossil fuels has contributed to global climate change by increasing atmospheric concentrations of greenhouse gases, in particular CO_2, ultimately resulting in global warming [1-3]. Recently, environmental concerns related to such climatic changes have motivated research towards the stabilization and eventual reversal of increased CO_2 concentrations in the atmosphere.

At present, there are three main strategies proposed for CO_2 capture: pre-combustion capture, post-combustion capture and oxy-combustion capture [2, 4], each with inherent advantages and disadvantages with respect to CO_2 capture from point sources. In summary, post-combustion capture processes involving novel solid sorbents [5] have created interest as promising alternatives to conventional techniques e.g. bulk amine absorption [6] due to their cost reductions for gas-fired plants and Table 1 shows a comparison of power station mitigation scenarios and their impacts on the overall plant efficiency [7].

Estimates show that Post–Combustion Carbon Capture (PCCC) has high comparative capture efficiencies of 47.4% for natural gas combined cycle and 34.8% for pulverised coal power plant, combined with the lowest capital costs, when compared to either pre or oxy-combustion capture, and is predicted to provide the cheapest electric costs per kilowatt. PCCC consequently shows the highest potential for CO_2 capture from point sources, offering some degree of flexibility, including ease of retrofitting into existing plant design [2, 7, 8]; however, PCCC is seen as having limited implementation due to financing issues; a recent example highlighting the problems facing PCCC is the cancellation of the proposed Longannet project [9], where, project sustainability was not possible without guaranteed continued funding. At present, commercially available PCCC can potentially

increase the cost of power generation in power plants (coal) by almost 80%, which would inadvertently reduce plant efficiency due to the parasitic energy requirements [10, 11]; and such systems need to be demonstrated at industrially relevant scales in order to address the following issues:

- development of materials with enhanced CO_2 separation and capture capacities e.g. physical sorbents and chemical solvents including ionic liquids, carbon fibers, molecular sieves, polymeric membranes etc.
- development of retrofittable CO_2 capture options for existing large point sources
- CO_2 capture integration with advanced power cycles
- development of advanced technologies for CO_2 compression

Recent work has focused on developing new and/or improving on existing PCCC materials, e.g. zeolites, metal oxides, metal organic frameworks, amine containing materials, and activated carbons [12-14], by capitalizing on the key attributes of these materials, which include low energies of regeneration, high CO_2 selectivity over competing species present in flue gas streams and, most importantly, high adsorption capacities coupled with fast process kinetics [15, 16]. To this end, two main methods have been used to develop materials for CO_2 capture; the most common and widely used approach involves the physical impregnation of a porous support with amine species, the second involves grafting and/or tethering aminosilanes/amines onto a support material, which itself must have a large surface area [12, 17-19].

To date, amine modification has been shown to increase CO_2 adsorption capacities, for example Wang *et al.* reported CO_2 adsorption capacities of ~2.12 mmol g^{-1} (348 K, 100 kPa) for silica gels impregnated with ≤ 30% Polyethyleneimine (PEI) [19], Zhang *et al* .impregnated tetraethylenepentamine on disordered mesoporous silicas (≤ 60% wt. tetraethylenepentamine) with CO_2 capacities ≤ 3.70 mmol g^{-1} (328 K) [20], and Heydari-Gorji reported adsorption capacities as high as 4.68 mmol g^{-1} for 55 wt.% PEI impregnation on pore-expanded MCM-41 (348 K) [21]. Although useful in-terms of CO_2 adsorption capacity, these approaches all suffer the same disadvantages i.e. the use of toxic chemicals during synthesis of the support material and during the impregnation process itself, amines do not covalently anchor to the silica, hence, there is the problem of amine leaching over repeated use. There is also the issue of synthetic complexity (multi-pot processes), which makes industrial scale up uneconomical, hence it is imperative to develop materials that are simple to make (single pot processes), cost effective (cheap and easily sourced starting materials) [19, 22] and efficient (meets the required sorbent specification).

In this study, a new route to amine in situ-impregnated silicas is reported, diethylenetriamine (DETA) was in situ-impregnated into aggregated silica, formed from the polycondensation of sodium metasilicate pentahydrate, and the effect of DETA loading on textural properties of the solid support, surface chemistry and overall effectiveness of the synthetic approach was investigated.

2. Experimental

2.1 Materials and Methods

All materials used for sorbent preparation were purchased from Sigma-Aldrich and used as received unless otherwise stated. For the synthesis of control (unmodified) samples, silica was prepared via the acid hydrolysis of a concentrated solution of 300 mM sodium metasilicate pentahydrate ($SiO_3Na_2{\cdot}5H_2O$). To achieve this, 3.182 g of silica precursor was dissolved in 21.7 ml deionized water before 28.3 ml of 1 M HCl was added slowly under continuous stirring, (reducing the pH from 13.00 ± 0.3 to 7.00 ± 0.05). As the rate of silica condensation is highest at neutral pH [23, 24], the solution was allowed to condense for ~5 min under continuous stirring at room temperature. Amine In situ-Impregnated Silicas (AIIS) were prepared by mixing 0.515 g diethylenetriamine with 20 ml methanol and adding the resulting solution to the silica sol-gel as detailed above. This amine-silica slurry was stirred for 2 h and allowed to dry either in a fume-cupboard at 303 K overnight or by using a vacuum

oven set at 358 K. Keeping the silicon concentration constant (300 mM), the concentration of DETA was varied in order to produce a range of AIIS samples; samples were labeled according to the molar concentration ratio of silicon to nitrogen ([Si]:[N]), , e.g. for [Si]:[N] = 2:1, sample was labeled D2-1 (Table 2). To produce unmodified silica, the silica sol-gel formed was centrifuged at 8000 rpm for 15 min washed twice with deionized water to effectively remove any salts formed and collected upon drying at 358 K for 4 h.

2.2 Characterization of Adsorbents

Textural characterization - all as-synthesized samples were analyzed using a Micrometrics ASAP 2420 analyzer. Samples were outgassed at vacuum and 383 K for 2 h to remove any physically adsorbed water or volatile gases before subsequent analysis using N_2 sorption at 77 K. Surface areas were determined using the Brunauer-Emmett-Teller (BET) method [25], pore sizes and pore volumes were determined via the Barrett-Joyner-Halenda (BJH) method [26]. *Elemental analysis* – as-synthesized samples were analyzed for wt% contents of carbon, hydrogen and nitrogen using a CHNS/0 analyzer (Series 11, E400, Perkin Elmer). *Fourier Transform Infrared Spectroscopy (FTIR)* – samples were analyzed to determine the chemical composition of the unmodified silica and AIIS. FTIR spectra were obtained using an ABB MB3000 FT-IR Laboratory Spectrometer (scanned 32 times over a frequency of 600 – 4000 cm^{-1}, resolution 4 $cm^{-1}$and all samples analyzed were finely ground before analysis). *Scanning Electron Microscopy (SEM)* – surface morphology was observed by SEM, to determine the effect of amine in situ-impregnation using a Hitachi Co. (Model: SU6600) analytical VP FE-SEM, operated at 20 keV and a scan resolution of 500 nm, all samples were ground and gold coated by sputtering before analysis. *Thermal Gravimetric Analysis (TGA)* – thermal stability, dehydration characteristics and amine content were investigated using a Netzsch STA 449 Fl Jupiter combined TGA-DSC instrument. The as-synthesized samples were heated from room temperature (298 K) to 1273 K, at a rate of 10 K min^{-1} under flowing air at 50 ml min^{-1}.

CO_2 sorption measurements - CO_2 sorption performance of synthesized sorbents was determined using an Intelligent Gravimetric Analyzer (IGA) supplied by Hiden Isochema Ltd, which uses gravimetry to accurately measure the magnitude and dynamics of gas/vapour sorption on a given sorbent [27]. ~ 43 ± 3 mg of sample was accurately weighed, before outgassing at vacuum and heating to 393 K (3 K min^{-1}) for 3 h to remove physically adsorbed water and volatiles from the sorbent surface. Samples were typically cooled to, and held, at 333 K before 99.99% CO_2 was introduced and the pressure increased from vacuum to the desired pressure step (10 kPa or 100 kPa at 50 mbar min^{-1}). The system was allowed to equilibrate at each set pressure. To investigate the recyclability of AIIS as a CO_2 capture sorbent, pressure swing adsorption was used; AIIS were regenerated by evacuating at 333 K for 60 min in vacuum before 99.99% CO_2 was introduced and the pressure increased from vacuum to 100 kPa for further 60 min; this process was repeated sequentially for 21 sorption cycles. Mixed composition studies, similar to those detailed above, were performed to determine CO_2/N_2 selectivities, CO_2 was replaced with N_2 following the same sorption process, molar selectivity was calculated as the ratio of capture capacities for both gases under the same conditions.

3. Results and Discussion

3.1 Sample Characterization

shows the textural properties obtained for AIIS, which show a reduction in BET specific surface area, total pore volume and average pore size with increased loading. D1-1 shows a deviation from the general trend exhibited by the other samples but this is attributable to DETA forming a greater number of interactions with the surface silanol groups of the silica rather than being deposited within the silica pores, reducing associated pore blocking. Figure 1 and

shows how these trends can be attributed to the partial filling of the pores inferred from the significantly reduced amount of N_2 adsorbed and the resulting pore-volume, when compared with the unmodified silica. These observations suggest that DETA has been progressively loaded into the porous structure via in situ-impregnation.

All five sorbents show similar adsorption isotherms, categorized as Type IV in the IUPAC classification [28] (Figure 1). Similarities in isotherm type suggest that the overall porous structure of the silica was not affected by in situ-impregnation with DETA. H2 Hysteresis loops observed at $0.46 \leq P/P^{o} \leq 0.9$, signify the presence of bottle shaped mesopores, and the differences in desorption mechanism for a wide pore size distribution [29, 30]; although, H2 has also been observed for regular pore distributions with no interconnecting channels [30]. All pore size distributions were well defined with an observed narrowing of the distributions with increasing DETA concentration; the results presented in
 show only a small decrease in average pore diameter, indicating that pore size was not significantly affected by DETA modification.

IR spectra for the prepared samples are shown in Figure 2; D1-1 is shown as a representative of AIIS, as all samples exhibited similar IR spectra with varying degree of intensities.The IR spectra of D1 shows several additional absorption peaks compared with that for unmodified silica, and these additional peaks are ascribed to the bonds within DETA (-NH_2 and C-N). Both samples show absorption peaks at 1065 cm^{-1} and 795 cm^{-1} corresponding to Si-O-Si asymmetric and symmetric stretching, respectively. In situ-impregnation produces further peaks at 2300 cm^{-1} – 2350 cm^{-1} (anti-symmetric stretching band of physisorbed CO_2 and vibration of gaseous CO_2 both arising from air [31]), 2969 cm^{-1}(C-H bond) and a broad band at 3280 – 3370 cm^{-1} representing the asymmetric and symmetric stretching modes of -NH_2 groups, as well as –OH vibration from adsorbed water and silanol groups. These results suggest that the O-H flexing vibration of the silanol groups has been replaced by N-H stretching vibrations of amine groups, indicating that amine groups were successfully attached on to the silica surface. This hypothesis is supported by observation of bending vibrations of N-H bond absorption peaks at 1320 cm^{-1} (C-N stretching vibrations), 1570 cm^{-1} and 1475 cm^{-1} (-CH_2 scissoring mode), in line with the elemental analyses of AIIS (Table 3).

Figure 3 shows that a linear correlation exists between amine loading and the subsequent wt% of amine present in the in situ-impregnated sorbent, which suggests that the amount of amine functionality within the silica framework can be controlled provided that the pore volume has not been exhausted. The reliability of this correlation was tested to allow for its use as a predictive tool to estimate wt% N from reaction concentration. D5-1 and D7-1 were synthesized with an amine loading of 16.67 wt% and 12.5 wt%, respectively; the correlation tool and elemental analysis were used to determine wt% N. Elemental analysis results showed that for D5-1 the wt% N = 3.63, while the correlation gave wt% N = 3.69. With similar accuracies observed for D7-1 (wt N=2.48 via CHN and wt% N= 2.44 from the correlation).

Knowledge of this relationship allows quantitative prediction of the reagents required to synthesize an unknown amount of sorbent, accurate to 95%. The major factors influencing sorbent synthesis are acid volume used during synthesis and the quantity of DETA needed to in situ impregnate a predefined amount of nitrogen functionality onto the sorbent, as discussed above. A linear correlation also exists between maximum silica yield and acid volume used to adjust the pH to neutral (7.00 +/- 0.05) during the acid hydrolysis step (Figure 4); subsequent analyses show the correlation to have an accuracy of 95%. With the increased synthetic control offered by these two correlations, sorbents can be tailored to specification (N-content) and demand (quantity).

Surface morphology was studied using SEM (Figure 5) and particles can be observed as pseudo-spherical in shape but aggregated with non-unform sizes. SEM analysis shows that the porous structure of the silica is maintained, however, the presence of DETA appears to cause the particles to be more tightly packed with less visible voids; greater agglomeration of smaller particles to form larger nano-size particles is also observed. However, the micrographs for both samples are relatively similar suggesting that, upon in situ-impregnation, the samples maintain the original morphology of

the unfunctionalized silica, and the amine does not necessarily coat the external silica surface during impregnation but fills the pore spaces during synthesis, as also shown by N_2 sorption analysis (Figure 1).

Thermal analyses were conducted on D1-1 and unmodified silica, (Figure 6). The calorimetric curve for D1-1 shows one endothermic peak and three exothermic peaks. The initial weight loss between 295 K and 450 K is ascribed to desorption of physisorbed water and/or volatiles [32]. Two exothermic peaks observed at 553 K and 690 K are due to the decomposition of molecular water and organic materials present, in this case DETA. The final exothermic peak at 1073 K is due to the decomposition of remaining silanol groups present in the materials, the intensity and mass loss at this stage suggests that are present at insignificant levels. The thermographs also show that the unfunctionalized silica demonstrates good thermal stability in the temperature range analyzed (298 K – 1273 K) indicating no significant losses other than those ascribed to H_2O and silanol groups (loss occurs at all temperatures). D1-1 displays relatively good thermal stability within the lower temperature range used, up to 400 K, before decomposition begins, continuing even after the boiling point of DETA (477 K) up to 790 K, which suggests that, although there was significant loss of organic groups at higher temperatures, the material can be used at temperatures up to 400 K.

3.2 CO_2 adsorption studies

CO_2 uptakes, with respect to pressure, were studied using an IGA system, allowing both equilibrium masses and kinetic data to be evaluated. Isothermal measurements were conducted at 333 K for two set pressures: 10 kPa and 100 kPa. These conditions best simulate the process gases requiring remediation; either pure CO_2 or a system typical of flue gas desulfurization, which produces a partial pressure of between 10 and 15 kPa CO_2 at a stream temperature of 333 K to 348 K [33]. CO_2 adsorption studies were performed for both unmodified silica and AIIS, allowing the effect of amine impregnation on sorbent CO_2 affinity to be investigated. The CO_2 adsorption data shown in Table 3 indicates that CO_2 capacity increases with increasing amine content; the relatively small adsorption capacity of unmodified silica is attributed to the presence of silanol groups on the silica surface and/or the sorbents minor textural properties. Impregnation with amine functionalities is expected to increase the interaction of acidic CO_2 molecules with the basic sites ($-NH_2$) incorporated into the silica. In theory, an increasing number of basic sites will increase the CO_2 adsorption capacity [3], and CHN analysis and sorption results confirm such a trend; however, a caveat of a minimum wt% amine exists (10 ± 3%), before which a significant influence on CO_2 capacity is observed. Hence, it can be proposed that amine contents ≥ 10%, produce an improvement in CO_2 uptake.

CO_2 selectivities were determined as the ratio of sorbent performance with individual pure streams of the two major flue gas components (CO_2 and N_2). It was evident that, for D1-1, the N_2 adsorption capacity was negligible compared to that for CO_2 (see Figure 7). At 333 K and 10 kPa, CO_2/N_2 molar selectivities ≤ 53 were recorded while values ≤ 9.6 were observed at 100 kPa.

For commercial application of solid sorbents for PCCC, it is essential that the materials used not only have high CO_2 capacities and selectivities but that they demonstrate stable sorption capacities during repetitive cycling [34]. In this study, pressure swing adsorption (PSA) was used; a typical PSA cycle uses a reduced pressure to shift the equilibrium position and cause desorption of adsorbed species and regeneration of the adsorbent [34], here the adsorption pressure was set at 100 kPa (50 mbar min^{-1} CO_2) and desorption at close to vacuum (0.1 kPa).

An 80 min, PSA cycle programme was performed for AIIS (333 K) allowing analysis over 21 cycles. Figure 8 shows that the CO_2 capacity reduces after the first cycle but remains fairly constant thereafter, reducing by only ~5% over the latter 20 cycles. The initial loss in capacity (~ 0.54 mmol g^{-1}) is attributed to the strong interaction between CO_2 and the sorbent which is not overcome by simple evacuation, complete thermal regeneration was achieved at 393 K, indicating regenerability of the sample. This retained uptake forms the new zero for adsorption and reproducible sorption behavior was observed for all subsequent cycles.

4. Conclusion

A new method of synthesizing DETA in situ-impregnated silica has been developed from the direct impregnation of DETA into aggregated silica, formed from the polycondensation of sodium metasilicate pentahydrate via acid hydrolysis. The presence and subsequent stability of DETA within the silica structure was confirmed and results obtained suggest that DETA can be in situ-impregnated within the aggregated silica in a controlled manner, forming a stable matrix with the solid support exhibiting a maximum CO_2 capacity of $\leq$ 1.779 mmol g^{-1} at 100 kPa and 333 K. Sorbent cycling studies indicated a 5% loss in capacity after 21 cycles, suggesting a relatively stable sorption capacity. CO_2/N_2 selectivities of $\leq$ 53 were obtained at 10 kPa and the inclusion of amine into the silica structure presents a practical method of enhancing CO_2 uptake, with evidence that the synthesis conditions can be tailored to material specification and demand.

Acknowledgements
EO thanks the University of Strathclyde for financial support

References

[1] G. Xu, L. Li, Y. Yang, L. Tian, T. Liu, K. Zhang, A novel CO_2 cryogenic liquefaction and separation system, Energy, 42 (2012) 522-529.
[2] R. Thiruvenkatachari, S. Su, H. An, X.X. Yu, Post combustion CO_2 capture by carbon fibre monolithic adsorbents, Progress in Energy and Combustion Science, 35 (2009) 438-455.
[3] C. Zhang, W. Song, G. Sun, L.-J. Xie, J. Wang, K. Li, C. Sun, H. Liu, C.E. Snape, T.C. Drage, CO_2 capture with activated carbon grafted by nitrogenous functional groups, Energy & Fuels, (2013).
[4] A. Samanta, A. Zhao, G.K.H. Shimizu, P. Sarkar, R. Gupta, Post-combustion CO_2 Capture Using Solid Sorbents–A Review, Industrial & Engineering Chemistry Research, (2012).
[5] A. Sayari, Y. Belmabkhout, R. Serna-Guerrero, Flue gas treatment via CO_2 adsorption, Chemical Engineering Journal, 171 (2011) 760-774.
[6] P.M.M. Blauwhoff, G.F. Versteeg, W.P.M. Van Swaaij, A study on the reaction between CO_2 and alkanolamines in aqueous solutions, Chemical Engineering Science, 39 (1984) 207-225.
[7] A. Samanta, A. Zhao, G.K.H. Shimizu, P. Sarkar, R. Gupta, Post-Combustion CO_2 Capture Using Solid Sorbents: A Review, Industrial & Engineering Chemistry Research, 51 (2011) 1438-1463.
[8] C.F. Martín, S. García, D. Beneroso, J.J. Pis, F. Rubiera, C. Pevida, Precombustion CO_2 capture by means of phenol–formaldehyde resin-derived carbons: From equilibrium to dynamic conditions, Separation and Purification Technology, 98 (2012) 531-538.
[9] M. Lupion, H.J. Herzog, NER300: Lessons learnt in attempting to secure CCS projects in Europe, International journal of greenhouse gas control, 19 (2013) 19-25.
[10] R.M. Davidson, Post-combustion carbon capture from coal fired plants: solvent scrubbing, IEA Clean Coal Centre London, 2007.
[11] T.C. Merkel, H. Lin, X. Wei, R. Baker, Power plant post-combustion carbon dioxide capture: an opportunity for membranes, Journal of Membrane Science, 359 (2010) 126-139.
[12] A. Heydari-Gorji, Y. Belmabkhout, A. Sayari, Polyethylenimine-Impregnated Mesoporous Silica: Effect of Amine Loading and Surface Alkyl Chains on CO_2 Adsorption, Langmuir, 27 (2011) 12411-12416.
[13] G. Qi, Y. Wang, L. Estevez, X. Duan, N. Anako, A.-H.A. Park, W. Li, C.W. Jones, E.P. Giannelis, High efficiency nanocomposite sorbents for CO_2 capture based on amine-functionalized mesoporous capsules, Energy Environ. Sci., 4 (2010) 444-452.
[14] H.C. Wang, C. Lu, H. Bai, J.F. Hwang, H.H. Lee, W. Chen, Y. Kang, S.-T. Chen, F. Su, S.-C. Kuo, Pilot-scale production of mesoporous silica-based adsorbent for CO_2 capture, Applied Surface Science, (2012).
[15] Y.G. Ko, H.J. Lee, H.C. Oh, U.S. Choi, Amines immobilized double-walled silica nanotubes for CO_2 capture, Journal of Hazardous Materials.

[16] A. Sayari, Y. Belmabkhout, R. Serna-Guerrero, Flue gas treatment via CO_2 adsorption, Chemical Engineering Journal, 171 (2011) 760-774.
[17] C. Chen, S.-T. Yang, W.-S. Ahn, R. Ryoo, Amine-impregnated silica monolith with a hierarchical pore structure: enhancement of CO_2 capture capacity, Chemical Communications, 0 (2009) 3627-3629.
[18] Z. Liang, B. Fadhel, C.J. Schneider, A.L. Chaffee, Adsorption of CO_2 on mesocellular siliceous foam iteratively functionalized with dendrimers, Adsorption, 15 (2009) 429-437.
[19] K. Wang, H. Shang, L. Li, X. Yan, Z. Yan, C. Liu, Q. Zha, Efficient CO_2 capture on low-cost silica gel modified by polyethyleneimine, Journal of Natural Gas Chemistry, 21 (2012) 319-323.
[20] X. Zhang, X. Zheng, S. Zhang, B. Zhao, W. Wu, AM-TEPA Impregnated Disordered Mesoporous Silica as CO_2 Capture Adsorbent for Balanced Adsorption–Desorption Properties, Industrial & Engineering Chemistry Research, 51 (2012) 15163-15169.
[21] A. Heydari-Gorji, A. Sayari, CO_2 capture on polyethylenimine-impregnated hydrophobic mesoporous silica: Experimental and kinetic modeling, Chemical Engineering Journal, 173 (2011) 72-79.
[22] D. Wang, C. Sentorun-Shalaby, X. Ma, C. Song, High-Capacity and Low-Cost Carbon-Based "Molecular Basket" Sorbent for CO_2 Capture from Flue Gas, Energy & Fuels, 25 (2010) 456-458.
[23] S.V. Patwardhan, S.J. Clarson, Silicification and biosilicification Part 1. Formation of silica structures utilizing a cationically charged synthetic polymer at neutral pH and under ambient conditions, Polymer Bulletin, 48 (2002) 367-371.
[24] C.J. Brinker, G.W. Scherer, Sol-gel science: the physics and chemistry of sol-gel processing, Gulf Professional Publishing, 1990.
[25] S. Brunauer, P.H. Emmett, E. Teller, Adsorption of Gases in Multimolecular Layers, Journal of the American Chemical Society, 60 (1938) 309-319.
[26] E.P. Barrett, L.G. Joyner, P.P. Halenda, The Determination of Pore Volume and Area Distributions in Porous Substances. I. Computations from Nitrogen Isotherms, Journal of the American Chemical Society, 73 (1951) 373-380.
[27] M. Benham, D. Ross, Experimental determination of absorption-desorption isotherms by computer-controlled gravimetric analysis, Z Phys Chem NF, 163 (1989) S25-S32.
[28] V. Zeleňák, M. Badaničová, D. Halamová, J. Čejka, A. Zukal, N. Murafa, G. Goerigk, Amine-modified ordered mesoporous silica: Effect of pore size on carbon dioxide capture, Chemical Engineering Journal, 144 (2008) 336-342.
[29] G. Duan, C. Zhang, A. Li, X. Yang, L. Lu, X. Wang, Preparation and characterization of mesoporous zirconia made by using a poly (methyl methacrylate) template, Nanoscale Research Letters, 3 (2008) 118-122.
[30] J.B. Condon, Surface area and porosity determinations by physisorption: measurements and theory, Elsevier Science, 2006.
[31] B. Aziz, N. Hedin, Z. Bacsik, Quantification of chemisorption and physisorption of carbon dioxide on porous silica modified by propylamines: Effect of amine density, Microporous and Mesoporous Materials, 159 (2012) 42-49.
[32] M. Bhagiyalakshmi, S.D. Park, W.S. Cha, H.T. Jang, Development of TREN dendrimers over mesoporous SBA-15 for CO2 adsorption, Applied Surface Science, 256 (2010) 6660-6666.
[33] Y. Zhao, Y. Shen, L. Bai, S. Ni, Carbon dioxide adsorption on polyacrylamide-impregnated silica gel and breakthrough modeling, Applied Surface Science, 261 (2012) 708-716.
[34] S.H. Liu, C.H. Wu, H.K. Lee, S.B. Liu, Highly stable amine-modified mesoporous silica materials for efficient CO_2 capture, Topics in Catalysis, 53 (2010) 210-217.

Tables

Table 1: Comparison of power stations with and without CO_2 capture

Technology	Thermal efficiency (% LHV)	Capital cost ($/kW)	Electricity cost (c/kWh)	Cost of CO_2 avoided ($/t CO_2)
gas-fired plants				
No capture	55.6	500	6.2	–
Post-combustion capture	47.4	870	8	58
Pre-combustion capture	41.5	1180	9.7	112
Oxy-combustion	44.7	1530	10	102
coal-fired plants				
No capture	44	1410	5.4	–
Post-combustion capture	34.8	1980	7.5	34
Pre-combustion capture	31.5	1820	6.9	23
Oxy-combustion	35.4	2210	7.8	36

Table 2: Surface areas, pore volumes, and average pore diameters for samples prepared within this study

Sample	[Si]:[N]	BET Surface Area m^2g^{-1}	Total pore volume cm^3g^{-1}	average Pore diameter nm
Unfunctionalized silica	-	546.0 ± 1.153	0.641	4.0
D8-1	1:0.125	312.9 ± 0.714	0.362	3.6
D4-1	1:0.25	179.5 ± 0.555	0.199	3.6
D2-1	1:0.5	134.1 ± 0.905	0.152	3.4
D1-1	1:1	250.8 ± 1.362	0.240	3.3

Table 3: Elemental analysis and CO_2 adsorption capacities at 10 kPa and 100 kPa for DETA in situ-impregnated silicas

Sample	wt% C	wt% H	wt% N	wt% Amine	Amine Conc. (mmol g^{-1})	CO_2 adsorption capacity at 10 kPa (mmol g^{-1})	CO_2 adsorption capacity at 100 kPa (mmol g^{-1})
Unmodified silica	trace	trace	trace	trace	trace	0.14	0.53
D1-1	18.7	6.71	12.72	31.17	9.08	1.14	1.779
D2-1	10.63	3.24	7.4	18.13	5.28	0.556	0.915
D4-1	5.95	3.21	4.45	10.9	3.18	0.352	0.704
D8-1	4.14	3	2.55	6.25	1.82	0.372	0.739

Figures

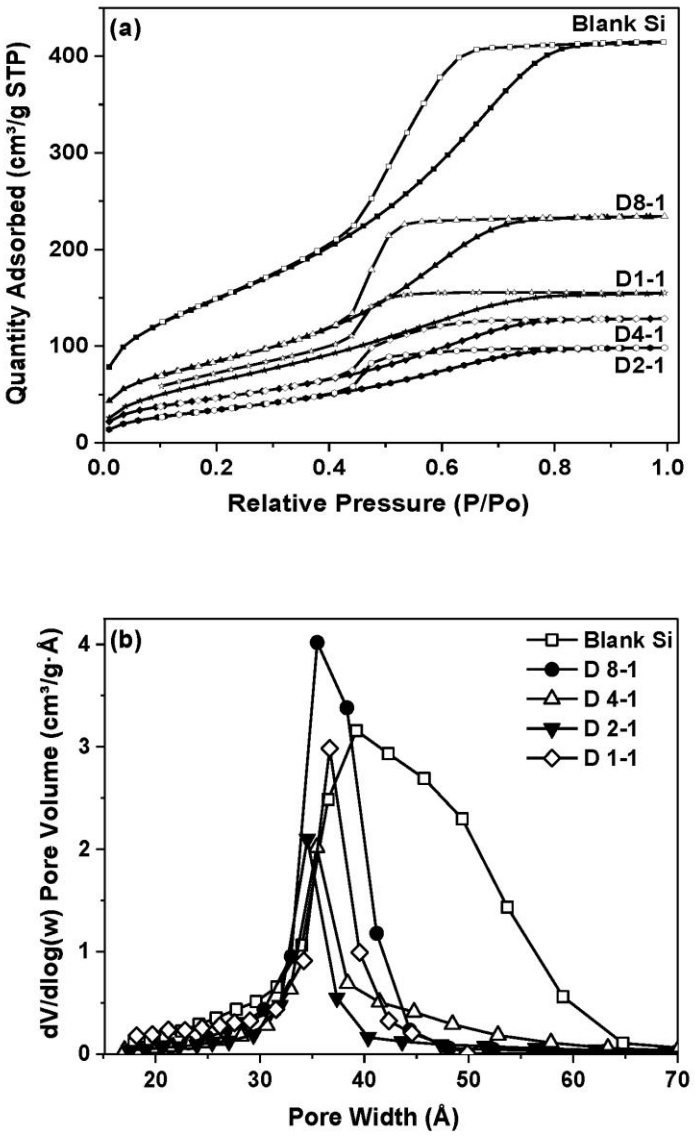

Figure 1: (a) N_2 sorption isotherms and (b) BJH desorption pore size distribution of unmodified and DETA in situ-impregnated silicas.

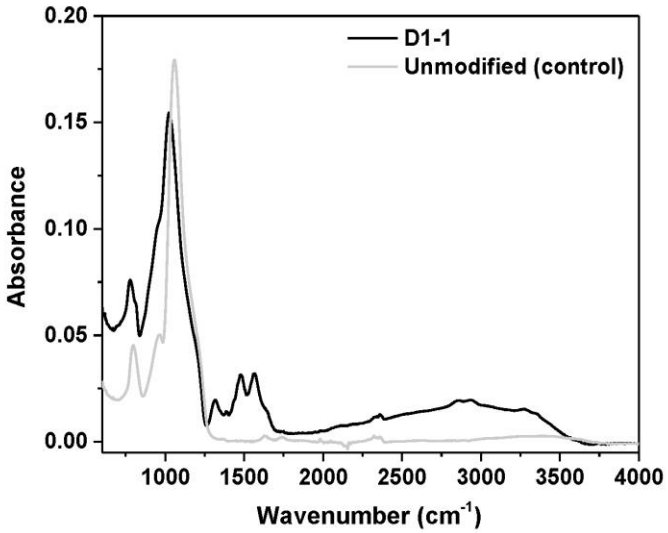

Figure 2: IR spectra for D1-1 and unmodified silica synthesized in this study.

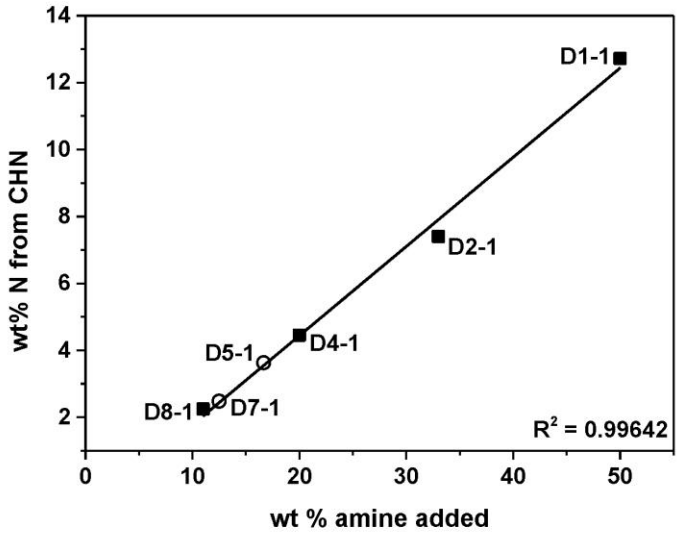

Figure 3: Correlation of amine loading with wt% of amine in situ-impregnated within the silica framework for materials synthesized in this study.

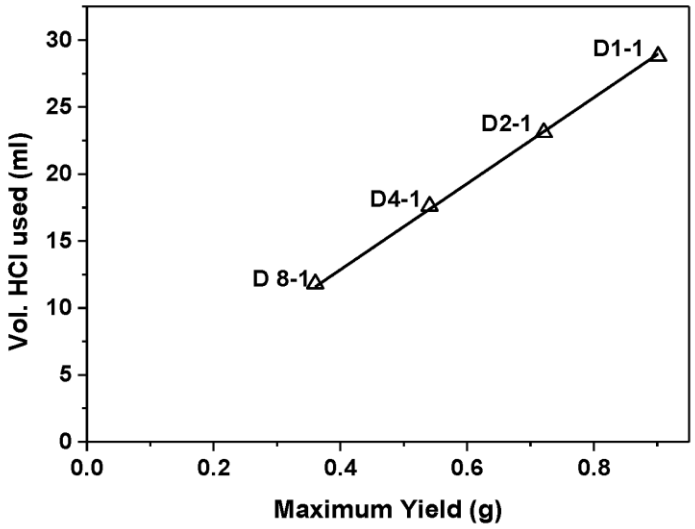

Figure 4: Correlation between the volume of acid needed and the calculated max yield

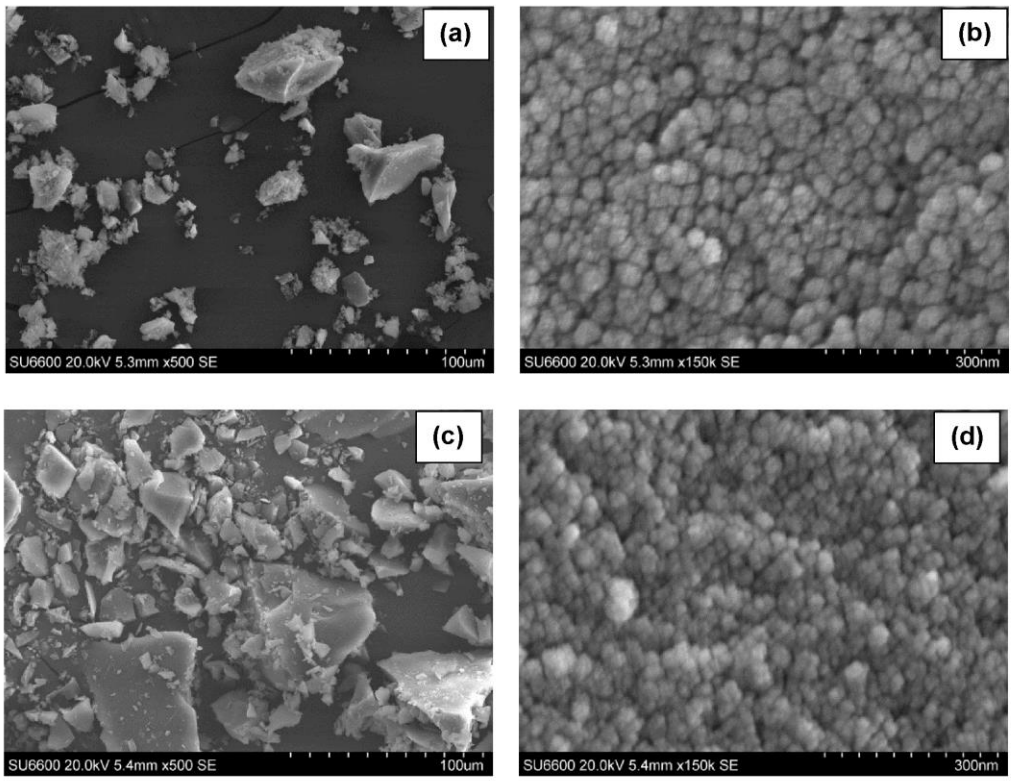

Figure 5: SEM images of unmodified silica (a & b) and D1-1 (c & d)

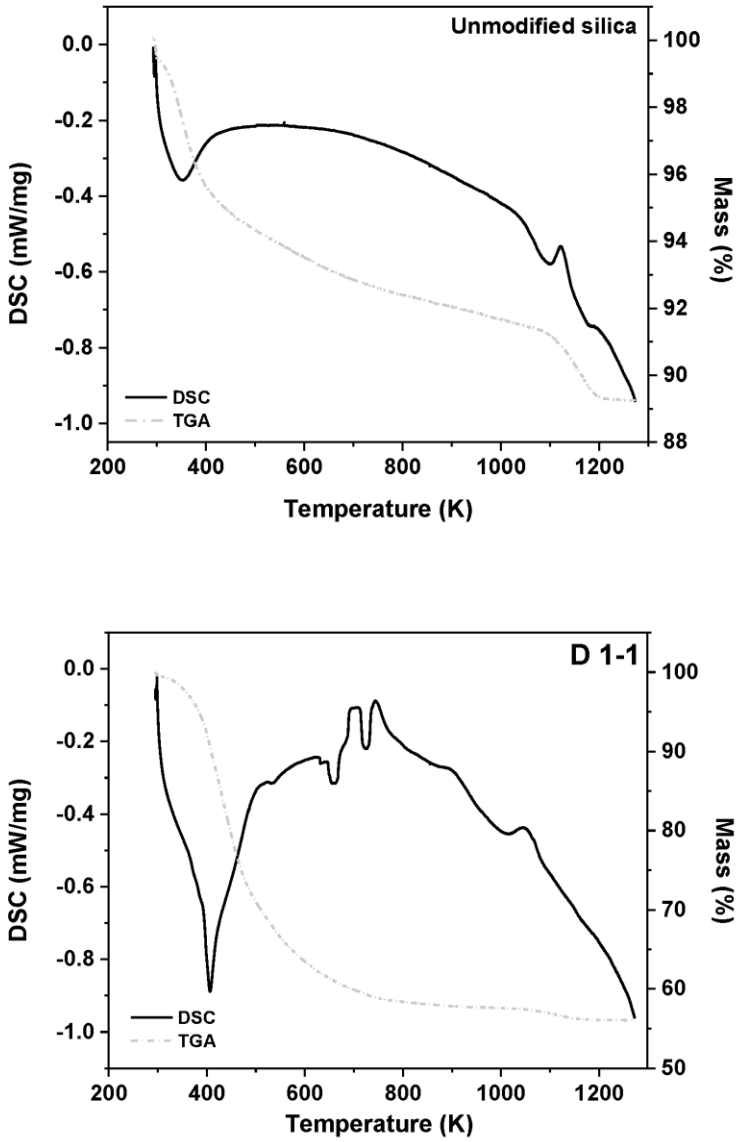

Figure 6: DSC-TGA thermographs of unmodified silica and D1-1 in the temperature range of ambient to 1273 K

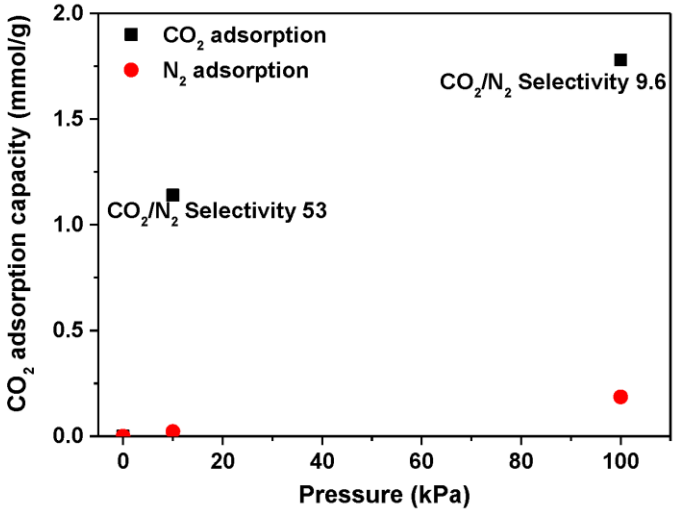

Figure 7: CO_2 and N_2 adsorption capacities for D1-1 at 10 kPa and 100 kPa (333 K, 60 min per pressure step)

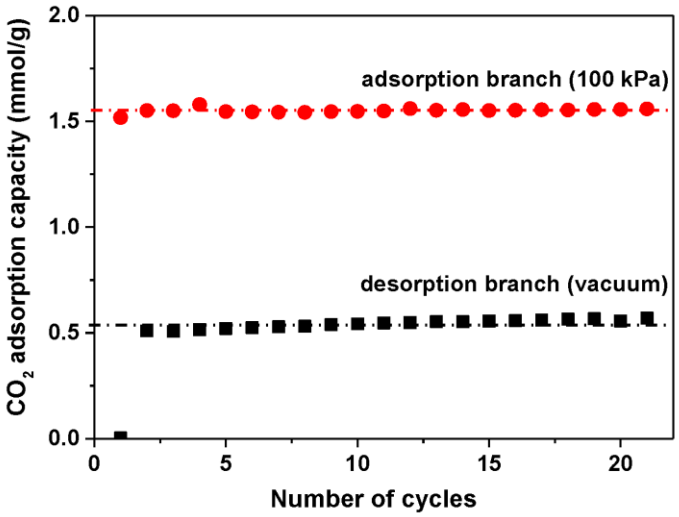

Figure 8: CO_2 adsorption-desorption runs on D1-1 at 333 K and 100 kPa (60 min per cycle)